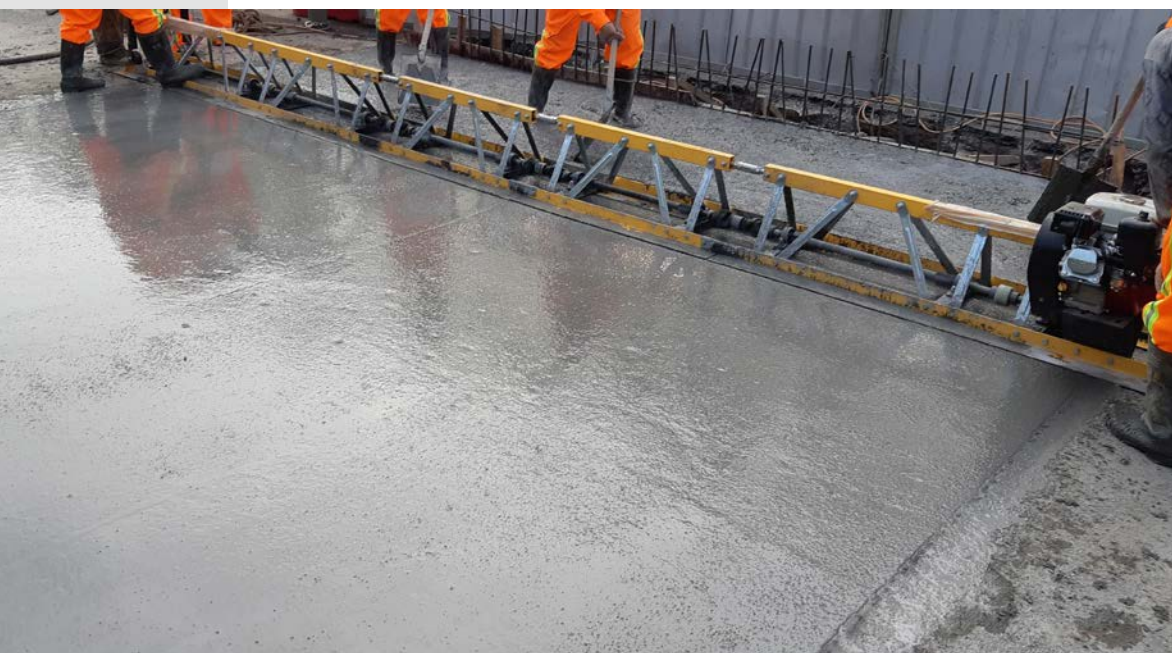


Shuai Yuan

Investigation of some Workability Issues Impeding the Large-scale Application of UHPC

SIB 11

MONOGRAPHIC SERIES TU GRAZ
SCHRIFTENREIHE DES INSTITUTS FÜR BETONBAU



Shuai Yuan

**Investigation of some Workability Issues Impeding
the Large-scale Application of UHPC**

Monographic Series TU Graz

Schriftenreihe des Instituts für Betonbau SIB

Series Editor:

Univ.-Prof. Dipl.-Wirtsch.-Ing. Dr.techn. Dirk Schlicke

Monographic Series TU Graz

Schriftenreihe des Instituts für Betonbau Volume 11

Shuai Yuan

**Investigation of some Workability Issues Impeding
the Large-scale Application of UHPC**

This work is based on the dissertation "*Investigation of some Workability Issues Impeding the Large-scale Application of UHPC*", presented at Graz University of Technology, Institute of Structural Concrete and Katholieke Universiteit Leuven in 2024.

Supervision / Assessment:

Viet Tue Nguyen (Graz University of Technology)

Jiabin Li (KU Leuven)

Cover Verlag der Technischen Universität Graz
Cover photo Institute of Structural Concrete, TU Graz
Print Buchschmiede (Dataform Media GmbH)

2025 Verlag der Technischen Universität Graz
www.tugraz-verlag.at

Print

ISBN 978-3-99161-026-7

E-Book

ISBN 978-3-99161-027-4

DOI 10.3217/978-3-99161-026-7



This work is licensed under the Creative Commons Attribution 4.0 International (CC BY 4.0) license.
<https://creativecommons.org/licenses/by/4.0/deed.en>

This CC license does not apply to the cover, third party material (attributed to other sources) and content noted otherwise.

Acknowledgement

This PhD research aims to improve the workability of UHPC to increase the fresh performances and keep the hardening performances, which is mainly supported by the Institute of Structural Concrete in the Graz University of Technology, Austria, including materials, equipment, etc. Part of the research on the recycled aggregate is carried out at KU Leuven.

Firstly, I would like to express my great gratitude to my supervisor at TU Graz, Prof. Dr.-Ing. Habil. Nguyen Viet Tue, for supporting me in doing my PhD research at TU Graz and giving me great guidance and help during my research period. His knowledge and authority in the field of concrete materials have greatly enriched my insights, and his rigorous and realistic attitude toward concrete experiments has also encouraged me to fully learn. Every discussion with him let me gain a fuller understanding of my research topic and understand which key issues in my research still needed to be considered. I would not be able to finish the research without his advice.

Secondly, I would like to thank my supervisor at KU Leuven, Prof. Dr.-Ing. Jiabin Li, for offering the opportunity to do joint PhD research at KU Leuven and giving me a lot of beneficial suggestions during my research period. He gave me great help with academic papers, assisted me in completing the publication of many research results, and also provided a lot of recommendations in the writing of the final thesis. His rigorous logic, profound theoretical literacy, and rich experimental experience have deeply infected me. He also mainly directed my research on the part of recycled aggregate concrete.

Thirdly, I want to thank the members of the supervisory committee in KU Leuven, Ing. Luc Boehme, Prof. Dr. Ir. Elke Gruyaert and Ir. Matthias Van Damme, for offering me very meaningful and valuable suggestions for my research in every meeting. I also want to appreciate Prof. Dr.-Ing. Markus Krüger, Prof. Dr.-Ing. Frank Dehn and Prof. Dr.-tech. Bernhard Freytag for providing me a lot of help in improving and optimising my thesis.

Fourthly, I would like to express my thanks to Prof. Dr.-tech. Dirk Schlicke, who continued to support me in completing my research and provided key guidance for my research to be more convincing. He also gave me a lot of assistance in my career. I also want to thank my colleagues in TU Graz, Dr.-tech. Kim Huy Hoang and Dipl.-Ing. Michael Huß, for providing invaluable comments and suggestions for my research and helping me to gain deeper insights into the field of concrete materials. And the colleagues in KU Leuven also helped me much with my research at KU Leuven. Besides, the colleagues in the Laboratory for Structural

Engineering and the Institute of Technology and Testing of Building Materials in TU Graz also offered a lot of help in implementing the experiments of this study.

Finally, I would like to thank my parents and wife, who have encouraged me and stood by me all the time during my doctoral period, so that I can persist in completing the PhD research.

Abstract

Ultra-high performance concrete (UHPC) represents one of the most important advances in concrete technology in the past thirty years. Through a careful selection of the constituents and proper mix design to create a dense structure, UHPC exhibits superior mechanical properties and durability aspects, compared with conventional normal strength concrete (NSC) and high-performance concrete (HPC). When containing steel fibre, it can also achieve very ductile behaviour in the post-peak branch, high flexural tensile strength, and possible strain hardening due to multiple cracking, providing this material with great potential in developing robust, durable and sustainable buildings and infrastructure.

In recent years, UHPC technology has been greatly developed. The engineering projects include not only new construction but also many maintenance and repair projects. Although the costs of the raw materials of UHPC are relatively high in comparison to that of NSC, thanks to its extremely high design strength, the size of the structure and the amount of steel reinforcements can be greatly reduced, leading to the fact that the total project cost may hardly increase. Moreover, the good mechanical performance and durability of UHPC can also significantly reduce life cycle costs.

However, at present in the world, the application of UHPC is still relatively limited, most of which are small structures or parts of large structures, and the real large-scale application of UHPC has rarely been realized. Many researchers are mainly paying attention to the mechanical properties of UHPC; while there are very few studies focusing on the workability of UHPC. It should be noted that the workability of UHPC is also an important issue that cannot be ignored in the large-scale application of UHPC, which refers to the ability of fresh concrete to be easily manipulated by the construction operations in each process (e.g. mixing, transporting, casting, compacting, etc.) and to obtain uniform quality and compact shape. Thus, on one hand, workability is of great importance when carrying out concreting operations, as it has a major influence on the efficiency of the work step; on the other hand, it also has a great influence on the hardened properties.

The ultra-high performance of UHPC is mainly because of the super dense microstructure, very low water content, and high powder material content. But this can also lead to incomplete hydration of the cement in concrete, little free water, and high viscosity, resulting in many problems in terms of workability. For example, due to the very low free water in fresh concrete and high viscosity, a hard viscoplastic layer (commonly called "elephant skin") often forms on the surface within only 30 seconds to a few minutes after the mixing. For

multi-layer UHPC structures, this layer would induce poor combination; when UHPC is used for road pavement, it will also cause a bad finishability of the concrete surface.

Besides, the introduction of a large amount of air during concrete mixing and casting will form big air bubbles in fresh concrete. For NSC, most of these air bubbles can rise and be discharged after pouring and vibrating. But for UHPC due to its high viscosity, the air bubbles would rise slowly and are very difficult to escape even with prolonged vibration, making many air bubbles remain in the hardened UHPC structure to form big air pores. Considering that UHPC can be applied to structures with very small thicknesses (as low as 3cm), and the big air pores can have a diameter of up to 5mm, this would negatively affect the mechanical performances and durability of the structure, which is an important problem for practical applications of UHPC in addition to the formation of the “elephant skin”.

Therefore, this doctoral dissertation mainly focuses on the workability issues of the “elephant skin” and the air bubbles in UHPC. Through experimental research and theoretical analysis, the formation mechanisms of the “elephant skin” on the concrete surface and the air bubbles formation and de-airing mechanisms in UHPC are summarized. Accordingly, the corresponding suggestions for enhancing the surface performance and the de-airing behaviours in UHPC are proposed, so as to realize the large-scale application of UHPC under the premise of ensuring the required properties.

Meanwhile, as the application of concrete containing recycled concrete aggregates (RCAs) is becoming more and more mature, the recycled aggregate (RCA), as a special aggregate with high water absorption and low density, may also have a great influence on the workability of concrete. Moreover, such RCA may be more widely used in the future, thus contributing to the reduction of construction and demolition waste and sustainable development. Therefore, the investigation of using RCAs to replace nature coarse aggregates in UHPC is also performed to further verify the proposed formation mechanisms of the “elephant skin” and air bubbles formation and de-airing mechanisms in UHPC.

It is anticipated that the results of this investigation will contribute to realizing the large-scale application of UHPC in structural engineering so as to benefit the safety, reliability and sustainable development of civil engineering.

Keywords:

Ultra-high performance concrete; workability; “elephant skin”; pore structure; recycled concrete aggregate

Untersuchung einiger Verarbeitbarkeitsprobleme, die die großflächige Anwendung von UHPC behindern

Kurzfassung

Ultrahochfester Beton (UHPC) stellt einen der wichtigsten Fortschritte in der Betontechnologie der letzten dreißig Jahre dar. Durch eine sorgfältige Auswahl der Bestandteile und eine geeignete Mischungszusammensetzung zum Erzielen einer dichten Struktur weist UHPC im Vergleich zu herkömmlichem normalfestem Beton (NSC) und Hochleistungsbeton (HPC) überlegene mechanische Eigenschaften und Dauerhaftigkeitsaspekte auf. Wenn Stahlfasern enthalten sind, kann er auch ein sehr duktileres Verhalten im Nachbruchbereich, eine hohe Biegezugfestigkeit und ein Strain-Hardening Verhalten aufgrund multipler Rissbildung erreichen, was diesem Material ein großes Potenzial für die Entwicklung robuster, langlebiger und nachhaltiger Gebäude und Infrastrukturen verleiht.

In den letzten Jahren hat sich die UHPC-Technologie stark weiterentwickelt. Zu den Bauprojekten gehören nicht nur Neubauten, sondern auch viele Instandhaltungs- und Sanierungsprojekte. Obwohl die Rohstoffkosten für UHPC im Vergleich zu NSC relativ hoch sind, können dank der extrem hohen Festigkeit die Größe der Bauteile und die Menge der Stahlbewehrung stark reduziert werden, was dazu führt, dass die Gesamtprojektkosten kaum steigen. Darüber hinaus können die guten mechanischen Eigenschaften und die Dauerhaftigkeit von UHPC die Lebenszykluskosten deutlich verringern.

Derzeit ist die Anwendung von UHPC weltweit jedoch noch relativ begrenzt, wobei es sich meist um kleine Gebäude oder Teile großer Bauwerke handelt, und die tatsächliche Anwendung von UHPC in großem Maßstab wurde bisher nur selten realisiert. Viele Forscher befassen sich hauptsächlich mit den mechanischen Eigenschaften von UHPC, während es nur sehr wenige Studien gibt, die sich mit der Verarbeitbarkeit von UHPC befassen. Es sei darauf hingewiesen, dass die Verarbeitbarkeit von UHPC ebenfalls ein wichtiger Aspekt ist, der bei der großflächigen Anwendung von UHPC nicht außer Acht gelassen werden darf. Dies bezieht sich auf die Fähigkeit des Frischbetons, sich bei den einzelnen Arbeitsschritten der Anwendung (z. B. Mischen, Transportieren, Gießen, Verdichten usw.) leicht verarbeiten zu lassen und eine einheitliche Qualität und kompakte Form zu erzielen. Demzufolge ist die Verarbeitbarkeit von großer Bedeutung bei der Durchführung von Betoniervorgängen, da sie einen großen Einfluss auf die Effizienz des Arbeitsschritts mit sich bringt. Des Weiteren kann sie die Qualität der Festbetoneigenschaften beeinträchtigen.

Die extrem hohe Leistungsfähigkeit des UHPC ist vor allem auf das sehr dichte Gefüge, den sehr geringen Wassergehalt und den hohen Anteil an Feinststoffen zurückzuführen. Dies führt jedoch auch zu einer unvollständigen Hydratation des Zements im Beton, wenig freiem Wasser und hoher Viskosität, was zu vielen Problemen bei der Verarbeitbarkeit führen kann. So bildet sich beispielsweise aufgrund des sehr geringen freien Wassers im Frischbeton und der hohen Viskosität oft schon 30 Sekunden bis wenige Minuten nach dem Mischen eine harte zähelastische Schicht (gemeinhin "Elefantenhaut" genannt) auf der Oberfläche. Bei mehrschichtigen UHPC-Strukturen würde diese Schicht zu schlechten Verbundeigenschaften führen; wenn UHPC für Straßenbeläge verwendet wird, führt dies auch zu einer schlechten Oberflächenqualität.

Außerdem führt das Einbringen einer großen Menge Luft beim Mischen und Gießen des Betons zur Bildung großer Luftblasen im Frischbeton. Bei NSC können die meisten dieser Luftblasen aufsteigen und nach dem Gießen und Rütteln ausgeschieden werden. Aufgrund der hohen Viskosität von UHPC steigen die Luftblasen jedoch nur langsam auf und können auch bei längerer Vibration nur schwer entweichen, so dass viele Luftblasen in der gehärteten UHPC-Struktur verbleiben und große Luftporen bilden. In Anbetracht der Tatsache, dass UHPC für Strukturen mit sehr geringen Dicken (bis zu 3 cm) verwendet werden kann und die großen Luftporen einen Durchmesser von bis zu 5 mm haben können, würde sich dies negativ auf die mechanischen Eigenschaften und die Dauerhaftigkeit der Struktur auswirken. Dies ist neben der Elefantenhautbildung auch ein wichtiges Problem für praktische Anwendungen von UHPC.

Daher konzentriert sich diese Dissertation hauptsächlich auf die Probleme der Verarbeitbarkeit von "Elefantenhaut" und Luftblasen in UHPC. Durch experimentelle Forschung und theoretische Analyse werden der Mechanismus der Bildung von "Elefantenhaut" auf der Betonoberfläche und der Mechanismus der Luftblasenbildung und Entlüftung in UHPC zusammengefasst. Dementsprechend werden Vorschläge zur Verbesserung der Oberflächenqualität und des Entlüftungsverhaltens von UHPC untersucht, um die großtechnische Anwendung von UHPC unter der Prämisse der Sicherstellung der geforderten Eigenschaften zu realisieren.

Da die Anwendung von Beton mit rezyklierten Betonzuschlägen (RCA) immer ausgereifter wird, kann der rezyklierte Zuschlag (RCA) als spezieller Zuschlag mit hoher Wasseraufnahme und geringer Dichte auch einen großen Einfluss auf die Verarbeitbarkeit von Beton haben. Darüber hinaus könnte diese RCA in Zukunft verstärkt eingesetzt werden, um die Bau- und Abbruchabfälle zu verringern und eine nachhaltige Entwicklung zu fördern.

Daher wird auch die Verwendung von RCAs als Ersatz für grobe Gesteinskörnungen in UHPC untersucht, um den beschriebenen Mechanismus der Bildung von "Elefantenhaut" und Luftblasenbildung sowie den Mechanismus der Entlüftung in UHPC weiter zu verifizieren.

Es ist zu erwarten, dass die Ergebnisse dieser Untersuchung dazu beitragen werden, die großflächige Anwendung von UHPC im Hochbau zu realisieren, um die Sicherheit, Zuverlässigkeit und nachhaltige Entwicklung des Bauwesens zu fördern.

Schlagwörter:

Ultrahochfester Beton; Verarbeitbarkeit; "Elefantenhaut"; Porenstruktur; rezyklierte Betonzuschläge

Onderzoek naar enkele verwerkbaarheidsproblemen die de grootschalige toepassing van UHPC belemmeren

Samenvatting

Ultrahoog performant beton (UHPC) vertegenwoordigt een van de belangrijkste ontwikkelingen in de betontechnologie in de afgelopen dertig jaar. Door een zorgvuldige selectie van de bestanddelen en het juiste mengselontwerp om een dichte structuur te creëren, vertoont UHPC superieure mechanische eigenschappen en duurzaamheidsaspecten, in vergelijking met conventioneel normaal sterktebeton (NSC) en high performance beton (HPC). Wanneer staalvezels aanwezig zijn, kan het ook zeer buigzaam gedrag in de postpiek tak bereiken, hoge buigtreksterkte en mogelijke spanningsuitharding door meervoudige scheuren, waardoor dit materiaal een groot potentieel heeft bij het ontwikkelen van robuuste, duurzame gebouwen en infrastructuur.

De afgelopen jaren is UHPC-technologie sterk ontwikkeld. De engineering projecten omvatten niet alleen nieuwbouw, maar ook veel onderhouds- en reparatieprojecten. Hoewel de kosten van de grondstoffen van UHPC relatief hoog zijn in vergelijking met die van NSC, dankzij de extreem hoge ontwerpsterkte, kunnen de grootte van de structuur en de hoeveelheid wapeningsstaal sterk worden verminderd, waardoor de totale projectkosten nauwelijks zouden stijgen. Bovendien kunnen de goede mechanische prestaties en duurzaamheid van UHPC de structurele veiligheid ook aanzienlijk verhogen.

Momenteel is de toepassing van UHPC wereldwijd echter nog meestal relatief beperkt tot bruggen met kleine spanwijdte, kleine gebouwen of delen van grote structuren, en de echte grootschalige toepassing van UHPC is zelden gerealiseerd. Veel onderzoekers besteden vooral aandacht aan de mechanische eigenschappen van UHPC; terwijl er zeer weinig studies zijn gericht op de verwerkbaarheid van UHPC. Opgemerkt moet worden dat de verwerkbaarheid van UHPC ook een belangrijk probleem is dat niet kan worden genegeerd bij de grootschalige toepassing van UHPC, wat verwijst naar het vermogen van vers beton om gemakkelijk gemanipuleerd te worden door de constructiewerkzaamheden in elk proces (bv. mengen, transporteren, gieten, verdichten, enz.) en om uniforme kwaliteit en compacte vorm te verkrijgen zonder enig probleem dat afbreuk doet aan de structurele veiligheid. Zo leidt enerzijds de verwerkbaarheid direct tot de haalbaarheid en efficiëntie van het gietproces van UHPC; Anderzijds heeft het ook een grote invloed op de verharde eigenschappen.

Voor UHPC zijn de ultra-hoge verhardingsprestaties hoofdzakelijk te wijten aan de super dichte microstructuur, lage water/cement verhouding, en hoge gelmateriaal inhoud. Maar dit

leidt ook tot onvolledige hydratatie van het cement in beton, weinig vrij water en hoge viscositeit, wat resulteert in veel problemen veroorzaakt door lage verwerkbaarheid. Bijvoorbeeld, door het zeer lage vrije water in het verse beton en de hoge viscositeit vormt zich vaak binnen 30 seconden tot enkele minuten na het gieten een harde viscoplastische laag (vaak "olifantenhuid" genoemd) op het oppervlak. Voor meerlaagse UHPC-structuren, zou deze harde laag slechte combinatie veroorzaken; Wanneer UHPC wordt gebruikt voor wegbestrating, zal dit ook een slechte afwerking van het betonoppervlak veroorzaken.

Bovendien zal de introductie van een grote hoeveelheid lucht tijdens het mengen en gieten van beton grote luchtbellen in het verse beton vormen. Voor NSC kunnen de meeste van deze luchtbellen stijgen en worden afgevoerd na het gieten en trillen. Maar voor UHPC vanwege zijn hoge viscositeit, zouden de luchtbellen langzaam stijgen en zijn zeer moeilijk te worden afgevoerd, zelfs bij langdurige trillingen, waardoor veel luchtbellen in de geharde UHPC-structuur blijven om grote luchtporiën te vormen. Aangezien UHPC kan worden toegepast op structuren met zeer kleine dikte (zo laag als 3cm), en de grote luchtporiën een diameter tot 5mm kunnen hebben, zou dit de mechanische prestaties en duurzaamheid van de structuur negatief beïnvloeden, wat een belangrijk probleem is voor praktische toepassingen van UHPC.

Daarom richt dit proefschrift zich voornamelijk op de verwerkbaarheidsproblemen van "olifantenhuid" en luchtbellen in UHPC. Aan de hand van experimenteel onderzoek en theoretische analyse wordt een overzicht gegeven van het ontstaansmechanisme van de "olifantenhuid" op het betonoppervlak en het mechanisme van luchtbelvorming en ontluchting in UHPC. Dienovereenkomstig worden de overeenkomstige suggesties voorgesteld om de oppervlakteprestaties en het ontluchtingsgedrag in UHPC te verbeteren, zodat UHPC op grote schaal kan worden toegepast met de vereiste eigenschappen.

Terwijl de toepassing van beton met gerecyclede betonaggregaten (RCA's) steeds meer wordt toegepast, kan het gerecycleerde granulaat (RCA), als speciaal aggregaat met hoge waterabsorptie en lage dichtheid, ook een grote invloed hebben op de verwerkbaarheid van beton. Daarom wordt het onderzoek naar het gebruik van RCA's om natuurlijke grove aggregaten in UHPC te vervangen ook uitgevoerd om het voorgestelde vormingsmechanisme van "olifantenhuid" en luchtbelvorming en ontluchtingsmechanisme in UHPC verder te verifiëren. Bovendien kunnen de nieuwe UHPC met RCA's ook gunstig zijn voor milieubescherming en duurzame ontwikkeling.

Verwacht wordt dat de resultaten van dit onderzoek zullen bijdragen aan het realiseren van de grootschalige toepassing van UHPC in de bouwkunde ten behoeve van de veiligheid, betrouwbaarheid en duurzame ontwikkeling van de civiele techniek.

Trefwoorden:

Ultrahoogwaardig beton; verwerkbaarheid; "olifantenhuid"; poriënstructuur; gerecycled betongranulaat

Contents

Acknowledgement	iii
Abstract	v
Kurzfassung	vii
Samenvatting	xi
Contents	xv
List of Figures	xix
List of Tables	xxvii
Notations and symbols	xxix
1 Introduction	1
1.1 History of UHPC development and application.....	1
1.2 UHPC fresh and hardened properties.....	6
1.3 Problem statement and motivation.....	8
1.4 Research objective and content.....	11
2 Materials and composition of UHPC	13
2.1 Materials	13
2.1.1 Cement	13
2.1.2 Mineral admixture.....	14
2.1.3 Superplasticizer	16
2.1.4 Aggregates	17
2.1.5 Steel fibre	18
2.2 Manufacture of UHPC mixtures and specimen preparation	20
2.3 Mix design	23

2.3.1	Silica fume and quartz powder contents	25
2.3.2	Water-to-binder ratio.....	28
2.3.3	Superplasticizer dosage.....	31
2.3.4	Paste volume	37
2.3.5	Coarse aggregate.....	40
2.3.6	Steel fibre	41
2.3.7	Cement type	43
2.4	Summary.....	45
3	“Elephant skin” on the surface of UHPC	47
3.1	Literature review.....	47
3.2	Materials and measuring methods	51
3.3	Influence of the “elephant skin” on the bonding performance between UHPC layers 60	
3.3.1	4-point bending test of 140×140×550mm ³ beams.....	60
3.3.2	3-point bending test of 150×150×700mm ³ beams.....	64
3.3.3	3-point bending tests of 40×40×160mm ³ prisms.....	67
3.4	Influencing factors on the growing of the “elephant skin”	73
3.4.1	Temperature and evaporation rate.....	73
3.4.2	UHPC components.....	78
3.4.3	Compressive strength.....	92
3.5	Formation and growing mechanisms of the “elephant skin”	93
3.5.1	Characteristics of the second layer after removing the “elephant skin”	93
3.5.2	“Elephant skin” formation and growing mechanisms analysis	96
3.6	Summary.....	98
4	Entrapped air bubbles and pore structure of UHPC	100
4.1	Literature review.....	100
4.2	Materials and measuring methods	106
4.3	Influence of the air pores on the hardened properties of UHPC	110

4.4	Influencing factors on the air content in fresh UHPC mixture and air pores in hardened UHPC mixture	113
4.4.1	Mixing parameters	113
4.4.2	Casting method	119
4.4.3	Concrete rheology	122
4.4.4	UHPC components.....	127
4.4.5	Defoaming agent.....	146
4.4.6	Release agent.....	153
4.5	Air bubbles formation and de-airing mechanisms	162
4.5.1	Distribution of air bubbles in UHPC columns	163
4.5.2	Influences of the specimen sizes on the percentage of air pores	166
4.5.3	Influences on the size of air bubbles	168
4.5.4	Air bubbles formation and de-airing mechanisms analysis.....	172
4.6	3D X-ray irradiation to detect air pores distribution	174
4.6.1	Results of the short cylinders	177
4.6.2	Results of the long columns	181
4.7	Summary.....	184
5	Influence of the RCA on the workability of UHPC	186
5.1	Literature review.....	186
5.2	Influence of RCA on the properties of normal strength concrete	189
5.2.1	Results in literature	190
5.2.2	Experimental research.....	194
5.3	Influence of RCA on the properties of UHPC	198
5.3.1	Preliminary tests at the first stage	199
5.3.2	Optimal compensation water content investigation	203
5.3.3	Influence of RCA on the de-airing and the “elephant skin”.....	206
5.4	Discussion of the influence mechanisms	211
5.5	Summary.....	213

6	Conclusions and recommendations	214
6.1	Main findings.....	214
6.2	Valorisations	216
6.3	Future investigation	217
6.3.1	More types of raw material	217
6.3.2	More in-depth study of the “elephant skin”	217
6.3.3	More in-depth study of air bubbles	218
6.3.4	A detailed study on UHPC with recycled aggregate	218
	Reference.....	219
	Appendix: Detailed UHPC recipes and properties	231

List of Figures

Figure 1.1 Sherbrooke Bridge [7].....	4
Figure 1.2 Mushill Bridge [10].....	4
Figure 1.3 Gärtnerplatz Bridge [11]	5
Figure 1.4 Haneda Airport Runway D [13].....	5
Figure 1.5 WILD Bridge in Austria [23].....	5
Figure 1.6 Mucem Museum [26].....	5
Figure 1.7 Jean Bouin Stadium [28].....	5
Figure 1.8 Sakata Mirai Footbridge [30].....	5
Figure 1.9 Difference of the packing skeleton between UHPC and conventional concrete [33].....	7
Figure 1.10 An “elephant skin” forming shortly after the casting of UHPC	9
Figure 1.11 Air pores remain in the hardened concrete structure.....	10
Figure 1.12 Schematic diagram of gel pores and capillary pores	10
Figure 2.1 Particle size distribution (PSD) curves of the used powders and sands [32]	19
Figure 2.2 Eirich R01 mixer (10L).....	21
Figure 2.3 ELBA EMS 60C mixer (75L).....	21
Figure 2.4 Small Hobart mixer (5L).....	21
Figure 2.5 Mixing procedure for UHPC.....	21
Figure 2.6 Spread-flow test to evaluate the flowability and viscosity of UHPC mixtures using the Haegermann cone [90].....	22
Figure 2.7 Influences of the content of Si on the properties of UHPC mixtures	26
Figure 2.8 Influences of content of QP on the properties of UHPC mixtures	28
Figure 2.9 Influences of W/B ratio on the properties of UHPC mixtures	30
Figure 2.10 Influence of SP/B ratio on the properties of UHPC mixtures	34
Figure 2.11 Relationship between SP/C ratio and flowability of UHPC.....	35
Figure 2.12 Parameters M and N for description of the changing of the flowability and viscosity over time	36
Figure 2.13 Relationship between SP/B ratio and the changing of the consistency of UHPC mixtures over time.....	37
Figure 2.14 Influences of paste volume (represented by cement content) on the properties of UHPC mixtures	39
Figure 2.15 Influence of coarse aggregate content on the compressive strength of UHPC mixtures with the same flowability	41
Figure 2.16 Influence of steel fibre content on the compressive strength of UHPC mixtures with the same flowability	43

Figure 2.17 Influence of cement type on the properties of UHPC	45
Figure 3.1 Light microscopy and mercury intrusion porosity (MIP) test results of Wetzel et al. [40]	48
Figure 3.2 Penetration tests with data collector to simulate conditions that promote the “elephant skin” formation on an exposed UHPC surface [44]	48
Figure 3.3 Measured values of penetration resistances against the time of exposure to radiation and airflow for slabs made with base UHPC mixture covered and not covered with plastic membrane (“T” refers to the top of concrete slab; “B” refers to the bottom of concrete slab) [44]	49
Figure 3.4 Flowing of UHPC in the 60cm length formwork (flowing time: 1min14s)	50
Figure 3.5 Sketch of the developed method for measuring the surface resistance of UHPC using different movable rods	52
Figure 3.6 Test procedure of the using method	55
Figure 3.7 Test photos of the surface resistance of the “elephant skin” using the Vicat apparatus	55
Figure 3.8 Sketch of the treatment under different high RHs	56
Figure 3.9 Photos of UHPC surfaces of plates 1 hour after casting	57
Figure 3.10 Surface resistance-time curves of the “elephant skin” of the reference UHPC mixture at different RH levels, which is fitted into a single parameter (A) quadratic equation (parameter A reflects the growing of the “elephant skin” over time)	58
Figure 3.11 Relationship between RH and parameter A	59
Figure 3.12 Percentage normalization of the results of all UHPC mixtures	59
Figure 3.13 Schematic diagram of a movable rod going through the "elephant skin"	60
Figure 3.14 Casting procedures of the two beams	61
Figure 3.15 Surface resistance-time curves of the UHPC mixtures subject to 4-point bending tests	62
Figure 3.16 4-point-bending tests of double-layer UHPC beams, the beam with the “elephant skin” has a clear crack in the joint zone (indicating a shear failure due to the relative slide between the upper and lower layers)	63
Figure 3.17 Bending stress-midspan displacement curves in the 4-point bending tests	63
Figure 3.18 Schematic diagram of 3-point bending test for double-layer UHPC beams	64
Figure 3.19 Photos of concrete surfaces 1 hour after casting	64
Figure 3.20 Surface resistance-time curves of the UHPC mixture subjected to 3-point bending tests	65
Figure 3.21 3-point-bending tests of double-layer UHPC beams, the crack of the beam with “elephant skin” is not clear but occurred in the joint zone	65
Figure 3.22 Bending stress-midspan displacement curves in the 3-point bending tests	66

Figure 3.23 Schematic diagram of three-point bending test of small prisms	68
Figure 3.24 Surface resistance-time curves of the concrete in the small 3-point bending tests	68
Figure 3.25 Broken UHPC prisms of Recipe “720 0%” with different cracking patterns after the 3-point bending tests	69
Figure 3.26 Broken UHPC prisms of Recipe “860 2%” with different cracking patterns after the 3-point bending tests	70
Figure 3.27 Relationship between the maximum bending stress and the surface resistance of the “elephant skin”	71
Figure 3.28 Reduction of the maximum bending stress of UHPC with the surface resistance of the “elephant skin”	72
Figure 3.29 Flow diagram of the mixing procedures (ii) and (iii)	74
Figure 3.30 Influence of different temperatures on the growing of the “elephant skin” over time	76
Figure 3.31 Nomograph to Estimate Rate of Evaporation on Concrete Surface in SI Unit [113]	77
Figure 3.32 Relationship between evaporation rate and parameter A for the UHPC mixtures with the same recipe “720 CEM A”	78
Figure 3.33 Relationship between evaporation rate and parameter A for the UHPC mixtures with the different recipes	78
Figure 3.34 Influences of the contents of Si and QP on the growing of the “elephant skin” over time	80
Figure 3.35 Influence of W/B ratio on the growing of the “elephant skin” over time	82
Figure 3.36 Influence of SP/B ratio on the growing of the “elephant skin” over time	84
Figure 3.37 Relationship between the changing of the consistency of UHPC over time and the growing of the “elephant skin” over time	86
Figure 3.38 Influence of paste volume on the growing of the “elephant skin” over time	88
Figure 3.39 Influence of coarse aggregate content and size on the growing of the “elephant skin” over time	91
Figure 3.40 Influence of the StF content on the growing of the “elephant skin” over time	92
Figure 3.41 Relationship between compressive strength and the growing of the “elephant skin” over time	92
Figure 3.42 Investigation of the second layer after removing the first layer of the “elephant skin”	93
Figure 3.43 Results of the new “elephant skin” layers of UHPC mixtures without BA and StF when putting the UHPC under different RH after removal of the “elephant skin” layer	95

Figure 3.44 Results of the new “elephant skin” layers of UHPC mixtures with StF or BA	.96
Figure 3.45 Schematic: coarse aggregates and steel fibres cause internal moisture to take a long way around to rise	98
Figure 4.1 UHPC surface with air pores	100
Figure 4.2 Air bubbles accumulate in a specific position in an enclosed formwork	101
Figure 4.3 Entrapped air contents of fresh UHPC mixtures at different mixing durations (Low mixing speed: 198rpm; high mixing speed: 361rpm) [120].....	102
Figure 4.4 Relationship between the content of entrapped air bubbles in hardened UHPC and plastic viscosity, which is tested by the RheoCAD400 rheometer (CAD Instruments, Les Essarts-le-Roi, France) [120].....	103
Figure 4.5 Air contents of fresh UHPC mixture with the addition of AFAs (defoaming agents) [120].....	103
Figure 4.6 Reconstructed pore structure model of fibre-reinforced UHPC (above 200 μm): (a) Analysis of pore structure characteristics. (I) was the whole structure, (II) was the upper area and (III) was the bottom area; (b) Top view of the pore structure; (c) Pore size distribution of fibre-reinforced UHPC [123].....	105
Figure 4.7 Schematic diagram of the testing cylinders.....	107
Figure 4.8 The test method to calculate the number of air pores in the hardened concrete	108
Figure 4.9 Several different cases of air pores at the cross-sections of hardened concrete specimens	109
Figure 4.10 Influence of P_{bubble} on the hardened properties of UHPC mixtures.....	112
Figure 4.11 Influence of P_{bubble} on the compressive strength of the UHPC mixtures in group 2.3.3-3	112
Figure 4.12 Influence of mixing time on the de-airing behaviours and properties of UHPC mixture	115
Figure 4.13 Influence of mixing time on the P_{fresh} after percentage normalization	116
Figure 4.14 Influence of the mixer type on the de-airing behaviours and UHPC properties	119
Figure 4.15 Schematic diagram of 3 casting method	120
Figure 4.16 Schematic diagram of the cutting position of the columns	121
Figure 4.17 Results of P_{bubble} with 3 casting method.....	121
Figure 4.18 Schematic diagram of concrete rebound	121
Figure 4.19 Influence of the flowability on P_{fresh}	123
Figure 4.20 Influence of flowability on the ($P_{fresh} - P_{bubble}$) values in UHPC mixtures	124
Figure 4.21 Influence of viscosity of concrete on the de-airing behaviours of UHPC.....	126
Figure 4.22 Influence of Si/C ratio on the de-airing behaviours in UHPC.....	129
Figure 4.23 Influence of QP/C ratio on the de-airing behaviours in UHPC.....	131

Figure 4.24 Influence of W/B ratio on the de-airing behaviours in UHPC	134
Figure 4.25 Influence of SP/B ratio on the de-airing behaviours in UHPC	136
Figure 4.26 Influence of paste content on the de-airing behaviours in UHPC	139
Figure 4.27 Results of group 2.3.4-2 after percentage normalization	141
Figure 4.28 Influence of BA content and size on the de-airing behaviours in UHPC.....	144
Figure 4.29 Influence of StF content and size on the de-airing behaviours in UHPC.....	146
Figure 4.30 Influence of Perfin/CEM ratio on the properties and P_{fresh} of UHPC.....	149
Figure 4.31 Influence of the Admixture/CEM ratios on the compressive strength of UHPC	150
Figure 4.32 Influence of the Admixture/CEM ratios on the de-airing behaviours of UHPC	151
Figure 4.33 Influence of defoaming agents on the bending performance of UHPC	152
Figure 4.34 Influence of the 2 release agents on P_{bubble}	154
Figure 4.35 Appearance of the surface of the UHPC samples with the two release agents.	155
Figure 4.36 Appearance of plywood formworks and the formed concrete surface with different release agents (RA No.1: a solvent-free release agent based on water-soluble emulsion; RA No.2: a release agent based on liquid wax; RA No.3: a release agent based on silicon oil; RA No.4: a release agent based on mineral oil.) [134].....	157
Figure 4.37 Appearances of UHPC cylinders using Recipe “750 0.25”	159
Figure 4.38 Appearances of UHPC cylinders using Recipe “800 0.25”	160
Figure 4.39 Appearances of UHPC cylinders using Recipe “850 0.25”	161
Figure 4.40 Examined P_{bubble} with 4 kinds of formwork release agents	162
Figure 4.41 Calculated ($P_{fresh} - P_{bubble}$) value with 4 kinds of formwork release agents.....	162
Figure 4.42 Schematic diagram of the cutting positions of the columns and cylinders.....	164
Figure 4.43 Air pores distribution along the longitudinal direction for the 9 columns	165
Figure 4.44 Air pores distribution along the longitudinal direction for the cylinders	166
Figure 4.45 Influence of surface area on the de-airing behaviours in UHPC	167
Figure 4.46 Influence of column length on the de-airing behaviours in UHPC	167
Figure 4.47 Relationship between the measured spread-flow values and the maximum air pore diameters	168
Figure 4.48 Relationship between the measured T_{200} values and the maximum air pore diameters	169
Figure 4.49 Relationship between the SP/B ratio and the maximum air pore diameter when the flowability is constant.....	170
Figure 4.50 UHPC mixtures stored in the open buckets for 90min of the de-airing process	171

Figure 4.51 Influence of casting time on the de-airing behaviours in UHPC.....	171
Figure 4.52 Relationship between casting time and maximum air pore diameter	172
Figure 4.53 Relationship between mixing time and maximum air pore diameter.....	172
Figure 4.54 Schematic diagram of the formation, de-airing and breaking of large air bubbles during the mixing process	173
Figure 4.55 Schematic diagram of the movement process of air bubbles	174
Figure 4.56 4 groups of cylinders and columns in this research.....	175
Figure 4.57 “UniTOM XL” from the company “TESCAN GmbH”	176
Figure 4.58 Scanning of one group of cylinder and column	176
Figure 4.59 3D analysis results of cylinder “IC_ES” by software “Dragonfly”	177
Figure 4.60 Distribution of the air pores along the longitudinal direction in the cylinder “IC_ES”	178
Figure 4.61 Distribution of the air pores along the longitudinal direction in the cylinder “IC_noES”	178
Figure 4.62 Distribution of the air pores along the longitudinal direction in the cylinder “DC_ES”	179
Figure 4.63 Distribution of the air pores along the longitudinal direction in the cylinder “DC_noES”	179
Figure 4.64 Scanned brightness of the upper part is slightly higher than that of the lower part in cylinder “IC_noES”	180
Figure 4.65 3D analysis of long column “IC_ES” by software “Dragonfly”	181
Figure 4.66 Distributions of air pores along the longitudinal direction in the immediate cast columns	182
Figure 4.67 Distributions of air pores along the longitudinal direction in the delayed cast columns	182
Figure 4.68 Scanned brightness of the middle part is slightly higher than those of the upper part and lower part in column “IC_noES”	183
Figure 4.69 Scanned percentages of air pores in the whole sample of the cylinders and columns	184
Figure 5.1 Production of RCAs in a recycling factory (http://www.obbc.be/nl/installaties)	187
Figure 5.2 Schematic diagram of recycled aggregate surface wrapped with mortar [57] ..	188
Figure 5.3 Influence of the volume replacement ratio of RCA and the content of compensation water on the slump value for CVC [59, 159-165]	191
Figure 5.4 Influence of the volume replacement ratio of RCA and the content of compensation water on the compressive strength for CVC [59, 159-165].....	192

Figure 5.5 Influence of the volume replacement ratio of RCA and the content of compensation water on the flowability for SCC [60, 166-170].....	193
Figure 5.6 Influence of the volume replacement ratio of RCA and the content of compensation water on the compressive strength for SCC [60, 166-170]	193
Figure 5.7 Photo of the used RCA	195
Figure 5.8 Particle size distribution of used NAs and RCAs in this section	195
Figure 5.9 Flow table test apparatus [172]	197
Figure 5.10 Photo of the flow table test apparatus [173].....	197
Figure 5.11 Photos of the flow table tests of concrete mixtures	198
Figure 5.12 Particle size distribution of used BAs and RCAs in this section.....	199
Figure 5.13 Flowability of 2 groups of UHPC mixtures	200
Figure 5.14 Photos of the flowability test of UHPC mixtures.....	201
Figure 5.15 Compressive strengths of these 2 groups of UHPC mixtures	202
Figure 5.16 P_{fresh} of the UHPC mixtures in Group “UHPC2 without StF”	203
Figure 5.17 Measured flowabilities of UHPC mixtures	204
Figure 5.18 Photos of the flowability test of UHPC mixtures.....	205
Figure 5.19 Measured 28d compressive strength of UHPC mixtures	206
Figure 5.20 Measured P_{fresh} of the UHPC mixtures.....	206
Figure 5.21 Photos of the flowability test of UHPC mixtures.....	208
Figure 5.22 Measured compressive strengths of UHPC mixtures.....	208
Figure 5.23 Influence of RCA on the de-airing behaviours in UHPC.....	210
Figure 5.24 Influence of the RCAs on the growing of the “elephant skin” over time.....	211

List of Tables

Table 2.1 Physical-mechanical properties and chemical components of the cement and mineral admixture	15
Table 2.2 Technical specifications of SP “Premment H500”	17
Table 2.3 Physical-mechanical properties and chemical components of the used fine aggregates (<0.8mm).....	18
Table 2.4 Physical-mechanical properties of the used coarse aggregates (<8mm)	18
Table 2.5 Starting and reference mix proportion developed by K. H. Hoang [32].....	24
Table 2.6 UHPC mixtures with different Si/C and QP/C ratios	25
Table 2.7 UHPC mixtures with different W/B ratios	29
Table 2.8 UHPC mixtures with different SP/B ratios	32
Table 2.9 UHPC mixtures with different cement contents (paste volumes).....	38
Table 2.10 UHPC mixtures with different coarse aggregates and the same flowability	41
Table 2.11 UHPC mixtures with different steel fibres and the same flowability	42
Table 2.12 UHPC groups with different cement types	43
Table 3.1 Water evaporation from UHPC mixtures (at the end of the 24h under 50% RH) [103]	49
Table 3.2 Information about the used movable rods	53
Table 3.3 UHPC mixtures for testing the influence of RH.....	56
Table 3.4 UHPC mixtures with different external and internal temperatures	75
Table 3.5 UHPC mixtures in Group 2.3.1-1	79
Table 3.6 UHPC mixtures in Groups 2.3.2-1~2.3.2-6 in Section 2.3.2	82
Table 3.7 UHPC mixtures in Groups 2.3.3-2, 2.3.3-6 and new Groups 3.4.2.3-1 and 3.4.2.3-2.....	84
Table 3.8 UHPC mixtures in Group 2.3.4-1	87
Table 3.9 UHPC mixtures in Group 2.3.5-1	90
Table 3.10 UHPC mixtures in Group 2.3.6-1	91
Table 3.11 UHPC mixture without BA and StF to test the new “elephant skin” layer	94
Table 3.12 UHPC mixtures with BA or StF to test the new “elephant skin” layer	95
Table 4.1 UHPC mixtures to test the influence of P_{bubble}	110
Table 4.2 UHPC groups tested with different mixing time	114
Table 4.3 UHPC mixtures mixed with different mixers.....	117
Table 4.4 UHPC mixtures to test the influence of the casting method and release agent ..	120
Table 4.5 UHPC mixtures to test the influence of flowability	122
Table 4.6 UHPC mixtures to test the influence of viscosity.....	125

Table 4.7 Influence of temperature in fresh concrete on the properties and de-airing behaviours of UHPC mixture	127
Table 4.8 UHPC mixtures in Group 2.3.1-2.....	128
Table 4.9 UHPC mixtures in Groups 2.3.2-7 and 2.3.2-8	132
Table 4.10 UHPC mixtures in Groups 2.3.3-3 and 2.3.3-7	135
Table 4.11 UHPC mixtures in Group 2.3.4-2 and new Group 4.4.4.4-1	138
Table 4.12 UHPC mixtures in Groups 2.3.5-2 and 2.3.5-3	143
Table 4.13 UHPC mixtures in Groups 2.3.6-2 and 2.3.6-3	144
Table 4.14 Technical specifications of the defoaming agents	146
Table 4.15 UHPC groups tested in this section	147
Table 4.16 UHPC groups tested in this section	149
Table 4.17 Technical specifications of these 2 release agents.....	154
Table 4.18 Technical specifications of these 4 tested release agents	158
Table 4.19 Mix proportions of UHPC mixtures for columns	163
Table 4.20 Casted samples to investigate the air bubble distribution.....	163
Table 4.21 UHPC mixtures in Groups 4.4.1.1-1 and 4.4.1.1-2	170
Table 4.22 Tested samples with 3D X-ray	174
Table 5.1 The CVCs tested for investigating the RCAs	196
Table 5.2 Technical parameters of the CEM C	196
Table 5.3 Tested UHPC mixtures with RCAs in preliminary tests	200
Table 5.4 Tested UHPC mixtures with RCAs and different compensation water content	203
Table 5.5 Tested UHPC mixtures with RCAs to investigate the workability issues	207

Notations and symbols

$\beta_{mix-actual}$	particle packing density [-]
ρ_a	apparent density [g/cm ³]
ρ_{rd}	oven-dry density [g/cm ³]
ρ_{ssd}	saturated surface dry density [g/cm ³]
Φ	capillary porosity [-]
A_{bubble}	average area of all the observed air bubbles [mm ²]
$A_{surface}$	area of the cross-section [mm ²]
CC	Cement content [kg/m ³]
D_{50}	median diameter. The portions of particles with diameters smaller and larger than this value are 50%. [μ m]
E	evaporation rate [kg/m ² /h]
N_{bubble}	number of air bubbles at the cross-section [-]
P_{bubble}	percentage of air bubbles at the cross-section [%]
$P_{bubble-all}$	percentage of air bubbles in the whole hardened sample [%]
$P_{difference}$	$(P_{fresh} - P_{bubble})$ value, the difference between P_{fresh} and P_{bubble} [%]
P_{fresh}	air content in fresh concrete [%]
R^2	correlation value of the fitting curve
S	spread-flow value of the concrete after mixing [cm]

T	the temperature in fresh UHPC mixture [$^{\circ}\text{C}$]
V_{bulk}	bulk volume occupied by the particles [m^3]
V_{solid}	total solid volume of the mixture [m^3]
Admixture/CEM ratio	admixture/cement mass ratios
AFA	antifoaming admixtures
Ag	aggregate
BA	basalt
BA/V(Ag) ratio	basalt/total aggregates volume ratio
BA _s	basalts
C&D W	construction and demolition waste
C ₃ A	tricalcium aluminate
CEM	Cement
CRC	Compact Reinforced Concrete
CVC	conventional vibrated concrete
CWA %	percentage of compensation water to water absorption of recycled aggregates
DC	delayed cast (95min after mixing)
ES	elephant skin
Foam/CEM ratio	BT3 Foam/cement mass ratio

GGBFS	ground granulated blast furnace slag
HPC	high-performance concrete
IC	immediately cast (2min after mixing)
MIP	mercury intrusion porosity
NA	nature aggregate
NAC	natural aggregate concrete
NAs	nature aggregates
NSC	normal strength concrete
PCE	comb copolymer polycarboxylate
PCEs	polycarboxylate superplasticizers
PEG	polyethylene glycol
PEO	polyethylene oxide
Perfin/CEM ratio	Sika Perfin/cement mass ratio
QP	quartz powder
QP/C ratio	quartz powder/cement mass ratio
QS	quartz sand
RAC	recycled aggregate concrete
RCA	recycled concrete aggregate
RCAs	recycled concrete aggregates
Re %	replacement ratio of recycled aggregates

RH	relative humidity
RHA	rice husk ash
RPC	Reactive Powder Concrete
SCC	self-compacting concrete
Si	silica fume
Si/C ratio	silica fume/cement mass ratio
SP	Superplasticizer
SP/C ratio	superplasticizer/cement mass ratio
SP/B ratio	superplasticizer/(cement+silica fume) mass ratio
StF	micro steel fibre
SUHPC	sprayed ultra-high performance concrete
UHPC	Ultra-high performance concrete
UHPFRC	Ultra-High-Performance-Fibre-Reinforced-Concrete
W/C ratio	water-to-cement mass ratio
W/B ratio	water-to-binder mass ratio
WA	water
WRA	water-reducing admixture

1 Introduction

1.1 History of UHPC development and application

In recent decades, concrete technology has made considerable progress. Many researchers in this field have developed concrete with exceedingly high performances that can be used in practical engineering applications. Among them, UHPC can have a compressive strength in the range of 150-200MPa and good performances in all other aspects.

The technology of high-performance concrete can be traced back to 1966. Kurt Walz [1] found that using a special production method can make concrete reach a compressive strength of 140MPa. However, it was not applied and further promoted at that time because the production method was too complicated and there were many other required configuration conditions, which made it unsuitable for large-scale construction applications [2].

Until the 1980s, some researchers discovered that a kind of excellent reactive powder material (such as silica fume, etc.) could be used with a suitable amount of superplasticizer to enhance the strength of concrete [3]. From then, concretes with strength grades as high as C100/115 had gradually been popularized and applied in practice.

With the further development of the various components of the high-strength concrete, new breakthroughs occurred in concrete technology. Danish researcher Hans Hendrik Bache developed a material with a high fibre content in 1981, which was also reinforced with a large number of steel bars when applied [4]. The material was called CRC (Compact Reinforced Concrete) and is still frequently used in structural elements such as stairs and balconies in the present time.

In 1993, the French contractor Bouygues Company cooperated with the Lafarge Company to further improve the compatibility of reactive powder with other components in concrete and developed a new type of concrete by adding a certain amount of superplasticizer, which was called "Reactive Powder Concrete (RPC)" [5]. Since then, ultra-high-strength concrete with a compressive strength in the range of 150-200 MPa could be produced.

In 1994, the Bouygues Company applied this RPC to the cooling tower of Cattenom Power Station in France. The concrete was used instead of steel to prevent corrosion damage in the extremely harsh environment inside the cooling tower [6]. It should be noted that in this application, the high strength of the concrete was not very necessary, but the high durability and long service life played a key role so that it could be used for a long time without unnecessary maintenance or repair. This showed that the new concrete could not only achieve high strength but also access other excellent properties through development. Therefore, the RPC was also called UHPC [6].

Over the years, the potential of this new high-performance structural material has been further developed. In 1997, the world's first pedestrian bridge made of UHPC materials was built in Sherbrooke, Quebec, Canada (see **Error! Reference source not found.** [7]). The bridge adopted a steel pipe UHPC truss structure with a span of 60m. Both the web and bottom chords were made of UHPC, which greatly reduced the self-weight of the bridge [8, 9].

In the autumn of 2005, the first UHPC bridge in the United States, the Marshall Bridge in Iowa (see **Error! Reference source not found.** [10]), was completed. The bridge was a high-grade single span simply supported beam highway bridge. The beam was composed of non-prestressed steel bars, and the shear force was borne by the steel fibres in the beam, which greatly simplified the steel bar structure [10].

The Gärtnerplatz Bridge, built in 2007, was the first UHPC-applied structure in Germany, as shown in Figure 1.3 [11]. It had a span of 132 meters and its slender structure consisted of a 3D steel truss combined with longitudinal girders and bridge decks. The bridge deck was made of UHPC with a thickness of only 85mm. The bonding of the longitudinal girders to the bridge deck was finished with epoxy mortar without any other mechanical combination [12]. This project also confirmed that UHPC could be firmly combined with steel structures without using complex mechanical connections.

In 2010, the expansion of Haneda Airport Runway D utilized the largest single project application of UHPC in the world to date, as shown in Figure 1.4 [13]. Approximately 7,000 UHPC slabs using special Ductal and Taiheiyo Cement from Lafarge provided an area of 200,000m², which could have an ultimate load-carrying capacity of 600KN/wheel. The UHPC slabs were ribbed, pre-tensioned with high-strength strands and had an effective depth of only 135mm. This project was an excellent example of how weight savings and durability made for an overall economical UHPC solution [14].

In the following twenty years, many UHPC structures have been built in Japan, the United States, South Korea, France, New Zealand and other countries [15]. The first design standard for UHPC was published in France in 2002 [16]. After more than ten years of research, the new design standard in France was completed in 2016 (NF-P-18-710 [17]). Besides, Japan's UHPC design guidelines were proposed in 2004 [18]. Switzerland's UHPC design standard was published in 2016 (SIA 2052 [19]). And the newest Austrian UHPC guideline was published in 2023 (ÖBV-Richtlinie "UHPC" [20]). Currently, the fib working group TG 8.6 is developing an international standard for UHPC [21].

On the other hand, due to the dense microstructure and high viscosity of UHPC, and the fact that UHPC can bond well with steel, steel fibres with high tensile strength are used to strengthen the concrete to achieve high ductile behaviour. For this Ultra-High-Performance-Fibre-Reinforced-Concrete (UHPFRC), the tensile strength can exceed 15MPa, and the flexible tensile strength can be as high as 50MPa [22]. Thus, this type of concrete can accommodate both tensile and compressive stress distributions, and with new appropriate design methods, the material costs can be saved regardless of whether or not conventional steel reinforcement is used.

In Austria, the arch road bridge WILD in Carinthia was assembled by the UHPFRC precast elements and completed in August 2010 (see Figure 1.5 [23]). Due to the high stiffness of the arch structure, a maximum utilization of the high compressive strength of UHPFRC was achieved. The main span of the two parallel arches was about 70 m. The wall thickness of the precast hollow box UHPFRC was only 60mm [24, 25]. This realized the application of the very slender (thickness less than 10cm) structures of UHPC.

The Mucem Museum, built in Marseille, France in 2013, used tree-like UHPC columns and delicate UHPC exterior walls (see Figure 1.6 [26]). Since UHPFRC had the advantages of the finesse and variety of geometrical shapes allowed by the absence of passive reinforcement, in this project, the UHPFRC was used for all peripheral support structures made of treelike-shaped columns, for the perforated panels of the south-east and the south-west facades and above the roof, for the peripheral gateway and its support structure [27].

In 2013, the roof of the Jean Bouin Stadium in Paris, France, was remodelled also with UHPFRC, allowing it to cover the entire stadium in a homogeneous manner while the roof rotated around the facade of the perimeter corridor (see Figure 1.7 [28]). The roof consisted of more than 3,000 different prefabricated UHPFRC triangles mounted on 78 metal beams, the largest of which cantilevers over 40m. The façade panels were open and the panels on the

roof were closed with glass granules to protect the audience from bad weather and sound disturbances. This unique technology was the subject of state-of-the-art engineering research at the time [29].

Although the current cost per cubic meter of UHPC is still four to five times that of conventional concrete when compared on a project-wide basis, UHPC solutions can be more economical and sustainable than conventional concrete when properly used. For example, the Japanese footbridge Sakata Mirai weighed only 20% of the traditional concrete bridge, as shown in Figure 1.8 [30]. According to the sponsors, the final cost of the project was 10% lower than comparable bridges in conventional concrete. Additionally, due to the ultra-high durability of UHPC, the cost of post-maintenance and risk assessment could also be greatly reduced.

In addition, future structural design will be largely based on whole-life design, where sustainability considerations play a greater role. For example, the Gärtnerplatz Bridge in Germany adopted the combination design of UHPC and steel structure and the UHPC integral bridge technology. When compared with traditional prestressed concrete bridges with the same span and bearing capacity in the whole life cycle, the CO₂ emission in the production and maintenance of the UHPC solution was only 40% [31]. Therefore, UHPC is not only with high performance and good durability but also conducive to the sustainable development of materials and the construction industry, which has a great development prospect.



Figure 1.1 Sherbrooke Bridge [7]



Figure 1.2 Mushill Bridge [10]



Figure 1.3 Gärtnerplatz Bridge [11]



Figure 1.4 Haneda Airport Runway D [13]



Figure 1.5 WILD Bridge in Austria [23]



Figure 1.6 Mucem Museum [26]



Figure 1.7 Jean Bouin Stadium [28]



Figure 1.8 Sakata Mirai Footbridge [30]

1.2 UHPC fresh and hardened properties

It is well known that the constituents of concrete are composed of cement, aggregate (sand and gravel), water and admixture. Thus, in order to achieve the high performance of UHPC, the basic rules for UHPC production have been applied to achieve the UHPC with a compressive strength in the region of 150-200 MPa, which are [2, 32]:

(1) The maximum particle size of UHPC should be smaller than that of conventional normal-strength concrete (NSC) since large particles can lead to stress concentration and hence strength reduction. The maximum particle size of UHPC is usually not more than 2 mm. However, up to now, coarse aggregate UHPC with a maximum aggregate size of 8 mm has also been developed, but with reduced strength compared to fine aggregate UHPC.

(2) The optimum packing density of particles in concrete is important. In order to reduce stresses on the contact surfaces between particles and to ensure that microcracks do not begin to form until a higher level of stress is reached, the microstructure needs to be very dense.

(3) The amount of cement used should be such that the water is fully bound. Then there will be extraordinarily little free water in the concrete thus achieving high strength.

(4) Fine steel fibres can be added to the concrete for the UHPFRC to guarantee ductile behaviour.

Accordingly, compared to NSC and high-performance concrete (HPC), UHPC uses exceptionally fine reactive powders and inert powders to fill the interspace, so that coarse and fine particles can be packed more densely. At the same time, UHPC also uses a large amount of cement and a high superplasticizer content to reduce the water content. The commonly used UHPC has a self-compacting capability. In addition, its internal microstructure is much denser than that of NSC, and the distribution of particles is relatively more homogeneous due to the high particle packing density, as shown in Figure 1.9 [33] (copyright permitted). Even for the UHPC mixtures containing coarse aggregates (2-8mm) in various applications, the difference in strength and deformation behaviour of the matrix and aggregate is much smaller than that of NSC or HPC [34].

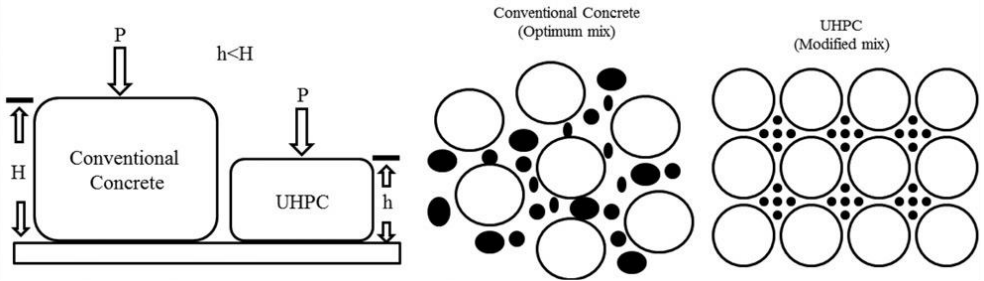


Figure 1.9 Difference of the packing skeleton between UHPC and conventional concrete [33]

In addition, the very dense microstructure and ultra-high strength of UHPC are mainly due to its extremely low water-to-binder ratio (W/B ratio, mass ratio of water/(cement + reactive powder)), which is only around 0.22-0.30. The matrix thus has very few capillary pores and is diffusion-resistant and impermeable to liquids and gases. Therefore, when UHPC is adopted as a material of civil engineering structure, it can show great resistance to the attack of chloride, alkali or de-icing salt without any additional protection [35]. And for the UHPFRC, the steel fibres within it hardly corrode. These are the reasons for the long durability and minimal maintenance requirements of this material.

However, these properties can also result in very high viscosity in the fresh state of UHPC. This is due to the enormous number of fine particles accumulating as well as the dense microstructure leading to increased inter-particle forces between the particles. They agglomerate to form larger “particles” and therefore can no longer act as optimum filler materials as intended [2]. The high viscosity in the fresh state of UHPC is very detrimental to the fresh properties of UHPC and can cause many workability problems.

At the same time, there is extraordinarily little free water in UHPC. Whilst the fine particles in UHPC require more water for wetting, and the dense microstructure requires water for lubrication to ensure adequate flowability, with the use of a superplasticizer, the free water in the concrete can be significantly reduced. This is mainly because the addition of comb-shaped superplasticizers to cement suspension improves cement particle dispersing as also paste flowability significantly due to a strong increase of electrostatic and steric repulsive force, in which the steric hindrance effect dominates the dispersion behaviour of superplasticizers [36].

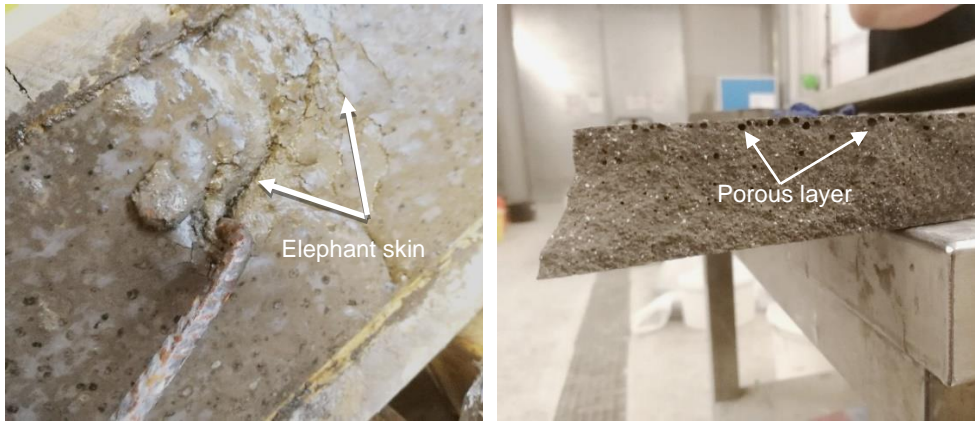
Thus, to date, there is still a contradiction between the high workability and high performances of UHPC. In order to ensure the strength and durability of UHPC, many workability issues still need to be resolved.

1.3 Problem statement and motivation

UHPC is superior to NSC and HPC in many aspects of performance, and UHPFRC can also replace the use of ordinary steel reinforcing bars to a certain extent. However, up to now, the applications of UHPC in the world are still very limited, especially for large-scale applications. Except for the immaturity of relevant industry norms, one of the most important reasons is that there are still some workability issues impeding UHPC's applications.

For example, the very high powder content and very low water content result in a very dense microstructure with very little free water, which triggers incomplete hydration of the powder as well as very sticky properties of UHPC in its fresh state [37, 38]. One big workability issue that affects UHPC surface properties is the so-called “elephant skin” [39, 40], as shown in Figure 1.10, which is a viscoplastic layer on the surface of fresh UHPC, forming in a period from only 30 seconds up to several minutes after casting. This layer prevents air bubbles in the concrete mixture from overflowing to the surface. As a result, the air bubbles accumulate below the “elephant skin” layer, forming a porous layer after the hardening of UHPC.

The formation of the “elephant skin” on the UHPC surface as well as the porous layer below it can induce several consequences: Firstly, it has a negative influence on the surface quality and aesthetics of UHPC. This is especially important for architectural precast concrete elements [41]; secondly, it can reduce the resistance of the concrete to some environmental actions, such as abrasion [42, 43]; thirdly, the presence of the “elephant skin” makes the surface of UHPC prone to crack after finishing, which negatively affects the mechanical and durability performance of UHPC elements and structures[44-46]; lastly, in the case of multi-layer UHPC elements, the presence of the “elephant skin” and the porous layer can cause an insufficient interconnection between adjacent layers, making the joint zone very sensitive to tensile and shears stress [47-50]. Therefore, this is a severe problem not only for the finish ability of concrete surfaces in cast-in-situ concrete projects but also for multi-layer concrete bonding in precast concrete projects.



(a) Appearance of the “elephant skin”

(b) Porous layer below the “elephant skin”

Figure 1.10 An “elephant skin” forming shortly after the casting of UHPC

Besides, the introduction of a large amount of air during concrete mixing and casting can form many big air bubbles in fresh concrete. For NSC, most of the air bubbles rise and escape after casting. But for UHPC, due to its high viscosity and dense microstructure, the discharging (de-airing) processes of air bubbles both during and after mixing are inefficient [51]. For some kinds of non-self-compacting UHPC, vibrating may help to eliminate parts of air bubbles [52, 53]. Nevertheless, a large amount of air bubbles would still remain in the concrete. Moreover, for self-compacting UHPC, vibrating may hardly have an effect on removing the air bubbles.

Thus, there are many big air pores in the hardened UHPC structure, as shown in Figure 1.11. Due to its extremely high performance and durability, UHPC can be applied to structures with very small dimensions (as low as 3cm). Considering that the big air pores may have a diameter of up to 5mm, this will negatively affect the mechanical performance and durability of the UHPC structure, which is another important problem for practical applications [54].

It should be noted that these air pores are not caused by the porosity in the concrete. According to Fehling E and Schmidt M et al. [2], in concrete there are several different types of pores. The smallest pores are the gel pores and capillary pores, as shown in Figure 1.12. The gel pores are the micropores with characteristic dimensions of 0.5-10nm, which are filled by the physically absorbed water during the hydration of the cement and may not influence the strength of concrete adversely. The capillary pores are the mesopores with average diameters ranging from 5 to 1000 nm, which are the voids between particles that have not been filled by the hydration products and will be reduced with the progress of hydration [55,

56]. The capillary porosity of concrete directly affects the hardening performance and is closely related to the particle packing density. In addition, there may also be small pores inside the aggregate, which depends on the quality of the aggregates. For example, recycled concrete aggregate (RCA) has more pores inside because it is wrapped in mortar [57].

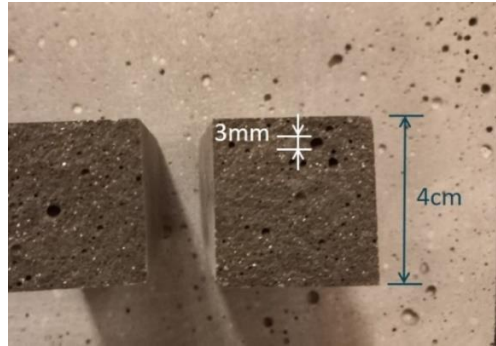


Figure 1.11 Air pores remain in the hardened concrete structure

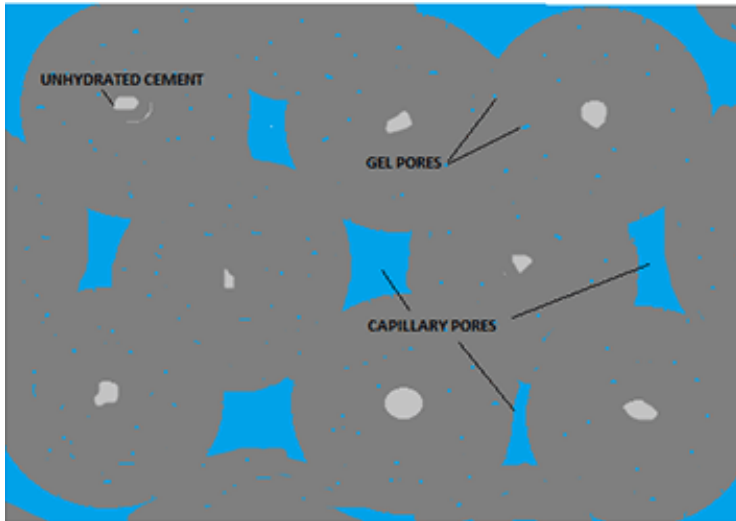


Figure 1.12 Schematic diagram of gel pores and capillary pores

For UHPC, due to the low W/B ratio, high particle packing density and very dense microstructure, the gel and capillary porosity are very small, resulting in ultra-high compressive strength [58]. And the natural aggregate used for UHPC is normally fine quartz sand or basalt, which also has very low porosity. Therefore, except for the pores left by insufficient vibration of conventional vibrating concrete (CVC), which are relatively rare in

self-compacting concrete (SCC), the big air pores in Figure 1.11 would be an important workability issue that influences directly the hardened properties.

Therefore, it is necessary to investigate these workability issues through a combination of theoretical analysis and experimental research. Additionally, in order to verify the influencing factors, the formation mechanisms of the “elephant skin” and the formation and de-airing mechanisms of air bubbles in UHPC, RCA as another kind of aggregate with special properties and a high water demand would be investigated to replace natural aggregate (NA) in UHPC at the end of this research. According to the existing results [59, 60], the NSC containing RCAs, also known as recycled aggregate concrete (RAC), shows different fresh properties and hydration reactions from the natural aggregate concrete (NAC) due to the high water absorption of the RCAs. Thus, it is also of great significance to study the workability of UHPC containing RCAs. At the same time, if the hardened properties of concrete can be maintained at an elevated level in the future through higher-quality and higher-performance RCAs, this new material is also beneficial to the economic and sustainable development in the field of civil engineering.

1.4 Research objective and content

The objective of this PhD research is to perform a thorough investigation of some important workability issues of UHPC, to achieve large-scale application of this superior material in both the precast and cast-in-situ concrete project. From the perspective of optimizing the production processes and mix proportions of UHPC, this research focuses on two main problems: the “elephant skin” and the air pores in the concrete. Several comparative experiments and theoretical analyses are conducted to investigate the influencing factors in various aspects, thereby the mechanisms are discussed, some solutions are suggested and the corresponding UHPC materials with suitable properties for various applications are developed.

The organization of this dissertation is as follows:

In Chapter 2, the material and composition of UHPC are introduced. The basics for the selections of each raw material in this research are explained. The influences of the contents of each raw material in the mix design on some properties of UHPC are investigated to determine the ranges of contents of these raw materials in order to satisfy the performances

of UHPC. The results in this chapter can provide great research foundations for the following research about workability issues.

Chapter 3 focuses on the problem of the “elephant skin”. An extensive laboratory study is first conducted on the formation and disadvantage of the “elephant skin”. Varied factors that affect the formation of the “elephant skin” on the concrete surface are investigated. Then, based on the test observations, the microscopic formation mechanisms of the “elephant skin” on the UHPC surface are discussed. Finally, some possible solutions are proposed to decrease the negative effect of the “elephant skin” on the surface performance of UHPC.

Chapter 4 systematically analyses the influences of various factors on the formation and de-airing mechanisms of the air bubbles, and considers the methods of improving the materials and mix proportions of the concrete to enhance the de-airing processes both during and after mixing. Based on the results of this research, the most suitable methods can be adopted for different practical engineering application requirements, which achieve the best efficiency.

In Chapter 5, to further verify the influencing factors on the workability issues, the formation mechanisms of the “elephant skin”, and the formation and de-airing mechanisms of air bubbles in UHPC, the research on using RCAs to replace the coarse aggregates in UHPC is conducted. Based on the investigations of the workability of normal RAC, the fresh and hardened properties of UHPC containing different replacement ratios of RCAs and different compensation water amounts are studied. Based on the special characteristics of RCA compared to NA (high water absorption, low density, etc.), the results of the “elephant skin” and de-airing behaviours in the concrete show consistency with the proposed mechanisms. At the same time, this study can also confirm the feasibility of using RCAs in UHPC for the sustainable developments.

Conclusions and prospects are drawn in Chapter 6.

2 Materials and composition of UHPC

The materials and mix designs used in this research are based on the research on the developing and optimisation of UHPC mix proportions by K. H. Hoang [32]. Further optimisation analyses for workability issues are presented in the respective sections.

2.1 Materials

As introduced in the first chapter, the UHPC's raw materials can usually be categorized as follows: cement, reactive admixture, inert admixture, water, superplasticizer, and aggregate. Steel fibre is also involved in the UHPFRC.

2.1.1 Cement

The commonly used cement (CEM) for UHPC is CEM I low-alkali Portland cement of strength classes 42.5 and 52.5 according to specification DIN EN 196 [61]. Additionally, cements with high sulphate resistance and low heat of hydration are the preferred choices, which have also high strength potential [2]. Since the fine-grained UHPC mixtures generally have high cement contents ($700\text{-}850\text{kg/m}^3$) and limited water demands, there is almost no alkali-silicon reaction expansion occurring [62]. It should be noted that the water demands of UHPC mixtures with different properties still need to be considered when selecting cement because they directly determine the flowability of UHPC and affect the amounts of superplasticizer.

In this research, in order to explore the influence of cement type on workability issues, two different types of Portland cement are used, which are produced in Austria according to EN 197-1 [63]. Table 2.1 shows the basic properties of these cements [32]. The CEM I 52.5 N (CEM A) from Lafarge Company combines the excellent chemical resistances of C_3A -free cement (for good workability of concrete) with the good hardening behaviour of Portland cement. Its applications range from the manufactures of prefabricated parts or pipes to tunnel inner shells, high-performance concretes, etc. The CEM I 42.5 R (CEM B) from W&P

company is a C_3A -free cement with relatively good workability due to favourable water requirements. It also has good early strength and post-hardening behaviour, increased resistance to sulphate attack, etc.

2.1.2 Mineral admixture

Mineral admixtures (or additives) with particle sizes less than 125 microns are used in UHPC to improve the performance of concrete in both fresh and hardened states. Mineral admixtures are usually classified into reactive and inert admixtures [64, 65].

Reactive admixture, such as natural pozzolan, silica fume, fly ash, ground blast furnace slag, etc., is crucial to improving the performance of UHPC. When fine cement particles fill the voids between larger particles, the reactive admixture, owing to its finer particle size, can result in a particle mixture of the concrete with better particle packing. From a physical point of view, as the fineness of the reactive admixture increases, the filling effect is also better. In addition, for the accumulation of fine particles under wet conditions, the particle properties (wettability, adhesion, particle shape, etc.) and the properties of the liquid have also a great influence on the packing of fine particles [32].

Papadakis [66-68] proposed a theoretical approach to estimate the maximum amount of some kinds of reactive admixtures capable of reacting with all the lime produced during the hydration of high water/cement ratio cement. He found that the maximum contents of silica fume, low calcium fly ash and high calcium fly ash were 18.3%, 24% and 50%, respectively. The addition of silica fume or fly ash above these optimum values would only act as a filler and have a negative effect on the workability of concrete. Even though these were only the results within the scope of his study and these contents were also related to the type of cement, the type of superplasticiser and the superplasticiser content, these results could provide great reference significance for the mix design of UHPC in this research. Moreover, the additional reactive admixtures that only acted as fillers could also be replaced by other more inert admixtures to reduce material cost and maintain workability.

Unlike reactive admixture, the inert admixture is primarily used for filling and can partially replace the reactive admixture as described above. They allow the "grain gaps" between the particles to be bridged. Usually, various fine quartz powders are used as inert admixtures to achieve an optimal grading of particle combinations, but they should be subjected to highly selective fractionation. For example, in some German Research Program [69] the quartz powders ground to a fineness from 12000 cm^2/g to 3600 cm^2/g (slightly coarser than the

cement) were used and proven to have a good effect. Quartz powder not only has high particle strength but also is easy to obtain various well-defined particles with different fineness.

In addition, limestone powder can also be used as an inert admixture, but its strength is lower than that of quartz powder. UHPC with limestone powder is usually more viscous and thicker, which is not good for workability. Due to this reason, limestone powder is only used in some specific applications.

K. H. Hoang [32] measured the packing densities of several types of silica fume, fly ash, ground granulated blast furnace slag, quartz powder and limestone powder using the superplasticizer-water solution demand test, which was to determine the mixing energy to measure the water demand so as to achieve the highest packing density of the powder and to assess the compatibility of the powder and the superplasticiser. The results showed that the use of very small amounts of silica fume (10-20% of the cement mass) ensured a high compressive strength compared to other reactive admixtures. Although the SP-water solution demand for silica fume was relatively higher, the combination of silica fume and quartz powder for mineral admixtures gave the best fresh and hardened properties of UHPC and lower cost in terms of overall efficiency.

Table 2.1 Physical-mechanical properties and chemical components of the cement and mineral admixture

Name	CEM A	CEM B	Si	QP
Type	CEM I 52.5 N	CEM I 42.5 R	RW-Füller Q1	Dorsilit® 16900
C₃A (wt.%)	<2.5	<2.5	-	-
D₅₀ (μm)	7.70	10.00	0.342	13.13
Dry density (g/cm³)	3.17	3.08	2.20	2.63
28d Compressive Strength (MPa)	61	57	-	-
SiO₂ (wt.%)	20.25	20.60	97.0	98.8
CaO (wt.%)	66.07	60.48	0.25	0.02
Al₂O₃ (wt.%)	2.76	4.5	0.15	0.69
Fe₂O₃ (wt.%)	4.91	5.65	0.03	0.02
Na₂O (wt.%)	0.21	0.21	0.05	0.01
K₂O (wt.%)	0.49	0.69	0.45	0.06
Na₂O equivalent (wt.%)	0.53	0.66	-	-
SO₃ (wt.%)	2.61	2.75	-	-
MgO (wt.%)	-	-	0.20	0.01
Grinding fineness (Blaine) (cm²/g)	4500	4300	-	-
Specific surface (BET) (m²/g)	-	-	16-20	1.2

Therefore, the reactive admixture used in this research is the silica fume RW Füller Q1 (Si) supplied by RW silicium GmbH – Germany, and the used inert powder is the quartz powder Dorsilit® 16900 (0.45-87.5 μ m) (QP) produced by Gebrüder Dorfner GmbH – Germany, which are also the products recommended by K. H. Hoang [32]. RW-Füller Q1 is a smooth, pozzolanic additive for producing dense and impermeable concrete mixtures according to EN 13263 [70]. When RW-Füller Q1 is used in mortars and concrete, the high stability and durability as well as high water and chemical impermeability can be guaranteed. The Dorsilit® crystal quartz powder is produced by iron-free, dry grinding of prepared quartz sand and subsequent air classification, which is characterized by a high SiO₂ content and contains only small amounts of secondary components. It has obvious beneficial effects on the workability and strength of concrete. The basic properties of these materials are also shown in Table 2.1.

2.1.3 Superplasticizer

Superplasticizer, also called “high-range water-reducing admixture”, is mainly used to ensure the flowability of concrete and reduce water demand. At present, comb copolymer polycarboxylate (PCE) superplasticizers are the most effective superplasticizers for the productions of self-compacting concrete and high-strength concrete [71, 72]. Through the functions of dispersion, lubrication (Adsorption), steric hindrance, the slow-release effect of grafted copolymerized branched chains, etc. of the PCE superplasticizer [73-76], the water demand of UHPC can be largely decreased, and the flowability can also be kept in a high level.

There are many different PCE superplasticizers, but most must be optimized for interaction with different types of cement. Some superplasticizer types also consist of two kinds of different polymer components. Experiences have shown that for UHPC containing large amounts of silica fume, the selected superplasticizer should be able to properly deagglomerate cement and other fine particles [77]. Increased silica fume content may reduce flowability and require more superplasticizers to achieve saturation. However, due to the very high surface area of silica fume, its effective dispersing ability is also necessary to obtain highly flowability UHPC.

Flatt and Houst [78] described the interaction and behaviour of three types of superplasticizer with cement suspensions. They reported that stepwise or delayed addition of the superplasticizer would result in better concrete fresh properties compared to direct addition.

In addition, the gradual addition of the superplasticizer was also crucial to improve the flowability of UHPC [79].

This research adopts the superplasticizer (SP) “Premment H500” from the company “BT3 Betontechnik”, which is an aqueous solution of superplasticiser with a solid content of about 30%. This superplasticizer is based on modified polycarboxylate ethers (a kind of PCEs) with a strong liquefying and homogenizing effect. It corresponds to EN 934-1 and EN 934-2 Tab. 3.1 and Tab. 3.2 [80, 81] and is suitable for concrete according to ÖNORM B 4710, DIN 1045-2 and EN 206 [82-84]. The technical specifications are seen in Table 2.2.

Table 2.2 Technical specifications of SP “Premment H500”

Form	Solid content	Density (kg/l)	PH value
liquid	30 wt.%	1.07 +/- 0.02	4.0 +/- 2.0

2.1.4 Aggregates

Except for the paste material composed of powder and liquid, the coarse particles in UHPC are mainly aggregates. As the main material contributing to volume stability, aggregate (Ag) plays the role of the rigid skeleton in concrete, which is mostly quartz sand. In order to let the concrete achieve higher strength and enhanced durability, the dense microstructure requires aggregates with finer particle size, but coarser than the particle size of the powder, usually between 0.1 and 1mm. However, UHPC mixtures containing coarse aggregates (2-8mm) have also been developed. The coarse aggregate is mostly basalt, and meanwhile, finer quartz sand must also be added to maintain a high particle packing density to achieve ultra-high performance.

In this research, three different types of crushed quartz sand QS1 (100-200 μ m), QS2 (300-800 μ m) and QS3 (100-500 μ m) produced by Gebrüder Dorfner GmbH – Germany were used as fine aggregates. QS1 (Geba® weiß) is a fine crystal quartz sand that is specially prepared for use in construction chemical products. QS2 (300-800 μ m) is a natural and light washed crystal quartz sand without humic substances, which can help to achieve super high strength of UHPC. QS3 (100-500 μ m) is a chemically inert, high melting point, high purity, hard type of quartz sand with a size range suitable for use in high fibre content UHPC. The basic properties of these three sands are shown in Table 2.3. The coarse aggregates included two crushed basalt rocks BA1 (2000-4000 μ m) and BA2 (4000-8000 μ m) from ALAS Klösch GmbH – Austria. The basic properties of these two coarse aggregates are shown in Table 2.4.

Table 2.3 Physical-mechanical properties and chemical components of the used fine aggregates (<0.8mm)

	QS1	QS2	QS3
D₅₀(μm)	103	510	330
Dry density (g/cm³)	2.65	2.65	2.65
Bulk density (g/cm³)	1.5	1.6	1.6
SiO₂ (wt.%)	99.0	98	97
Al₂O₃ (wt.%)	0.29	0.8	1.5
Fe₂O₃ (wt.%)	0.08	0.01	0.02
Ti₂O (wt.%)	0.16	0.04	0.09
K₂O (wt.%)	0.03	0.3	0.7
Na₂O (wt.%)	0.01	0.03	0.05
CaO (wt.%)	0.02	0.02	0.02
MgO (wt.%)	0.01	0.1	0.01
BaO (wt.%)	0.02	0	0

Table 2.4 Physical-mechanical properties of the used coarse aggregates (<8mm)

	BA1	BA2
Apparent density (g/cm³)	2.978	2.978
Dry density (g/cm³)	2.893	2.899
Saturated and surface-dried density (g/cm³)	2.921	2.926
Water absorption (%)	0.82	0.80
LA coefficient (EN 1097-2 [85])	10.8	10.8

2.1.5 Steel fibre

It is well known that for NSC, due to the high capillary porosity, the internal microstructure will change with the increase of compressive stress, allowing the plain concrete after the peak to still have certain ductility [86]. However, for UHPC without steel fibres, the dense microstructure will suddenly be brittle after the peak compressive stress, causing the complete failure of the structure [87]. Therefore, the use of sufficient high-strength micro steel fibre (StF) is crucial to the post-peak ductility of UHPC, which can also significantly improve the tensile strength. Compared with conventional steel reinforcement, the use of steel fibres can also provide possible strain hardening due to the multiple cracking, decrease the crack width, and provide improved resistance to carbonation and freeze-thaw cycles of UHPC.

Elongated fibres with a maximum diameter of 0.20 mm and a length of 9-17 mm made of high-strength steel with a tensile strength ≥ 2000 MPa according to DIN EN 14889-1 [88] can provide good flexural strength and ductile behaviour for UHPC [32, 89]. This size range is also good for the workability of the concrete, especially steel fibres with a length/diameter ratio of at least 65.

In this research, the micro steel fibres WIRE FIBRE from the company KrampeHarex GmbH – Germany are used to investigate their influence. Due to the grid effect, the addition of steel fibres has a great influence on the flowability of the concrete. This research considers two types of steel fibres with different dimensions, which are DM 12.5/0.175 (StF1) with a length of 12.5mm and a diameter of 0.175mm and DG 20/0.3 (StF2) with a length of 20mm and a diameter of 0.3mm. Both steel fibres are straight steel fibres with round cross-sections and tensile strengths of more than 2100MPa.

In order to determine the particle size distribution of the materials, the laser diffraction technique with HELOS-RODOS instrument, Sympatec GmbH was used for the cement, silica fume and quartz powder, while the image analysis technique with QICPIC-RODOS instrument, Sympatec GmbH was applied for the quartz sands. Other tests for material characterization were carried out partly in the own lab, while in some cases the data was available from materials suppliers. The particle size distributions of the powders and sands are displayed in Figure 2.1 [32].

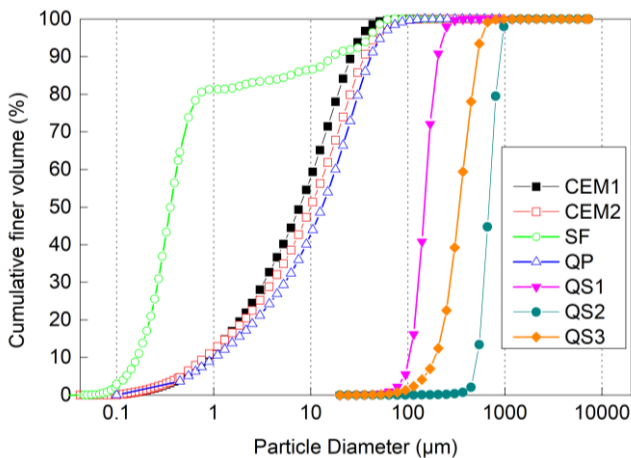


Figure 2.1 Particle size distribution (PSD) curves of the used powders and sands [32]

2.2 Manufacture of UHPC mixtures and specimen preparation

The UHPC mixtures in this research are produced with an Eirich mixer, an ELBA mixer or a small Hobart mixer. The Eirich RV01 mixer is a powerful intensive mixer with a driven, rotating mixing pan and a mixing tool which rotates eccentrically, as shown in Figure 2.2. The mixer power can reach 4.0kW. It is especially suitable for mixing high-viscosity UHPC with a capacity of 8~10L. It can also record the speed, current, power and other information in real-time and export it to Excel for later data analysis. The ELBA EMS 60C mixer is a single-shaft high-capacity laboratory compulsory mixer with a capacity of 60~75L. It has a two-zone counter-flow mixing system with the mixer lining and the mixer spirals of highly wear-resistant steel cast as shown in Figure 2.3. The mixer power can reach 3.0kW, which can complete the mixing of UHPC. The small Hobart N50 mixer with a capacity of 5L can mix hydraulic cement pastes and mortar of plastic consistency, as shown in Figure 2.4. The planetary action of the beater assures thorough blending and mixing to create predictable finished batches. Its selective agitator transmission has 3-speed settings: 139, 285, and 591rpm. Due to its small capacity, the Hobart mixer is only used to initially optimize the UHPC mix proportion.

The mixing procedure is shown in Figure 2.5. At first, the CEM, Si and QP are mixed in the mixer with a low mixing speed of 100rpm until a homogenous mixture; then the WA and SP are added in sequence, and the mixing speed is increased to 400rpm to promote the reaction of CEM, WA and SP; after the generation of the paste, the mixing speed is decelerated back to 250rpm and both kinds of QS are mixed to engender the concrete; after that, the machine is stopped for 2min to reduce the temperature in the concrete; finally, for the fibre reinforced UHPC, the StF is manually added into the concrete mixtures gradually to avoid fibre balls or clumps. The mixing time is the period from the time when water and superplasticizer are added to the end of mixing.



Figure 2.2 Eirich R01 mixer (10L)



Figure 2.3 ELBA EMS 60C mixer (75L)



Figure 2.4 Small Hobart mixer (5L)

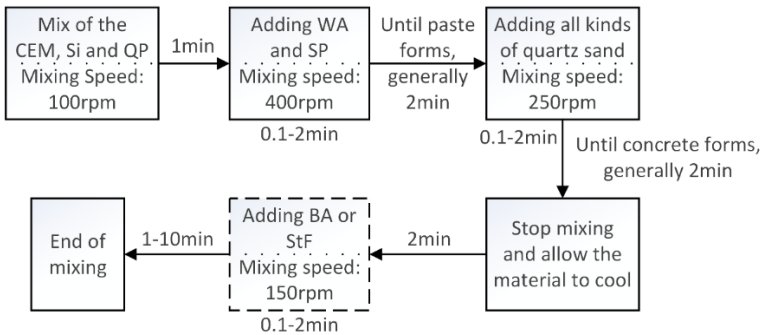


Figure 2.5 Mixing procedure for UHPC

The temperature and humidity of the environment during the concrete manufacture are monitored by a hygrothermograph. The normal temperature and humidity of the laboratory are around 20°C and 60%, controlled by the air conditioner and humidifier.

Regarding the fresh properties of the manufactured UHPC mixtures, the flowability and viscosity are measured by the use of the Haegermann cone, as shown in Figure 2.6 [90, 91] (copyright permitted), which is rapid and convenient. The flowability is represented by the spread-flow value. The viscosities can be evaluated by the flowing time to 20cm when the concrete mixtures have the same flowability due to the limitations of this device, marked as “ T_{200} ”. The shorter the flow time, the lower the viscosity. The temperature in fresh concrete is tested shortly after mixing with a thermometer according to ASTM C1064 [92], which is used to calculate the evaporation rate for analysing its influence on the “elephant skin” in Chapter 3. The changing of consistency over time is considered by measuring the changing of the flowability and viscosity over time, which is obtained by measuring the flowability and viscosity every half hour, so as to examine the effect of retarding on the workability issues.

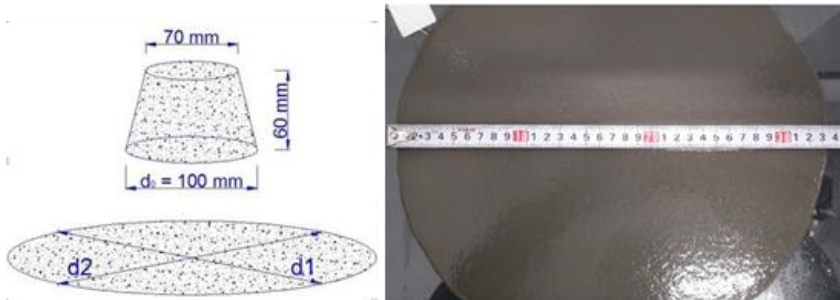


Figure 2.6 Spread-flow test to evaluate the flowability and viscosity of UHPC mixtures using the Haegermann cone [90]

Regarding the hardened properties, due to the relatively small scattering in the compressive strength results of the UHPC specimens after grinding the pressure surfaces with a grinding machine every time [93], each mixed concrete mixture is cast into 2~4 100×100×100mm³ cubes and tested the 28-day compressive strength according to EN 12390-3 [94]. Some are stored for 28 days in room temperature water, while the others are cured in 80°C hot water for 48h to quickly reach the 28d compressive strength under standard curing conditions. In addition, several 3-point bending tests, 4-point bending tests and elastic modulus tests are also carried out in order to investigate the effect of workability issues on the bending performance and modulus of elasticity of UHPC, which will be described in the following sections.

2.3 Mix design

For the determination of the dosage ranges of the components and the mix proportions of UHPC, in order to achieve ultra-high performances, high particle packing density is the key requirement, which is defined by Eq (1.1) [32, 90].

$$\beta_{mix-actual} = \frac{V_{solid}}{V_{bulk}} = 1 - \phi \quad (2.1)$$

where: $\beta_{mix-actual}$ is the particle packing density; V_{bulk} is the bulk volume occupied by the particles; V_{solid} is the total solid volume of the mixture; Φ is the porosity, which is the void content within the granular structure (pores between particles).

The particle packing density directly affects the performance of concrete, because when the porosity between particles is higher, the strength and durability of concrete are generally lower. Thus, the used raw materials and mix design in UHPC need to be considered based on high particle packing density for superior performances.

K. H. Hoang et al. [32, 90] used the modified superplasticizer-water solution demand test and the stepwise optimization method of particle packing density to develop several mix proportions of UHPC with different maximum grain sizes. Many of them have already been applied to industrial projects, such as the UHPFRC hollow box girder [32], the UHPFRC composite column [95], the prefabricated UHPC girders for viaducts “Quickway System” [96], integral bridge Fehring and integral bridge in Trautenfels [97], Karl-Heine-Bogen foot and cycle path bridge in Leipzig [98], etc.

Thus, the mix design in this study is based on the research on the development of UHPC mix proportions with high particle packing density and good performances by K. H. Hoang et al. [32, 90]. As shown in Table 2.5, the mix proportion of fine aggregate UHPC is considered as the starting and reference recipe for the investigation of the workability issues. The mix design of coarse aggregate UHPC needs to be analysed after the incorporation of BA1 or BA2. QS3 is used only in some specific applications with a high content of StFs [32].

In order to minimize the adverse effects of workability issues and explore the mechanisms, it is necessary to adjust the contents of some components of UHPC in order to explore their

influences. However, to ensure the hardening performances of the UHPC, certain limitations must exist in the tuning of these parameters. To this end, the following mix design parameters are investigated in this study:

- Silica fume content
- Quartz powder content
- Water-to-binder ratio
- Superplasticizer dosage
- Paste volume (including cement, mineral admixture, superplasticizer and water)
- Coarse aggregate
- Steel fibre

Table 2.5 Starting and reference mix proportion developed by K. H. Hoang [32]

	Reference recipe
CEM (kg/m³)	720
Si (kg/m³)	86.4
QP (kg/m³)	216
WA (kg/m³)	164.9
SP (kg/m³)	21.6
QS1 (kg/m³)	236.6
QS2 (kg/m³)	946.4
BA (kg/m³)	-
StF (kg/m³)	-
Water-to-cement (W/C) ratio	0.25
Water-to-binder (W/B) ratio	0.223
Si/C ratio	12%
QP/C ratio	30%
SP/C ratio	3%
QS1/(QS+BA)	20V%
QS2/(QS+BA)	80V%
BA/(QS+BA)	-
StF volume content	-

Considering the fact that the properties of raw materials may vary slightly depending on the batches, storage times, and storage conditions, they can also have an effect on the fresh and hardened properties of UHPC. Therefore, each group of UHPC mixtures should be mixed and tested on the same day, and only one parameter can be changed while the other parameters are kept constant. When combining the results of different groups of UHPC mixtures, the results need to be percentage normalized from the reference recipe in Table 2.5, so that multiple groups of results can be statistically analysed to calculate the mean values and standard deviations, which are also percentage normalized from the mean values of

results of reference recipe in Table 2.5. Detailed mix recipes and properties of all UHPC mixtures in this section can be found in Table A.1 in the appendix.

2.3.1 Silica fume and quartz powder contents

For the mix design of UHPC, the silica fume and quartz powder contents are usually considered as a mass ratio to cement. According to the results of K. H. Hoang [32], the silica fume/cement mass ratio (Si/C ratio) can range from 10%~20%, the quartz powder/cement mass ratio (QP/C ratio) can range from 30%~40%, which would not have a big influence on the particle packing density as well as the compressive strength of concrete.

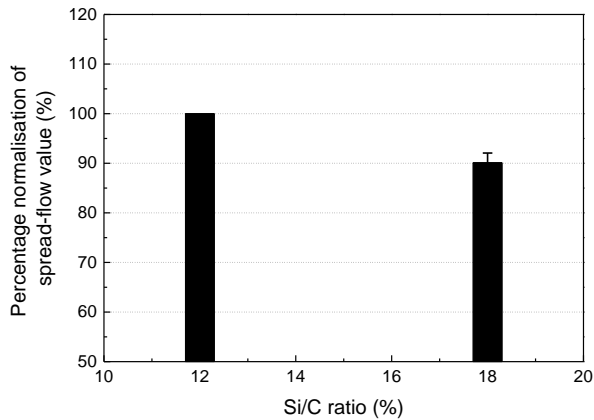
In this research, the Si/C ratio of 12% and 18%, and the QP/C ratio 30% and 40% are considered. In order to keep the volume of total concrete constant, when the Si/C ratio and QP/C ratio are increased, the total content of aggregates is slightly reduced accordingly. As shown in Table 2.6, 2 groups of 8 UHPC mixtures with 12% and 18% Si/C ratios and 30% and 40% QP/C ratios were tested. These 2 groups had different cement contents, which were represented as “720” and “860” in the names of UHPC mixtures. The investigation of cement content (paste volume) will be introduced in section 2.3.4. The results of temperature in fresh concrete show that both the Si/C ratio and the QP/C ratio may not have a big influence.

Table 2.6 UHPC mixtures with different Si/C and QP/C ratios

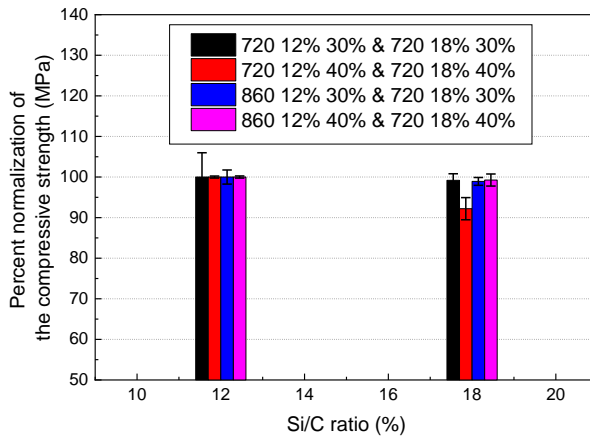
Group	UHPC mixture	Si/C ratio (%)	QP/C ratio (%)	Temperature in fresh concrete (°C)
2.3.1-1	720 12% 30%	12	30	28,6
	720 18% 30%	18	30	27,5
	720 12% 40%	12	40	29,9
	720 18% 40%	18	40	28,5
2.3.1-2	860 12% 30%	12	30	26,4
	860 18% 30%	18	30	26,3
	860 12% 40%	12	40	27,1
	860 18% 40%	18	40	26,7

When the other variables are kept constant and only the Si/C content is varied, these 8 UHPC mixtures can generate 4 sets of data. Due to the different specific values, after percentage normalization from the UHPC mixtures with 12% Si/C ratio and statistical analysis, the results of the influence of Si content on the flowability and compressive strength of UHPC can be shown in Figure 2.7.

It can be found that, when the value of the Si/C ratio is between 10% and 20%, the compressive strength of UHPC hardly changes, but the spread-flow value decreases by about 10%, which is consistent with the results of K. H. Hoang [32]. Therefore, a Si/C ratio of 12% is sufficient for UHPC without steel fibres. However, the Si/C ratio should not be more than 20% considering the workability and packing density of UHPC.



(a) Flowability



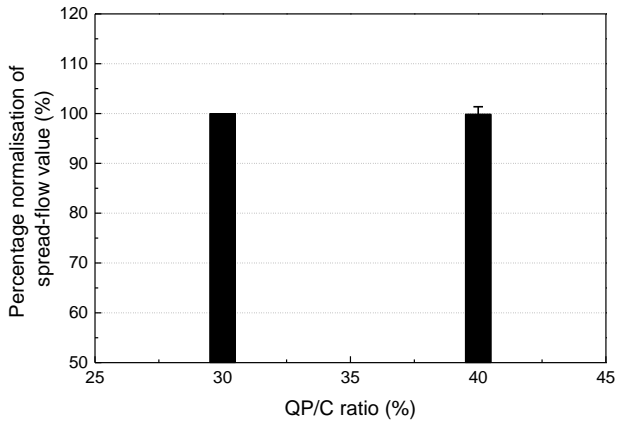
(b) Compressive strength

Figure 2.7 Influences of the content of Si on the properties of UHPC mixtures

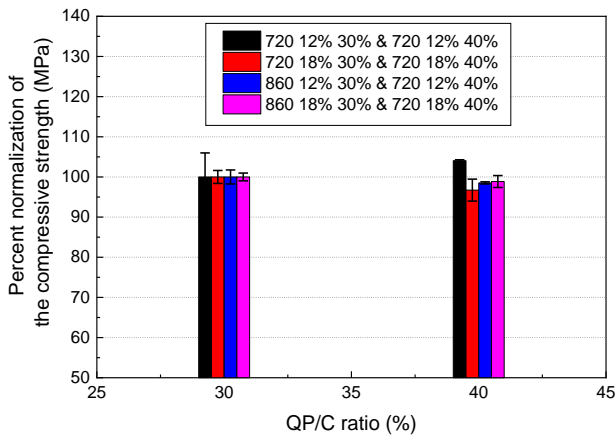
For the influence of quartz powder content, when the other variables are kept constant and only the QP/C content is varied, these 8 UHPC mixtures can also generate 4 sets of data. After percentage normalization from the UHPC mixtures with a 30% QP/C ratio and

statistical analysis, the results of the influence of QP content on the flowability and compressive strength of UHPC can be shown in Figure 2.8.

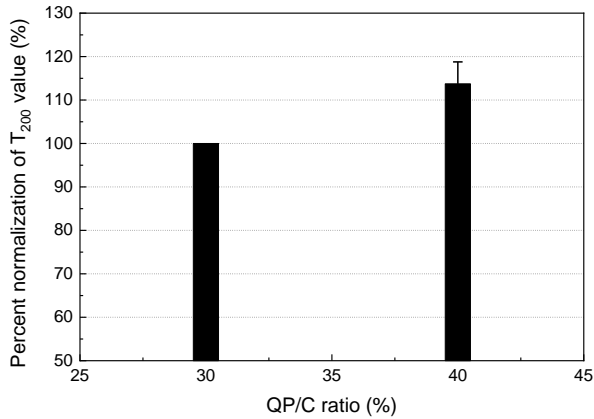
It can be found that, when the value of the QP/C ratio is between 30% and 40%, the flowability and compressive strength of UHPC hardly change significantly. Thus, the T_{200} values (flowing time to 20cm) of each group can also be compared to represent the viscosity, as shown in Figure 2.8(c). This time, a higher QP/C ratio causes the T_{200} value to increase by about 13%, indicating an increase in the viscosity of UHPC, which is consistent with the results of K. H. Hoang [32]. Therefore, a QP/C ratio of 30% is also better for UHPC without steel fibres. And the QP/C ratio should also better be no more than 40%.



(a) Flowability



(b) Compressive strength



(c) Viscosity

Figure 2.8 Influences of content of QP on the properties of UHPC mixtures

According to the ÖBV-Richtlinie “UHPC” [20], for different kinds of UHPC, the combined mass of reactive and inert admixtures should be between 40~58% of the cement mass. Therefore, this is also consistent with the results of the mix design analysis described above.

2.3.2 Water-to-binder ratio

For the performance of UHPC, water is a very important factor. Due to the hydration reaction, the water content in UHPC is normally considered as the water-to-binder ratio (W/B ratio), which directly affects the flowability, compressive strength, and other performances of UHPC.

According to the ÖBV-Richtlinie “UHPC” [20], for UHPC, the W/B ratio should not be higher than 0.25. K. H. Hoang [32] estimated the effect of the water-to-cement ratio (W/C ratio, mass ratio of water/cement) ranging from 0.22 to 0.28 on the compressive strength of hardened pastes. His results showed that the lower the W/C ratio, the higher the compressive strength. However, considering the workability of the concrete, he suggested a W/C ratio of 25%. Accordingly, when the Si/C ratio is around 12~18%, the corresponding W/B ratio is about 0.21-0.22.

For further investigation, this study examined 8 groups of UHPC mixtures with different W/B ratios. As shown in Figure 2.7, except for changing the water contents in the UHPC mixtures “720 12% 30%”, “720 18% 30%”, “720 12% 40%” and “720 18% 40%” in Table 2.6, the UHPC mixtures with different paste volumes, cement types and StF contents were also tested

to verify whether the effect of W/B ratio on concrete properties would be similar for the UHPC mixtures with different recipes. In the names of the groups, “720”, “620” and “860” represent the cement contents (kg/m^3), and “0%” and “2%” are the StF volume contents. The groups “CEM A 2%” and “CEM B 2%” were with 2 vol. % of StF1. Other groups were without StF. And except for the group “CEM B 2%”, other groups all used the CEM A.

Table 2.7 UHPC mixtures with different W/B ratios

Group	Name	Tested W/B ratio	Corresponding W/C ratio
2.3.2-1	720 12% 30%	0.223, 0.241	0.25, 0.27
2.3.2-2	720 18% 30%	0.212, 0.223	0.25, 0.264
2.3.2-3	720 12% 40%	0.223, 0.228	0.25, 0.255
2.3.2-4	720 18% 40%	0.212, 0.223	0.25, 0.264
2.3.2-5	620 CEM A 0%	0.223, 0.25	0.25, 0.285
2.3.2-6	860 CEM A 0%	0.205, 0.223	0.23, 0.25
2.3.2-7	720 CEM A 2%	0.223, 0.25	0.25, 0.285
2.3.2-8	720 CEM B 2%	0.223, 0.232	0.25, 0.26

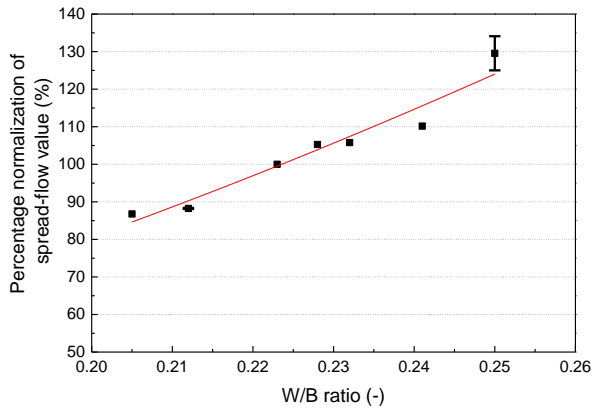
After percentage normalization from the UHPC mixtures with 0.223 W/B ratio and statistical analysis, the results of the influences of W/B ratio on the flowability, temperature and compressive strength of UHPC can be shown in Figure 2.9. It can be found that a higher W/B ratio can lead to a higher flowability and a lower temperature in fresh concrete. After the linear fitting, the relationship between the percentage change in spread-flow value and the W/B ratio (correlation value $R^2=0.922$), and the relationship between the percentage change in fresh concrete temperature and the W/B ratio ($R^2=0.811$) can be expressed as the following equations:

$$\frac{S_{W/B}}{S_{W/B=0.223}} = 8.9217 \times W / B - 0.9895 \quad (2.2)$$

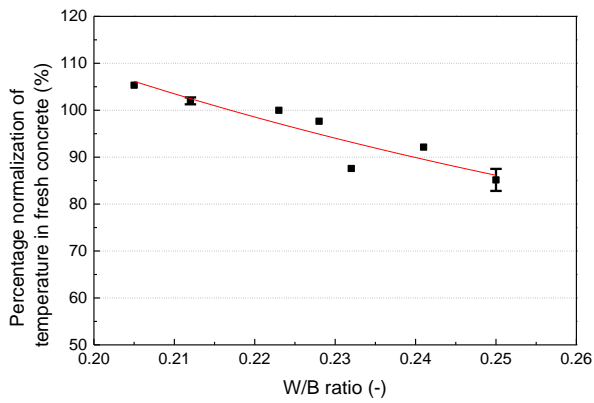
where: $S_{W/B}$ is the required spread-flow value of the UHPC (cm); $S_{W/B=0.223}$ is the spread-flow value of the UHPC when the W/B ratio is 0.223 and other factors remain unchanged (cm).

$$\frac{T_{W/B}}{T_{W/B=0.223}} = -4.4368 \times W / B + 1.9894 \quad (2.3)$$

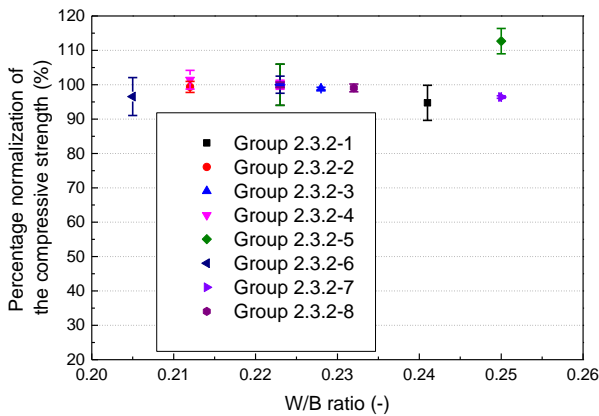
where: $T_{W/B}$ is the required temperature in fresh UHPC ($^{\circ}\text{C}$); $T_{W/B=0.223}$ is the temperature in fresh UHPC when the W/B ratio is 0.223 and other factors remain unchanged ($^{\circ}\text{C}$).



(a) Flowability



(b) Temperature in fresh UHPC mixture



(c) Compressive strength

Figure 2.9 Influences of W/B ratio on the properties of UHPC mixtures

However, the relationship between the W/B ratio and compressive strength is not as regular as expected, which may be because for some UHPC mixtures, a slightly higher W/B ratio may not only increase the free water in the concrete but also increase the flowability of the UHPC mixture, which leads to a denser microstructure and a higher particle packing density, thus leading to an increase in compressive strength [2, 32]. Nevertheless, the value of the W/B ratio should be between 0.21 and 0.25. A W/B ratio greater than 0.25 can be detrimental to hardened properties of UHPC according to ÖBV-Richtlinie “UHPC” [20] and K. H. Hoang [32].

2.3.3 Superplasticizer dosage

As introduced before, superplasticizer (SP) has also a direct influence on the workability of concrete. For UHPC, owing to its extremely low W/B ratio, the use of a PCE superplasticizer is necessary to achieve sufficient flowability. However, unlike NSC and HPC, UHPC also contains reactive admixtures, which can absorb the molecules of superplasticizers. For example, for mortars containing silica fume, silica fume with a higher negative surface charge requires a higher PCEs content to achieve the desired flowability. In the cement paste, Ca^{2+} is also adsorbed on the surface of the silica fume, and the surface charge of the silica fume changes from negative to positive. Consequently, silica fume with a high negative surface charge has a higher adsorption capacity for Ca^{2+} and thereby requires a higher PCEs content, and is less dispersible after adsorption than other particles with a low negative surface charge [32, 77]. In addition, the very fine silica fume can also cause increased inter-particle forces between the particles [2]. Therefore, an increase in silica fume content will reduce the flowability of UHPC mixtures and more superplasticizer is required to achieve saturation.

Thus, the superplasticizer dosage should also be represented as superplasticizer/binder ratio (SP/B ratio, mass ratio of superplasticizer/(cement+reactive powder)). According to the ÖBV-Richtlinie “UHPC” [20], for UHPC, the superplasticiser/cement mass ratio (SP/C ratio) should be between 2-4%. K. H. Hoang [32] also tested the compatibility of three kinds of superplasticiser with cement and silica fume using the method of mixing energy measurement. The results showed that the product “Premment H500” used in this research could have a very good dispersion effect. At the same time, an SP/C ratio in the range of 2-3.5% could be used to ensure sufficient particle packing density of the UHPC. When considering that the Si/C ratio is 12%, the corresponding SP/B ratio is approximately 1.79-3.13%.

Additionally, after the content of the superplasticiser exceeds the saturation value, higher superplasticizer content will not disperse aggregate to improve the flowability of concrete

anymore, and may also hardly lead to segregation due to the high viscosity of the concrete. In most cases, the SP/B ratio higher than 3.13% will be a useless consumption. However, due to the slow-release effect of grafted copolymerized branched chains [76] and the retarding effect of the cement hydration process [99], more PCE superplasticizer may also have a retention effect on the consistency of concrete.

2.3.3.1 Influences on the concrete properties

In this research, 7 groups of UHPC mixtures were tested for further investigation, as shown in Table 2.8, the UHPC mixtures with different paste volumes, cement types, W/B ratios and StF contents were also tested to verify whether the effect of SP/B ratio on concrete properties would be similar for the UHPC mixtures with different recipes.

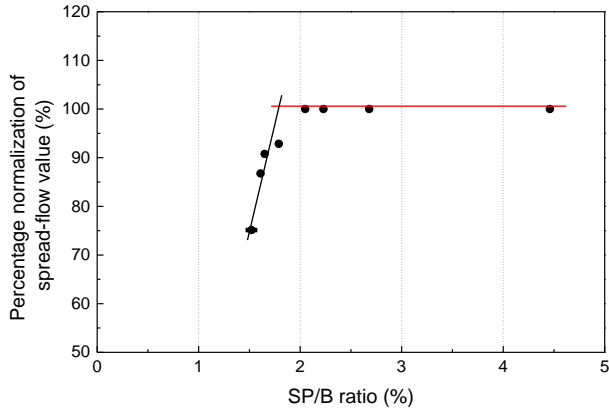
In the names of the UHPC mixtures, “720, 750, and 860” are the cement contents (kg/m^3), “0.223, 0.241, and 0.25” are the W/B ratios, and “2%” means the volume content of StF1. Except for the group “720 0.223” using CEM B, all the other groups used CEM A. Except for the groups “720 0.25 2%” and “860 0.223 2%”, all the other groups were without StF. In each group, although the SP/B ratio varies in different values, all UHPC mixtures were designed as self-compacting concrete mixtures without vibration. After percentage normalization from the UHPC mixtures with 2.68% SP/B ratio (3% SP/C ratio) and statistical analysis, the results of the influences of SP/B ratio on the flowability, temperature and compressive strength of UHPC can be shown in Figure 2.10.

Table 2.8 UHPC mixtures with different SP/B ratios

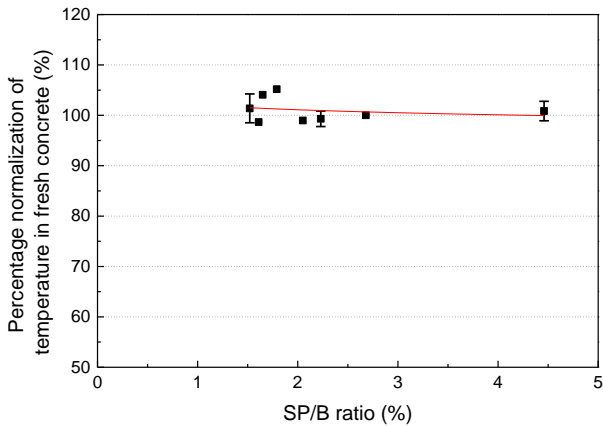
Group	Name	Tested SP/B ratio (%)	Corresponding SP/C ratio (%)
2.3.3-1	720 0.223	2.05, 2.68, 4.46	2.3, 3, 5
2.3.3-2	720 0.241	1.52, 1.65, 2.68	1.7, 1.85, 3
2.3.3-3	720 0.25 2%	1.52, 1.79, 2.23, 2.68, 4.46	1.7, 2, 2.5, 3, 5
2.3.3-4	750 0.223	2.68, 4.46	3, 5
2.3.3-5	750 0.241	2.68, 4.46	3, 5
2.3.3-6	860 0.223	1.52, 1.61, 2.68	1.7, 1.8, 3
2.3.3-7	860 0.223 2%	2.23, 2.68, 4.46	2.5, 3, 5

Based on the results of the flowability, a relationship can be assumed between the superplasticiser used in this research and the flowability of UHPC. As shown in Figure 2.11, when the type and content of other materials remain unchanged, the flowability of concrete

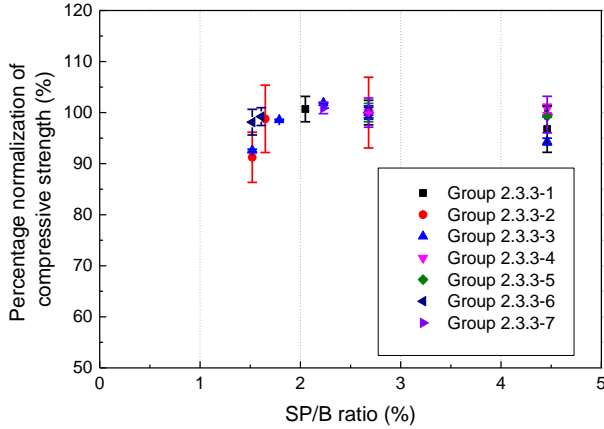
increases with the increase of the SP/B ratio at the beginning. After reaching a critical value, a further increase of the SP/B ratio does not further increase the flowability of the UHPC mixtures, irrespective of the cement type and mix proportion, and the flowability of the UHPC mixtures may remain constant.



(a) Flowability



(b) Temperature in fresh UHPC mixture



(c) Compressive strength

Figure 2.10 Influence of SP/B ratio on the properties of UHPC mixtures

Therefore, according to the results in Figure 2.10, the following equation can be estimated ($R^2=0.88$):

$$\frac{S_{SP/B}}{S_{SP/B=2.68\%}} = \begin{cases} 62.156 \times SP/B - 0.1571, & SP/B \leq 1.86\% \\ 1, & SP/B \geq 1.86\% \end{cases} \quad (2.4)$$

where: $S_{SP/B}$ is the required spread-flow value (cm); $S_{SP/B=0.0268}$ is the spread-flow value (cm) when the SP/B ratio is 2.68% and other factors remain unchanged.

This critical value can be estimated to be around 1.86%. Considering that the flowability of concrete can be related to workability issues, when studying the influences of the superplasticizer, it is suggested to consider two cases where the SP/B ratio is lower than the critical value and higher than the critical value, so as to distinguish whether the influences of the superplasticiser on workability issues are through an influence on the flowability of the concrete, or through a retarding effect (see the analysis in the next section).

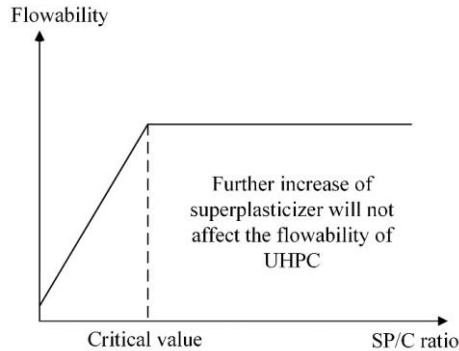


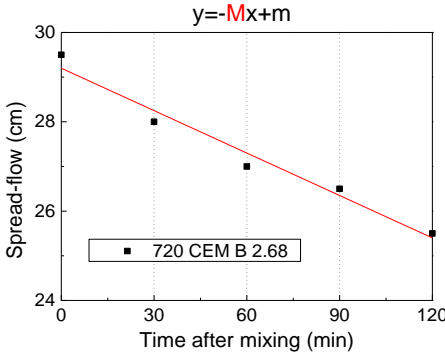
Figure 2.11 Relationship between SP/C ratio and flowability of UHPC

The results of temperature and compressive strength show little effect of superplasticiser. However, it is worth noting that when the SP/B ratio is very low, the low flowability can also cause a lot of air pores in the hardened UHPC, leading to a decrease in compressive strength. The research on air pores will be presented in Chapter 4.

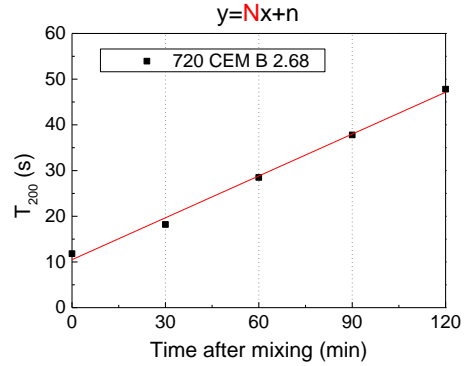
2.3.3.2 Influence on the changing of the consistency over time

In this research, the influence of the SP/B ratio on the changing of the consistency over time of the UHPC mixture was also investigated by testing the changing of the flowability and viscosity over time. The experimental results of the UHPC mixture “720 CEM B 2.68” (Table A.1 in Appendix) are shown in Figure 2.12. After mixing, due to the hardening of the concrete, the flowability gradually decreased over time, and the viscosity gradually increased over time. To easily show the differences in changing over time, new parameters M and N were introduced to describe the slopes of the trend lines. The larger the parameters M and N, the faster the changing of the flowability and viscosity over time.

Consequently, the groups “720 0.223 CEM B”, “720 0.241”, “750 0.223”, “750 0.241” and “860 0.223” were chosen to test the changing of the consistency over time. After percentage normalization from the UHPC mixtures with a 2.68% SP/B ratio and statistical analysis, the results of the influence of the SP/B ratio on the changing of the consistency over time can be shown in Figure 2.13. Even though the result possessed a certain amount of dispersion, it could be found that whether the SP/B ratio was higher or lower than the critical value, a higher SP/B ratio would decrease the parameters M and N, which meant retarding the changing of the flowability and viscosity over time. It should be noted that, however, the above conclusion is only applicable to a PCEs-based SP.



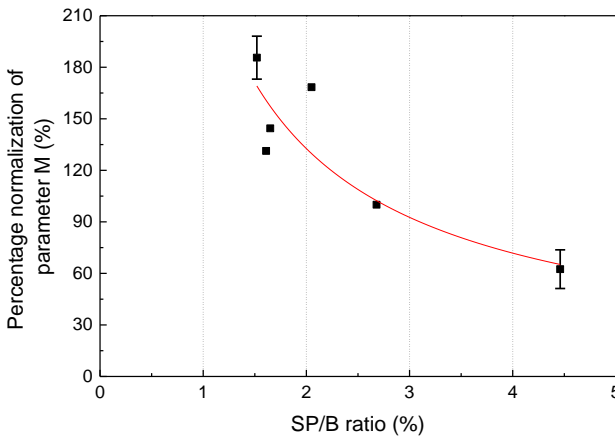
(a) Changing of spread-flow over time



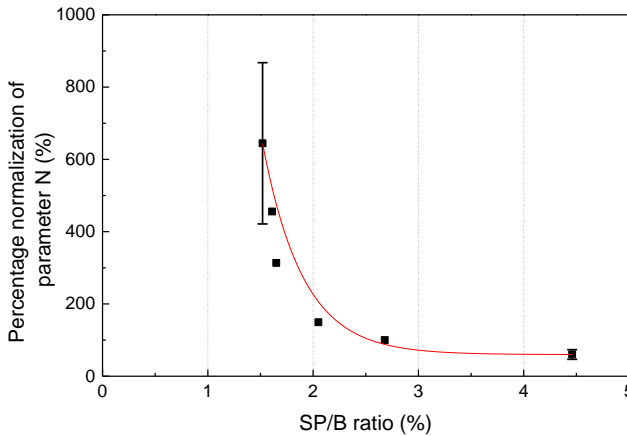
(b) Changing of T₂₀₀ over time

Figure 2.12 Parameters M and N for description of the changing of the flowability and viscosity over time

In summary, the value of the SP/B ratio is suggested to be in the range of 1.79-3.57% (corresponding to the SP/C ratio in the range of 2-4%) according to ÖBV-Richtlinie “UHPC” [20] and K. H. Hoang [32] to ensure sufficient flowability and no waste of material. Moreover, considering that there are few retarder products suitable for UHPC containing C₃A-free cement, and there may also be an interaction between the retarder and SP, which will affect the workability of concrete, if SP can be used to replace the retarder to extend the consistency of concrete, then this can have many benefits in some UHPC cast-in-place large-scale engineering applications.



(a) Parameter M



(b) Parameter N

Figure 2.13 Relationship between SP/B ratio and the changing of the consistency of UHPC mixtures over time

2.3.4 Paste volume

In the paste of UHPC, when keeping the Si/C ratio, QP/C ratio, W/B ratio and SP/B ratio, the changing of the paste volume can be represented by the changing of the cement content. According to the test results in the above sections, UHPC mixtures with various paste volumes (including CEM, Si, QP, WA and SP) would have different properties. Hence, in this research, the influences of paste volume on the fresh and hardened properties of UHPC are also examined.

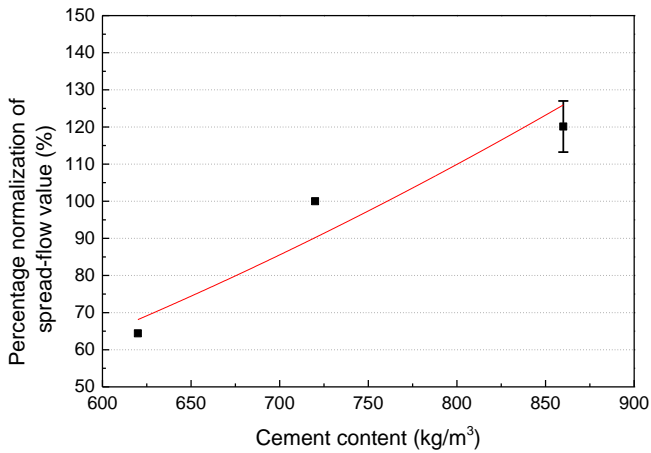
According to the ÖBV-Richtlinie “UHPC” [20], for UHPC, the cement content could be between 600-850kg/m³. UHPC mixtures with coarse aggregates usually contain lower paste volumes, while UHPC mixtures with steel fibres usually contain higher paste volumes. Combined with the cement content of 720kg/m³ suggested by K. H. Hoang (Table 2.5) [32], when the value of Si/C ratio is taken as 12%, QP/C ratio as 30%, W/B ratio as 0.25 and SP/B ratio as 2.68%, the paste volume for UHPC can be calculated to be between 464.7-649.9L/m³.

In this research, 2 groups of UHPC mixtures were tested, as shown in Table 2.9. The group “0.223 2.68 0%” was without StF, while the group “0.223 2.68 2%” was with 2 vol. % StF1. “0.223” is the W/B ratio and “2.68” is the SP/B ratio in %. Detailed mix recipes and properties of each group of UHPC mixtures can be found in Table A.1 in the appendix, in which the paste volumes are marked in the names of the recipes. After percentage

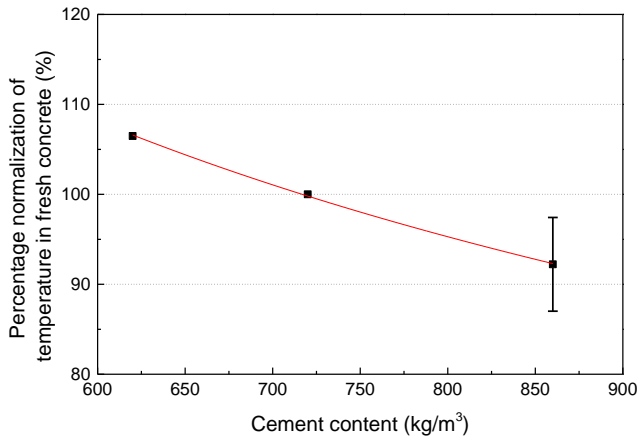
normalization from the UHPC mixtures with 720kg/m³ cement content and statistical analysis, the results of the influences of paste volume (represented by cement content) on the flowability, temperature and compressive strength can be shown in Figure 2.14.

Table 2.9 UHPC mixtures with different cement contents (paste volumes)

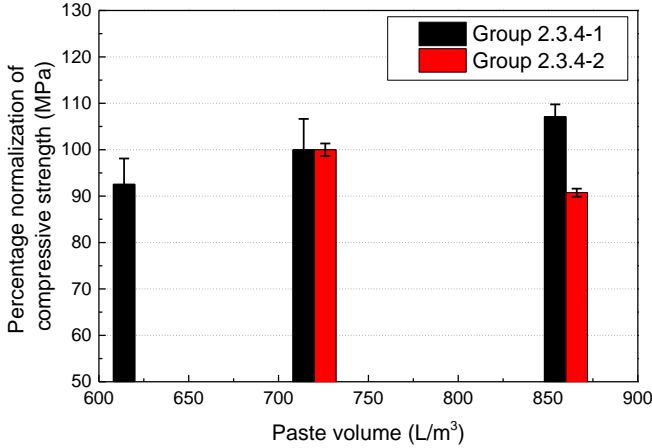
Group	Name	CEM content (kg/m ³)	Corresponding paste volume (L/m ³)
2.3.4-1	0.223 2.68 0%	620, 720, 860	479.5, 553.6, 657.4
2.3.4-2	0.223 2.68 2%	720, 860	553.6, 657.4



(a) Flowability



(b) Temperature in fresh UHPC mixture



(c) Compressive strength

Figure 2.14 Influences of paste volume (represented by cement content) on the properties of UHPC mixtures

It can be found that a higher cement content (paste volume) can lead to a higher flowability and a lower temperature in fresh concrete. After the linear fitting, the relationship between the percentage change in spread-flow value and the cement content ($R^2=0.873$), and the relationship between the percentage change in fresh concrete temperature and the cement content ($R^2=0.996$) can be expressed as the following equations:

$$\frac{S_{CC}}{S_{CC=720}} = 0.00226 \times CC - 0.6272 \quad (2.5)$$

where: CC is the cement content of the UHPC (kg/m^3); S_{CC} is the required spread-flow value of the UHPC (cm); $S_{CC=720}$ is the spread-flow value of the UHPC when the cement content is $720\text{kg}/\text{m}^3$ and other factors remain unchanged (cm).

$$\frac{T_{CC}}{T_{CC=720}} = -0.0006 \times CC + 1.432 \quad (2.6)$$

where: CC is the cement content of the UHPC (kg/m^3); T_{CC} is the required temperature in fresh UHPC ($^{\circ}\text{C}$); $T_{CC=720}$ is the temperature in fresh UHPC when the cement content is $720\text{kg}/\text{m}^3$ and other factors remain unchanged ($^{\circ}\text{C}$).

For the results of the influence of paste volume on compressive strength, although these two groups showed different behaviours, the overall difference in compressive strength didn't exceed 10%. Therefore, it could be concluded that when the cement content was between 620kg/m^3 and 860kg/m^3 (paste volume between 479.5L/m^3 and 657.1L/m^3), the change in compressive strength was not significant. Combining the ÖBV-Richtlinie "UHPC" [20] and the results of K. H. Hoang [32], it was concluded that the cement content should ideally be between $620\text{-}850\text{kg/m}^3$, corresponding to a paste volume between $479.5\text{-}649.9\text{L/m}^3$.

2.3.5 Coarse aggregate

The coarse aggregates used for UHPC are usually basalts (BA) with a particle fraction of 2-8mm, which are added into the concrete mixture to enhance the volume stability of UHPC. Based on the mix proportion of coarse aggregate UHPC recommended by K. H. Hoang [32], the BAs account for about 30-50% of the volume of total aggregates to replace QS2 when the volume content of QS1 remains constant.

It should be noted that with the same paste content, the total specific surface area of the particles in the coarse aggregate is smaller than that in the fine aggregate, which would also decrease with the increase of particle size. According to the ÖBV-Richtlinie "UHPC" [20], the paste volume (CEM, Si, QP, WA and SP) of UHPC containing coarse aggregates should be reduced in comparison to that of fine aggregate UHPC to prevent segregation or uneven distribution of aggregates to keep good hardened properties.

In this research, 3 groups of UHPC mixtures were tested. Two kinds of basalts (BA1 and BA2) with different fractions were used to replace QS2 with 30% basalt/total aggregate volume ratio (BA/V(Ag) ratio), respectively, as shown in Table 2.10. The paste content was adjusted accordingly to achieve the same flowability for each UHPC mixture to avoid the influence of uneven distribution. In the names of UHPC mixtures, "0.25" and "0.27" are the W/C ratios, and "0%" and "30%" are the V(BA)/V(Ag) ratios. For the results of T_{200} value and temperature, it can be found that with the same flowability, the UHPC mixtures have similar temperatures and viscosities.

After percentage normalization from the UHPC mixtures without BA (720kg/m^3 of cement content) and statistical analysis, the results of the influence of BA on the compressive strength can be shown in Figure 2.15. These results also indicate that when the paste volume is adjusted, 30% incorporation of coarse aggregate of both sizes will not have a significant

effect on the performances of UHPC. In some applications, coarse aggregates can be used instead of a percentage of fine aggregates, which also reduces material costs.

Table 2.10 UHPC mixtures with different coarse aggregates and the same flowability

Group	UHPC mixture	CEM content (kg/m ³)	Paste volume (L/m ³)	Coarse aggregates	Spread-flow (cm)	T ₂₀₀ (s)	Temperature in fresh UHPC (°C)
2.3.5-1	(1) 0.25 0% BA	720	553.6	Without BA	24.5	21	29.4
	(1) 0.25 30% BA1	660	509.1	V(BA1)/V(Ag)=30%		20	29.4
	(1) 0.25 30% BA2	630	486.9	V(BA2)/V(Ag)=30%		20	29.2
2.3.5-2	(2) 0.25 0% BA	720	553.6	Without BA	25	29	27.4
	(2) 0.25 30% BA1	660	509.1	V(BA1)/V(Ag)=30%		28	26.4
2.3.5-3	(3) 0.27 0% BA	720	568	Without BA	24	20	27.1
	(3) 0.27 30% BA1	660	522.3	V(BA1)/V(Ag)=30%		20	26.8
	(3) 0.27 30% BA2	630	499.5	V(BA2)/V(Ag)=30%		20	27.4

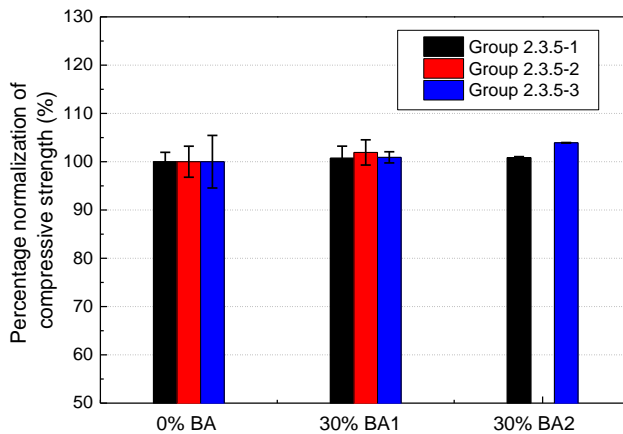


Figure 2.15 Influence of coarse aggregate content on the compressive strength of UHPC mixtures with the same flowability

2.3.6 Steel fibre

According to the ÖBV-Richtlinie “UHPC” [20], the content of steel fibre (StF) used for UHPC is usually less than 5 vol.% of the concrete and replaces aggregates by volume percentage to keep the paste volume constant. Although the total surface area of the particles of the UHPC with StF is also smaller than that without StF with the same paste content, the cross-grid effect of the steel fibre can impede the flow of particles and reduce the flowability of UHPC. Thus, the paste volume of UHPC containing steel fibres should be increased in comparison to that of UHPC without steel fibre to prevent fibre balls or clumps and keep good hardened properties.

In this research, 3 groups of UHPC mixtures were also tested. Two kinds of steel fibres (StF1 and StF2) with different dimensions were used with 2 vol.% of the concrete, as shown in Table 2.11. The paste content was adjusted accordingly to achieve the same flowability for each UHPC mixture to avoid undesirable effects. In the names of UHPC mixtures, “0.25” and “0.27” are the W/C ratios, and “0%” and “2%” are the volume content of steel fibres. For the results of T_{200} value and temperature, it can be found that with the same flowability, the UHPC mixtures have similar temperatures and viscosities.

After percentage normalization from the UHPC mixtures without StF (720kg/m³ of cement content) and statistical analysis, the results of the influence of StF on the compressive strength can be shown in Figure 2.16. These results also indicate that when the paste volume is adjusted, 2% incorporation of steel fibres of both sizes will not have a significant effect on the performances of UHPC.

Table 2.11 UHPC mixtures with different steel fibres and the same flowability

Group	UHPC mixture	CEM content (kg/m ³)	Paste volume (L/m ³)	Steel fibres	Spread-flow (cm)	T ₂₀₀ (s)	Temperature in fresh UHPC (°C)
2.3.6-1	(1) 0.25 0% StF	720	553.6	Without StF	24.5	21	29.4
	(1) 0.25 2% StF1	750	575.8	With 2 vol.% StF1		20	29.2
2.3.6-2	(2) 0.25 0% StF	720	553.6	Without StF	25	29	27.4
	(2) 0.25 2% StF1	750	575.8	With 2 vol.% StF1		28	27.8
2.3.6-3	(3) 0.27 0% StF	720	568	Without StF	26	11	27.3
	(3) 0.27 2% StF1	790	621.3	With 2 vol.% StF1		11	26
	(3) 0.27 2% StF2	780	613.7	With 2 vol.% StF2		11	27

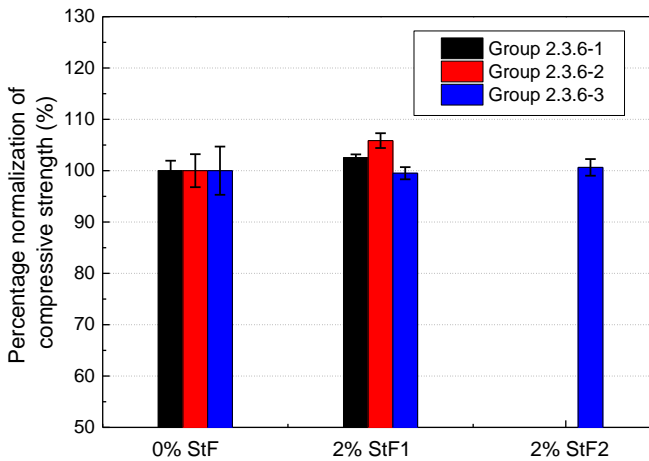


Figure 2.16 Influence of steel fibre content on the compressive strength of UHPC mixtures with the same flowability

Therefore, considering the beneficial effects of steel fibres on the UHPC's tensile properties, ductility, etc., it is necessary to use steel fibres in many UHPC applications, but at the same time, the paste volume has to be increased accordingly, which is also noteworthy in specific applications.

2.3.7 Cement type

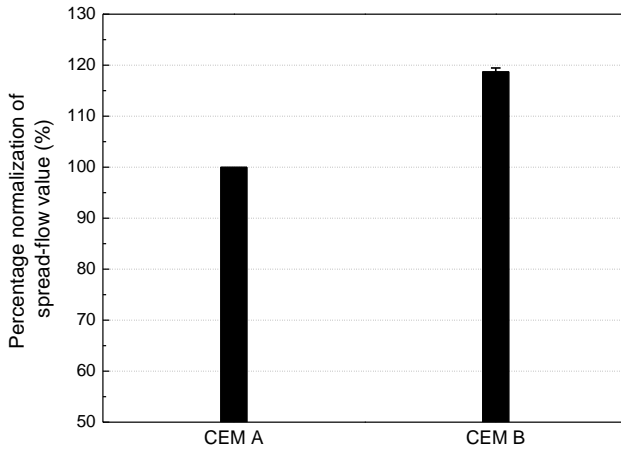
Based on the previous results, the cement type may also have an influence on the properties of concrete. In this study, 2 groups of UHPC mixtures with CEM A and CEM B were tested, as shown in Table 2.12. In the names of the recipe group, "720" and "750" are the cement contents (kg/m^3), and "0.25" and "0.27" are the W/C ratios.

Table 2.12 UHPC groups with different cement types

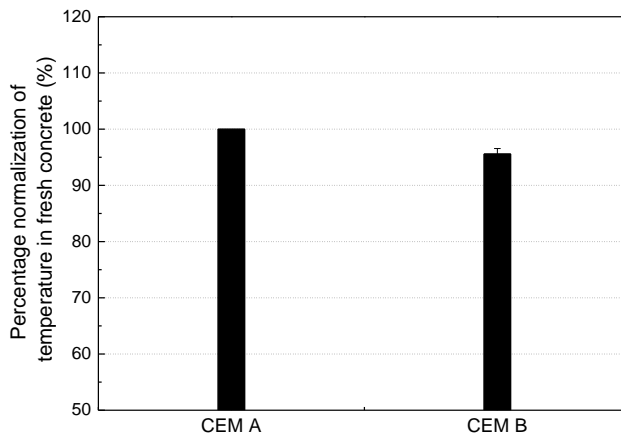
Group	Name	Cem type
2.3.7-1	720 0.25	CEM A, CEM B
2.3.7-2	750 0.27	CEM A, CEM B

After percentage normalization from the UHPC mixtures with CEM A and statistical analysis, the results of the influences of cement type on the flowability, temperature and compressive strength can be shown in Figure 2.17. When the recipes, other raw materials, and mixing conditions were all the same, the UHPC mixtures with CEM B exhibited a higher flowability, a lower temperature in the fresh concrete, and a lower compressive strength than

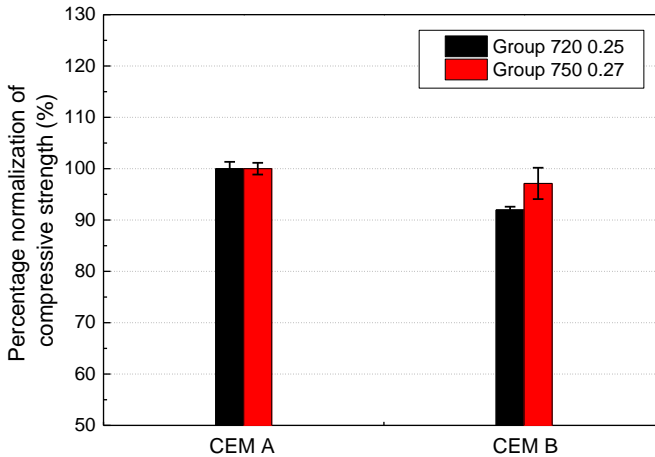
the UHPC mixtures with CEM A. This means that the workability of UHPC with CEM B may be better than that with CEM A. Hence, CEM B may also be beneficial in solving the workability issues, but the compressive strength may need to be sacrificed. As a result, the choice of cement type should be made according to the requirements of the specific practical application.



(a) Flowability



(b) Temperature in fresh UHPC mixture



(c) Compressive strength

Figure 2.17 Influence of cement type on the properties of UHPC

2.4 Summary

This chapter focuses on the material and composition of UHPC, explains the basis for the selection of each raw material in this research, explores the influence of the content of each raw material in the mix design on some properties of UHPC, and determines the range of content of these raw materials in order to satisfy the performances of UHPC. The main conclusions are drawn as follows:

- (1) The value of the Si/C ratio should be between 12-18%, and the value of the QP/C ratio should be between 30-40%. Unless it is to solve some specific problems, less Si and QP content would be better;
- (2) The value of the W/B ratio should be between 0.21 and 0.25. The value of the W/B ratio has an increasing relationship with the flowability and decreasing relationships with the temperature in fresh concrete and the compressive strength;
- (3) The value of the SP/B ratio should be between 1.79-3.57%. With the increase of the SP/B ratio, the flowability of fresh UHPC mixtures firstly increases gradually, then keeps constant after a critical value. The PCE superplasticizer can have a retarding effect on the changing of the consistency of the UHPC mixture over time;

- (4) The paste volume should be between 479.5-649.9L/m³, corresponding to a cement content between 620-850kg/m³ when the Si/C ratio is 12%, QP/C ratio is 30%, W/B ratio is 0.223 and SP/B ratio is 2.68%;
- (5) The coarse aggregate can be incorporated into UHPC up to 50% of the total aggregate volume in place of QS2. The steel fibre can be incorporated into UHPC up to 5% of the total concrete volume in place of aggregates. In order to avoid problems such as aggregate segregation and fibre ball, UHPC mixtures with coarse aggregates usually contain less paste and UHPC mixtures with steel fibres usually contain more paste.

The introduction and investigation in this chapter would provide a great research basis for the following research about workability issues. However, further investigation is still needed with the development of new raw materials that can be used in UHPC.

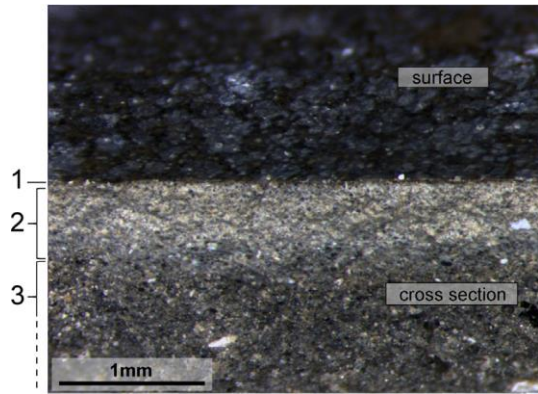
3 “Elephant skin” on the surface of UHPC

As mentioned before, the “elephant skin” and the resulting porous layer below the surface can greatly compromise the surface performance and hardened properties of UHPC. This chapter mainly investigates how to minimize the formation of the “elephant skin” so as to enhance the surface performance of UHPC.

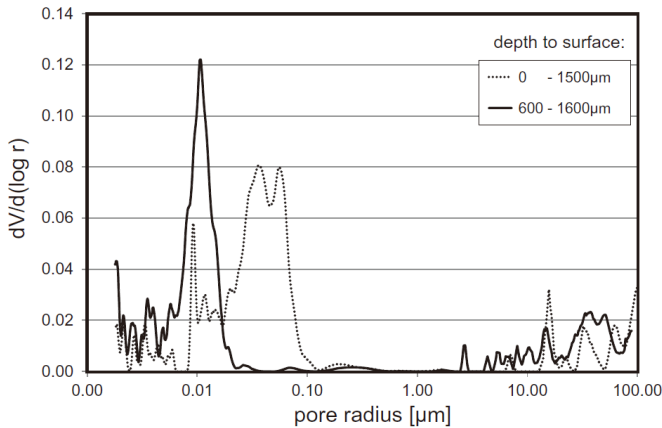
3.1 Literature review

Some research on the characteristics of the “elephant skin” on UHPC surfaces and on how to avoid its formation has been carried out in previous studies. Wetzel et al. [40, 50, 100] investigated the microstructural features of the “elephant skin” on UHPC surface by means of optical microscopy and porosity testing. It was identified that the thickness of the “elephant skin” and the porous layer below it were about 50 μm and 500 μm , respectively, as shown in Figure 3.1 (copyright permitted). Besides, they also found that the formation of the “elephant skin” was heavily influenced by the relative humidity (RH) of the environment. Based on those observations, it was suggested to put UHPC specimens in an environment with 100% RH to avoid the formation of the “elephant skin” on the surface.

Chen et al. [44] used the penetration test according to ASTM C403 [101] to investigate the way to avoid the formation of the “elephant skin” on UHPC surface, as shown in Figure 3.2 (copyright permitted). By comparing the penetration resistance of the top and bottom positions of the concrete slab, they found that the only effective way was to spray water on the UHPC surface and cover it with a plastic membrane, as shown in Figure 3.3. This was in fact consistent with the proposal of Wetzel et al. [40].



(a) Stereoscopic image of the fracture edge of a UHPC sample in an oblique view (layer 1: the “elephant skin”; layer 2: porous layer; layer 3: UHPC matrix)



(b) Porosity of the layers one, two and three (0–1500μm) and the only layer three (600–1600μm) of a UHPC sample with the “elephant skin”

Figure 3.1 Light microscopy and mercury intrusion porosity (MIP) test results of Wetzel et al. [40]

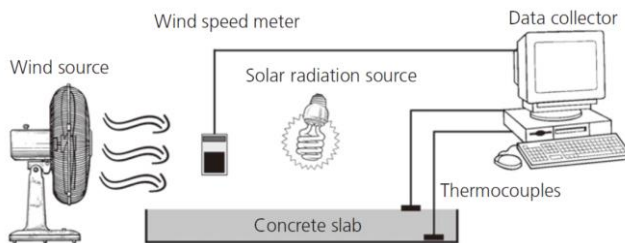


Figure 3.2 Penetration tests with data collector to simulate conditions that promote the “elephant skin” formation on an exposed UHPC surface [44]

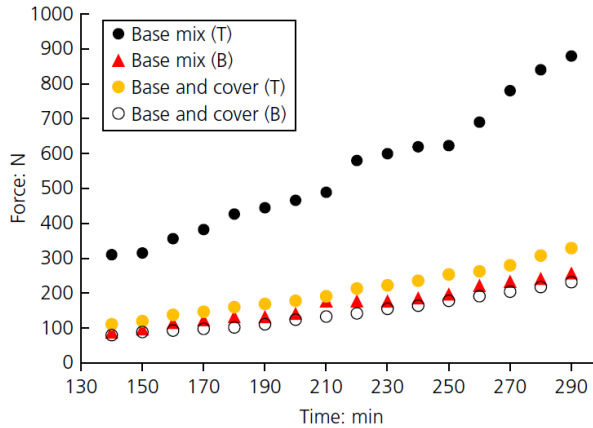


Figure 3.3 Measured values of penetration resistances against the time of exposure to radiation and airflow for slabs made with base UHPC mixture covered and not covered with plastic membrane (“T” refers to the top of concrete slab; “B” refers to the bottom of concrete slab) [44]

Çağlar Y and Oğuzhan Ç [102] assessed the influence of the “elephant skin” formation on the macropore profile by micro-computed tomography scan (X-ray). They clearly observed the porous layer beneath the “elephant skin” and found that a high humidity of 95% and lower temperature benefit to decrease the formation of the “elephant skin” as well. In addition, their results showed that the increase of ground granulated blast furnace slag (GGBS) replacement enhanced the formation of the “elephant skin” on UHPC (increased porosity of the porous layer), albeit with a reduced demand for superplasticizer.

Çağlar Y and Halit Y [103] found the increase in the amount of fly ash (FA) enhanced the formation of the “elephant skin”, compared with the silica fume (Si) and blast furnace slag (BFS). As shown in Table 3.1 (copyright permitted), only in the UHPC mixture with FA (UHPC-FA), increasing the exposure temperature didn’t cause a steep rise in evaporation because the “elephant skin” acted as a barrier and hindered the water evaporation even at high temperatures.

Table 3.1 Water evaporation from UHPC mixtures (at the end of the 24h under 50% RH) [103]

Mixtures	Temperature (°C)		
	20	30	40
Evaporation (kg/m ²)			
UHPC-C	1.0	1.2	1.6
UHPC-BFS	1.4	1.7	2.2
UHPC-FA	1.0	1.3	1.4

Küchler [104] attempted to avoid the formation of the “elephant skin” on UHPC surface by gently poking the concrete with a thin steel bar in order to permit early venting and by subsequently spraying water on the surface. Such a solution was found to be helpful in preventing the formation of the “elephant skin” on the UHPC surface; however, it was less practical for large-scale applications.

To summarize, the existing research has only tried to give some solutions to the “elephant skin” through the experiments, but not studied the specific formation mechanisms of the “elephant skin”. In addition, as shown in Figure 3.4, for the coarse aggregate UHPC with steel fibres under 67% relative humidity, the “elephant skin” appears only 4min after casting. But in the 60cm length formwork, the flowing time of the concrete is about 1min14s. Consequently, during the real production of large-scale UHPC elements, there is often not sufficient time to spray water, cover a plastic membrane or perform other treatments on the surface before the formation of the “elephant skin” on the UHPC surface.



Figure 3.4 Flowing of UHPC in the 60cm length formwork (flowing time: 1min14s)

Therefore, in order to efficiently improve the surface quality and performance of UHPC by controlling the “elephant skin” on the surface, the mechanisms of its formation need to be well understood. To this end, it is necessary to investigate the effects of various influencing factors and to identify the key ones that influence the formation of the “elephant skin” in UHPC.

In the next sections, extensive laboratory studies are carried out on the formation of the “elephant skin” by use of UHPC mixtures with different mix proportions. Various factors that affect the formation of the “elephant skin” on UHPC surface are investigated. Based on the test observations, the microscopic formation mechanisms of the “elephant skin” on UHPC

surface are discussed. Then some feasible solutions are proposed to decrease the negative effects of the “elephant skin” on the surface performance of UHPC.

3.2 Materials and measuring methods

The raw materials employed in this study are the same raw materials including CEM, Si, QP, WA, SP, Ag and StF, as introduced in Section 2.1. The recipes of the UHPC mixtures used in this study are introduced in each section to facilitate the identification. All the UHPC mixtures are endowed with self-compacting ability. Each group of UHPC mixtures should be mixed and tested on the same day, and only one parameter can be changed while the other parameters are kept constant. When combining the results of different groups of UHPC mixtures, the results need to be percentage normalized from the reference recipe in Table 2.5, so that multiple groups of results can be statistically analysed to calculate the mean values and standard deviations.

Except for the UHPC mixture used to produce large beams in Section 3.3.2, which is mixed with an ELBA mixer, the rest of the UHPC mixtures are mixed with an Eirich mixer. The temperature and humidity of the environment during the concrete manufacture are monitored by a hygrothermograph. The normal temperature and humidity of the laboratory are around 20°C and 60%, controlled by the air conditioner and humidifier. The mixing procedure and measurement methods of temperature in fresh concrete, flowability, and viscosity of UHPC mixtures in this chapter are the same as that in Chapter 2. Unless otherwise stated, the samples cast in the tests in each section are mostly cured in 80°C hot water for 48h in order to quickly reach the 28-d compressive strength.

To investigate the effects of the “elephant skin” on the surface performance of UHPC, it is necessary to find an appropriate approach to quantify the surface performance of the concrete. In existing studies, several methods were generally used, which included the observation of the thickness of the “elephant skin” on the UHPC surface by means of a microscope, the analysis of the porosity below the “elephant skin” and the testing of the hardness of the “elephant skin” through a penetration tester [40, 44, 102]. In the first two methods, slices of hardened concrete specimens required to be cut and examined, which was rather time-consuming, while the latter needed advanced experimental devices with high accuracy and sophisticated operations.

In this work, an alternative test method was developed and used, based on a modification of the method for testing the setting time of cement paste using the Vicat apparatus according to EN 196-3 [105], as shown in Figure 3.5. Due to the formation of the “elephant skin”, the surface of the concrete hardens much faster than the initial setting of the concrete below the surface over time. Therefore, in order to characterize the hardening of the concrete surface over time, the objective of this test approach is to determine the change of the surface resistance (strength) of the UHPC over time to represent the growing of the “elephant skin” over time.

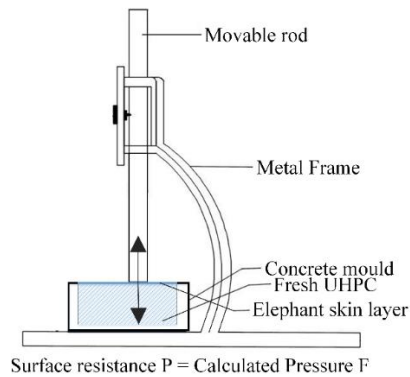




Figure 3.5 Sketch of the developed method for measuring the surface resistance of UHPC using different movable rods

Thus, the movable rod of the original Vicat apparatus was turned upside down so that its circular cross-section with a diameter of about 10mm faces downward. At the same time, another 5 cylindrical rods with diameters of about 10 mm but different weights were used. The weight and the diameter of the circular cross-section of all 6 cylindrical rods were measured, including the movable rod of the original Vicat apparatus, and the pressure at the downward end section of each rod was calculated, as shown in Table 3.2.

Table 3.2 Information about the used movable rods

Material	Weight	Lower section diameter	Calculated Pressure	Photo
Wood	12g	11.16mm	1.21kPa	
Plastics	28g	10.35	3.26kPa	
Aluminum	39g	10.23	4.65kPa	
Aluminum	64.9g	10.25	7.71kPa	

Material	Weight	Lower section diameter	Calculated Pressure	Photo
Steel	175.7g	9.8	22.83kPa	
Steel	301g	9.95	37.94kPa	

As shown in Figure 3.6, the test procedure is described as follows: immediately after the mixing, the fresh UHPC mixture is cast into the formwork of a $100 \times 250 \times 30 \text{ mm}^3$ plate; then the plate formwork is placed and positioned on the base of the Vicat apparatus; after that, the movable rod is gently lowered until it is in contact with the UHPC surface; finally, the movable rod is released quickly and fall freely on the UHPC surface.

During the test, the rods with varying weights were tried every 3-4min starting from the one with the minimum weight, and the time required for the “elephant skin” to develop sufficient strength to prevent each rod from falling through it, was recorded. The resistance of the UHPC surface (i.e., the “elephant skin”) is defined as the maximum pressure it can withstand before the rod penetrates into the UHPC mixture. That pressure is calculated as the weight of the rod divided by its bottom cross-section area. The calculated pressure is assumed to equal the surface resistance of UHPC (strength of the “elephant skin”). Through tracing the development of the UHPC surface resistance over time, the growing of the “elephant skin” on the UHPC surface over time can be derived.

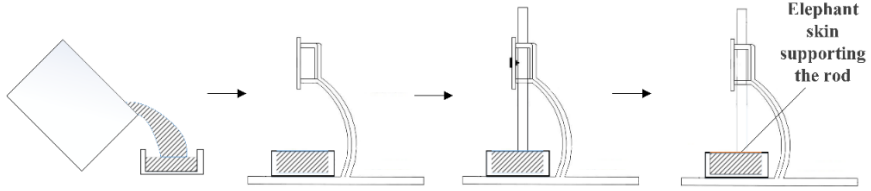


Figure 3.6 Test procedure of the using method

It is worth noting that according to the observation of the “elephant skin” (Figure 1.10), the hardness distribution of the “elephant skin” on the concrete surface is relatively uniform, but the distance between the test position and the edge of the formwork will affect the surface resistance results due to the bending effect. In this test method, the distance between each test position and the edge of the formwork should be as same as possible, as shown in the photos in Figure 3.7.

It is obvious that in comparison to the test methods in previous research [40, 44, 102], the developed method in this study does not require a long time to wait for the concrete to set, highly sophisticated instruments, and an extremely high degree of testing accuracy. It is easier to perform with more efficiency to evaluate the growing of the “elephant skin” on the UHPC surface.



Figure 3.7 Test photos of the surface resistance of the “elephant skin” using the Vicat apparatus

According to the literature review, relative humidity (RH) is regarded as one of the main factors affecting the formation of the “elephant skin”. A higher RH may lead to a slower formation of the “elephant skin” over time. Thus, in order to verify the validity of the test method, the influence of RH was further explored using the test method developed in this study.

As shown in Figure 3.8, a bucket was used to test the fresh UHPC mixtures at different RHs. The water was put in the bucket at first, then after 1~2 days, the fresh UHPC mixture was stored in the bucket to examine the growing of the “elephant skin” on the surface. The different RHs were achieved by the different durations of time the water was stored in the bucket before placing the UHPC mixtures.

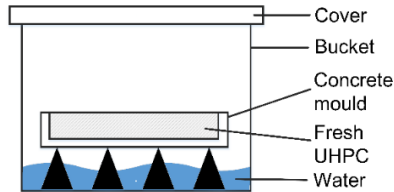


Figure 3.8 Sketch of the treatment under different high RHs

Therefore, 5 batches of UHPC mixtures with different recipes were tested to investigate the growing of the “elephant skin” over time at various RH levels, as shown in Table 3.3. Detailed mix recipes of all UHPC mixtures can be found in Table A.2 in the appendix. The UHPC mixtures with different paste volumes, cement types, BA contents and StF contents were also tested to verify whether the effect of RH on the “elephant skin” would be similar for the UHPC mixtures with different recipes. In the names of the UHPC mixtures, “720, 620 and 860” are the cement contents, “30%” is the BA/V(Ag) ratio, and “1%” and “3%” are the volume contents of StF. Except for the groups “720 CEM B”, all the other groups used the CEM A.

Table 3.3 UHPC mixtures for testing the influence of RH

Group	UHPC mixture	Tested RH
3.2-1	720 CEM B	40%, 76%, 100%
3.2-2	720 CEM A	46%, 60%, 76%, 80%, 100%
3.2-3	620 30% BA2	70%, 85%, 100%
3.2-4	620 30% BA2 1% StF	68%, 85%, 100%
3.2-5	860 QS3 3% StF	64%, 87%, 100%

Each batch of UHPC mixtures was mixed on the same day. The RH in the laboratory was measured to be 40-64% (due to the different opening conditions of the humidifier); A RH of 100% was directly spraying water on the UHPC surface; and RH 68-87% was measured by a hygrometer in the box in Figure 3.8. Since this research was only to verify the accuracy of the test method and the effect of different mix proportions on the properties of UHPC has been analysed in Chapter 2, each UHPC mixture was only cast one 100×250×30mm³ plate

to test the growing of the “elephant skin”, and the properties such as flowability and compressive strength were not measured.

The photos of the surfaces of the UHPC mixture “720 CEM B” under different RH levels can be seen in Figure 3.9. It is clear that the surface under lower RH shows a stronger “elephant skin”. With the test method, the surface resistance (P)-time (t) curves of these surfaces are shown in Figure 3.10. To manifest the experimental results more explicitly, a new parameter A was introduced to describe the slope of the curve and the growing of the “elephant skin” on the UHPC surface over time. The surface resistance-time curve was fitted to a single parameter (parameter A) quadratic equation. The correlation values R^2 of the curves “RH 40%”, “RH 76%” and “RH 100%” are 0.986, 0.989 and 0.94 respectively, which could be considered high enough. Thus, the larger the parameter A, the faster the growing of the “elephant skin” over time. Since the surface resistance (P)-time (t) curves in the research were all able to fit the values of parameter A with the R^2 values exceeding 0.9, the correlation value of R^2 for each parameter A will not be given in the subsequent content.

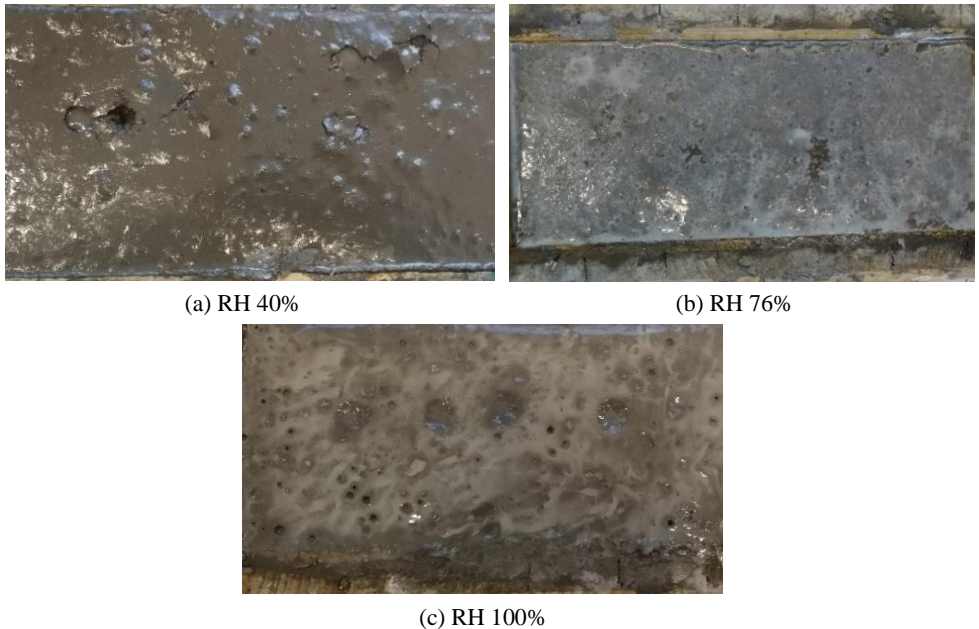


Figure 3.9 Photos of UHPC surfaces of plates 1 hour after casting

It is worth noting that the surface under 100% RH has almost no the “elephant skin”. The surface resistance-time curve in this case actually represents the initial stage of the setting of the concrete but not the growing of the “elephant skin” over time. Moreover, according to

BA Graybeal [106], MA Bajaber et al. [107] and CW Chung et al. [108], the initial setting of UHPC can have a surface resistance of 3.4MPa at 15 hours after casting and can be retarded by high superplasticizer dosage. Therefore, the curves fitted by the test method developed in this research can be considered numerically accurate.

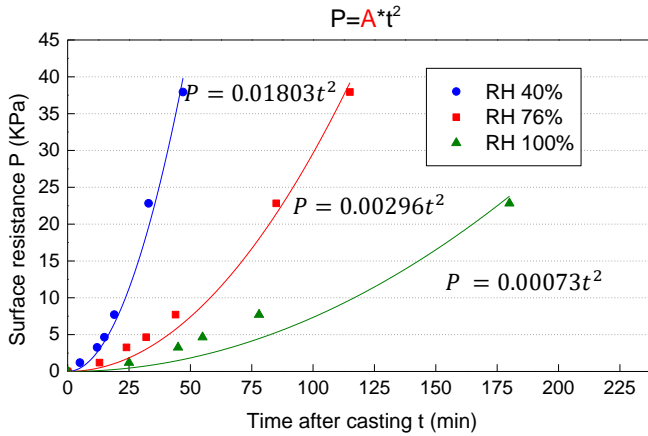


Figure 3.10 Surface resistance-time curves of the “elephant skin” of the reference UHPC mixture at different RH levels, which is fitted into a single parameter (A) quadratic equation (parameter A reflects the growing of the “elephant skin” over time)

The relationship between parameter A and RH for the UHPC mixtures in Table 3.3 is shown in Figure 3.11. It can be found that when comparing the results of each UHPC mixture, higher RH can result in a slower growing of the “elephant skin” over time. When all the UHPC mixtures are analysed together, after percentage normalization from the “RH 100%” and statistical analysis, the result is shown in Figure 3.12. At this time, there is a large dispersion, which is due to the different slopes of the curves for the different UHPC mixtures, indicating that other factors are also co-related to influence the growing of the “elephant skin” over time.

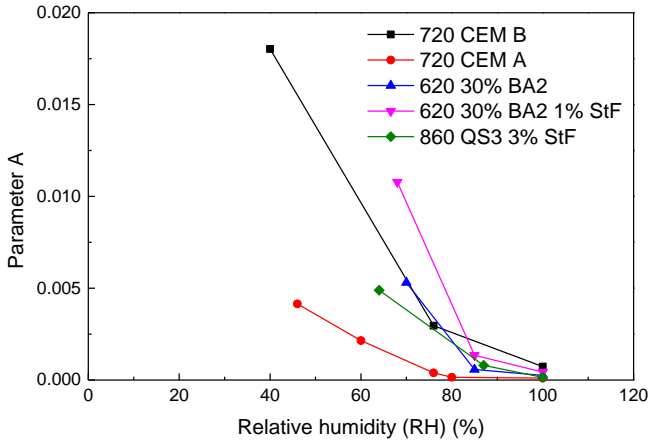


Figure 3.11 Relationship between RH and parameter A

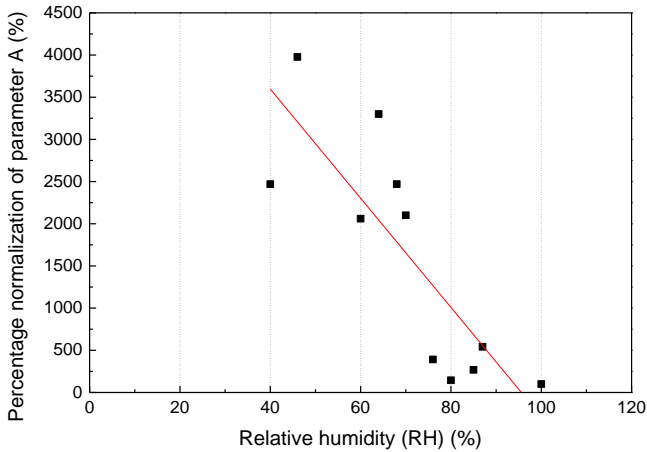


Figure 3.12 Percentage normalization of the results of all UHPC mixtures

In summary, the results of this research with the new test method are apparently in good agreement with existing test results in the literature. This demonstrates the validity of the developed test method in this research.

Additionally, when using this test method, it was observed that the “elephant skin” was present in almost all cases except for spraying water on the surface (RH 100%). When an “elephant skin” was present, the concrete underneath was much softer than the “elephant skin” (when the movable rods penetrated the “elephant skin”, they could be lowered a certain depth further, as shown in Figure 3.13). Even though the calculated surface resistance should be the sum of the resistance of the “elephant skin” and the resistance of the UHPC matrix

underneath, the results in Figure 3.10 show that the resistance of the UHPC matrix is much smaller than that of the "elephant skin" when the RH is low. Therefore, for UHPC with a similar superplasticiser dosage (the initial setting time is nearly the same, causing the resistance of the UHPC matrix in each time point to be also nearly the same), the growing of the “elephant skin” over time can be represented through comparing the growing of surface resistance over time, which is reflected by the value of parameter A. When the superplasticizer dosage is different, such as the study in Section 3.4.2.3, each mixture was tested under around RH50%. According to the results in Figure 3.11 and Figure 3.12, the parameter A measured under RH100% is usually much smaller than that under RH50%, so it can be approximated that the tested growing of surface resistance over time can represent the growing of the “elephant skin” over time.

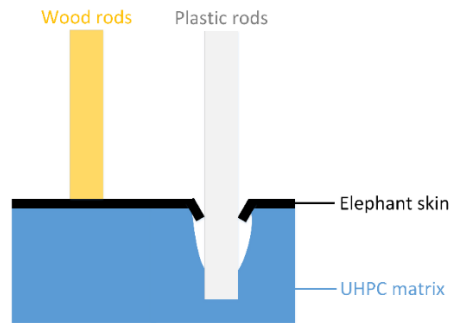


Figure 3.13 Schematic diagram of a movable rod going through the "elephant skin"

3.3 Influence of the “elephant skin” on the bonding performance between UHPC layers

To study the influence of the “elephant skin” on the bonding performance of multi-layer UHPC, a number of double-layered UHPC beam specimens have been fabricated and subjected to 3-point bending and 4-point bending tests to observe cracking patterns and maximum bending stresses. The purpose is to show the prevalence of the “elephant skin” in UHPC and to investigate the effect of the growing of the “elephant skin” over time on the bonding performance of multilayer UHPC elements. Thus, in each bending test, only the maximum bending load was recorded and the failure mode was examined.

3.3.1 4-point bending test of 140×140×550mm³ beams

In this research, 6.5L of UHPC mixture with the same recipe as “720 CEM B” in Table 3.3 (Table A.2 in Appendix) were mixed four times (26L in total) by the Eirich mixer to cast two $140 \times 140 \times 550 \text{mm}^3$ beams to compare the bending behaviours of the double-layer beams with and without the “elephant skin”. The temperature and humidity of the environment were about 21°C and 40%, respectively.

With regard to the cast of the beams, as shown in Figure 3.14, firstly one-half beam was produced. Then water was sprayed on the surface of the UHPC. After 1h, the second half of the beam was cast to formulate a double-layer UHPC beam. For the second beam, after the half was cast, the UHPC was exposed to air to form the “elephant skin”. Then, after 1h, the second half was cast. In this way, two beams containing and not containing the “elephant skin” at the bonding surface were produced.

The surface resistance-time curves of the UHPC mixtures are shown in Figure 3.15. It could be found that 1h after casting, the “elephant skin” was already very hard with a surface resistance of about 64.9kPa. Therefore, after two UHPC beams were placed in an open environment for 28 days, the 4-point bending tests were performed with a span of 450mm (150-150-150mm) according to ÖBV-Richtlinie “Faserbeton”, 2008 [109].

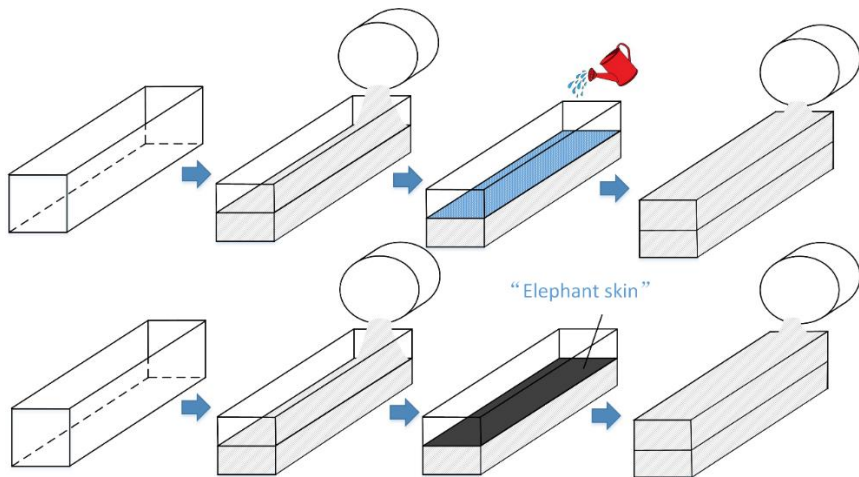


Figure 3.14 Casting procedures of the two beams

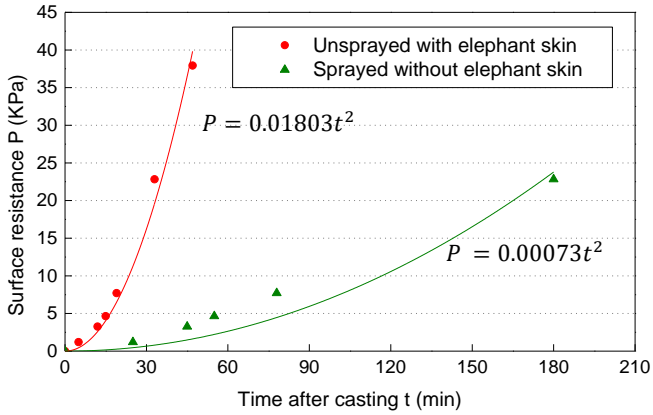
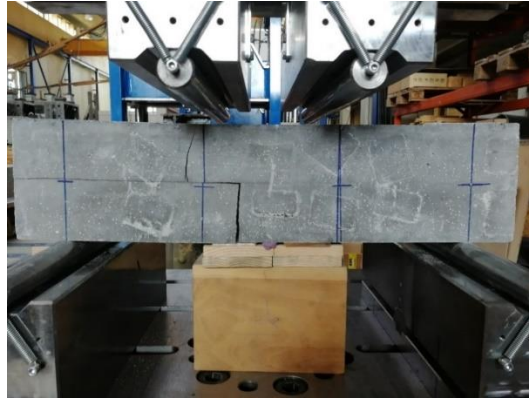


Figure 3.15 Surface resistance-time curves of the UHPC mixtures subject to 4-point bending tests

Figure 3.16 shows the failure modes of these two UHPC beams. It can be clearly seen that the first one was composed of two layers with no “elephant skin” in the lower layer and exhibited a typical bending failure with flexural cracks firstly starting from the bottom side of the beam and then propagating to the top surfaces of the beam; while the second one was composed of two layers with the “elephant skin” in the lower layer and the porous layer. One can clearly see that a crack in the joint zone between the upper and lower layer of the beam occurred, which affected the failure mode and maximum load of the beam.



(a) No “elephant skin” in the joint zone



(b) With an “elephant skin” in the joint zone

Figure 3.16 4-point-bending tests of double-layer UHPC beams, the beam with the “elephant skin” has a clear crack in the joint zone (indicating a shear failure due to the relative slide between the upper and lower layers)

Figure 3.17 shows the bending stress-midspan displacement curves of these two beams. The maximum bending stress of the beam with the “elephant skin” decreased by approximately 34.7%. This indicated that when there was no "elephant skin", the maximum bending stress could be considered to be the bending strength of the beam. However, when there was an "elephant skin" at the bond surface, the maximum bending stress was actually due to the horizontal shear force at the bond surface exceeding the shear bonding strength of the two elements, which was not the bending strength of the beam anymore. Based on these results, the existence of the “elephant skin” can decrease the bonding performance between the adjacent layers of UHPC in a multi-layer structure.

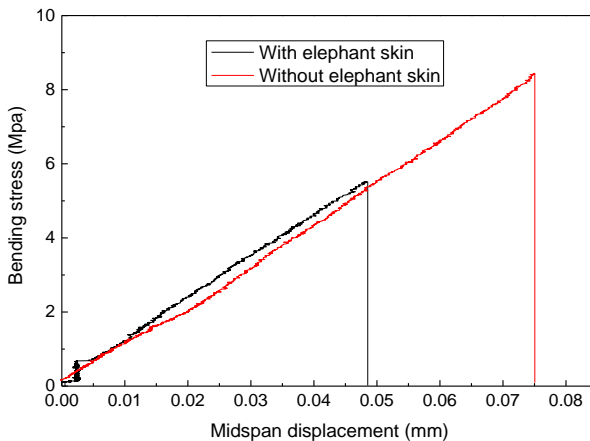


Figure 3.17 Bending stress-midspan displacement curves in the 4-point bending tests

3.3.2 3-point bending test of 150×150×700mm³ beams

Since the mid-span stress in the 3-point bending test was larger than that in the 4-point bending test due to the larger span and bending moment, for clearer detecting the detrimental impacts of the “elephant skin”, another group of 3-point bending tests was also performed. In this group, 40L of UHPC mixture with the same recipe as “720 CEM A” in Table 3.3 was mixed with the ELBA mixer to manufacture two 150×150×700mm³ beams. The temperature and humidity of the environment were about 19.1°C and 55%, respectively. The casting process of the beams was similar to the last group used for 4-point bending tests in Figure 3.14. Firstly, half of each beam was cast. Then water was sprayed on the concrete surface of one beam, while that of the other beam was exposed to air to form the “elephant skin”. After 1h, the second half of each beam was cast to make two double-layer UHPC beams. After curing the beams in the 80°C hot water for 48h, the 3-point bending tests were performed with a span of 600mm (300-300mm), as shown in Figure 3.18.

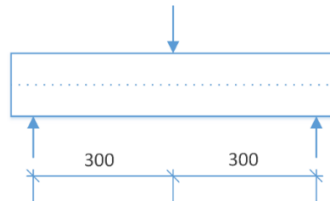


Figure 3.18 Schematic diagram of 3-point bending test for double-layer UHPC beams

The photos of the UHPC surfaces after casting for 1h are shown in Figure 3.19. The surface resistance-time curves of this UHPC mixture are shown in Figure 3.20. The cracks of the beams are shown in Figure 3.21. It can be seen that the “elephant skin” in this test was not as strong as that in the previous 4-point bending test, this might be due to the lower temperature and higher humidity of the environment. Although the crack was not that clear, it could also be seen that the beam with the “elephant skin” had a horizontal crack along the bonding surface between the upper and lower layers.



(a) Unsprayed surface



(b) Sprayed surface

Figure 3.19 Photos of concrete surfaces 1 hour after casting

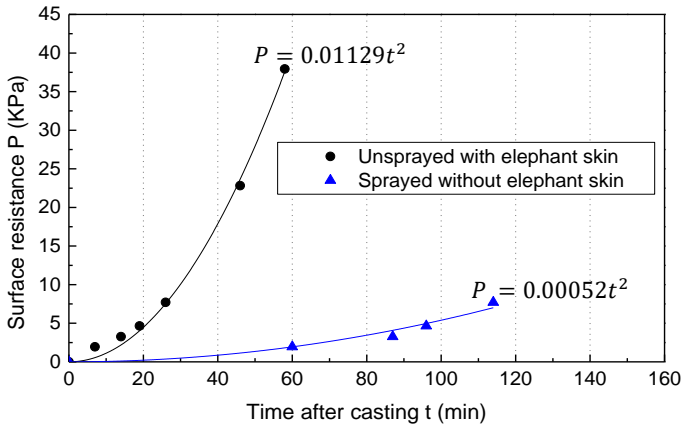
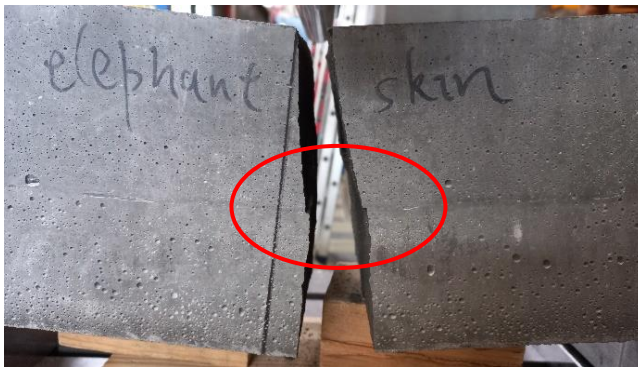


Figure 3.20 Surface resistance-time curves of the UHPC mixture subjected to 3-point bending tests



(a) No “elephant skin” in the joint zone



(b) With an “elephant skin” in the joint zone

Figure 3.21 3-point-bending tests of double-layer UHPC beams, the crack of the beam with “elephant skin” is not clear but occurred in the joint zone

Figure 3.22 shows the bending stress-midspan displacement curves of these two beams under the 3-point bending tests. At this time, the maximum bending stress of the beam with the “elephant skin” decreased by approximately 18%, which also showed the adverse impact of the existence of the “elephant skin” on the bonding performance of the double-layer UHPC beam.

It should be noted that there was a large difference between the results of the maximum bending stresses of these two groups of UHPC beams. The reasons can be as follows: 1) the UHPC mixture in 3-point bending tests contained CEM A, which was stronger than the CEM B used in the UHPC mixture in previous 4-point bending tests; 2) the UHPC beams in 3-point bending tests cured in 80°C hot water for 48h had higher compressive strength than those in 4-point bending tests placed in the open environment for 28 days (the maximum compressive strength of the UHPC mixture in 3-point bending tests was measured to be 184.3MPa, while unfortunately, the compressive strength of the UHPC mixture in 4-point bending test was not available); 3) when the UHPC specimen was placed in an open environment after final setting, the continuous loss of water caused a certain degree of shrinkage near the surface, while the core area wasn’t influenced, which would cause some small failures or microcrack inside the specimen before the test, leading to a significant decrease on the bending strength of plain UHPC.

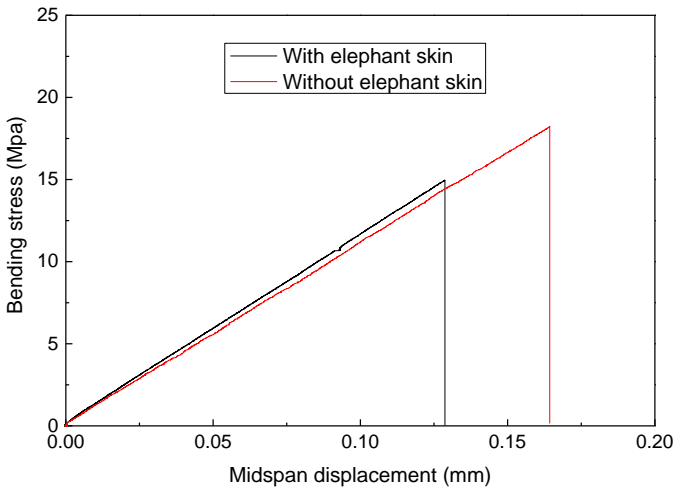


Figure 3.22 Bending stress-midspan displacement curves in the 3-point bending tests

Nonetheless, according to the results, it can be seen that the existence of the “elephant skin” in the joint surface between the upper and lower UHPC layers can cause a change in the

failure mode and a decrease in the bending strength of the beams, irrespective of the concrete properties and loading conditions.

3.3.3 3-point bending tests of 40×40×160mm³ prisms

To further study the influence of the “elephant skin” on the bonding performance between adjacent UHPC elements, 3-point bending tests of small beams (prisms) were also performed [110]. According to the results in Section 3.3.1 and 3.3.2, it can be found that the higher the surface resistance, the lower the maximum bending stress, which means, the stronger the “elephant skin”, the larger its influence on the bending strength. Therefore, the aim of this section is to find the relationship between the maximum bending stress and the surface resistance of the “elephant skin” and try to give acceptable values of surface resistance in order to provide a basis for determining the range of values for parameter A.

The UHPC mixture mixed in the ELBA mixer in Section 3.3.2 with the recipe “720 CEM A” was also cast into 15 prisms with a size of 40×40×160mm³ through upper and lower layers, and one 100×250×30mm³ plate to test the growing of the “elephant skin”. Additionally, to investigate the results of UHPC mixtures with StF, two more UHPC mixtures (“750 1%” and “860 2%”) containing 1 vol. % and 2 vol. % of StF1, respectively, were also mixed in an Eirich mixer. For each UHPC mixture, 10 prisms and 1 plate were cast due to the smaller mixing capacity. Detailed mix recipes of these UHPC mixtures can be found in Table A.2 in the appendix. In the names of the UHPC mixtures, “750” and “860” are the cement contents, and the “1%” and “2%” are the StF volume contents.

The casting method of the prisms was: the lower layers (20×40×160mm³) of all the prisms were cast directly after mixing, and the upper layers (20×40×160mm³) of 3 (or 2) prisms were also cast directly. Afterwards, every 30 minutes, the upper layers (20×40×160mm³) of 3 (or 2) prisms were cast. The centre line in the mould was marked before casting to ensure that each prism was cast exactly in layers of the same size. This means that the upper layers of the prisms were cast after the formation of the “elephant skin” on the surface of the lower layers for 0min, 30min, 60min, 90min and 120min respectively, so as to investigate the influence of the “elephant skin” with difference surface resistances, as shown in Figure 3.23. The temperature and humidity of the environment during the manufacture of the prisms were about 21.2°C and 57%.

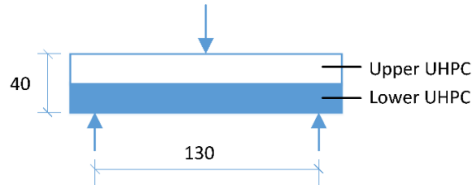


Figure 3.23 Schematic diagram of three-point bending test of small prisms

Figure 3.24 shows the surface resistance-time curves of the “elephant skin” for the tested UHPC mixtures. Through fitting by use of the quadratic equation, the surface resistance of each “elephant skin” can be estimated. However, the curves in Figure 3.24 cannot be directly compared with each other due to their different raw material batches and mixing conditions. The influence of StF will be analysed in Section 3.4.2.

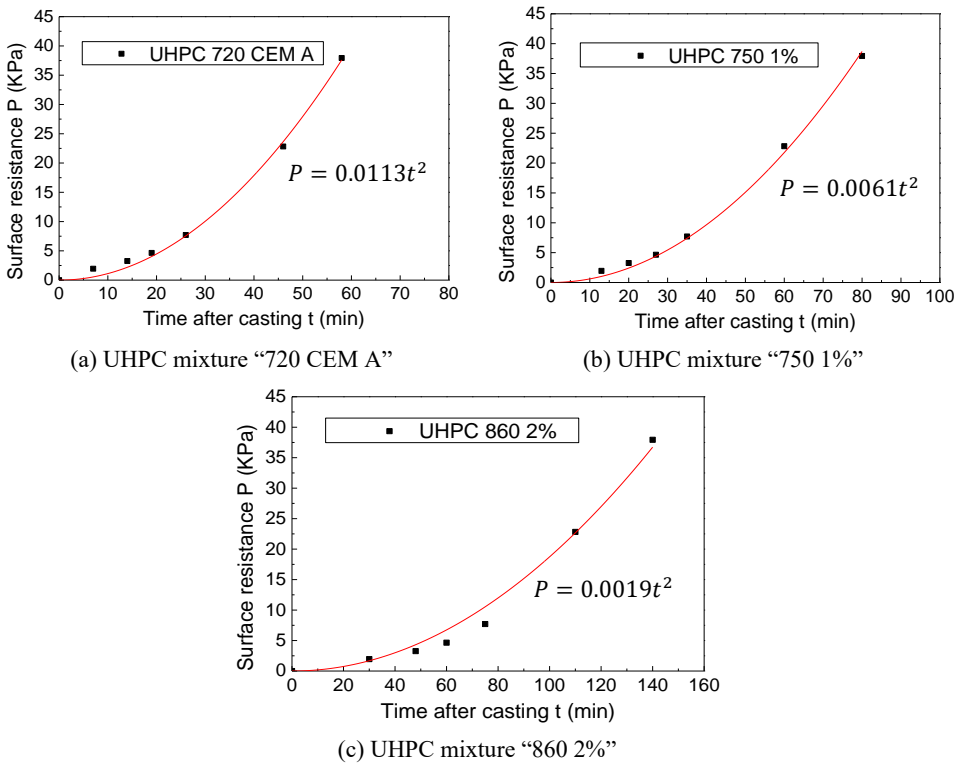


Figure 3.24 Surface resistance-time curves of the concrete in the small 3-point bending tests

Figure 3.25 shows the broken samples of the UHPC mixture with recipe “720 CEM A” without StF of different casting time intervals. Figure 3.26 shows the broken samples of the UHPC mixture with recipe “860 2%” with 2% StF of different casting time intervals. From

the photos of the broken samples without StF, the cracks on the interface were not very clear due to the low loading force, only a little occurred on the samples with a casting time interval of 120mm. But from the photos of the broken samples with 2% StF, it could be seen that the cracks of the sample of 60min were close to the bonding surface, and the cracks of the sample with a casting time interval of 120min occurred directly on the bonding surface.



(a) 0min



(b) 60min



(c) 120min

Figure 3.25 Broken UHPC prisms of Recipe “720 0%” with different cracking patterns after the 3-point bending tests

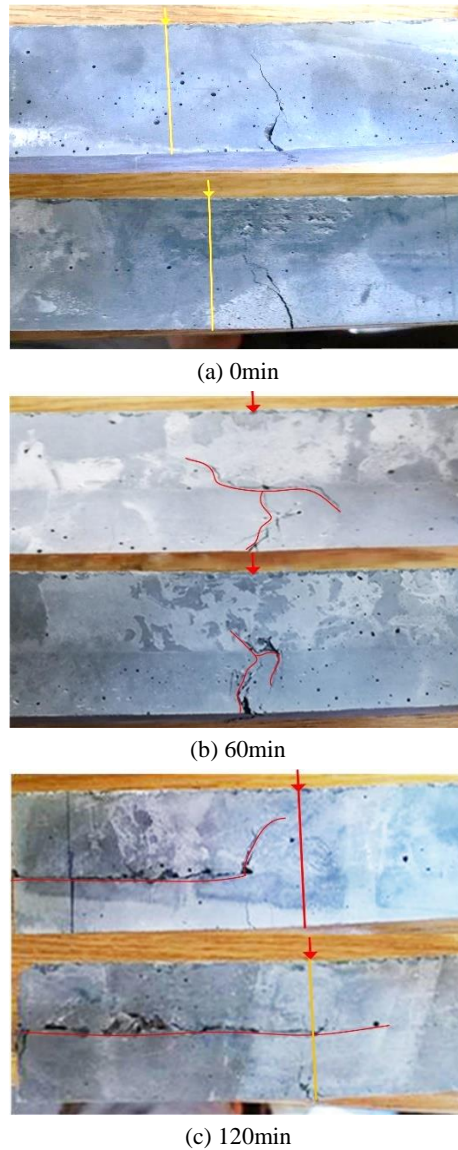
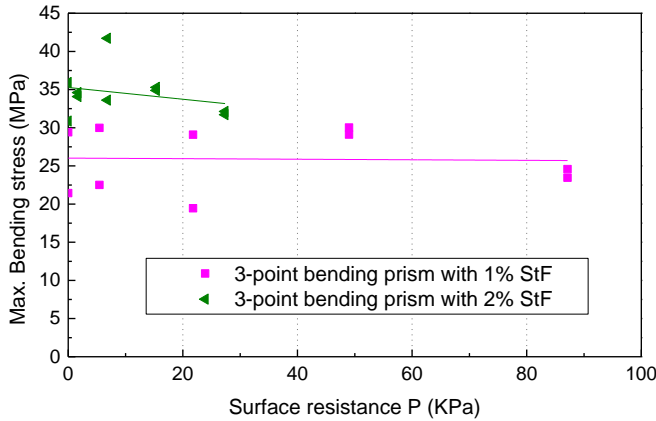


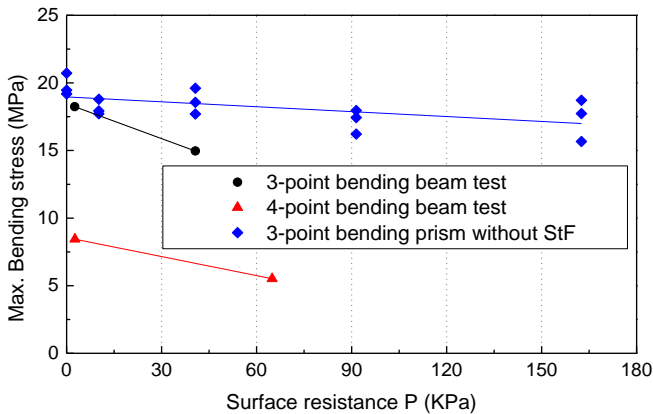
Figure 3.26 Broken UHPC prisms of Recipe “860 2%” with different cracking patterns after the 3-point bending tests

Combined with the results of 3-point bending tests and 4-point bending tests for the beams and prisms, the surface resistance-maximum bending stress relationship curves can be drawn, as shown in Figure 3.27. Since the materials, mix recipes and curing processes of these UHPC mixtures were different, the maximum bending stresses were also different. It can be found that although the cracks at the interface were evident in the broken samples with a casting

interval of 60min-120min, the results of UHPC mixtures with StF (Figure 3.27(a)) showed very significant scattering. It should be noticed that when StF was incorporated into the concrete mixture, the maximum bending stress of the UHPC was mainly influenced by the fibre distribution and orientation. Thus, in this case, the effect of the “elephant skin” on the bonding performance couldn’t be simply explored by comparing the maximum bending stress. However, when the experimental results containing StF were excluded, it could be seen from the other results (Figure 3.27(b)) that a higher surface resistance P, meaning a stronger “elephant skin”, could lead to a lower maximum bending stress of double-layer beams by reducing the bonding performance.



(a) UHPC mixtures with StF



(b) UHPC mixtures without StF

Figure 3.27 Relationship between the maximum bending stress and the surface resistance of the “elephant skin”

In order to investigate the clear relationship between the maximum bending stress and the surface resistance of the “elephant skin”, Figure 3.28 shows the percentage normalization of the results of three groups of UHPC mixtures without StF and the fitting curves. It can be found that when the growing of the “elephant skin” over time (as shown in Figure 3.20 and Figure 3.24) is similar, with the increase in the surface resistance, the bending strength of the small double-layered concrete prisms appeared to decrease to a lesser extent than that of the big beams. This may be because the shear stress in the middle section was higher in the small prism than in the large beam due to the smaller size. The effect of the “elephant skin” led to the destruction of the specimen not because the bending stress reached the bending strength but because the shear stress in the middle section reached the bonding strength of the two layers. Nevertheless, from the results in Figure 3.28, when considering a maximum bending stress drop of not more than 80%, the concrete surface resistance caused by the “elephant skin” should be better not to exceed 40kPa.

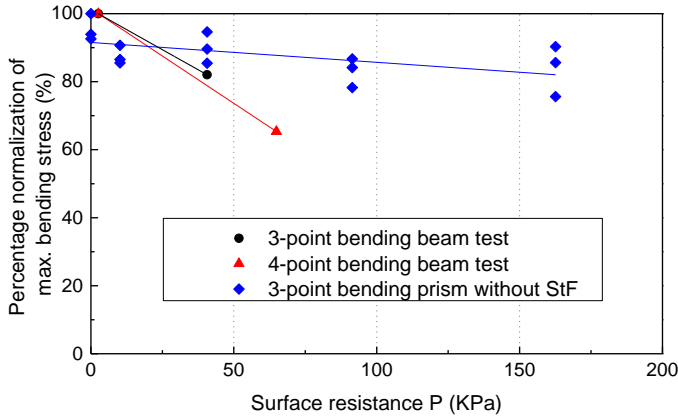


Figure 3.28 Reduction of the maximum bending stress of UHPC with the surface resistance of the “elephant skin”

In addition, when multiple-layer concrete elements are produced, the second layer can also be poured by means of a falling impact from a height to break through the “elephant skin” that has been formed, in order to prevent the “elephant skin” from adversely affecting the bond performance and to achieve a good combination. However, it should be noted that the free fall height of concrete has a limit, otherwise separation may occur during pouring. Standard IS 456 [111] specifies a maximum permissible free fall height for NSC of 1.5m. Since UHPC may be able to reduce the probability of separation due to its high viscosity and small particle size, the ÖBV-Richtlinie “UHPC” [20] states that the maximum fall height of UHPC can be up to 5m.

Accordingly, considering the possibility of pouring NSC on the surface of UHPC with the “elephant skin” (UHPC-NSC combined element), the maximum free fall height should be taken as 1.5m. Considering the density of concrete is about 2400 kg/m^3 , the impact pressure in contact with the “elephant skin” can be calculated as 35.28kPa. Therefore, from this point of view, combined with the results of the bending tests, the surface resistance of the “elephant skin” can be considered acceptable when it is less than 35.28kPa. In the large-scale application of UHPC, it is considered that the concrete surface can be sprayed with water and other treatments within 1h at the longest after the concrete is poured, so the surface resistance caused by the “elephant skin” within 60min should be less than 35.28kPa. After taking these into the quadratic equation “ $P=At^2$ ”, it can be concluded that when the parameter A is less than 0.0098, the “elephant skin” on the surface is acceptable.

It is worth noting that the initial setting time of the UHPC mixture in Figure 3.15 is different from that of the UHPC mixture in Figure 3.20. However, it can be seen in Figure 3.28 that when 1h after casting, the surface resistance contributed by the initial setting of the concrete is much smaller than the surface resistance due to the “elephant skin”. Moreover, the two UHPC mixtures with different initial setting times show similar effects, thus this also proves that the growing of surface resistance over time can be used to represent the growing of the “elephant skin” over time when the RH is not very high.

3.4 Influencing factors on the growing of the “elephant skin”

3.4.1 Temperature and evaporation rate

3.4.1.1 Temperature

According to Section 3.1, many studies also reported that temperature was another important factor that influenced the growing of the “elephant skin” on UHPC surface. According to Section 3.2, humidity can have a direct effect on the growing of the “elephant skin”. Thus, it can be considered that the growing of the “elephant skin” is related to surface evaporation.

Consequently, in this section, the influence of temperature on the “elephant skin” formation was investigated in terms of the external temperature and internal temperature of the UHPC mixtures. The external temperature was the temperature of the environment, which was monitored by the air conditioner in the laboratory. The internal temperature was the

temperature in UHPC after mixing, which was controlled by altering the mixing processes on the premise of preserving materials and recipes.

This study considered three different mixing procedures to generate different temperatures in freshly mixed UHPC: (i) the mixing process introduced in Section 2.2 with gradual addition of the raw materials and a cooling interval; (ii) the powder materials and aggregates were mixed together before adding water and superplasticizer, and the mixing was continuous during the process without stop; (iii) the aggregates were heated to 40°C prior to the concrete manufacture to simulate the possible solar heating in practical project, there was also no stop during the mixing process. Compared with Figure 2.5, the mixing procedures (ii) and (iii) in these tests are shown in Figure 3.29. Although these three mixing procedures were different, considering that the total mixing time might have an influence on the workability issues (see analysis in Chapter 4), the total mixing time for all three was kept at 15min.

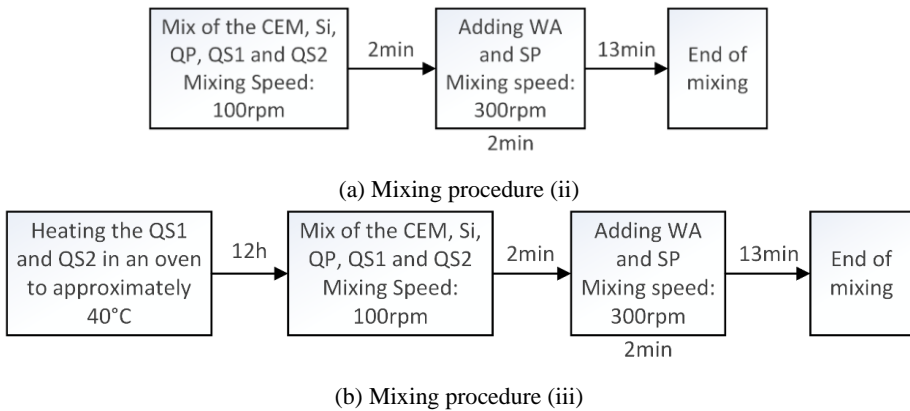


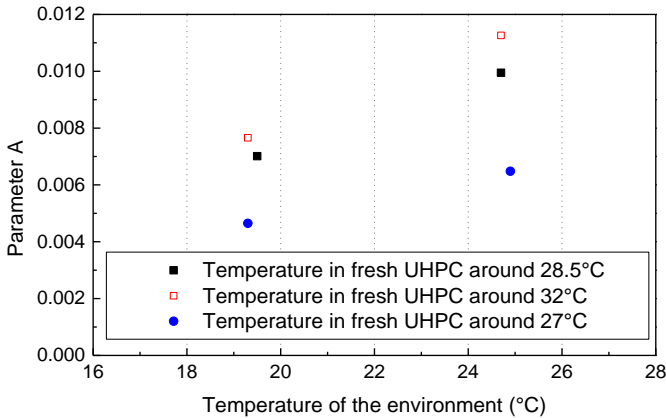
Figure 3.29 Flow diagram of the mixing procedures (ii) and (iii)

Considering the co-influences of RH and temperature, UHPC mixtures with the same recipe as “720 CEM A” in Table 3.3 were mixed at various external temperatures and internal temperatures with the same RH of 37%. As shown in Table 3.4, 7 batches of UHPC mixtures were mixed on the same day with 3 mixing procedures (to control the internal temperature in the UHPC mixture) and 2 external temperature conditions by changing the setting of the air conditioner in the laboratory. The measured flowability and compressive strength of each UHPC mixture with different temperatures exhibited similar properties, which were not significantly affected by the temperature and mixing procedures.

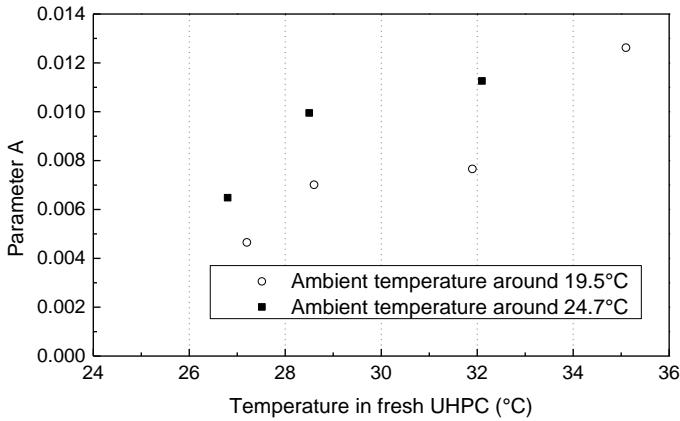
The relationship between parameter A (which reflects the growing of the “elephant skin” over time on the UHPC surface) and the external temperature, as well as the relation between parameter A and the internal temperature, are respectively shown in Figure 3.30. It can be found that the increase of both the external temperature and the internal temperature may increase the growing of the “elephant skin” over time.

Table 3.4 UHPC mixtures with different external and internal temperatures

UHPC mixture	Ambient temperature (°C)	Temperature in fresh UHPC (°C)	Spread-flow (cm)	Compressive strength (MPa)	Parameter A
3.4.1-1	19.3	27.2	26	193.8	0.00465
3.4.1-2	19.3	28.5	26	197.9	0.00701
3.4.1-3	19.6	35.1	26.5	193.1	0.01262
3.4.1-4	24.9	26.8	26	189.9	0.00648
3.4.1-5	24.7	28.5	25	191.1	0.00995
3.4.1-6	24.7	32.1	25.5	192.3	0.01126
3.4.1-7	19.3	31.9	25	-	0.00766



(a) Effect of ambient temperature



(b) Effect of temperature in fresh UHPC mixtures

Figure 3.30 Influence of different temperatures on the growing of the “elephant skin” over time

3.4.1.2 Evaporation rate

To characterise the combined effect of external temperature, internal temperature, and RH, the evaporation rate of the concrete surface was calculated according to Paul J Uno as the following formula [112]:

$$E = 5 \left([T_c + 18]^{2.5} - r \cdot [T_a + 18]^{2.5} \right) (V + 4) \times 10^{-6} \tag{3.1}$$

where: E is the evaporation rate of the concrete (kg/m²/h); T_c is the temperature in fresh concrete (°C); T_a is the ambient temperature (°C); r is the relative humidity (-); and V is the wind velocity (km/h).

This formula is based on the popular evaporation rate nomograph from ACI 305R, as shown in Figure 3.31 [113].

Thus, for the UHPC mixtures with the same recipe “720 CEM A” in Section 3.2, 3.3 and 3.4.1, the evaporation rates can be calculated considering the general wind velocity in the laboratory of 1~1.5 km/h according to Baldwin P and Maynard A [114]. When correlated with the results of parameter A, the relationship between the evaporation rate and parameter A can be shown in Figure 3.32. The results are essentially linear, so after fitting the relationship equation can be assumed to be ($R^2=0.991$):

$$A = 0.0479E - 0.0078 \tag{3.2}$$

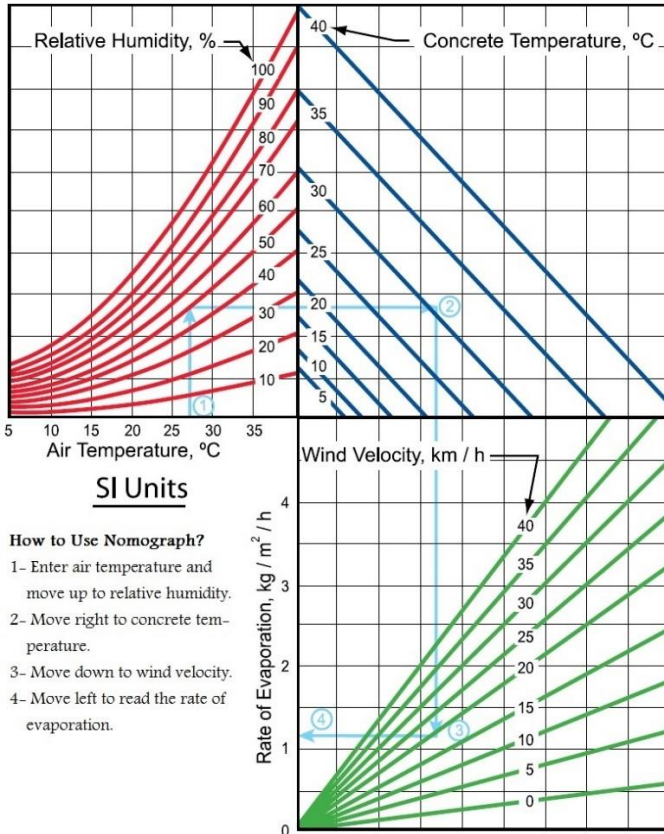


Figure 3.31 Nomograph to Estimate Rate of Evaporation on Concrete Surface in SI Unit [113]

Combining Equations (3.1), and (3.2), the following equation can be obtained:

$$A = 0.04795 \left([T_c + 18]^{2.5} - r \cdot [T_a + 18]^{2.5} \right) (V + 4) \times 10^{-6} - 0.0078 \tag{3.3}$$

Therefore, according to the conclusions of Section 3.3, the parameter A should better not exceed 0.0098 so that the “elephant skin” can be treatable. Consequently, it can be calculated that the evaporation rate should not exceed 0.36kg/m²/h for the UHPC mixture with the recipe "720 CEM A", which is also the reference mix proportion in this research (Table 2.5). When the mixing procedure in Figure 2.5 is used, the temperature in the fresh state is typically around 29°C for UHPC mixtures with the "720 CEM A" ratio. As a result, the evaporation rate can be controlled by the ambient temperature, RH and wind velocity in large-scale applications.

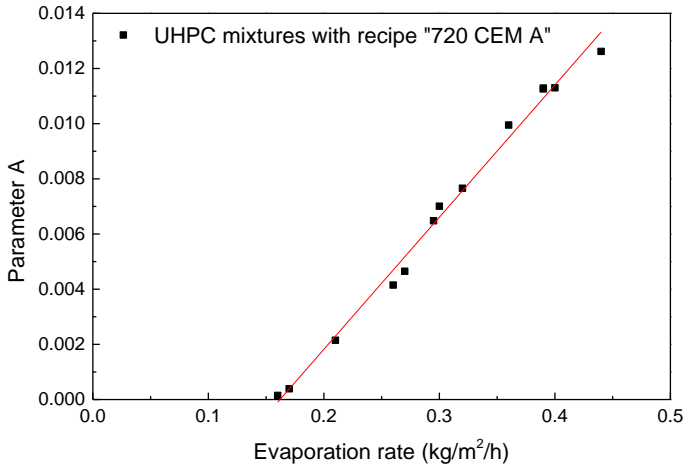


Figure 3.32 Relationship between evaporation rate and parameter A for the UHPC mixtures with the same recipe “720 CEM A”

Figure 3.33 shows the relationship between the evaporation rate and parameter A for the UHPC mixtures with different recipes. It can be seen that there is a certain degree of discreteness, indicating that in addition to the evaporation rate, the mix proportion of concrete seems also to have an influence on the growing of the “elephant skin” over time. As a result, the moisture evaporation of the concrete surface may not be the only reason for the formation and growing of the “elephant skin”.

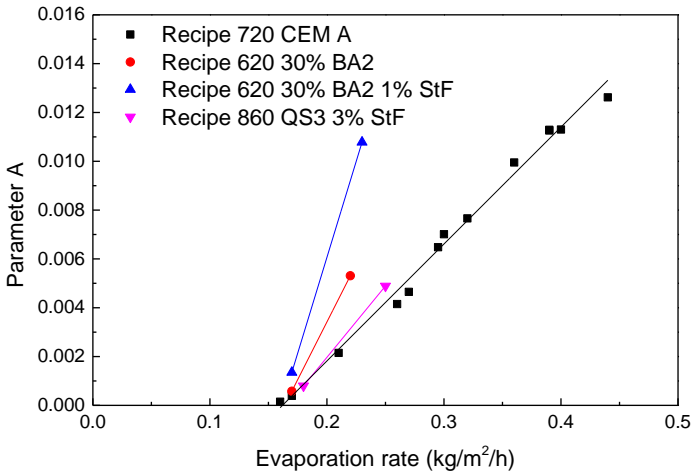


Figure 3.33 Relationship between evaporation rate and parameter A for the UHPC mixtures with the different recipes

3.4.2 UHPC components

Based on the investigation in the previous section, it can be seen that different UHPC recipes lead to different effects of evaporation rates on the "elephant skin". Therefore, based on the research in Section 2.3, this section investigates the effects of different contents of UHPC components on the growing of the "elephant skin" over time, while trying to keep the evaporation rates of the concrete surfaces the same (same RH, ambient temperature, mixing process, etc.).

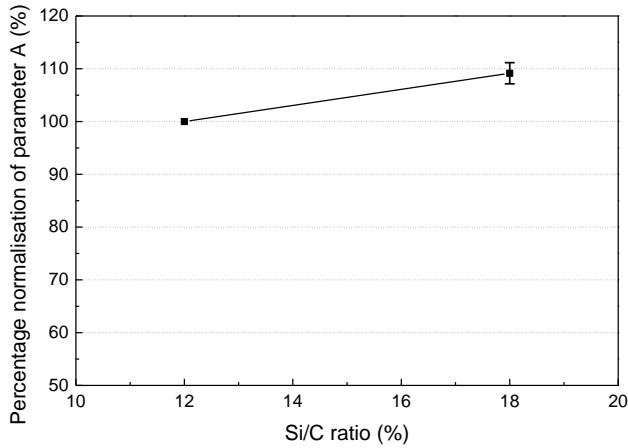
3.4.2.1 Silica fume and quartz powder

According to the research in Section 2.3.1, the dosages of Si and QP in UHPC can range between 12-18% and 30-40% of the cement mass, respectively. For investigation of the influences of the Si/C ratio and QP/C ratio on the growing of the “elephant skin” over time, the UHPC mixtures in the group 2.3.1-1 were also cast into the 100×250×30mm³ plates to compare the parameters A, as shown in Table 3.5. The ambient RH and temperature for this group were the same as 70% and 21.2°C. The temperatures in these fresh UHPC mixtures didn’t have big differences (Table 2.6). It can be assumed that these UHPC mixtures had similar surface evaporation rates.

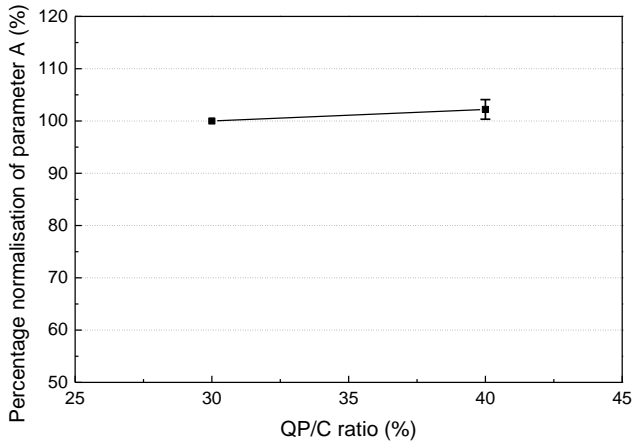
Table 3.5 UHPC mixtures in Group 2.3.1-1

Group	UHPC mixture	Si/C ratio (%)	QP/C ratio (%)	Parameter A
2.3.1-1	720 12% 30%	12	30	0.00269
	720 18% 30%	18	30	0.00299
	720 12% 40%	12	40	0.0028
	720 18% 40%	18	40	0.003

Figure 3.34 shows the results of the influences of the Si/C ratio and QP/C ratio on the parameter A after percentage normalization from the UHPC mixtures with 12% Si/C ratio and 30% QP/C ratio and statistical analysis. It can be seen that both a higher Si/C ratio and higher QP/C can enhance the growing of the “elephant skin” over time. Although only two sets of Si/C and QP/C ratios were tested in this study, considering that when the W/C ratio remained unchanged, more Si and QP powders directly led to a higher powder (CEM, Si, QP) content on the UHPC surface, it could be assumed that Si/C and QP/C ratios linearly affected the growing of the "elephant skin" over time. Thus, the following equations can be estimated:



(a) Si/C ratio



(b) QP/C ratio

Figure 3.34 Influences of the contents of Si and QP on the growing of the “elephant skin” over time

$$\frac{A_{Si/C}}{A_{Si/C=0.12}} = 1.5246 \times Si / C + 0.8171 \tag{3.4}$$

where: $A_{Si/C}$ is the required parameter A; $A_{Si/C=0.12}$ is the parameter A when the Si/C ratio is 0.12 and other factors remain unchanged.

$$\frac{A_{QP/C}}{A_{QP/C=0.3}} = 0.2212 \times QP / C + 0.9337 \tag{3.5}$$

where: $A_{QP/C}$ is the required parameter A; $A_{QP/C=0.3}$ is the parameter A when the Si/C ratio is 0.3 and other factors remain unchanged.

Combining Equations (3.2), (3.4) and (3.5), it can be concluded that when the evaporation rate, Si/C ratio and QP/C ratio are varied from the reference recipe of UHPC in Table 2.5, the parameter A of the growing of the “elephant skin” can be calculated by the following equation:

$$A = (0.0479 * E - 0.0078) (1.5246 * Si / C + 0.8171) (0.2212 * QP / C + 0.9337) \quad (3.6)$$

Combined with the results of Section 2.3.1, unless special application requirements, the Si/C ratio and the QP/C ratio should be as low as possible above 12% and 30%, respectively, which is also beneficial in slowing down the growing of the “elephant skin”.

3.4.2.2 Water-to-binder ratio

In this research, the influence of the W/B ratio on the growing of the “elephant skin” over time was also investigated. Based on the research in Section 2.3.2, the parameter A was also tested for the UHPC mixtures in the groups “2.3.2-1”~“2.3.2-6”, as shown in Table 3.6. The ambient RH and temperature for this group were the same as 70% and 21.2°C. However, according to the results in Figure 2.9, the W/B ratio is approximately linearly related to the normalised percentage of temperature in fresh UHPC mixtures. With a constant laboratory wind velocity, it can be assumed that the normalised percentage of evaporation rate on the surface of the UHPC mixtures in this section has also a relationship with the W/B ratio. This can also be estimated from Equation (2.3) and Equation (3.1) according to Paul J Uno [112] to the following equation:

$$\sqrt[2.5]{\frac{E_{W/B}}{E_{W/B=0.223}}} = -4.4368 \times W / B + 1.9894 \quad (3.7)$$

where: $E_{W/B}$ is the required evaporation rate ($\text{kg}/\text{m}^2/\text{h}$); $E_{W/B=0.223}$ is the evaporation rate when the W/B ratio is 0.223 and other factors remain unchanged ($\text{kg}/\text{m}^2/\text{h}$). From this equation, it can be concluded that an increase in the W/B ratio may lead to a decrease in the evaporation rate of concrete.

Table 3.6 UHPC mixtures in Groups 2.3.2-1~2.3.2-6 in Section 2.3.2

Group	Name	Tested W/B ratio	Corresponding W/C ratio	Parameter A
2.3.2-1	720 12% 30%	0.223, 0.241	0.25, 0.27	0.00269, 0.00083
2.3.2-2	720 18% 30%	0.212, 0.223	0.25, 0.264	0.00299, 0.00145
2.3.2-3	720 12% 40%	0.223, 0.228	0.25, 0.255	0.00275, 0.00234
2.3.2-4	720 18% 40%	0.212, 0.223	0.25, 0.264	0.003, 0.00141
2.3.2-5	620	0.223, 0.25	0.25, 0.285	0.01022, 0.00182
2.3.2-6	860	0.205, 0.223	0.23, 0.25	0.00228, 0.00068

Figure 3.35 shows the results of the influence of the W/B ratio on the parameter A after percentage normalization from the UHPC mixtures with 0.223 W/B ratio and statistical analysis. It can be seen that a higher W/B ratio can decrease the growing of the “elephant skin” over time. There seems to be a relationship between the parameter A and the W/B ratio with a high degree polynomial equation. When the curve is fitted with a small error ($R^2=0.994$), the following equation can be estimated:

$$\sqrt[7.8]{\frac{A_{W/B}}{A_{W/B=0.223}}} = -8.7244 \times W / B + 2.954 \tag{3.8}$$

where: $A_{W/B}$ is the required parameter A; $A_{W/B=0.223}$ is the parameter A when the W/B ratio is 0.223 and other factors remain unchanged.

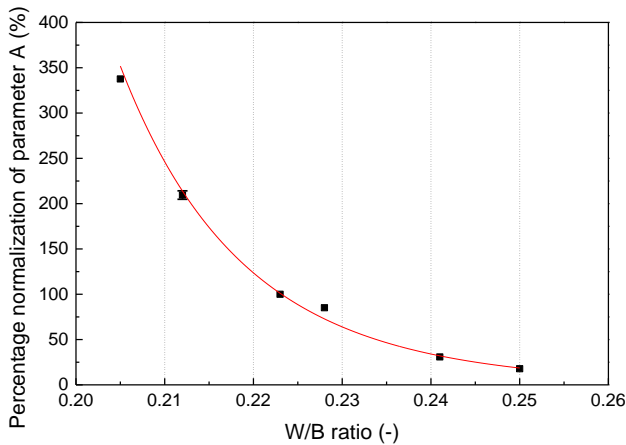


Figure 3.35 Influence of W/B ratio on the growing of the “elephant skin” over time

Comparing Equation (3.7) with Equation (3.8), it can be concluded that the effect of the W/B ratio on parameter A is not only through the effect of the W/B ratio on the temperature in the fresh concrete and thus on the evaporation rate. A higher W/B ratio also increases the free water in the UHPC mixture, which may be the main reason for slowing down the growing of the “elephant skin” over time. Nonetheless, when bringing Equation (3.7) and Equation (3.8) into Equation (3.6), the following equation can be obtained:

$$A = \left(\frac{0.0479E}{(-4.4368 \times W / B + 1.9894)^{2.5}} - 0.0078 \right) (1.5246 \times Si / C + 0.8171) \quad (3.9)$$

$$\times (0.2212 \times QP / C + 0.9337) (-8.7244 \times W / B + 2.954)^{7.8}$$

In summary, an increase in the W/B ratio will be beneficial in slowing down the growing of the “elephant skin” over time. According to the results of Section 2.3.2, when the W/B ratio is not higher than 0.25, a higher W/B ratio is preferable.

3.4.2.3 Superplasticizer dosage

As shown from the investigation carried out in Section 2.3.3, the superplasticizer has a particular effect on the flowability of the UHPC mixture: the flowability of concrete increases with the increase of the SP/B ratio before reaching a critical value. After that, a further increase of the SP/B ratio no longer affects the flowability of the UHPC mixtures, but only has a retarding effect on the changing of the consistency over time. Therefore, the investigation of the influence of the SP/B ratio on the growing of the “elephant skin” can also be considered from two parts: the SP/B ratio higher than the critical value and the SP/B ratio lower than the critical value.

As shown in Table 3.7, the groups “720 0.241” (2.3.3-2) and “860 0.223” (2.3.3-6) in Table 2.8 were chosen to investigate the influence of low SP/B ratio on the formation of the “elephant skin”. The UHPC mixtures in these two groups were also tested for the parameters A. Except that, two more groups “720 0.223” and “860 0.223 (high)” of UHPC mixtures with different high SP/B ratios were tested. In the name of the recipes, “720” and “860” represent the cement contents (kg/m³) and “0.223” and “0.241” are the W/B ratios. Detailed mix recipes and properties of the groups “720 0.223” and “860 0.223 (high)” can be found in Table A.3 in the appendix. The UHPC mixtures in each group had similar temperatures in fresh concrete. The ambient RH and temperature were also the same for each group. Thus, the evaporation rates of the UHPC mixtures in each group could also be considered the same, which were calculated as shown in Table 3.7.

Table 3.7 UHPC mixtures in Groups 2.3.3-2, 2.3.3-6 and new Groups 3.4.2.3-1 and 3.4.2.3-2

Group	Name	Tested SP/B ratio (%)	Corresponding SP/C ratio (%)	Parameter A	Evaporation rate (kg/m ² /h)
2.3.3-2	720 0.241	1.52, 1.65, 2.68	1.7%, 1.85%, 3%	0.00771, 0.00288, 0.00083	0.25
2.3.3-6	860 0.223	1.52, 1.61, 2.68	1.7%, 1.8%, 3%	0.00791, 0.00479, 0.00068	0.21
3.4.2.3-1	720 0.223	2.23, 2.68, 4.46	2.5%, 3%, 5%	0.00423, 0.00275, 0.00165	0.25
3.4.2.3-2	860 0.223 (high)	1.96, 2.68, 4.46	2.2%, 3%, 5%	0.00309, 0.00215, 0.00121	0.19

Figure 3.36 shows the results of the influences of the SP/B ratio on parameter A after percentage normalization from the UHPC mixtures with a 2.68% SP/B ratio and statistical analysis. When considering from two parts, a higher SP/B ratio can decrease the growing of the “elephant skin” over time, while the low SP/B ratio part has a greater influence (steeper slope of the curve) than the high SP/B ratio part. Considering the critical value of the SP/B ratio is 1.86% according to the results in Section 2.3.3 when the curve is fitted with a small error ($R^2=0.892$), the following equations can be estimated:

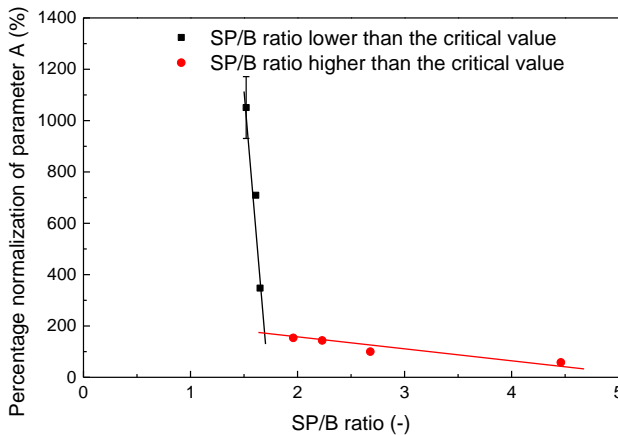


Figure 3.36 Influence of SP/B ratio on the growing of the “elephant skin” over time

$$\frac{A_{SP/B}}{A_{SP/B=2.68\%}} = \begin{cases} -5137.1 \times SP/B + 88.88, & SP/B \leq 1.86\% \\ -37.253 \times SP/B + 2.194, & SP/B \geq 1.86\% \end{cases} \quad (3.10)$$

where: $A_{SP/B}$ is the required parameter A; $A_{SP/B=2.68\%}$ is the parameter A when the SP/B ratio is 2.68% and other factors remain unchanged.

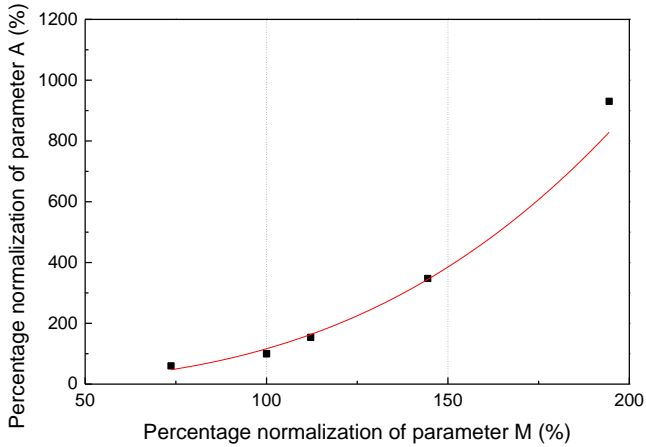
When bringing the Equation (3.10) into Equation (3.9), the following equation can be obtained:

$$A = \begin{cases} \left(\frac{0.0479E}{(-4.4368 \times W/B + 1.9894)^{2.5}} - 0.0078 \right) \\ \times (1.5246 \times Si/C + 0.8171) (0.2212 \times QP/C + 0.9337), & SP/B \leq 1.86\% \\ \times (-8.7244 \times W/B + 2.954)^{7.8} (-5137.1 \times SP/B + 88.88) & (3.11) \\ \\ \left(\frac{0.0479E}{(-4.4368 \times W/B + 1.9894)^{2.5}} - 0.0078 \right) \\ \times (1.5246 \times Si/C + 0.8171) (0.2212 \times QP/C + 0.9337), & SP/B \geq 1.86\% \\ \times (-8.7244 \times W/B + 2.954)^{7.8} (-37.253 \times SP/B + 2.194) & \end{cases}$$

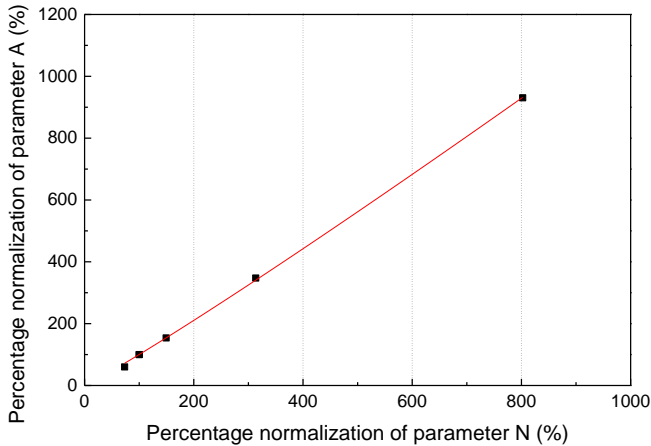
For the low SP/B ratio part, an increase in the SP/B ratio results in an increase in the flowability and a decrease in the viscosity of the UHPC mixture, which is actually due to more free water being released in the UHPC mixture. Consequently, like the influence of the W/B ratio, a higher SP/B ratio may have an effect on slowing down the growing of the "elephant skin" when the evaporation rate is nearly the same. For the high SP/B ratio fraction, according to the results in Section 2.3.3, an increase in the SP/B ratio may not change the flowability and viscosity of the UHPC mixture, which means no more free water can be released, but the changing of the concrete consistency over time can be slowed down. Consequently, when the evaporation rate, flowability and viscosity are nearly the same, the growing of the "elephant skin" over time may be influenced by the changing of the concrete consistency over time.

In order to verify this conclusion, the values of parameter M and parameter N were also examined for each UHPC mixture in groups "720 0.241" (2.3.3-2) and "720 0.223" (3.4.2.3-1) in Table 3.7 to characterise the changing of flowability and viscosity over time. After percentage normalization from the UHPC mixtures with a 2.68% SP/B ratio, the relationship between parameter A and parameter M and the relationship between parameter A and parameter N are shown in Figure 3.37. It can be seen that no matter whether the SP/B ratio is lower or higher than its critical value, an increase of parameter M or parameter N will lead to an increase of parameter A. In other words, a slower changing of the consistency of concrete over time can decrease the growing of the "elephant skin" over time. This is also

the reason why in Figure 3.36, when the SP/B ratio is lower than the critical value, as the SP/B ratio increases, parameter A decreases much more rapidly than when the SP/B ratio is higher than the critical value.



(a) Flowability changing over time



(b) Viscosity changing over time

Figure 3.37 Relationship between the changing of the consistency of UHPC over time and the growing of the “elephant skin” over time

Accordingly, a higher dosage of PCEs-based SP to slow down the changing of the consistency of the UHPC mixture over time could be helpful to decrease the growing of the “elephant skin” over time. In this way, some effective retarders can also be used to replace excess SP to save costs. However, in this research, 3 kinds of concrete retarding admixtures were tested, which were “Premment L 201”, “Premment H 1000” and “Premtard VZG 100

Long Time” from the company “BT3 Betontechnik”. But unfortunately, none of them had a good retarding effect for the UHPC mixtures with CEM A or CEM B in this research. This might be because both CEM A and CEM B are C₃A-free cement, which was not compatible with the above retarding admixtures. Thus, in the aspect of retarder, further investigation needs to be performed in the future.

In conclusion, combined with the results in Section 2.3.3, when the SP/B ratio is not higher than 3.57%, a higher SP/B ratio would be preferable.

3.4.2.4 Paste volume

In this research, to investigate the influence of the paste volume on the growing of the “elephant skin” over time, the UHPC mixtures in group 2.3.4-1 in Table 2.9 in Section 2.3.4 were also cast into the 100×250×30mm³ plates to compare the parameters A, as shown in Table 3.8. The ambient RH and temperature for this group were the same as 70% and 21.2°C. However, according to the results in Figure 2.14, the paste volume is approximately linearly related to the normalised percentage of temperature in fresh UHPC mixtures. With a constant laboratory wind velocity, it can be assumed that the normalised percentage of evaporation rate on the surface of the UHPC mixtures in this section has also a relationship with the paste volume. This can also be estimated from Equation (2.5) and Equation (3.1) to the following equation:

Table 3.8 UHPC mixtures in Group 2.3.4-1

Group	Name	CEM content (kg/m ³)	Corresponding paste volume (L/m ³)	Parameter A
2.3.4-1	0.223	620	479.5	0.01022
	2.68 0%	720	553.6	0.00275
		860	657.4	6.753E-4

$$\sqrt[2.5]{\frac{E_{CC}}{E_{CC=720}}} = -0.0006 * CC + 1.432 \quad (3.12)$$

where: CC is the cement content of the UHPC (kg/m³); E_{CC} is the required evaporation rate (kg/m²/h); $E_{CC=720}$ is the evaporation rate when the cement content is 720kg/m³ and other factors remain unchanged (kg/m²/h). From this equation, it can be concluded that an increase in the cement content (paste volume) leads to a decrease in the evaporation rate of concrete.

Figure 3.38 shows the results of the influences of the cement content (paste volume) on parameter A after percentage normalization from the UHPC mixtures with 720kg/m³ cement content. It can be seen that higher cement content (paste volume) can decrease the growing of the “elephant skin” over time. There seems to be a relationship between the parameter A and the cement content with multiple equation curves. When the curve is fitted with a small error (R²=0.995), the following equation can be estimated:

$$\sqrt[8.9]{\frac{A_{CC}}{A_{CC=720}}} = -0.0015 * CC + 2.08 \tag{3.13}$$

where: *CC* is the cement content of the UHPC (kg/m³); *A_{CC}* is the required parameter A; *A_{CC=720}* is the parameter A when the cement content is 720kg/m³ and other factors remain unchanged.

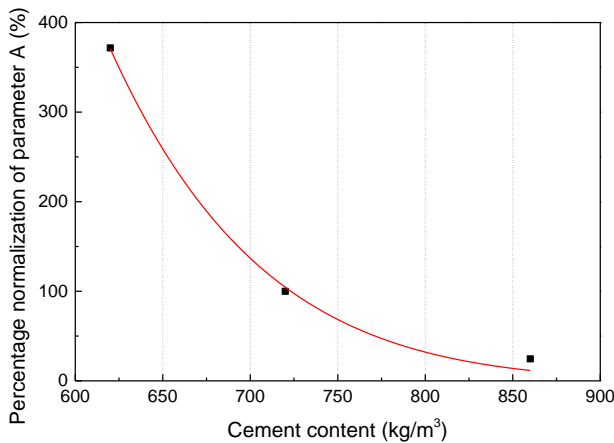


Figure 3.38 Influence of paste volume on the growing of the “elephant skin” over time

Comparing Equation (3.12) with Equation (3.13), it can also be concluded that the effect of the paste volume on the parameter A is not only through the effect of the cement content (paste volume) on the temperature in the fresh concrete and thus on the evaporation rate. In this case, when the cement content (paste volume) is higher, although the powder (CEM, Si, QP) content of the UHPC increased, the W/B ratio doesn’t change, it can be considered that the decrease in the growing of the “elephant skin” over time at this point is not a function of the powder content of the surface, nor of the free water in the UHPC mixture, but may only be a result of the consistency of the concrete.

Therefore, in combination with the results of Section 3.4.2.1-3.4.2.3, it can be surmised that the higher flowability and lower viscosity of the UHPC mixture may also slow down the growing of the "elephant skin" over time. However, this conclusion needs to be further confirmed by more experiments. Nonetheless, when bringing Equation (3.12) and Equation (3.13) into Equation (3.11), the following equation can be obtained:

$$A = \begin{cases} \left(\frac{0.0479E}{(-4.4368 \times W/B + 1.9894)^{2.5} (-0.0006 * CC + 1.432)^{2.5}} - 0.0078 \right) \\ \quad \times (1.5246 \times Si/C + 0.8171) (0.2212 \times QP/C + 0.9337) & , SP/B \leq 1.86\% \\ \quad \times (-8.7244 \times W/B + 2.954)^{7.8} (-5137.1 \times SP/B + 88.88) \\ \quad (-0.0015 * CC + 2.08)^{8.9} \end{cases} \quad (3.14)$$

$$A = \begin{cases} \left(\frac{0.0479E}{(-4.4368 \times W/B + 1.9894)^{2.5} (-0.0006 * CC + 1.432)^{2.5}} - 0.0078 \right) \\ \quad \times (1.5246 \times Si/C + 0.8171) (0.2212 \times QP/C + 0.9337) & , SP/B \geq 1.86\% \\ \quad \times (-8.7244 \times W/B + 2.954)^{7.8} (-37.253 \times SP/B + 2.194) \\ \quad (-0.0015 * CC + 2.08)^{8.9} \end{cases}$$

Combining Equations (3.1), and (3.14), the following equation can be obtained:

$$A = \begin{cases} \left(\frac{0.0479 \left([T_c + 18]^{2.5} - r \cdot [T_a + 18]^{2.5} \right) (V + 4) \times 10^{-6}}{(-4.4368 \times W/B + 1.9894)^{2.5} (-0.0006 * CC + 1.432)^{2.5}} - 0.0078 \right) \\ \quad \times (1.5246 \times Si/C + 0.8171) (0.2212 \times QP/C + 0.9337) & , SP/B \leq 1.86\% \\ \quad \times (-8.7244 \times W/B + 2.954)^{7.8} (-5137.1 \times SP/B + 88.88) \\ \quad (-0.0015 * CC + 2.08)^{8.9} \end{cases} \quad (3.15)$$

$$A = \begin{cases} \left(\frac{0.0479 \left([T_c + 18]^{2.5} - r \cdot [T_a + 18]^{2.5} \right) (V + 4) \times 10^{-6}}{(-4.4368 \times W/B + 1.9894)^{2.5} (-0.0006 * CC + 1.432)^{2.5}} - 0.0078 \right) \\ \quad \times (1.5246 \times Si/C + 0.8171) (0.2212 \times QP/C + 0.9337) & , SP/B \geq 1.86\% \\ \quad \times (-8.7244 \times W/B + 2.954)^{7.8} (-37.253 \times SP/B + 2.194) \\ \quad (-0.0015 * CC + 2.08)^{8.9} \end{cases}$$

In summary, an increase in the cement content (paste volume) will be beneficial in slowing down the growing of the "elephant skin" over time. According to the results of Section 2.3.4, when between 620-850kg/m³, a higher cement content is preferable.

3.4.2.5 Coarse aggregate

According to the research in Section 2.3.5, for investigation of the growing of the “elephant skin” over time in the UHPC mixtures with coarse aggregates, the UHPC mixtures in the group 2.3.5-1 were also cast into the 100×250×30mm³ plates to compare the parameters A, as shown in Table 3.9. The ambient RH and temperature for this group were the same as 48% and 23.1°C. The temperatures in these fresh UHPC mixtures didn’t have big differences (Table 2.10). It could be assumed that these UHPC mixtures have similar surface evaporation rates.

Table 3.9 UHPC mixtures in Group 2.3.5-1

Group	UHPC mixture	CEM content (kg/m ³)	Paste volume (L/m ³)	Coarse aggregates	Parameter A
2.3.5-1	(1) 0.25 0% BA	720	553.6	Without BA	0.00636
	(1) 0.25 30% BA1	660	509.1	V(BA1)/V(Ag)=30%	0.00881
	(1) 0.25 30% BA2	630	486.9	V(BA2)/V(Ag)=30%	0.01142

Figure 3.39 shows the results of the influences of the BA content and BA size on parameter A after percentage normalization from the UHPC mixture without BA. It can be seen that when the UHPC mixtures have the same flowability and viscosity (results of Section 2.3.5), both a higher BA content and a larger BA size can lead to an increase in parameter A. This means that except for the evaporation rate, the consistency of concrete, and the changing of the consistency over time, the coarse aggregate itself contributes to the growing of the "elephant skin" over time. Therefore, UHPC mixtures without coarse aggregates, with less coarse aggregates or with smaller-sized coarse aggregates can be beneficial in slowing down the growing of the “elephant skin” over time.

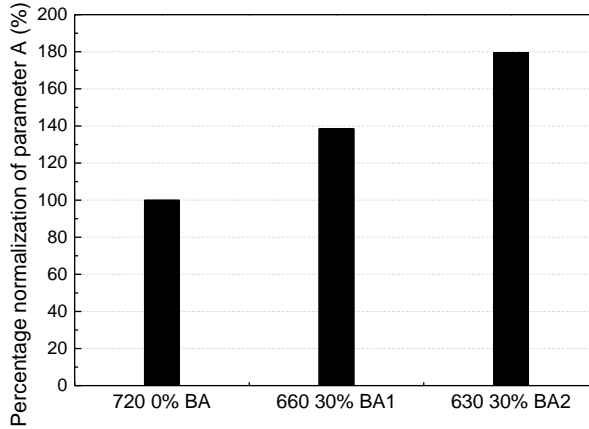


Figure 3.39 Influence of coarse aggregate content and size on the growing of the “elephant skin” over time

3.4.2.6 Steel fibre

Like the research about coarse aggregate, according to the research in Section 2.3.6, the UHPC mixtures in Group 2.3.6-1 were tested with the parameters A, as shown in Table 3.10. The ambient RH and temperature for this group were the same as 48% and 23.1°C. The temperatures in these fresh UHPC mixtures didn’t have big differences (Table 2.11). It could be assumed that these UHPC mixtures have similar surface evaporation rates.

Table 3.10 UHPC mixtures in Group 2.3.6-1

Group	UHPC mixture	CEM content (kg/m ³)	Paste content (L/m ³)	Steel fibres	Parameter A
2.3.6-1	(1) 0.25 0% StF	720	553.6	Without StF	0.00636
	(1) 0.25 2% StF1	750	575.8	With 2 vol.% StF1	0.00935

Figure 3.40 shows the results of parameter A in the UHPC mixtures with and without StF after percentage normalization from the UHPC mixture without StF. It can be seen that when the UHPC mixtures have the same flowability and viscosity (results of Section 2.3.6), the existence of StF can lead to an increase in the parameter A. This means that the StF itself can also contribute to the growing of the "elephant skin" over time. Therefore, UHPC mixtures without or with fewer steel fibres can be beneficial in slowing down the growing of the “elephant skin” over time.

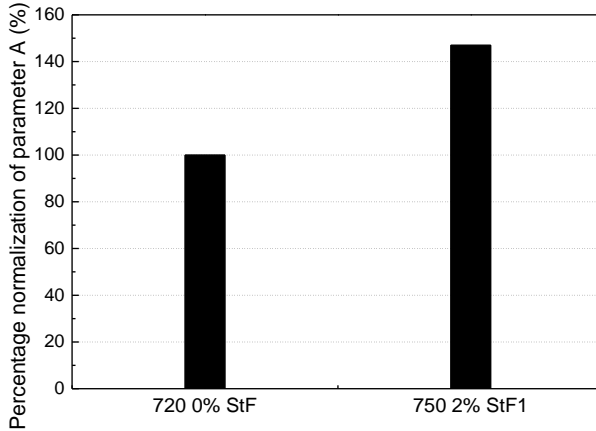


Figure 3.40 Influence of the StF content on the growing of the “elephant skin” over time

3.4.3 Compressive strength

Figure 3.41 presents the relationship between the parameter A measured from the plates and the results of the cubic compressive strength (maximum value) of the same UHPC mixture. It can be found that the existence of the “elephant skin” does not appear to affect the maximum compressive strength. Regardless of whether the parameter A is larger than 0.0098, there is almost no influence on the compressive strength of the UHPC mixture. This also means that by changing the composition of the UHPC mixture or making other treatments, the growing of the “elephant skin” over time can be slowed down without compromising the compressive strength of UHPC.

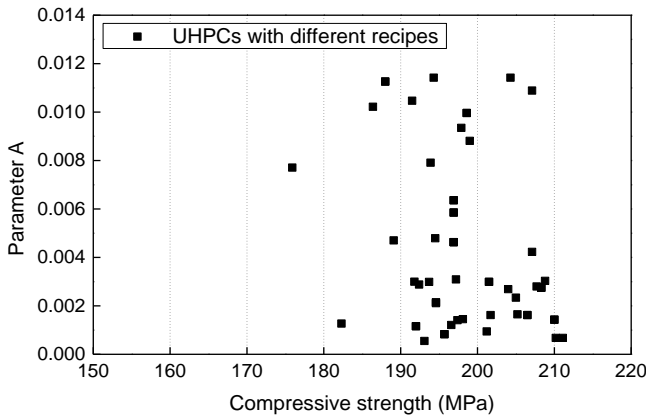


Figure 3.41 Relationship between compressive strength and the growing of the “elephant skin” over time

3.5 Formation and growing mechanisms of the “elephant skin”

3.5.1 Characteristics of the second layer after removing the “elephant skin”

To further explore the formation and growing mechanisms of the “elephant skin”, in combination with previous experimental results, the new surface characteristics after removing the “elephant skin” were considered. A small spatula was used to remove the hard “elephant skin” 30 minutes or 1 hour after casting, as shown in Figure 3.42(a). Figure 3.42(b) displays the exterior of the new surface shortly after the removal of the first layer. The new “elephant skin” still formed and increased the surface resistance rapidly. Hence, the growing of the new “elephant skin” second layer over time was investigated to be compared with that of the first layer.



(a) Using a spatula to remove the first layer of elephant skin



(b) A new layer holding the wood rod

Figure 3.42 Investigation of the second layer after removing the first layer of the “elephant skin”

3.5.1.1 UHPC without BA and StF

For this investigation, the UHPC mixtures with the same recipe as “720 CEM B” in Table 3.3 were mixed three times. Three 100×250×30mm³ plates were cast each time to test the growing of the “elephant skin”. As shown in Table 3.11, in the first mixture (Mix1), the surface of one plate was removed 15min after casting (removing time: 15min) and the surface of another plate was removed 30min after casting (removing time: 30min). The last one was not removed to test the formation of the first layer (removing time: 0min). In the second mixture (Mix2), the surface of one plate was removed 30min after casting (removing time: 30min) and the surface of another plate was removed 1h after casting (removing time: 1h). The last one was not removed to test the formation of the first layer (removing time: 0min). In the third mixture (Mix3), three plates were all removed in 1h. One plate was under the humidity of 60% before and after removal. One plate was under the humidity of 60% before the removal and 80% after the removal. The last one was under the humidity of 80% before the removal and 60% after the removal.

Table 3.11 UHPC mixture without BA and StF to test the new “elephant skin” layer

Recipe	UHPC mixture	Removing time	RH	Parameter A
720 CEM B	Mix1	0min	40	0.01803
		15min		0.01716
		30min		0.01703
	Mix2	0min	65	0.0011
		30min		0.00116
		1h		0.00108
	Mix3	before removal	60	0.0021
		1h		0.00217

From the results of parameters A in Table 3.11, it can be found that when the UHPC mixture is without BA and StF, the growing of the new “elephant skin” layer over time is almost the same as that of the old layer over time, and the removal time seems to have no obvious influence. Figure 3.43 shows the experimental results of Mix3 under different humidity before and after removing the “elephant skin”. In this condition, the growing of the “elephant skin” over time was not affected by the removal, but only by the humidity.

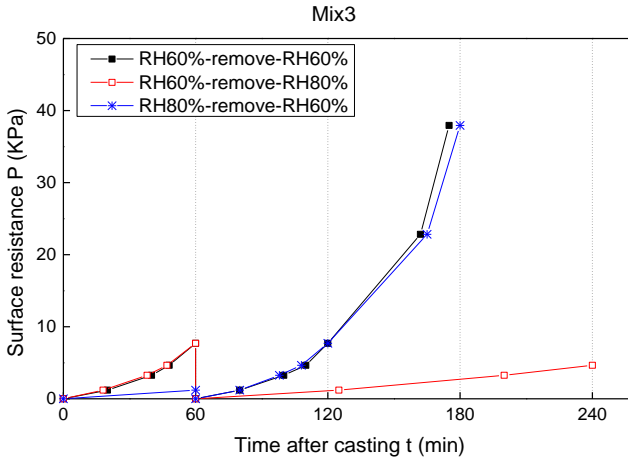


Figure 3.43 Results of the new “elephant skin” layers of UHPC mixtures without BA and StF when putting the UHPC under different RH after removal of the “elephant skin” layer

3.5.1.2 UHPC with BA or StF

For this investigation, the parameters A of the new “elephant skin” layer (layer 2) and that of the old “elephant skin” layer (layer 1) of the UHPC mixtures “620 30% BA2”, “620 30% BA2 1% StF”, “860 QS3 3% StF” in Table 3.3, “(1) 0.25 30% BA2” in Table 3.9, and “(1) 0.25 2% StF1” in Table 3.10 were also tested, as shown in Table 3.12. All the old “elephant skin” layers (layer 1) were removed 1h after casting.

Table 3.12 UHPC mixtures with BA or StF to test the new “elephant skin” layer

UHPC mixture	Removing time	RH	Parameter A
620 30% BA2	0min	70	0.00531
	1h		0.00311
620 30% BA2 1% StF	0min	68	0.01078
	1h		0.00268
860 QS3 3% StF	0min	64	0.00489
	1h		0.0027
(1) 0.25 30% BA2	0min	48	0.01142
	1h		0.0066
(1) 0.25 2% StF1	0min	48	0.00935
	1h		0.00534

Figure 3.44 shows a comparison of parameter A of the two layers for these UHPC mixtures after percentage normalization from parameter A of layer 1 and statistical analysis. The

results should be divided into 3 groups: the UHPC mixtures with BA without StF (the UHPC mixtures “620 30% BA2” and “(1) 0.25 30% BA2”), the UHPC mixtures with StF without BA (the UHPC mixtures “860 QS3 3% StF” and “(1) 0.25 2% StF1”), and the UHPC mixtures with BA and StF (the UHPC mixture “620 30% BA2 1% StF”). It can be found that for all the UHPC mixture, the growing of the new “elephant skin” over time is slower than that of the old “elephant skin”. And the more BA or StF are added, the greater the percentage of the parameter A in the second layer is reduced. Combined with the results in the last section, these results also indicate that the growing of the “elephant skin” over time should be not only due to the evaporation of water on the surface of the concrete but also due to the upward movement of the moisture from inside of the UHPC.

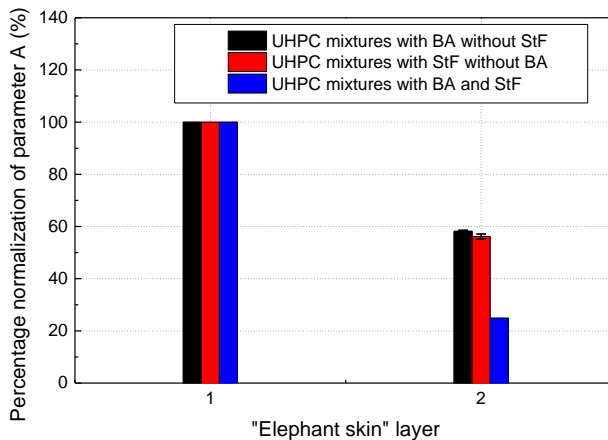


Figure 3.44 Results of the new “elephant skin” layers of UHPC mixtures with StF or BA

3.5.2 “Elephant skin” formation and growing mechanisms analysis

According to the present test results and those in previous studies, the evaporation rate is a mean factor that influences the growing of the “elephant skin” over time on the UHPC surface. In addition, the consistency of the UHPC mixture and the changing of the consistency over time have also a degree of influence over the growing of the “elephant skin”. The coarse aggregates and steel fibres themselves have also an effect on the growing of the “elephant skin”. Present experimental results from the second “elephant skin” layer

demonstrate that the upward movement of the moisture in the mixture to the concrete top surface can also affect the formation and growing of the “elephant skin”.

Based on the above discussions and in combination with previous findings [40, 44, 102], the formation and growing mechanisms of the “elephant skin” on UHPC surface are proposed in this research as follows: after mixing and casting, the top surface of UHPC is exposed to ambient conditions. The water on the UHPC surface evaporates rapidly with low RH levels and high temperatures. Owing to the rather limited amount of free water in the UHPC mixture, the loss of water on the concrete surface is often significant. On the other hand, due to the high viscosity of UHPC, the rising rate of internal water in the mixture is generally very low, which is normally (much) lower than the evaporation rate of water on the concrete surface. This is obviously different from that in normal strength concrete, where no “elephant skin” is observed. As a result, there is an absence of sufficient water on the UHPC top surface that acts as a substitute for the evaporated water. The loss of water on the UHPC surface accelerates the hardening process of the mixture, resulting in the rapid formation of a hard layer on the surface, that is, the (first) “elephant skin” layer.

Therefore, reducing the evaporation rate from the surface of UHPC, increasing the consistency of UHPC or increasing the free water in UHPC to promote the rapid rise of internal moisture, and slowing down the decrease in consistency of UHPC over time to provide more time for the internal moisture to rise can all contribute to slowing down the growing of the “elephant skin” over time. Coarse aggregates and steel fibres accelerate the growing of the “elephant skin” due to the large size and tortuosity of the particles themselves, which prevents the internal moisture from rising (as shown in Figure 3.45, the internal moisture needs to take a long way round to rise).

For the UHPC mixture without coarse aggregates and steel fibres, as the first layer of the “elephant skin” forms and grows, the “elephant skin” blocks the evaporation of the concrete below it, thus gradually stopping the rise of internal moisture. When the first layer is removed, the new concrete surface is the same as it was when the UHPC mixture was just cast, and the action of surface evaporation and internal moisture rise begins anew. However, when the UHPC mixture contains coarse aggregates and/or steel fibres, the internal moisture needs to take a long way around to rise, causing the first layer of the “elephant skin” to grow quickly. Although this also stops evaporation and results in the internal moisture gradually stopping rising, the internal moisture that has taken a long way around is delayed in reaching the surface of UHPC and accumulates below the “elephant skin”. Thus, when the first layer

is removed, more moisture is actually present on the new UHPC surface than on the first layer, which causes the slower growing of the second "elephant skin" layer over time.

The proposed mechanisms of the formation of the “elephant skin” seems to be consistent with most of the test findings in this research as well as that reported in previous work.

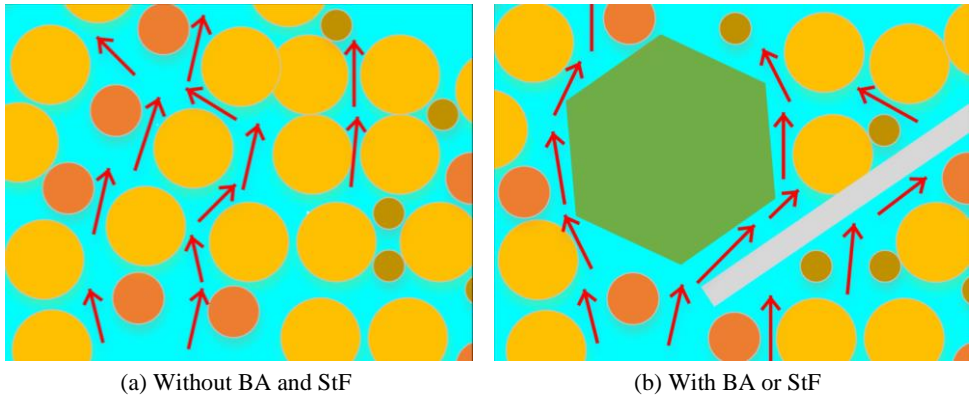


Figure 3.45 Schematic: coarse aggregates and steel fibres cause internal moisture to take a long way around to rise

3.6 Summary

This chapter mainly investigates the “elephant skin” problem that affects the surface performance of UHPC. By use of a newly developed method based on the Vicat experiments to investigate various influencing factors, the formation mechanisms of the “elephant skin” are discussed. Accordingly, several feasible methods to mitigate the formation of the “elephant skin” on the UHPC surface can be developed. The main conclusions are drawn as follows:

- (1) In order to ensure that the "elephant skin" does not adversely affect structural safety in large-scale applications of UHPC, and to provide sufficient time for surface treatment, the growing of the "elephant skin" over time should be below a certain limit. After analysis, the surface resistance within 60 min after cast should be less than 35.28 kPa, which is calculated from the maximum falling height of the concrete to break through the “elephant skin”;
- (2) The evaporation rate of the concrete surface is an important factor in the formation and growing of the “elephant skin”. Therefore, in engineering applications, the

evaporation rate should be as low as possible. The evaporation rate was calculated to be less than $0.36 \text{ kg/m}^2/\text{h}$ for the reference mix proportion of UHPC in this study to fulfil the requirements of conclusion (1);

- (3) The composition and content of UHPC will influence the formation and growing of the “elephant skin”. Within the scope and the test method of this research, the parameter A can be calculated by referring to Equation (3.15) in terms of the proportion of each constituent of UHPC so that the parameter A can be controlled below 0.0098 to fulfil the requirements of conclusion (1);
- (4) The UHPC mixtures without or with lower contents of steel fibres and coarse aggregate will contribute to a decrease in the growing of the “elephant skin” over time;
- (5) According to the formation and growing mechanisms of the “elephant skin” proposed in this study, a favourable approach to resolve the workability issue of the “elephant skin” should be based on the following three aspects: reducing surface evaporation, increasing internal moisture, and promoting the rise of internal moisture.

In conclusion, based on the requirements of different large-scale engineering applications of UHPC, on the requirements of maintaining performances, corresponding methods of decreasing the growing of the “elephant skin” over time can be considered to provide more time for spraying water on the surface. However, further experimental and theoretical research is still needed in the future.

4 Entrapped air bubbles and pore structure of UHPC

4.1 Literature review

As mentioned before, due to the dense microstructure and high viscosity of the UHPC, the air entrapped during the manufacture of the UHPC cannot be easily removed even with prolonged vibration, and a large amount of air bubbles will remain in the hardened material to form big air pores.

As shown in Figure 4.1, since the surface of UHPC is very flat, there is usually no need to add a special coating to the surface of UHPC structures, but when there are many air pores, it will have a very bad appearance. At the same time, people will have less confidence in such elements or structures, especially when the structure is very thin. Taping the side of the formwork with a rubber hammer after casting and grinding to create better uniformness on the surface might help, but with limited efficiency [115, 116].



Figure 4.1 UHPC surface with air pores



Figure 4.2 Air bubbles accumulate in a specific position in an enclosed formwork

Besides, as shown in Figure 4.2, when UHPC is cast into an enclosed formwork, the air bubbles will accumulate in a specific position after casting to form larger air pores, seriously affecting local safety, especially when the structure is very thin.

For sprayed ultra-high performance concrete (SUHPC), suitable accelerators should be added to form a suitable sprayed thickness and early strength by instantaneous reaction and spraying process. But this may cause the air bubbles to be easily entrapped into the fresh mixtures and lately transfer to macro-pores in hardened SUHPC and result in poor hardened properties [117].

For widening and repairing existing concrete bridges with cast-in-situ UHPC, the effect of vehicle-bridge coupling vibration in the through-traffic section may cause part of the air bubbles to gradually move to the upper part of the fresh casted concrete in the repaired section. The coupling effect of frequency and amplitude causes a high heterogeneous redistribution of steel fibres and air bubbles characterized by the aggregation of air pores in the top part of specimens, which could be detrimental to the performances of UHPC (mainly tensile and flexural strengths) [118].

Therefore, air pores in UHPC can negatively affect many aspects of the hardened properties of this material. At present, many studies have given some possible methods to reduce the air pores in the UHPC structure, which provide a good research basis for this study. For example, Schachinger I et al. [119] carried out an investigation on the practical methods to reduce the air pores in hardened UHPC. They found that the flowability of concrete had an influence on the air content in fresh concrete. Pumping concrete also appeared to be beneficial in reducing the air pores in the structure compared to direct pouring and placement. A spiral pump with an operating pressure of 25 bars could reduce the air content of the fresh concrete by about

1.3-2.9 vol.%. In addition, low-pressure mixing was effective in reducing the air content in fresh concrete due to the less entrapped air in the concrete mixture, with vacuum mixing being the best. However, these methods are currently less suitable for large-scale applications of UHPC.

Huang H et al. [120] investigated the effects of rheological performance, antifoaming admixtures (AFA, also known as defoaming agent), and mixing procedures on the air content in fresh UHPC mixtures. According to their results, longer mixing time and higher mixing speed were helpful for decreasing the air content in fresh UHPC mixtures, as shown in Figure 4.3 (copyright permitted). The low viscosity of UHPC and some defoaming agents could also benefit to decrease the air pores in the hardened samples, as shown in Figure 4.4 and Figure 4.5 (copyright permitted), respectively. These findings will be further verified in this study.

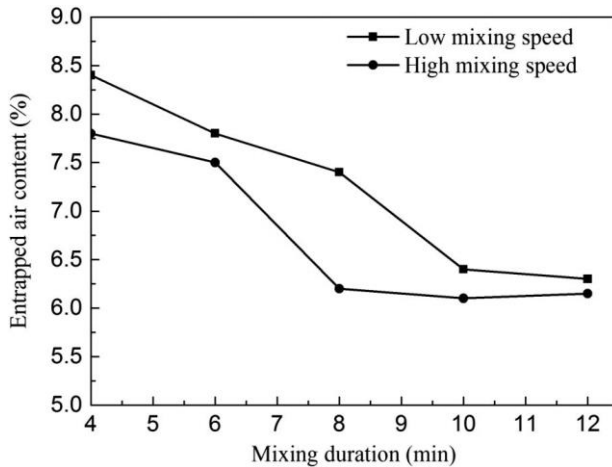


Figure 4.3 Entrapped air contents of fresh UHPC mixtures at different mixing durations (Low mixing speed: 198rpm; high mixing speed: 361rpm) [120]

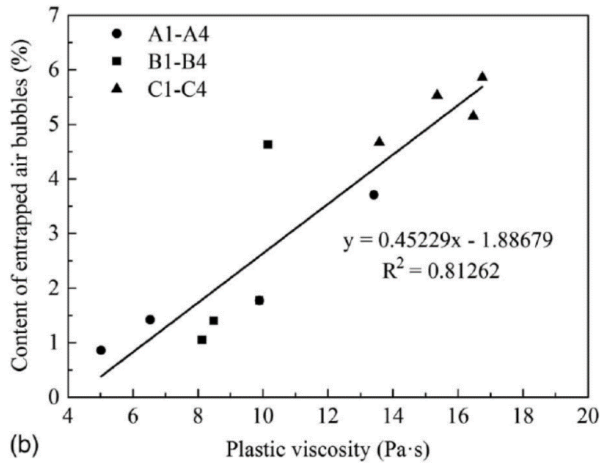


Figure 4.4 Relationship between the content of entrapped air bubbles in hardened UHPC and plastic viscosity, which is tested by the RheoCAD400 rheometer (CAD Instruments, Les Essarts-le-Roi, France) [120]

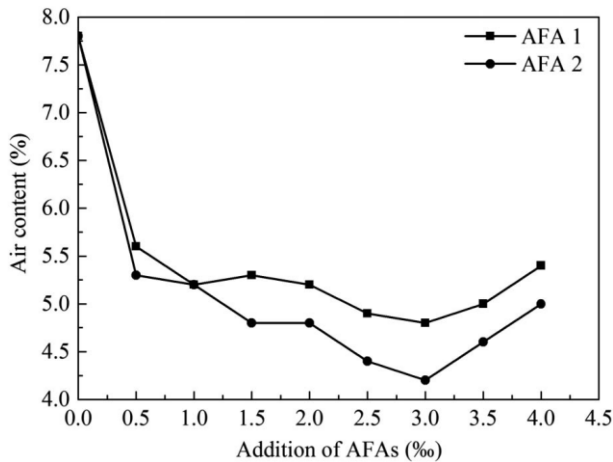


Figure 4.5 Air contents of fresh UHPC mixture with the addition of AFAs (defoaming agents) [120]

Yu R et al. [121] carried out dynamic modelling of air bubbles in fresh UHPC based on Stokes's law, which was also used to clarify the appropriate UHPC rheological model. They used image analysis technology to study the effect of some factors in the rheological properties of UHPC on the total air void content. They also found that with an increase in the UHPC viscosity, the total voids content (the voids including all diameters) showed an increasing tendency. In addition, with an increase in the added defoamer content, the amount of air voids (diameter > 1 mm) first decreased, and then sharply increased. The minimum value of the air voids (diameter > 1 mm) content could be obtained when the defoamer is

added with 0.5% of cementitious material in UHPC. The influence of the defoamer (defoaming agent) will be further investigated in this study.

Dils J et al. [54] used a special mixer to test the influence of air pressure during mixing on the air content in fresh UHPC mixture. They concluded that lower air pressure during mixing would lead to lower air content in fresh UHPC mixture. This conclusion is consistent with the results of Schachinger I et al. [119].

Wang R et al. [122] used the X-ray CT method to measure the spatial distribution of steel fibres and entrapped air pores (bigger than 2mm) in UHPC cylinders with a size of $\Phi 100 \times H 200 \text{mm}^3$. They found that more superplasticizers (SP) seemed to be able to reduce air bubbles. At the same time, they also found that more steel fibres could also decrease the air bubble content. However, in their results, the quantitative analysis of the sizes and numbers of air bubbles is not precise enough.

Li T et al. [123] also used X-ray CT and image analysis techniques to establish a three-dimensional model to perform visualization and quantitative analysis of the distribution of steel fibres and air pores in UHPC cylinders with a size of $\Phi 100 \times H 100 \text{mm}^3$. They observed the upper part of the sample had a higher amount and size of air pores than the lower part, and more steel fibres would reduce the number of air bubbles, as shown in Figure 4.6 (copyright permitted). However, they didn't give a clear analysis and discussion about the results.

Shi K et al. [124] found that mixing the correct amount of steel slag powder could slow down the setting speed of UHPC, which could remove the entrapped air bubbles during mixing in time, and the particle size of steel slag powder could fill the particle size range of the break in mineral powder particle grading, thus improving the continuity of the overall gelling material grading. However, the incorporation of steel slag powder also led to a reduction in the continuous hydration degree of cement and ground granulated blast furnace slag (when used) at the time of initial setting, which also reduced the generation of the hydration product and increased the porosity of the hardened matrix, especially the harmful pores, leading to a reduction of mechanical properties.

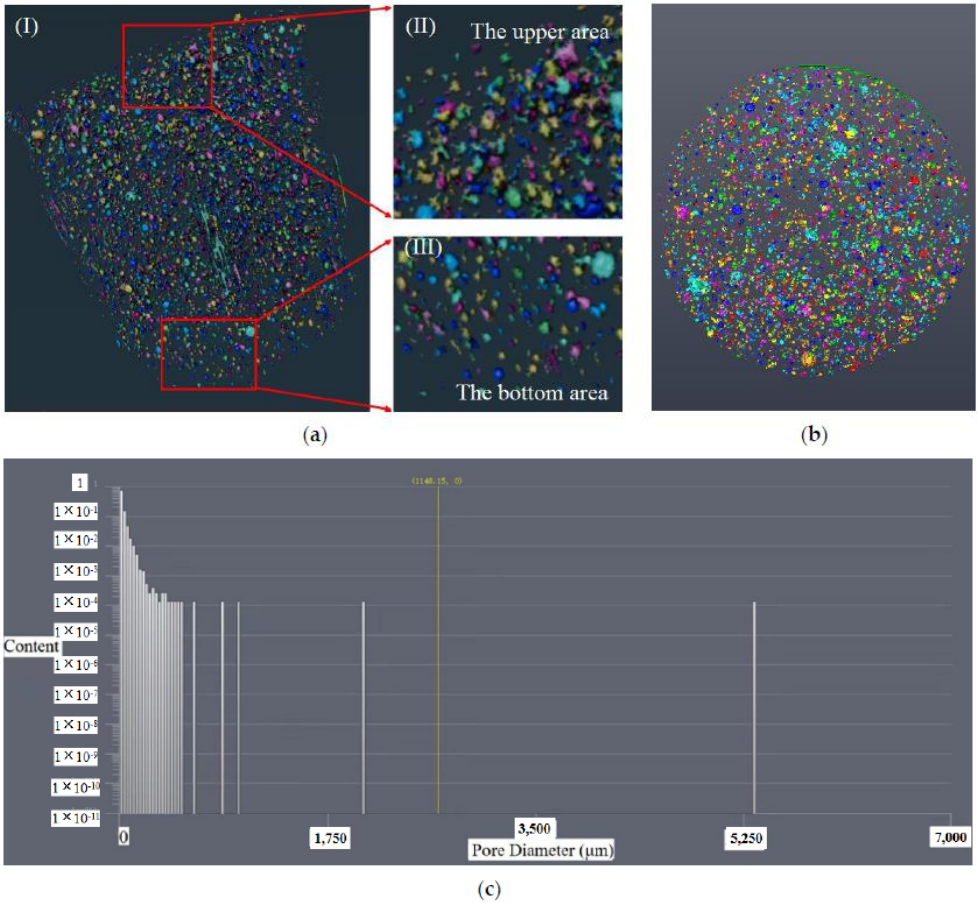


Figure 4.6 Reconstructed pore structure model of fibre-reinforced UHPC (above 200 μm): (a) Analysis of pore structure characteristics. (I) was the whole structure, (II) was the upper area and (III) was the bottom area; (b) Top view of the pore structure; (c) Pore size distribution of fibre-reinforced UHPC [123]

Huang H et al. [125] studied the influences of rice husk ash on the strength and permeability of UHPC. They measured the flowability and air content in fresh UHPC mixture and the compressive and flexural strengths of the hardened concrete at different curing ages, assessed the permeability before and after loading by water absorption and chloride ion penetration, and evaluated the pore structure for selected samples by using mercury intrusion porosity (MIP) measurement. The results showed that the addition of rice husk ash (RHA) to replace Si decreased the flowability of the fresh UHPC mixture and increased the number of entrapped air bubbles. But it could enhance the compressive strength and impermeability of UHPC due to the refined pore structure.

Accordingly, most of the existing literature focused on how to reduce air pores in UHPC structures by different possible methods. However, the specific de-airing mechanisms in UHPC are not yet clear. At the same time, if the de-airing in the UHPC can be enhanced from the perspective of concrete mix proportion while ensuring the hardened properties, it will be applicable to more large-scale engineering applications.

Therefore, it is necessary to develop effective measures to enhance the de-airing behaviours in UHPC. In this research, the de-airing process is divided into two parts: the de-airing during mixing, which is tested by the air content in fresh concrete after mixing; and the de-airing after mixing, which is evaluated by examining the air pores in the hardened concrete. This research systematically analyses the influences of different factors on the de-airing behaviours in UHPC during and after mixing, and considers the efficient methods to reduce the air pores in the UHPC structures. Based on the results of this research, the optimal solutions can be adopted for different practical engineering applications, which could achieve the best efficiency.

4.2 Materials and measuring methods

The raw materials used in this research are the same raw materials including CEM, Si, QP, WA, SP, Ag and StF introduced in Section 2.1. Additionally, 2 kinds of defoaming agents and some formwork release agents are also studied, which will be introduced in the following sections. The recipes of the UHPC mixtures used in this study are also based on the research of Section 2.3. Each group of UHPC mixtures should be mixed and tested on the same day, and only one parameter can be changed while the other parameters are kept constant. When combining the results of different groups of UHPC mixtures, the results need to be percentage normalized from the reference recipe in Table 2.5, so that multiple groups of results can be statistically analysed to calculate the mean values and standard deviations.

Most UHPC mixtures are mixed with an Eirich mixer; the UHPC mixtures mixed with other mixers are specified in the sections. The temperature and humidity of the environment are not considered in this research due to their negligible effects on the de-airing behaviours in UHPC. The mixing procedure and the measurement methods of temperature, flowability, and viscosity of fresh UHPC mixtures in this chapter are the same as that in Chapter 2 and Chapter 3. The samples cast in the tests in each section are mostly cured in room temperature water for 28 days unless otherwise stated.

In this research, the air content in fresh concrete after mixing is tested by the apparatus according to EN 12350-7 [126]. The air pores in the hardened concrete are examined by the optical technique of image analysis. As shown in Figure 4.7, the cylinders with a size of $\Phi 100 \times H 200 \text{mm}^3$ are cast and cut from three different positions 2-3 days after casting to examine the air bubbles in the sections. A special equipment with a high-resolution camera is used to take photos of the cut sections, as shown in Figure 4.8(a) [127] (this photo is taken from the report). The photos are then analysed with the software “ImageJ” to recognise the numbers and sizes of air pores at the cross-sections, as shown in Figure 4.8(b). This method is very popular for examining the distribution of air pores and steel fibres in concrete. Although this test method is based on 2-dimensional image analysis, which may deviate from the actual 3-dimensional distribution, compared with some methods that directly detect the 3-dimensional distribution, this method is faster and more convenient to analyse the factors that influence the air pores in the UHPC structures. In this research, air pores larger than 0.5mm in mean Feret diameter (the mean value of the minimum and maximum Feret diameters of each object's boundary over a sufficient number of orientations [128]) are only considered, so that the other types of pores mentioned in Section 1.3 cannot be involved.

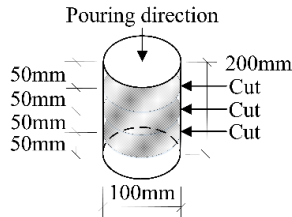
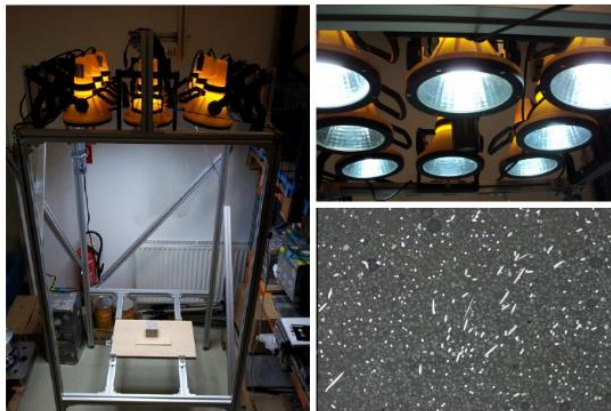
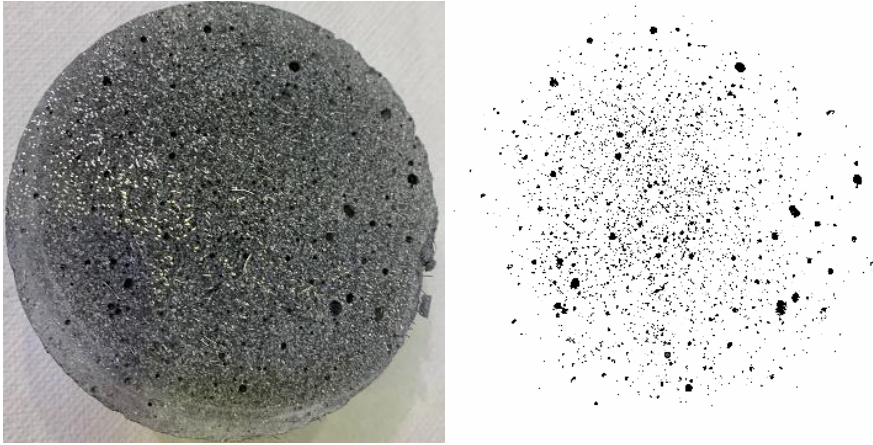


Figure 4.7 Schematic diagram of the testing cylinders



(a) Special equipment with a camera [127]



(b) Air pores in the section analysed by ImageJ

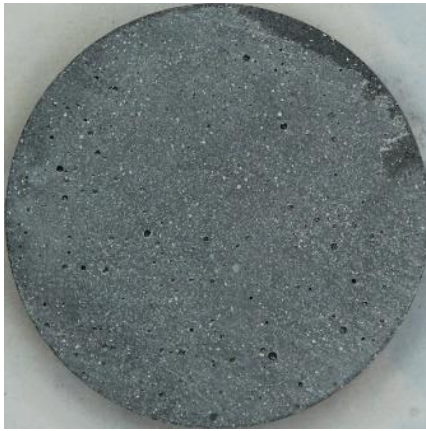
Figure 4.8 The test method to calculate the number of air pores in the hardened concrete

Through the test method, the numbers and sizes of air pores in the hardened concrete specimens can be measured. However, as shown in Figure 4.9, when the air pores at the cross-section are examined, there are several different cases, including a few small pores (Figure 4.9(a)), many small pores (Figure 4.9(b)), a few large pores (Figure 4.9(c)) and many large pores (Figure 4.9(d)). Therefore, it is not comprehensive to simply consider the number or average size of air pores. In this research, the following equation is used to integrally analyse the percentage of air pores at the cross-section P_{bubble} (%):

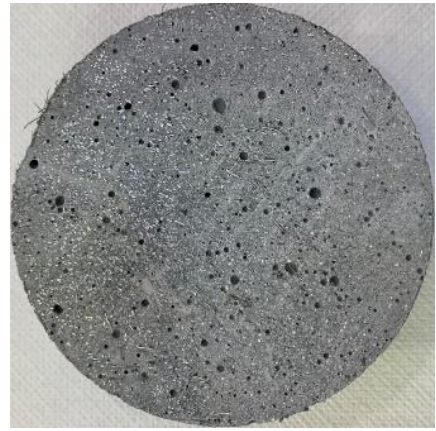
$$P_{bubble} = \frac{N_{airpore} \times A_{airpore}}{A_{surface}} \quad (4.1)$$

where $N_{airpore}$ (-) is the number of air pores at the cross-section; $A_{airpore}$ (mm²) is the average area of all the observed air pores; $A_{surface}$ (mm²) is the area of the cross-section.

As mentioned before, the 2-dimensional percentage of air pores at the cross-section P_{bubble} (%) is not equal to the 3-dimensional percentage of air pores in the whole hardened UHPC sample $P_{bubble-all}$ (%), which is very difficult to be accurately obtained. Nonetheless, assuming that the distribution of air bubbles in the sample is relatively uniform and that the area of each cross-section of the cylinder is the same, the average value of the P_{bubble} of all the cut sections in the cylinder can be very close to $P_{bubble-all}$. Therefore, when studying the influence of various factors on $P_{bubble-all}$, the variation of P_{bubble} can be used to represent that of $P_{bubble-all}$.



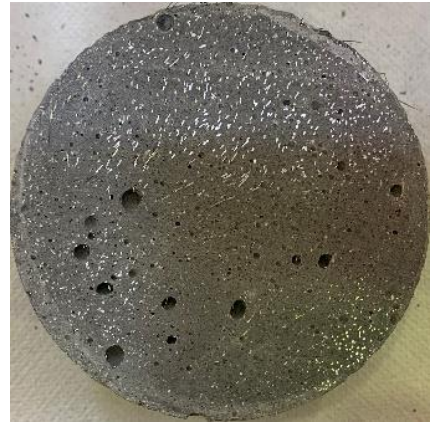
(a) A few small pores



(b) Many small pores



(c) A few large pores



(d) Many large pores

Figure 4.9 Several different cases of air pores at the cross-sections of hardened concrete specimens

It is also possible to cut the cylinder in the longitudinal direction, but this is only to detect the distribution of air pores within the cylinder along the longitudinal direction. Since the areas of the cross-sections are not the same after the longitudinal cut, the percentage of air pores in the middle cross-section is not representative of $P_{bubble-all}$. In comparison, the results along the transverse cut can be closer to the actual percentage of air pores.

With this test method, the de-airing behaviour during mixing can be evaluated by the air content in the fresh UHPC mixture (P_{fresh}). The de-airing behaviour after mixing can be evaluated by the difference of the P_{fresh} and P_{bubble} , when the entrapped air during casting and other factors remain constant.

4.3 Influence of the air pores on the hardened properties of UHPC

According to the results of Section 2.3.3, the SP/B ratio has insignificant effect on the temperature and compressive strength of UHPC mixtures. However, according to the test results of this research, the SP/B ratio can influence the percentage of air pores (P_{bubble}) in hardened concrete. Thus, in order to characterise the influence of P_{bubble} on the hardened properties, UHPC mixtures containing various SP/B ratios were mixed by an ELBA mixer, as shown in Table 4.1. Detailed mix recipes and properties can be found in Table A.4 in the appendix. In the names of the mixtures, “860” is the cement content (kg/m^3), and “0.25” is the W/C ratio.

Each mixture was mixed with 30L and cast into two $\Phi 100 \times H200\text{mm}^3$ cylinders to test the P_{bubble} , one $\Phi 100 \times H200\text{mm}^3$ cylinder to test the elastic modulus, two $50 \times 150 \times 550\text{mm}^3$ beams and two $30 \times 150 \times 550\text{mm}^3$ beams to test the bending strength, and four to five $100 \times 100 \times 100\text{mm}^3$ cubes to test the compressive strength. The elastic modulus was tested according to the EN 12390-13 [129]. The bending strength of the beam was tested by a 4-point bending test according to ÖBV-Richtlinie “UHPC” [20]. The modified beam dimension of $30 \times 150 \times 550\text{mm}^3$ was to be expected a clearer result of the influence for thinner beam specimens, although the actual results were not as different as expected. From the results of average P_{bubble} in Table 4.1, it can be found that a higher SP/B ratio can certainly decrease the P_{bubble} , which will be analysed in chapter 4.4.4.

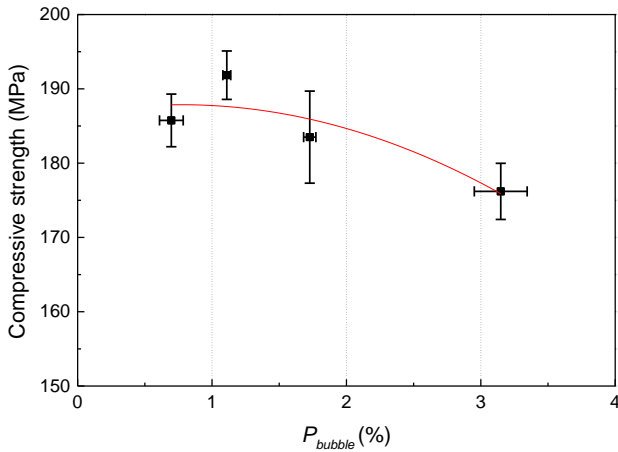
Table 4.1 UHPC mixtures to test the influence of P_{bubble}

Group	UHPC mixture	SP/B ratio (%)	Corresponding SP/C ratio (%)	Spread-flow (cm)	P_{fresh} (%)	Average P_{bubble} (%)
4.3-1	860 0.25 ELBA 1.15	1.15	1.55	21	4.8	3.15
	860 0.25 ELBA 1.51	1.51	1.7	27	4	1.73
	860 0.25 ELBA 2.68	2.68	3	32	3.6	1.11
	860 0.25 ELBA 4.46	4.46	5	32	3.6	0.70

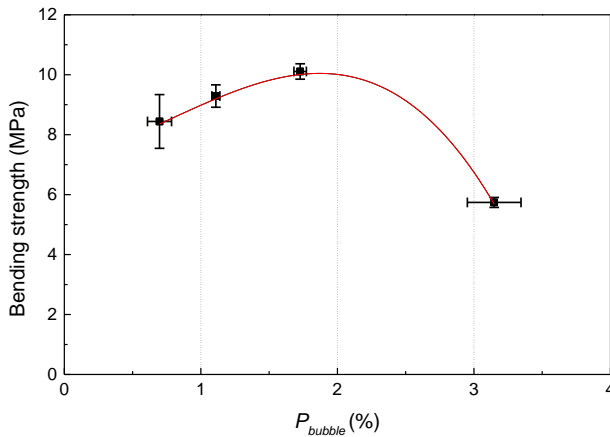
Figure 4.10 shows the results of the influences of P_{bubble} on the compressive strength, bending strength and elastic modulus of the UHPC mixture. It can be seen that a higher P_{bubble} will cause a lower compressive strength, a lower bending strength and a lower elastic modulus.

This result is consistent with the description in the literature and also validates the validity of the experimental methodology employed.

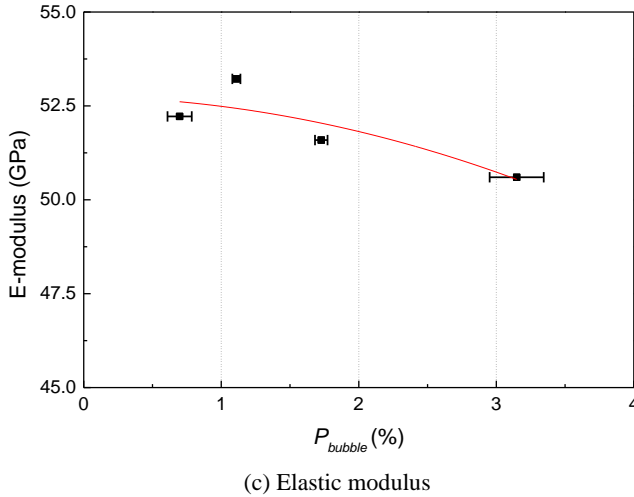
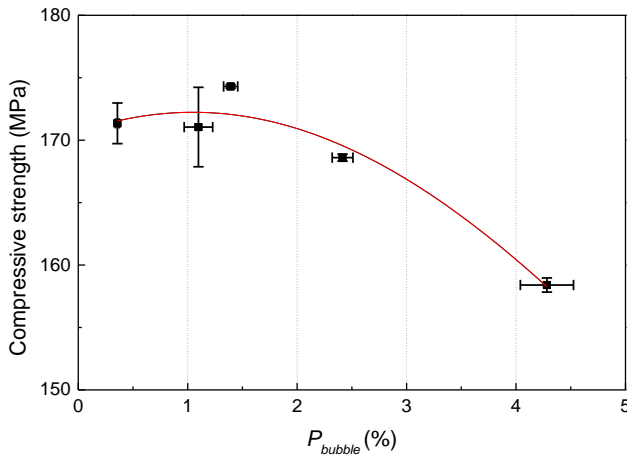
To further determine the P_{bubble} values that can be recommended, the P_{bubble} values of the UHPC mixtures in Groups 2.3.3-3 (Section 2.3.3) were also tested. The effect of their P_{bubble} values on compressive strength is shown in Figure 4.11.



(a) Compressive strength



(b) Bending strength

Figure 4.10 Influence of P_{bubble} on the hardened properties of UHPC mixturesFigure 4.11 Influence of P_{bubble} on the compressive strength of the UHPC mixtures in group 2.3.3-3

Combining the test results in Figure 4.10 and Figure 4.11, it can be seen that there would be a significant decrease in the hardened properties of UHPC mixtures when the P_{bubble} is greater than about 1.7%. In addition, according to ACI 347.3R-13 [130], for very important concrete surfaces, the surface total void ratio (including the air pores with all sizes) should be less than 1.2% (observed in a $610 \times 610 \text{ mm}^2$ area) and the maximum diameter of the voids on the surface should be less than 19 mm in order to ensure adequate surface quality and people confidence. Accordingly, considering the ability of UHPC to be applied in very thin

components, it is concluded in this research that when the P_{bubble} is less than 1.7%, the air pores in hardened UHPC structures can be acceptable.

It is worth noting that when the mixing of the UHPC mixture is completed, on the one hand, the process of de-airing in the stationary concrete continues, and on the other hand, part of the new air is entrapped during the casting process. Considering that the capillary porosity of UHPC is very small as stated in Section 1.3, the air content in the fresh UHPC mixture (P_{fresh}) is mostly due to the entrapped air bubbles. Therefore, there seems to be a relationship between the P_{fresh} and the $P_{bubble-all}$ in the hardened UHPC elements. However, since the percentage of de-airing and the percentage of entrapped air cannot be examined, and also, there may be some other factors influencing the air content, it is not possible to give a direct recommended value for P_{fresh} based on P_{bubble} .

At the same time, there is temporarily no guideline that gives requirements of air content in fresh UHPC mixtures. Considering that due to the high viscosity, the air content in the fresh UHPC mixture could be much higher than that in the NSC mixture, based on the P_{fresh} values of the UHPC mixtures in Groups 4.3-1 and 2.3.3-3 (Table A.1 and Table A.4 in the Appendix) and the results in Figure 4.10 and Figure 4.11, it can only be concluded that UHPC mixtures with a P_{fresh} of less than 4% are preferable.

4.4 Influencing factors on the air content in fresh UHPC mixture and air pores in hardened UHPC mixture

4.4.1 Mixing parameters

The mixing parameters may mainly affect the de-airing behaviour during mixing, resulting in different air content values in the fresh UHPC mixtures. In this research, the influences of mixing time and the type of mixer are investigated, respectively. Other parameters in each group remain the same.

4.4.1.1 Mixing time

It has been shown in the literature [120] that an increase in mixing time may help to reduce P_{fresh} . To verify this result, 3 groups of UHPC mixtures were mixed with the Eirich mixer, as shown in Table 4.2. Detailed mix recipes and properties of these UHPC mixtures can be

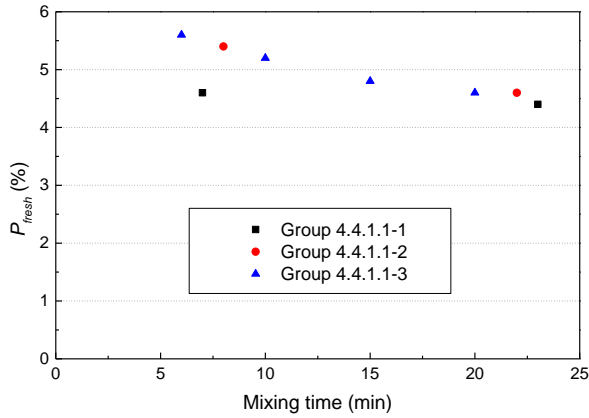
found in Table A.4 in the appendix. In the names of the UHPC mixtures, “720” and “750” are the cement contents, and “0.223” and “0.241” are the W/B ratio. Each group was mixed at different mixing times. The mixing process was the same for all UHPC mixtures as introduced in Section 2.2. The differences in mixing time were mainly caused by the different speeds of materials feeding and the length of mixing time in the end (the mixing process in Figure 2.5 takes only 6 min if the material is added very quickly). All the UHPC mixtures were directly poured from the top of the cylinder, the entrapped air during casting can be considered to be similar.

Table 4.2 UHPC groups tested with different mixing time

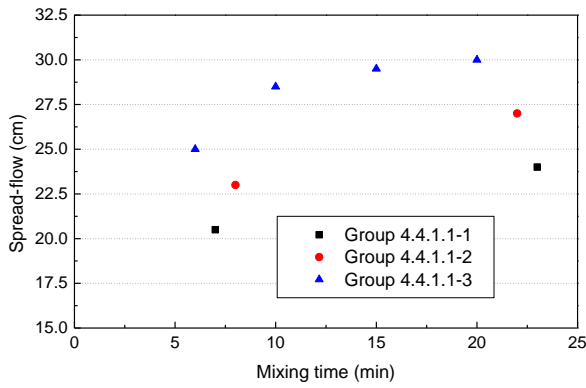
Group	Name	Mixing time	P_{fresh} (%)
4.4.1.1-1	720 0.241	7min, 23min	4.6, 4.4
4.4.1.1-2	750 0.223	8min, 22min	5.4, 4.6
4.4.1.1-3	720 0.223	6min, 10min, 15min, 20min	5.6, 5.2, 4.8, 4.6

Figure 4.12 shows the results of P_{fresh} , the flowability and the compressive strength of each UHPC mixture. It can be found that a longer mixing time can decrease P_{fresh} , which is consistent with the literature (Figure 4.3). However, on the one hand, a longer mixing time allows for longer de-airing process during mixing; on the other hand, a longer mixing time slightly increases the flowability of the UHPC mixture, which also leads to an enhanced de-airing process during mixing (will be analysed in Section 4.4.3). Since both factors affect the P_{fresh} at the same time, the relationship between mixing time and P_{fresh} may not be linear. Besides, the resultant curves of these three groups also showed different patterns of change, indicating that different recipes would have different effects on P_{fresh} . From the results for compressive strength, it can be seen that when the mixing time is shorter and the air content is higher, the compressive strength of the UHPC mixture may be slightly lower, which is also consistent with the results in Section 4.3.

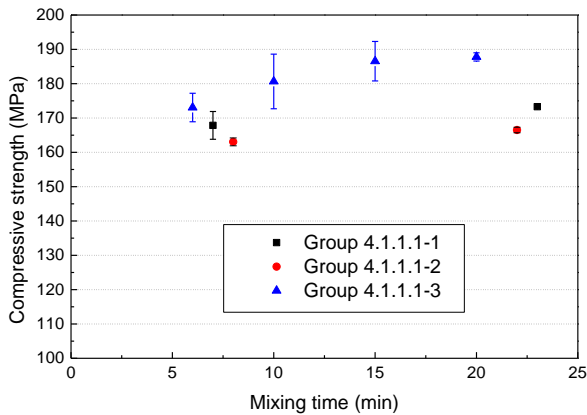
Therefore, considering that the UHPC mixtures in Groups 4.4.1.1-3 used the reference recipe in this research, and the general mixing time for a typical UHPC mixture is about 15min for the mixing process in Figure 2.5, the results for Groups 4.4.1.1-3 after percentage normalization from the UHPC mixtures with the mixing time of 15min can be obtained in Figure 4.13. After fitting, the following equation can be obtained ($R^2=0.998$):



(a) Measured P_{fresh}



(b) Flowability



(c) Compressive strength

Figure 4.12 Influence of mixing time on the de-airing behaviours and properties of UHPC mixture

$$\frac{P_{fresh}}{P_{fresh,MT=15}} = 0.00067 \times MT^2 - 0.0325 \times MT + 1.337 \quad (4.2)$$

where: MT is the mixing time (min), $P_{fresh,MT=15}$ is the P_{fresh} when the mixing time is 15min and other factors remain unchanged.

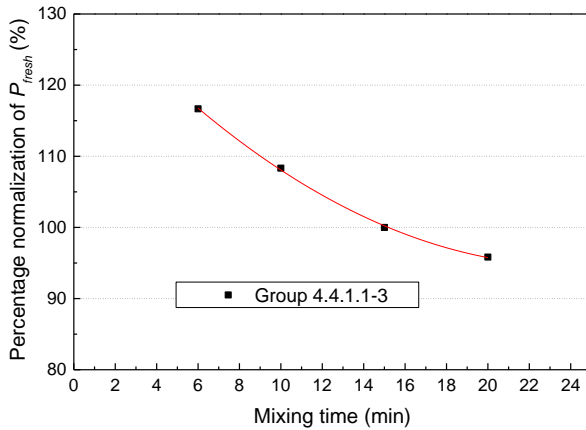


Figure 4.13 Influence of mixing time on the P_{fresh} after percentage normalization

It is noteworthy that the above equation is only applicable to the reference recipe, and the value of $P_{fresh,MT=15}$ is not always the same due to the influence of material batches. In all subsequent tests, the mixing time should be kept at about 15 min.

4.4.1.2 Type of mixer

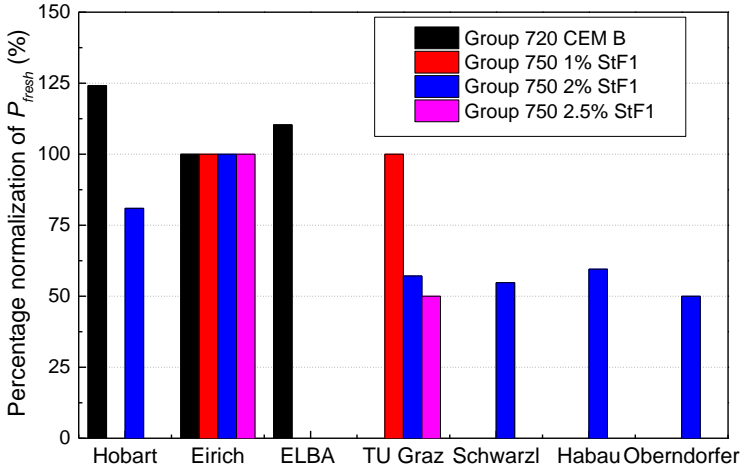
Considering that there are many different types of mixers for mixing UHPC, this section mainly investigates the influence of the type of mixer on P_{fresh} . Except for the previously mentioned Eirich intensive mixer (10L, 4kW), the ELBA single-shaft laboratory compulsory mixer (75L, 3kW), and the small Hobart planetary mixer (5L, 0.35kW), four large mixers are also employed in this study based on the research project “UHPC Austria” [131], which are the twin-shaft mixer (2.5m³, 55kW) in the mix station “Schwarzl”, the ring-pan mixer with swirlers (1.5m³, 45kW) in the mix station “Habau”, the planetary mixer (2.25m³, 75kW) in the mix station “Oberndorfer”, and the cone mixer with eccentric swirler (0.75m³, 22kW) from the Laboratory for Structural Engineering (LKI) at TU Graz. Although the mixers are different, the mixing procedure, mixing speed and mixing time are all similar.

A total of 4 groups of UHPC mixtures were mixed within some of these 7 mixers, as shown in Table 4.3. Detailed mix recipes and properties of these UHPC mixtures can be found in Table A.4 in the appendix. In the names of the UHPC mixtures, “720” and “750” are the cement contents, and “1%”, “2%” and “2.5%” are the volume contents of steel fibre. The first group used CEM B and the other 3 groups used CEM A. The UHPC mixtures mixed by Eirich mixer and ELBA mixer were cast into several cylinders to examine the air pores in hardened UHPC. The UHPC mixtures mixed by a small Hobart mixer were only tested with the P_{fresh} and the 28-day compressive strength due to the small capacity. The UHPC mixtures mixed with large mixers based on the research project were partly cast to some cylinders, and partly only tested the P_{fresh} and the 28-day compressive strength.

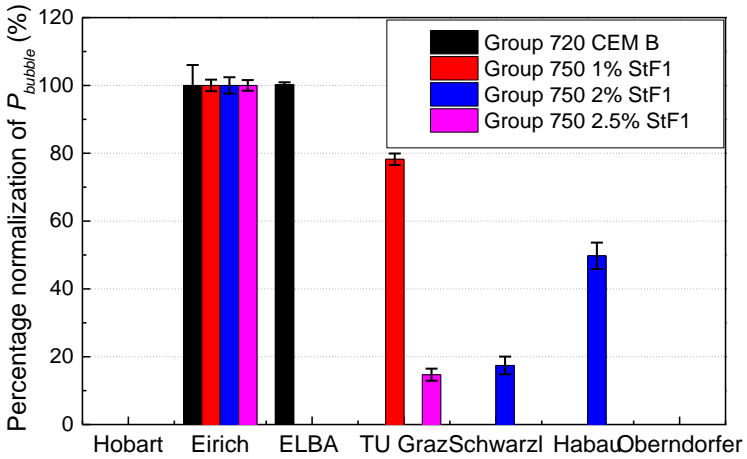
Table 4.3 UHPC mixtures mixed with different mixers

Group	Mixers
720 CEM B	Hobart, Eirich, ELBA
750 1% StF1	Eirich, TU Graz
750 2% StF1	Hobart, Eirich, TU Graz, Schwardl, Habau, Oberndorfer
750 2.5% StF1	Eirich, TU Graz

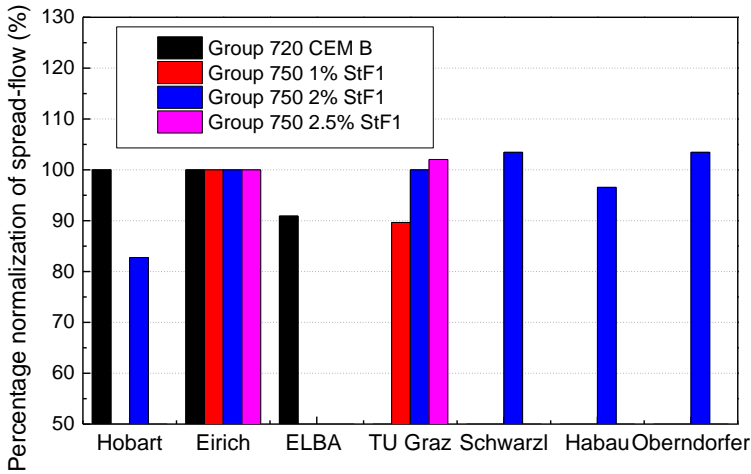
Figure 4.14 shows the results of P_{fresh} , P_{bubble} , flowability and compressive strength after percentage normalization from the results of the Eirich mixer and statistical analysis. In general, it seems that a larger mixer would result in a smaller P_{fresh} and P_{bubble} . A larger mixer may also have higher flowability and lower compressive strength. It should be noted that due to the project progress, the UHPC mixtures in each group were not mixed on the same date, and the differences between raw material batches might also have an influence. The influence of mixers still requires further investigation. Nevertheless, since the type of mixer has an influence on the workability of UHPC, in all subsequent tests, only the concretes from the same mixer can be compared.



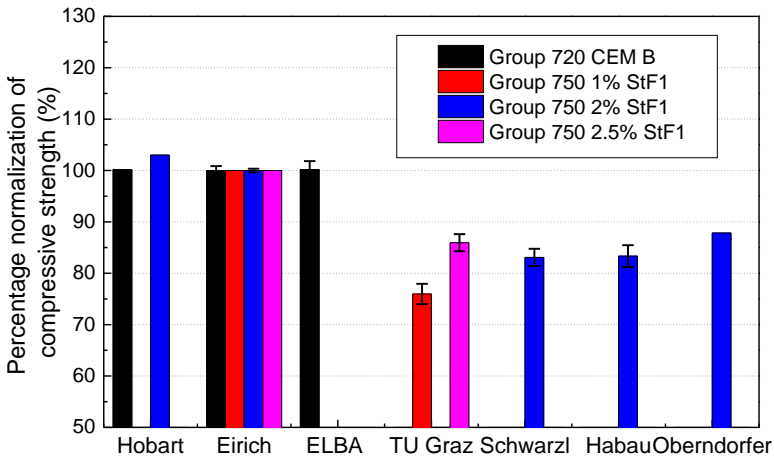
(a) Measured P_{fresh}



(b) Examined P_{bubble}



(c) Flowability



(b) Compressive strength

Figure 4.14 Influence of the mixer type on the de-airing behaviours and UHPC properties

4.4.2 Casting method

As mentioned before, the casting method of the concrete may influence the entrapped air during casting. Thus, when the UHPC mixture has the same P_{fresh} , the P_{bubble} may also be different when the casting method is different. To investigate the influence of the casting method, 3 casting methods are designed to compare their influence in this study, based on the research project “MABA”. As shown in Table 4.4, a batch of UHPC was mixed with an

ELBA mixer to cast 6 big $\Phi 150 \times H1000 \text{mm}^3$ columns and 6 $100 \times 100 \times 100 \text{mm}^3$ cubes. The mix proportion and materials for the UHPC mixture were not available due to the project confidentiality. P_{fresh} was measured to be 2.5% and the maximum 28d compressive strength of the UHPC was 165MPa. In each group, 2 kinds of release agents for formwork (“MFRL 456” and “SPSP IQ P08”) were used. The influence of the release agent will be analysed in Section 4.4.6.

Table 4.4 UHPC mixtures to test the influence of the casting method and release agent

Group	UHPC mixture	Cast method	Release agent	P_{fresh} (%)
4.4.2-1	MABA 1	Vert	MFRL 456	2.5
	MABA 2	Vert. Ho	MFRL 456	2.5
	MABA 3	GEN 70°	MFRL 456	2.5
	MABA 4	Vert	SPSP IQ P08	2.5
	MABA 5	Vert. Ho	SPSP IQ P08	2.5
	MABA 6	GEN 70°	SPSP IQ P08	2.5

As shown in Figure 4.15, “Vert” was to directly pour the concrete from the top; “Vert. Ho” was to use a hose to let the concrete flow from the bottom; “GEN 70°” was to tilt the formwork to about a 70° angle to the ground, and pour the concrete from the top. As shown in Figure 4.16, the columns were cut in three positions 2-3 days after casting and examined the three P_{bubble} with the method introduced in Section 4.2.

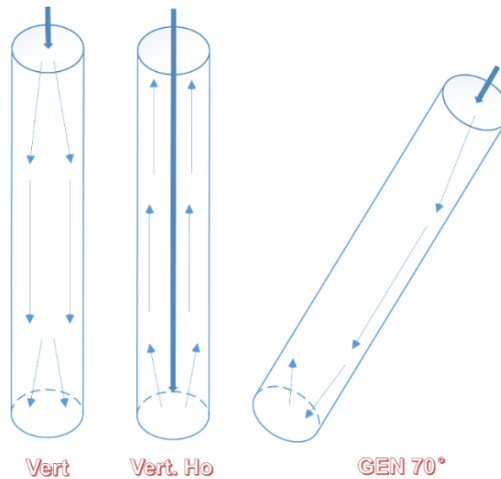


Figure 4.15 Schematic diagram of 3 casting method

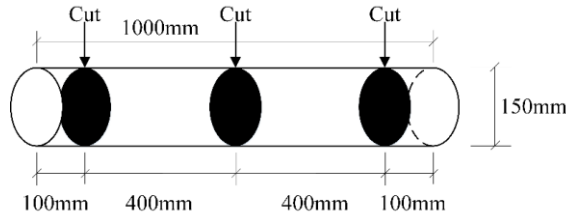


Figure 4.16 Schematic diagram of the cutting position of the columns

Figure 4.17 shows the examined results of P_{bubble} after percentage normalization from the casting method “Vert” and statistical analysis. Since for the same UHPC mixture, the de-airing behaviour after mixing can also be considered the same, it can be found that casting with a hose can cause lower entrapped air to achieve a lower P_{bubble} , while a tilted formwork may lead to higher entrapped air during casting, resulting in a larger P_{bubble} . This may be due to the fact that when the formwork is tilted, the concrete may rebound at the bottom or when it hits the edge of the formwork, covering more air, as shown in Figure 4.18.

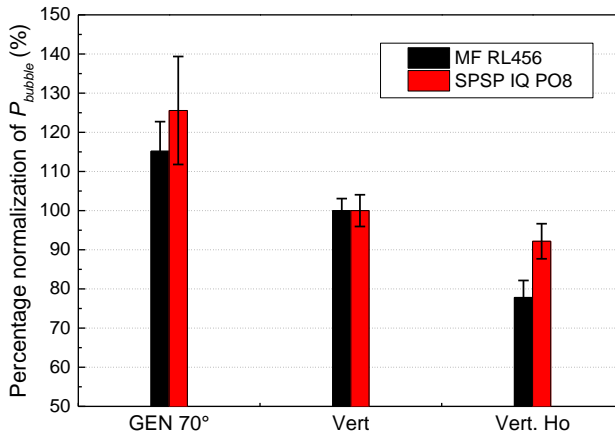


Figure 4.17 Results of P_{bubble} with 3 casting method

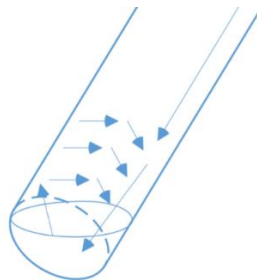


Figure 4.18 Schematic diagram of concrete rebound

In summary, using some casting methods like casting with a hose can contribute to reducing the air pores in hardened concrete to a certain extent. According to the literature, pumping concrete can also be beneficial for this, which will be further studied in the future. However, in the tests of the following sections, the UHPC mixtures are all cast directly from the top to keep the entrapped air during casting as same as possible so that the difference of P_{fresh} and P_{bubble} can be used to reflect the de-airing after mixing.

4.4.3 Concrete rheology

4.4.3.1 Flowability

According to Schachinger I et al. [119], the flowability may affect P_{fresh} in many cases. For verification, a total of 4 groups of UHPC mixtures with different spread-flow values are compared, as shown in Table 4.5. Group 2.3.3-3 is the same group tested in Section 2.3.3. Detailed mix recipes and properties of these UHPC mixtures can be found in Table A.4 in the appendix. In each group, the UHPC mixtures have the same type and batch of raw materials, the same mixer and mixing process, the same casting method and formwork release agent. Only the recipes are different (e.g. different W/B ratio or SP/C ratio) to achieve different flowability. In the names of the UHPC mixtures, “720”, “750”, and “860” are the cement content (kg/m^3), “0.223”, “0.241”, and “0.25” are the W/B ratio, “1.51%”, “1.79%”, etc. are the SP/B ratio. Except for the group 4.4.3-2, the UHPC mixtures in other groups all use CEM A.

Table 4.5 UHPC mixtures to test the influence of flowability

Group	UHPC mixture	Cement content (kg/m^3)	W/B ratio (%)	Spread-flow (cm)	P_{fresh} (%)
4.4.3.1-1	720 0.223 StF	720	0.223	22	4.3
	720 0.25 StF	720	0.25	27.5	3.5
	860 0.223 StF	860	0.223	27.5	3.5
	750 0.241 StF	750	0.241	26	3.8
4.4.3.1-2	720 CEM B 0.223	720	0.223	26	3.6
	720 CEM B 0.232	720	0.232	27.5	3.2
	750 CEM B 0.241	750	0.241	31	2.6
4.4.3.1-3	860 0.223 1.51%	860	0.223	26	4.5
	860 0.223 4.46%	860	0.223	31	3.7
2.3.3-3	720 0.25 1.51%	720	0.25	21	5
	720 0.25 1.79%	720	0.25	26	4.2
	720 0.25 2.23%	720	0.25	28	3.7
	720 0.25 2.68%	720	0.25	28	3.7
	720 0.25 4.46%	720	0.25	28	3.7

Figure 4.19 shows the relationship between the spread-flow value and P_{fresh} after percentage normalization from the UHPC mixture with a 26cm spread-flow value in each group and statistical analysis. It can be observed that there is an almost linear relationship between the spread-flow value and the percentage normalization of P_{fresh} . After fitting, the following equation can be obtained ($R^2=0.991$):

$$\frac{P_{fresh}}{P_{fresh,S=26}} = -0.0415 \times S + 2.079 \quad (4.3)$$

where: S is the spread-flow value, $P_{fresh,S=26}$ is the P_{fresh} when the spread-flow value is 26cm and other factors remain unchanged.

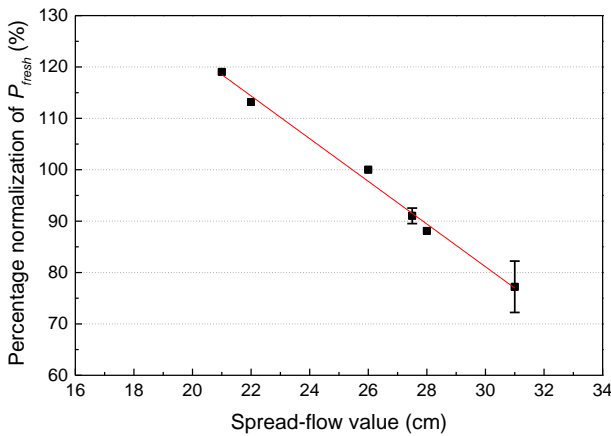
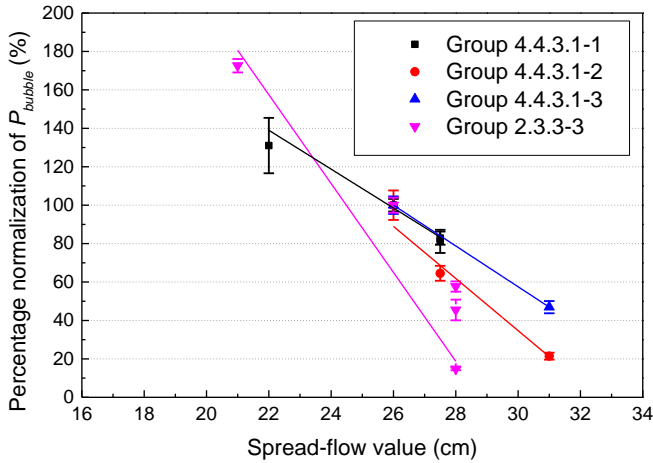
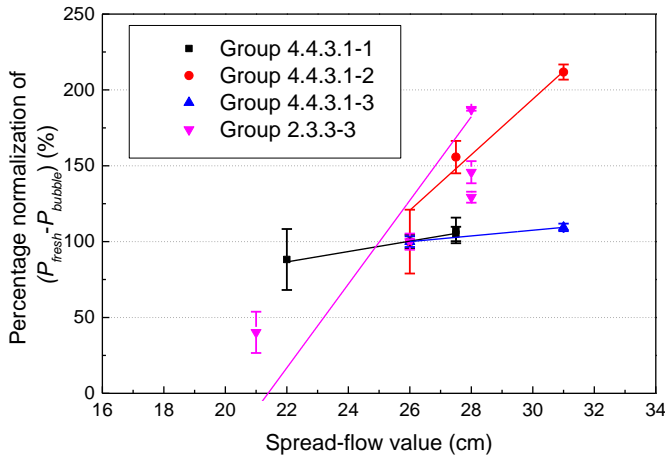


Figure 4.19 Influence of the flowability on P_{fresh}

According to this result, it may be doubtful whether this is caused by increased particle packing density due to increased flowability, leading to further reduced porosity. However, the formation of large air pores does not come from the porosity of the concrete, but rather from the entrapped air of the materials during mixing, as distinguished in Section 1.3. At the same time, the process of de-airing is already going on during mixing. Thus, the real reason should be that higher flowability may enhance the de-airing process during mixing, resulting in a lower P_{fresh} . Additionally, the UHPC mixtures in Group 4.4.3.1-2 contain CEM B, suggesting that the effect of cement type on the de-airing behaviours is through the consistency of concrete.

Figure 4.20 shows the results of P_{bubble} and the $(P_{fresh} - P_{bubble})$ value for these groups of UHPC mixtures. It can be found that the flowability of concrete may not have an influence on the de-airing after mixing. A higher flowability can lead to a lower P_{bubble} by decreasing the P_{fresh} .

(a) Examine P_{bubble} (b) Calculated $P_{fresh} - P_{bubble}$ Figure 4.20 Influence of flowability on the $(P_{fresh} - P_{bubble})$ values in UHPC mixtures

4.4.3.2 Viscosity

According to Huang H et al. [120], and Yu R et al. [121], the viscosity may influence the de-airing behaviours in UHPC. Thus, in this study, 3 groups of UHPC mixtures with the same

flowability and different viscosity are compared, as shown in Table 4.6. The UHPC mixtures in Group 4.4.3.2-1 are the same as that in Group 4.4.3.1-1 tested in Section 4.4.3.1. The UHPC mixtures in Group 4.4.3.2-2 are the same as that in Group 2.3.1-2 tested in Section 2.3.1. Detailed mix recipes and properties of the UHPC mixtures in Group 4.4.3.2-3 can be found in Table A.4 in the appendix. Each group have the same batch of raw materials, the same mixer and mixing process, the same casting method and formwork release agent. Only the recipes and QP/C ratios are different to achieve different viscosity. From the results of P_{fresh} in Table 4.6, the viscosity (reflected by T_{200} value) may not influence P_{fresh} , which may mostly be determined by the flowability.

Table 4.6 UHPC mixtures to test the influence of viscosity

Group	UHPC mixture	Cement content (kg/m ³)	W/B ratio (%)	Spread-flow (cm)	T_{200} (s)	P_{fresh} (%)
4.4.3.2-1	720 0.25 StF	720	0.25	27.5	9	3.5
	860 0.223 StF	860	0.223	27.5	8.5	3.5
4.4.3.2-2	860 12% 30%	860	0.223	27	9	4.3
	860 12% 40%	860	0.232	27	11	4.3
4.4.3.2-3	750 0.241 1% StF	750	0.241	29	11	3.6
	750 0.223 0% StF	750	0.223	29	9	3.6

After the percentage normalization from the UHPC mixtures with a T_{200} value of 9s and statistical analysis, the results are shown in Figure 4.21. It can be seen that a higher viscosity (larger T_{200} value) may lead to a lower ($P_{fresh} - P_{bubble}$) value and thereby a higher P_{bubble} . This means that the viscosity of concrete may not affect the de-airing behaviour during mixing, but only affect the de-airing behaviour after mixing.

It should be noted that the method used to compare the viscosity of UHPC mixtures in the scope of this research can only be based on UHPC mixtures with the same flowability. Therefore, even though the UHPC mixtures in Table 4.6 have the same T_{200} value, due to the difference in flowability, it is incorrect to assume that these UHPC mixtures have the same viscosity. The results in Figure 4.21(b) simply illustrate that the T_{200} value is almost linearly related to the ($P_{fresh} - P_{bubble}$) value and P_{bubble} . It does not make sense to directly derive an equation for the relationship between the T_{200} value and the percentage normalization of P_{bubble} .

Therefore, the results in this section only provide a basis for later studies that illustrate the effects of the viscosity of UHPC mixtures. When an effective method can be found to directly

assess the viscosity of UHPC mixtures with various flowability, an equation for the relationship between the viscosity and the percentage normalization of P_{bubble} can be derived, which will be further investigated in the future.

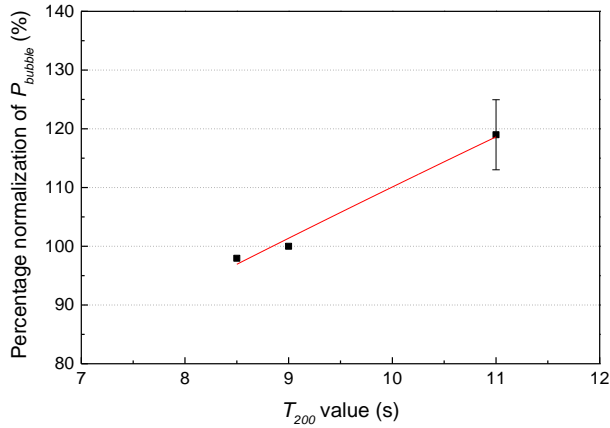
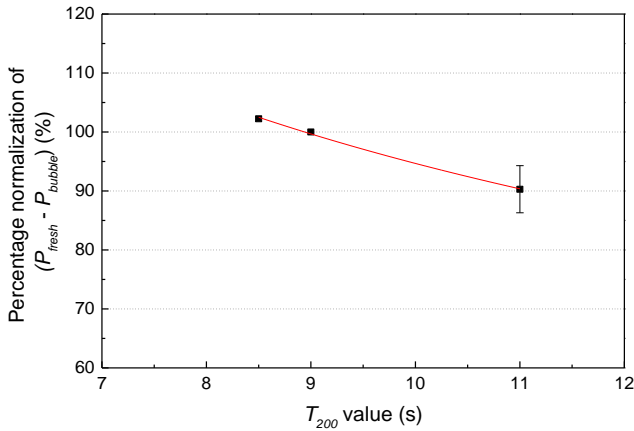
(a) Examined P_{bubble} (b) Calculated $P_{fresh} - P_{bubble}$

Figure 4.21 Influence of viscosity of concrete on the de-airing behaviours of UHPC

4.4.3.3 Temperature in fresh UHPC mixture

According to the investigation in Section 3.4, the temperature in the fresh UHPC mixture may have some influences on the workability issues. Thus, as in Section 3.4.1.1, this study also considers three different mixing procedures in Figure 2.5 and Figure 3.29 ((i), (ii) and (iii)) to examine the different temperatures in fresh concrete.

A total of 3 batches of UHPC mixtures with the same recipe as the UHPC mixture “750 0.223” in Table 4.2 were mixed at various mixing procedures but with similar mixing durations (15min). Detailed mix recipes and properties of these UHPC mixtures can be found in Table A.4 in the appendix (750 0.223 Temp1, 750 0.223 Temp2 and 750 0.223 Temp3). The measured flowability, viscosity, average compressive strength, P_{fresh} and average P_{bubble} of each UHPC mixture with different temperatures in the fresh mixed mixtures are shown in Table 4.7. It can be seen that all the UHPC mixtures exhibit similar properties and are not affected by temperature. Moreover, neither P_{fresh} nor P_{bubble} is significantly affected by the temperature in fresh concrete within the scope of this study.

Table 4.7 Influence of temperature in fresh concrete on the properties and de-airing behaviours of UHPC mixture

Recipe	Temperature in fresh UHPC (°C)	Spread-flow (cm)	T ₂₀₀ (s)	Average compressive strength (MPa)	P_{fresh} (%)	Average P_{bubble} (%)
750 0.223	30.2	24	20	170.35	5.7	3.636
	33.2	24	20	171.15	5.7	3.578
	37.1	24	20	175.1	5.7	3.611

As a result, it seems that the temperature in fresh concrete does not significantly influence either P_{fresh} or P_{bubble} , which will then not be considered a separate influencing factor in the next studies. It is worth noting that the different mixing procedures used in this study did not change the mixing speed and mixing time, but only the temperature in fresh concrete. Therefore, the results of this study cannot explain whether the mixing procedures have an influence on P_{fresh} or P_{bubble} . The mixing procedures may have some influence, which needs to be investigated in the future.

4.4.4 UHPC components

According to the results in Section 2.3, the content of the UHPC components may influence the flowability and viscosity of the mixture. Thus, like the investigation in Chapter 3, this section also investigates the influences of the content of the UHPC components on the de-airing behaviours during and after mixing.

4.4.4.1 Silica fume and quartz powder

As analysed in Section 2.3.1, when the Si/C ratio is within the range of 12-18% and the QP/C ratio is within the range of 30-40%, a higher Si/C ratio decreases the flowability and a higher

QP/C ratio increases the viscosity of the UHPC mixture. Consequently, for further investigation of the influence of the amount of Si and QP on the de-airing behaviours, the UHPC mixtures in Group 2.3.1-2 were also measured the P_{fresh} and cast into several cylinders to examine P_{bubble} , as shown in Table 4.8.

Table 4.8 UHPC mixtures in Group 2.3.1-2

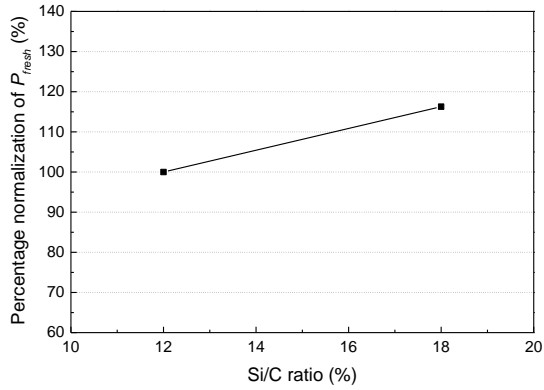
Group	UHPC mixture	Si/C ratio (%)	QP/C ratio (%)	P_{fresh} (%)	Average P_{bubble} (%)
2.3.1-1	860 12% 30%	12	30	4.3	1.442
	860 18% 30%	18	30	5	2.12
	860 12% 40%	12	40	4.3	1.659
	860 18% 40%	18	40	5	2.418

Figure 4.22(a)(b) shows the influence of the Si/C ratio on the P_{fresh} and P_{bubble} after percentage normalization from the UHPC mixtures with 12% Si/C ratio and statistical analysis. Figure 4.22(c) shows the influence of the Si/C ratio on the difference between P_{fresh} and P_{bubble} . It can be seen that a higher Si/C ratio can increase the P_{fresh} and thereby increase the P_{bubble} . But the value of $(P_{fresh} - P_{bubble})$ may not change.

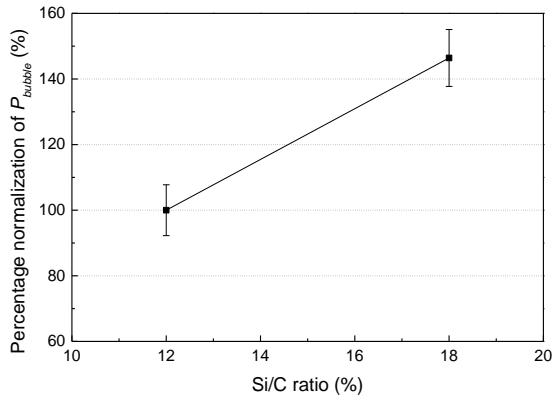
Considering that the silica fume material itself may not have a chemical effect on the de-airing behaviours and all other external factors remain constant, it can be assumed that the increase in silica fume content leads to an increase in P_{fresh} through its reduction in flowability. Consequently, based on the results in Section 4.4.3.1, linear relationships can be assumed between the Si/C ratio and percentage normalization of P_{fresh} . According to the result in Figure 4.22(a), the following equation can be estimated when the Si/C ratio is between 0.12~0.18:

$$\frac{P_{fresh}}{P_{fresh, Si/C=0.12}} = 2.71 \times Si / C + 0.6748 \quad (4.4)$$

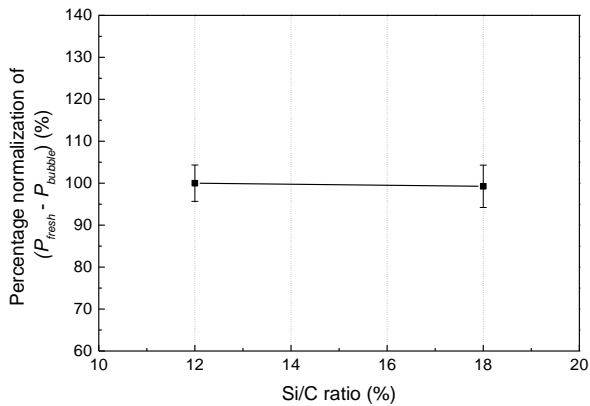
where: $P_{fresh, Si/C=0.12}$ is the P_{fresh} when the Si/C ratio is 0.12 and other factors remain unchanged.



(a) Measured P_{fresh}



(b) Examined P_{bubble}



(c) Calculated $P_{fresh} - P_{bubble}$

Figure 4.22 Influence of Si/C ratio on the de-airing behaviours in UHPC

Assuming that $(P_{fresh} - P_{bubble}) = P_{difference}$, $(P_{fresh, Si/C=0.12} - P_{bubble, Si/C=0.12}) = P_{difference, Si/C=0.12}$, and $P_{difference} = P_{difference, Si/C=0.12}$ (the result in Figure 4.22(c)), the Equation (4.4) can be transformed into:

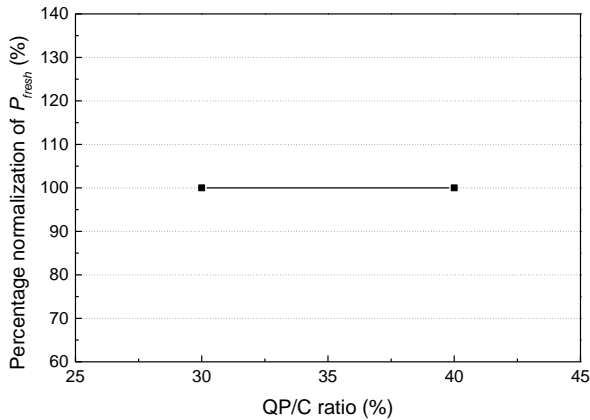
$$\frac{P_{bubble} + P_{difference}}{P_{bubble, Si/C=0.12} + P_{difference, Si/C=0.12}} = 2.71 \times Si / C + 0.6748 \quad (4.5)$$

$$P_{bubble} = (2.71 \times Si / C + 0.6718) P_{bubble, Si/C=0.12} + 2.71 \times Si / C \times P_{difference, Si/C=0.12} - 0.3252 \times P_{difference, Si/C=0.12} \quad (4.6)$$

$$P_{bubble} = P_{bubble, Si/C=0.12} + (2.71 \times Si / C - 0.3252) P_{difference, Si/C=0.12} \quad (4.7)$$

where: $P_{bubble, Si/C=0.12}$ is the P_{bubble} when the Si/C ratio is 0.12 and other factors remain unchanged. $P_{difference, Si/C=0.12}$ is the $(P_{fresh} - P_{bubble})$ value when the Si/C ratio is 0.12 and other factors remain unchanged.

Figure 4.23(a)(b) shows the influence of the QP/C ratio on the P_{fresh} and P_{bubble} after percentage normalization from the UHPC mixtures with a 30% QP/C ratio and statistical analysis. Figure 4.23(c) shows the influence of the QP/C ratio on the difference between P_{fresh} and P_{bubble} . It can be seen that a higher QP/C ratio may not affect P_{fresh} but causes a higher P_{bubble} , which means the QP/C ratio has an effect on the de-airing behaviour after mixing.



(a) Measured P_{fresh}

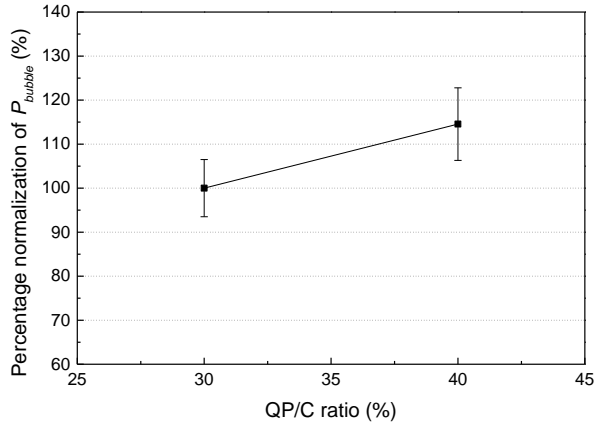
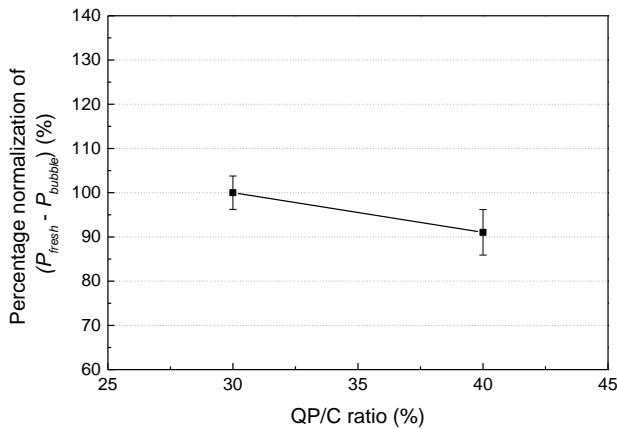
(b) Examined P_{bubble} (c) Calculated $P_{fresh} - P_{bubble}$

Figure 4.23 Influence of QP/C ratio on the de-airing behaviours in UHPC

Considering that the quartz powder material itself may not have a chemical effect on the de-airing behaviours and all other external factors remain constant, it can be assumed that the increase in quartz powder content leads to an increase in the P_{bubble} through its increase in viscosity. Consequently, based on the results in Section 4.4.3.2, linear relationships can be assumed between the QP/C ratio and percentage normalization of the $(P_{fresh} - P_{bubble})$ value. According to the result in Figure 4.23(c), the following equation can be estimated when the QP/C ratio is between 0.3~0.4:

$$\frac{P_{fresh} - P_{bubble}}{P_{fresh, QP/C=0.3} - P_{bubble, QP/C=0.3}} = -0.896 \times QP / C + 1.2688 \quad (4.8)$$

where: $P_{fresh, QP/C=0.3}$ is the P_{fresh} when the QP/C ratio is 0.3 and other factors remain unchanged. $P_{bubble, QP/C=0.3}$ is the P_{bubble} when the QP/C ratio is 0.3 and other factors remain unchanged.

Considering that $P_{fresh} = P_{fresh, QP/C=0.3}$, the Equation (4.8) can be transformed into:

$$P_{bubble} = (0.896 \times QP / C - 1.2688) P_{bubble, QP/C=0.3} + (0.896 \times QP / C - 0.2688) P_{fresh, QP/C=0.3} \quad (4.9)$$

where: $P_{bubble, QP/C=0.3}$ is the P_{bubble} when the QP/C ratio is 0.3 and other factors remain unchanged. $P_{difference, QP/C=0.3}$ is the $(P_{fresh} - P_{bubble})$ value when the QP/C ratio is 0.3 and other factors remain unchanged.

In summary, more Si and QP may be detrimental to the de-airing behaviours in UHPC. Combined with the results of Section 2.3.1, unless special application requirements, the Si/C ratio and the QP/C ratio should be as low as possible above 12% and 30%, respectively.

4.4.4.2 Water-to-binder ratio

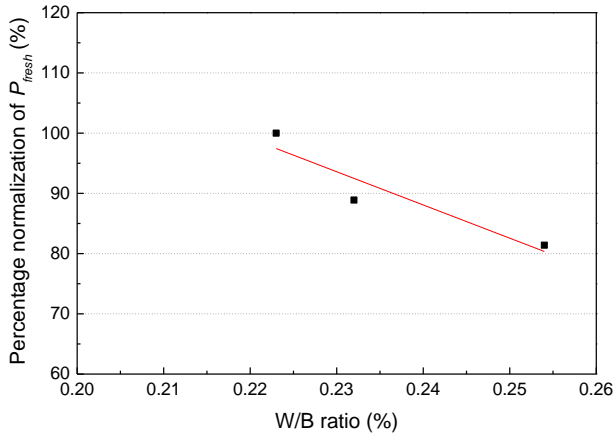
According to the existing research, it is well known that a higher W/B ratio will lead to a higher flowability, a lower viscosity and a lower compressive strength of the UHPC. Consequently, for further investigation of the influence of the W/B ratio on the de-airing behaviours, the UHPC mixtures in Group 2.3.2-7 and 2.3.2-8 were also measured the P_{fresh} and cast into several cylinders to examine P_{bubble} , as shown in Table 4.9.

Table 4.9 UHPC mixtures in Groups 2.3.2-7 and 2.3.2-8

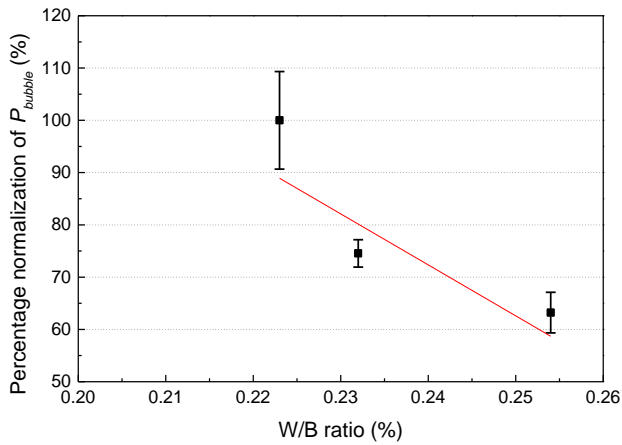
Group	Name	Tested W/B ratio	Corresponding W/C ratio	P_{fresh} (%)
2.3.2-7	720 CEM A 2%	0.223, 0.254	0.25, 0.285	4.3, 3.5
2.3.2-8	720 CEM B 2%	0.223, 0.232	0.25, 0.26	3.6, 3.2

Figure 4.24(a)(b) shows the influence of the W/B ratio on the P_{fresh} and P_{bubble} after percentage normalization from the UHPC mixtures with 0.223 W/B ratio and statistical analysis. Figure 4.24(c) shows the influence of the W/B ratio on the difference between P_{fresh} and P_{bubble} . It

can be seen that a higher W/B ratio can decrease the P_{fresh} and increase the $(P_{fresh} - P_{bubble})$ value, thereby decreasing the P_{bubble} .



(a) Measured P_{fresh}



(b) Examined P_{bubble}

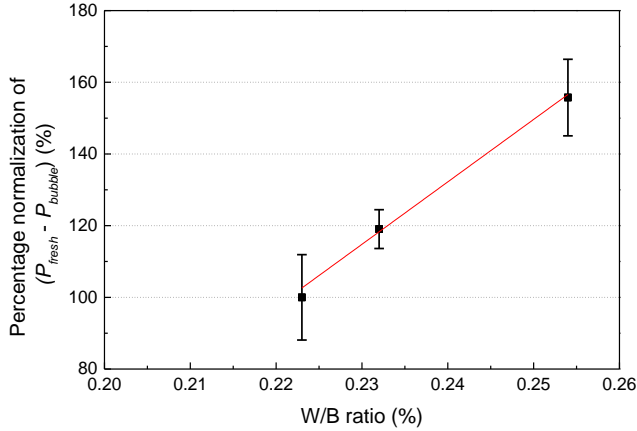
(c) Calculated $P_{fresh} - P_{bubble}$

Figure 4.24 Influence of W/B ratio on the de-airing behaviours in UHPC

According to the results in Section 2.3.2, the W/B ratio is almost linearly related to the flowability of UHPC mixtures. The result in Figure 4.24(c) also shows that the W/B ratio is linearly related to the $(P_{fresh} - P_{bubble})$ value ($R^2=0.994$). Thus, based on the results in Section 4.4.3.1, linear relationships can be assumed between the W/B ratio and P_{fresh} (although the R^2 value is only 0.766 in these tests). According to the result in Figure 4.24(a) and Figure 4.24(c), the following equations can be estimated:

$$\frac{P_{fresh}}{P_{fresh,W/B=0.223}} = -5.515 \times W / B + 2.23 \quad (4.10)$$

where: $P_{fresh,W/B=0.223}$ is the P_{fresh} when the W/B ratio is 0.223 and other factors remain unchanged.

$$\frac{P_{fresh} - P_{bubble}}{P_{fresh,W/B=0.223} - P_{bubble,W/B=0.223}} = 17.74 \times W / B - 2.956 \quad (4.11)$$

where: $P_{bubble,W/B=0.223}$ is the P_{bubble} when the W/B ratio is 0.223 and other factors remain unchanged.

Combining the Equation (4.10) and (4.11), the following equation can be estimated:

$$P_{bubble} = (17.74 \times W / B - 2.956) P_{bubble,W/B=0.223} - (23.255 \times W / B - 5.186) P_{fresh,W/B=0.223} \quad (4.12)$$

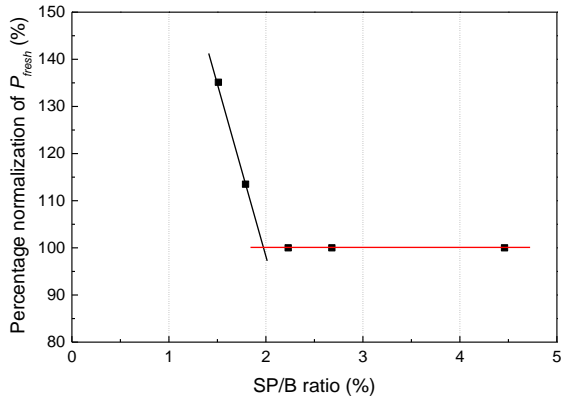
4.4.4.3 Superplasticizer (SP)

On the basis of the research results in Section 4.3, the superplasticizer content may have an influence on P_{fresh} and the $(P_{fresh} - P_{bubble})$ value. The investigation of the influence of the SP/B ratio should also be considered from two parts: the SP/B ratio higher than the critical value and the SP/B ratio lower than the critical value. Thus, as shown in Table 4.10, for further investigation of the influence of SP/B ratio on de-airing behaviours, except for Group 2.3.3-3, the UHPC mixtures in Group 2.3.3-7 (Table 2.8) were also cast into cylinders and examined the P_{bubble} . The UHPC mixtures in group 4.3-1 were mixed with an ELBA mixer, which cannot be compared together with the UHPC mixtures in group 2.3.3-3 and group 2.3.3-7 mixed with an Eirich mixer.

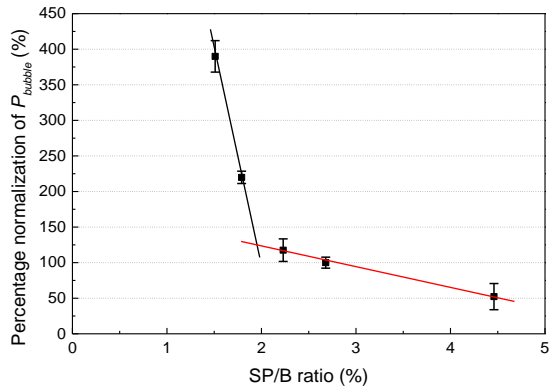
After percentage normalization and statistical analysis, the results are shown in Figure 4.25. When the SP/B ratio is smaller than the critical value, with the increase of SP/B ratio, the increase of flowability leads to the decrease of P_{fresh} , thus the decrease of P_{bubble} . Interestingly, when the SP/B ratio is larger than the critical value, as the SP/B ratio continues to increase, the flowability and P_{fresh} remain unchanged, but P_{bubble} is still decreasing. From the results of the $(P_{fresh} - P_{bubble})$ value, it can also be found that as the SP/B ratio increases, the $(P_{fresh} - P_{bubble})$ value increases very rapidly at first, which may be due to the decrease of the viscosity of the concrete [32], and later when the viscosity remains constant, the $(P_{fresh} - P_{bubble})$ value still increases, but at a slightly slower rate. It can thus be deduced that when the flowability and viscosity are constant, an increase in SP/B ratio may have a retarding effect on the changing of the consistency of the fresh UHPC over time (results in Section 2.3.3.2), which provides more time for the de-airing process after mixing and thereby causes an increase in the $(P_{fresh} - P_{bubble})$ value.

Table 4.10 UHPC mixtures in Groups 2.3.3-3 and 2.3.3-7

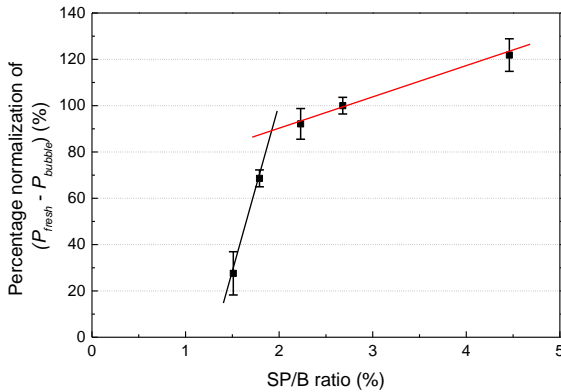
Group	UHPC mixture	SP/B ratio (%)	Corresponding SP/C ratio (%)	Spread-flow (cm)	P_{fresh} (%)
2.3.3-3	720 0.25 1.51%	1.51	1.7	21	5
	720 0.25 1.79%	1.79	2	26	4.2
	720 0.25 2.23%	2.23	2.5	28	3.7
	720 0.25 2.68%	2.68	3	28	3.7
	720 0.25 4.46%	4.46	5	28	3.7
2.3.3-7	860 0.223 (2% StF) 2.23%	2.23	2.5	27.5	4.2
	860 0.223 (2% StF) 2.68%	2.68	3	27.5	4.2
	860 0.223 (2% StF) 4.46%	4.46	5	27.5	4.2



(a) Measured P_{fresh}



(b) Examined P_{bubble}



(c) Calculated $P_{fresh} - P_{bubble}$

Figure 4.25 Influence of SP/B ratio on the de-airing behaviours in UHPC

Considering that the superplasticizer material itself may not have a chemical effect on the de-airing behaviours and all other external factors remain constant, it can be assumed that the increase in SP/B ratio leads to a decrease in the P_{bubble} through its increase in flowability, decrease in viscosity and the retarding effect. From the results, linear relationships can be assumed between the SP/B ratio and percentage normalization of P_{fresh} and that of the $(P_{fresh} - P_{bubble})$ value ($R^2=0.991$) when the SP/B ratio is smaller and larger than the critical value, respectively. Hence, considering the critical value of SP/B ratio is 1.86% according to the results in Section 2.3.3, based on the result in Figure 4.25(a) and Figure 4.25(c), the following equation can be estimated:

$$\frac{P_{fresh}}{P_{fresh,SP/B=2.68\%}} = \begin{cases} -77.22 \times SP/B + 2.5174, & SP/B \leq 1.86\% \\ 1, & SP/B \geq 1.86\% \end{cases} \quad (4.13)$$

where: $P_{fresh,SP/B=2.68\%}$ is the P_{fresh} when the SP/B ratio is 2.68% and other factors remain unchanged.

$$\frac{P_{fresh} - P_{bubble}}{P_{fresh,SP/B=2.68\%} - P_{bubble,SP/B=2.68\%}} = \begin{cases} 146.5 \times SP/B - 1.936, & SP/B \leq 1.86\% \\ 13.026 \times SP/B + 0.651, & SP/B \geq 1.86\% \end{cases} \quad (4.14)$$

where: $P_{bubble,SP/B=2.68\%}$ is the P_{bubble} when the SP/B ratio is 2.68% and other factors remain unchanged.

According to the conclusion in Section 2.3.3, the value of the SP/B ratio is suggested to be in the range of 1.79-3.57%. Therefore, Combining the Equation (4.13) and (4.14), the following equation can be estimated:

$$P_{bubble} = \begin{cases} (146.5 \times SP/B - 1.936) P_{bubble,SP/B=2.68\%} \\ - (223.72 \times SP/B - 4.4534) P_{fresh,SP/B=2.68\%} \\ (13.026 \times SP/B + 0.651) P_{bubble,SP/B=2.68\%} \\ - (13.026 \times SP/B - 0.349) P_{fresh,SP/B=2.68\%} \end{cases}, \begin{matrix} SP/B \leq 1.86\% \\ SP/B \geq 1.86\% \end{matrix} \quad (4.15)$$

Consequently, when no higher than 3.57%, a higher SP/B ratio would be preferable.

4.4.4.4 Paste volume

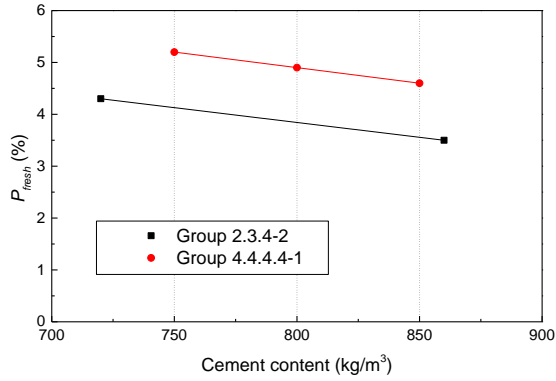
According to the results in Section 2.3.4, a higher paste content can lead to a higher flowability of concrete. To further investigate the influence of paste content on the de-airing

behaviours of UHPC, the UHPC mixtures in Group 2.3.4-2 were also tested P_{fresh} and P_{bubble} . Additionally, one more group was introduced to investigate the influence of paste volume, as shown in Table 4.11. Detailed mix recipes and properties of the UHPC mixtures in Group 4.4.4.4-1 can be found in Table A.4 in the appendix. In each group, the UHPC mixtures had the same W/B ratio, SP/B ratio, Si/C ratio and QP/C ratio, so the different cement contents represented the different paste volumes. In the names of the UHPC mixtures in Group 4.4.4.4-1, “750”, “800” and “850” are the cement contents, and “0%” is the volume contents of StF, which is different from the “2%” of StF content in Group 2.3.4-2.

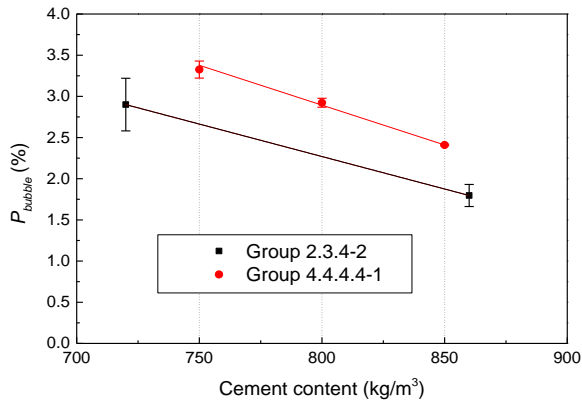
Table 4.11 UHPC mixtures in Group 2.3.4-2 and new Group 4.4.4.4-1

Group	UHPC mixture	CEM content (kg/m ³)	Corresponding paste content (L/m ³)	P_{fresh} (%)
2.3.4-2	0.223 2.68 2% 553.6	720	553.6	4.3
	0.223 2.68 2% 657.4	860	657.4	3.5
4.4.4.4-1	750 0%	750	575.8	5.2
	800 0%	800	612.9	4.9
	850 0%	860	649.9	4.6

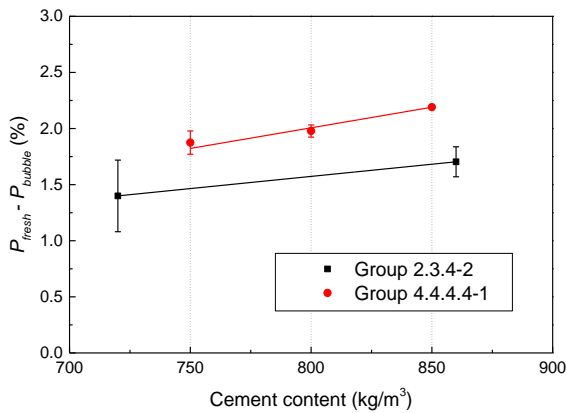
Since the same cement content and paste volume do not exist in both UHPC mixtures, the results cannot be percentage normalised together. Thus, Figure 4.26 shows the results of measured P_{fresh} , examined P_{bubble} and calculated ($P_{fresh} - P_{bubble}$) value for these two groups. It can be found that a higher cement content (paste volume) can decrease P_{fresh} and increase ($P_{fresh} - P_{bubble}$) value, resulting in a lower P_{bubble} . The relationship between cement content and P_{fresh} , and the relationship between cement content and ($P_{fresh} - P_{bubble}$) value are almost linear. Therefore, an increase in the cement content (paste volume) in UHPC mixtures can enhance the de-airing behaviours both during and after mixing. Considering that an increase in the cement content (paste volume) can also lead to an increase in flowability and a decrease in viscosity, these results are consistent with the results in Section 4.4.3.



(a) Measured P_{fresh}



(b) Examined P_{bubble}



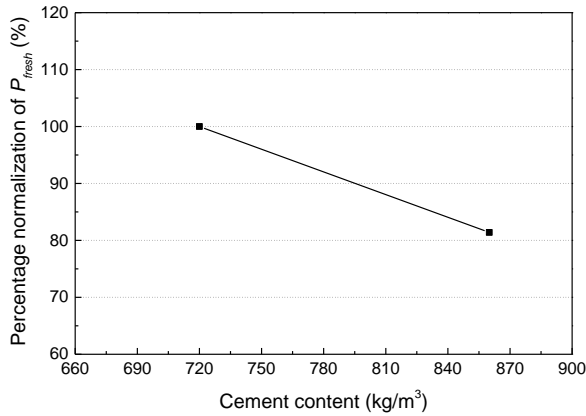
(c) Calculated $P_{fresh} - P_{bubble}$

Figure 4.26 Influence of paste content on the de-airing behaviours in UHPC

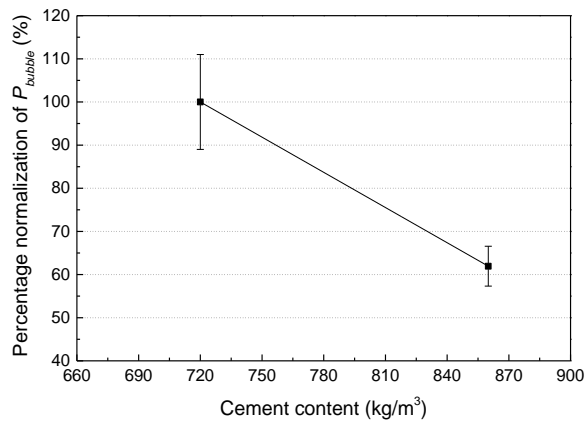
Considering the reference recipe contains 720kg/m^3 cement content (Table 2.5), for Group 2.3.4-2, after percentage normalization from the UHPC mixtures with 720kg/m^3 cement content and statistical analysis, the results of P_{fresh} , P_{bubble} and the $(P_{fresh} - P_{bubble})$ value can be seen in Figure 4.27. Accordingly, the following equations can be estimated:

$$\frac{P_{fresh}}{P_{fresh,CC=720}} = -0.00133 \times CC + 1.958 \quad (4.16)$$

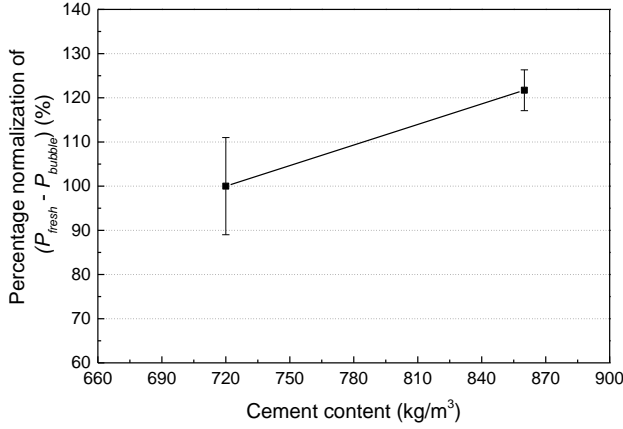
where: CC is the cement content of the UHPC (kg/m^3); $P_{fresh,CC=720}$ is the P_{fresh} when the cement content is 720kg/m^3 and other factors remain unchanged.



(a) Measured P_{fresh}



(b) Examined P_{bubble}



(c) Calculated $P_{fresh} - P_{bubble}$

Figure 4.27 Results of group 2.3.4-2 after percentage normalization

$$\frac{P_{fresh} - P_{bubble}}{P_{fresh,CC=720} - P_{bubble,CC=720}} = 0.00155 \times CC - 0.116 \quad (4.17)$$

where: $P_{bubble,CC=720}$ is the P_{bubble} when the cement content is 720kg/m^3 and other factors remain unchanged.

Combining the Equation (4.16) and (4.17), the following equation can be estimated:

$$P_{bubble} = (0.00155 \times CC - 0.166) P_{bubble,CC=720} - (0.00288 \times CC - 2.074) P_{fresh,CC=720} \quad (4.18)$$

Co-relating the Equations (4.4) ~ (4.18), it can be concluded that:

$$P_{fresh} = \begin{cases} \left((2.71 \times Si / C + 0.6748)(-5.515 \times W / B + 2.23) \right. \\ \quad \times (-77.22 \times SP / B + 2.5174) \\ \quad \times (-0.00133 \times CC + 1.958) P_{fresh,reference} \\ \left. (2.71 \times Si / C + 0.6748)(-5.515 \times W / B + 2.23) \right. \\ \quad \times (-0.00133 \times CC + 1.958) P_{fresh,reference} \end{cases}, \begin{matrix} SP / B \leq 1.86\% \\ SP / B \geq 1.86\% \end{matrix} \quad (4.19)$$

$$P_{bubble} = \begin{cases} \left(\begin{array}{l} (0.896 \times QP / C - 1.2688)(17.74 \times W / B - 2.956) \\ \times (0.00155 \times CC - 0.166)(146.5 \times SP / B - 1.936) \end{array} \right) P_{bubble,reference} \\ \left(\begin{array}{l} (0.896 \times QP / C - 1.2688)(17.74 \times W / B - 2.956) \\ \times (0.00155 \times CC - 0.166)(223.72 \times SP / B - 4.4534) \\ - (0.896 \times QP / C - 1.2688)(17.74 \times W / B - 2.956) \\ \times (0.00288 \times CC - 2.074) \\ - (0.896 \times QP / C - 1.2688)(23.255 \times W / B - 5.186) \\ + (0.896 \times QP / C - 0.2688) + (2.71 \times Si / C - 0.3252) \end{array} \right) P_{fresh,reference} \\ \left(\begin{array}{l} (0.896 \times QP / C - 1.2688)(17.74 \times W / B - 2.956) \\ \times (0.00155 \times CC - 0.166)(13.026 \times SP / B + 0.651) \end{array} \right) P_{bubble,reference} \\ \left(\begin{array}{l} (0.896 \times QP / C - 1.2688)(17.74 \times W / B - 2.956) \\ \times (0.00155 \times CC - 0.166)(13.026 \times SP / B - 0.349) \\ - (0.896 \times QP / C - 1.2688)(17.74 \times W / B - 2.956) \\ \times (0.00288 \times CC - 2.074) \\ - (0.896 \times QP / C - 1.2688)(23.255 \times W / B - 5.186) \\ + (0.896 \times QP / C - 0.2688) + (2.71 \times Si / C - 0.3252) \end{array} \right) P_{fresh,reference} \end{cases} \quad \begin{array}{l} , SP / B \leq 1.86\% \\ \\ \\ , SP / B \geq 1.86\% \end{array} \quad (4.20)$$

where: $P_{fresh,reference}$ is the P_{fresh} when the recipe of UHPC mixture is the reference mix proportion; $P_{bubble,reference}$ is the P_{bubble} when the recipe of UHPC mixture is the reference mix proportion. As mentioned before, it is not possible to derive specific values for $P_{fresh,reference}$ and $P_{bubble,reference}$ as the raw material batch of UHPC, storage time, etc. may have some effect on the properties. However, according to equations (4.19) and (4.20), for UHPC mixtures without coarse aggregate and steel fibres, P_{fresh} and P_{bubble} can be calculated based on the results of the reference mix proportion.

4.4.4.5 Coarse aggregate and steel fibre

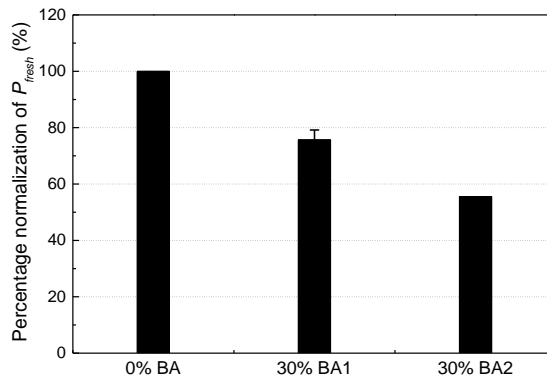
As introduced in Sections 2.3.5 and 2.3.6, when the concrete has the same paste content, an increase in the amount or maximum size of the coarse aggregates tends to change the flowability and causes segregation because of the decreased total surface area of the particles. An increase in the amount or maximum size of steel fibres also tends to change the flowability because the network formed by the intersection of steel fibres will prevent the flow of concrete. Thus, in order to keep the flowability of concrete and prevent it from affecting P_{fresh} , the paste content of UHPC mixtures was adjusted to investigate the influence of the amount and size of coarse aggregates (BAs) and steel fibres on the de-airing behaviours.

For the investigation of coarse aggregate, the UHPC mixtures in Group 2.3.5-2 and Group 2.3.5-3 were also tested for the P_{fresh} and cast into cylinders to examine P_{bubble} , as shown in Table 4.12.

Table 4.12 UHPC mixtures in Groups 2.3.5-2 and 2.3.5-3

Group	UHPC mixture	CEM content (kg/m ³)	Paste content (L/m ³)	Coarse aggregates	P_{fresh} (%)	Average P_{bubble} (%)
2.3.5-2	(2) 0.25 0% BA	720	553.6	Without BA	4.8	2.154
	(2) 0.25 30% BA1	660	509.1	V(BA1)/V(Ag)=30%	3.8	1.55
2.3.5-3	(3) 0.27 0% BA	720	568	Without BA	5.4	4.027
	(3) 0.27 30% BA1	660	522.3	V(BA1)/V(Ag)=30%	3.9	2.629
	(3) 0.27 30% BA2	630	499.5	V(BA2)/V(Ag)=30%	3	1.863

After percentage normalization from the UHPC mixtures without BA (720kg/m³ of cement content) and statistical analysis, the results of the influence of BA content and size on the de-airing behaviours of the UHPC mixture can be seen in Figure 4.28. It can be found that a higher BA content and a larger size may cause a lower P_{fresh} and a slightly lower ($P_{fresh} - P_{bubble}$) value, leading to a lower P_{bubble} . Considering that the flowability and viscosity do not change when the paste volume is adjusted (the results in Section 2.3.5), it can be assumed that when the concrete contains more or larger coarse aggregates, whose density is much higher than other components, the mixing process would be more intense, resulting in more rapid de-airing during mixing, thereby a lower P_{fresh} . After casting, because of the long way around the rise (Figure 3.45), the de-airing after mixing may decrease slightly.

(a) Measured P_{fresh}

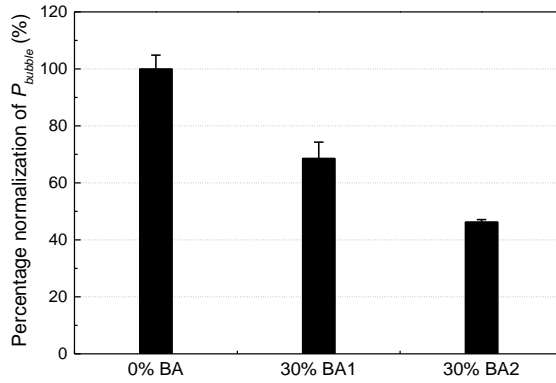
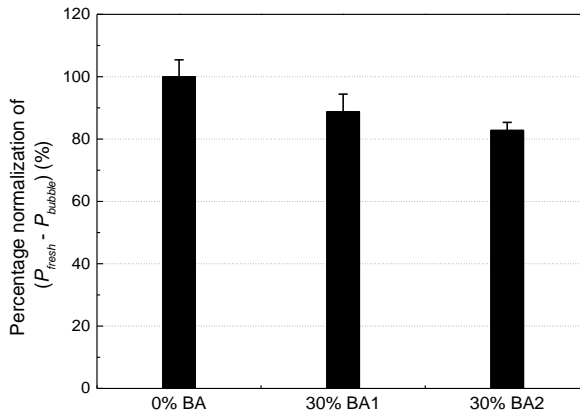
(b) Examined P_{bubble} (c) Calculated $P_{fresh} - P_{bubble}$

Figure 4.28 Influence of BA content and size on the de-airing behaviours in UHPC

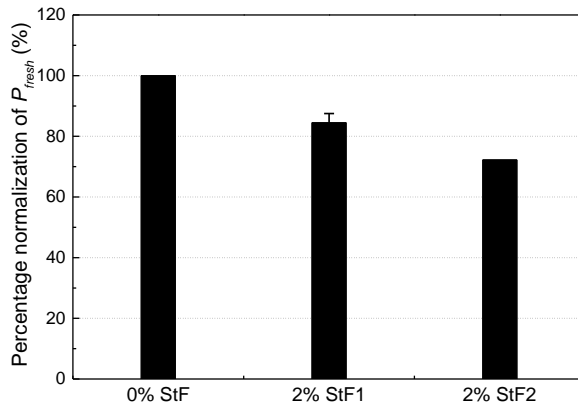
According to Wang R et al. [122] and Li T et al. [123], more steel fibres may decrease the air bubbles in UHPC. For the investigation of steel fibre, Groups 2.3.6-2 and 2.3.6-3 were also tested P_{fresh} and P_{bubble} , as shown in Table 4.13.

Table 4.13 UHPC mixtures in Groups 2.3.6-2 and 2.3.6-3

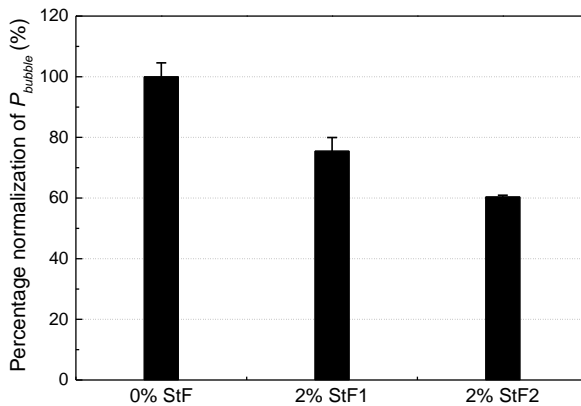
Group	UHPC mixture	CEM content (kg/m ³)	Paste content (L/m ³)	Steel fibres	P_{fresh} (%)	Average P_{bubble} (%)
2.3.6-2	(2) 0.25 0% StF	720	553.6	Without StF	4.8	2.154
	(2) 0.25 2% StF1	750	509.1	With 2V% StF1	4.2	1.713
2.3.6-3	(3) 0.27 0% StF	720	568	Without StF	5.4	3.352
	(3) 0.27 2% StF1	790	522.3	With 2V% StF1	4.4	2.395

(3) 0.27 2% StF2	780	499.5	With 2V% StF2	3.9	2.024
------------------	-----	-------	---------------	-----	-------

After percentage normalization from the UHPC mixtures without StF (720kg/m³ of cement content) and statistical analysis, the results of the influence of StF content and size on the de-airing behaviours of the UHPC mixture can be seen in Figure 4.29. It can be found that a higher StF content and a larger size may also cause a lower P_{fresh} and a slightly lower ($P_{fresh} - P_{bubble}$) value, leading to a lower P_{bubble} . Considering that the flowability and viscosity don't change (Section 2.3.6), it can be assumed that when the concrete contains more or larger steel fibres, the mixing process would also be more intense, resulting in more rapid de-airing during mixing, thereby a lower P_{fresh} . After casting, also because of the long way around the rise (Figure 3.45), the de-airing after mixing may decrease slightly.



(a) Measured P_{fresh}



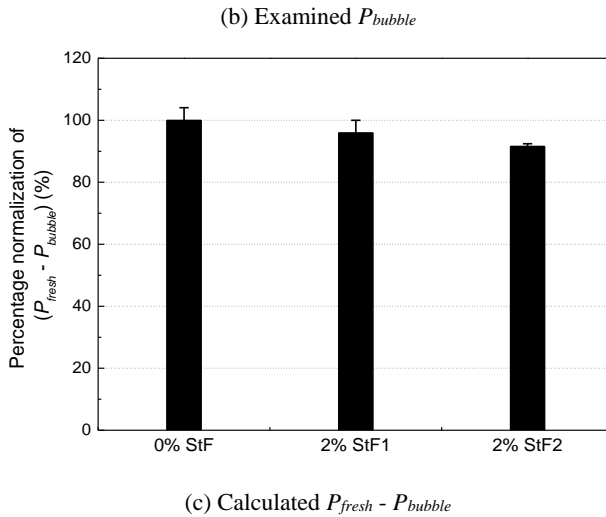


Figure 4.29 Influence of StF content and size on the de-airing behaviours in UHPC

From these results, it can be found that large particles in concrete such as BA and StF can be beneficial to enhance the de-airing behaviours in UHPC to a certain extent. Therefore, this can also be considered in some practical engineering applications.

4.4.5 Defoaming agent

According to Huang H et al. [120] and Yu R et al. [121], some defoaming agents might also contribute to the reduction of P_{fresh} . The defoaming agents can be powders or solutions, which are added as an admixture with the superplasticizer during the mixing. In order to investigate the functional mechanisms, this research considered two products to test their influence on the de-airing behaviours, which were the “Perfin-300” (Perfin) from the company “Sika AG” and the “Premadd foam EXT” (Foam) from the company “BT3 Betontechnik”. The technical specifications of the two defoaming agents are shown in Table 4.14. Sika® PerFin-300 is a liquid concrete admixture to reduce pores on the concrete surface, which complies with EN 934-2 Table 9 (sealant) [132]. It can be used in concrete with alkali-sensitive aggregate. BT3 Premadd Foam EX T is a high-quality defoaming agent with very high stability and a good defoaming effect for use in fresh concrete in precast concrete plants.

Table 4.14 Technical specifications of the defoaming agents

Name	Form	Density (kg/l)	PH value	Solid content:
Sika Perfin	liquid	0.97	3.7 +/- 0.5	30 wt.%
BT3 Foam	liquid	1.07 +/- 0.02	-	30 wt.%

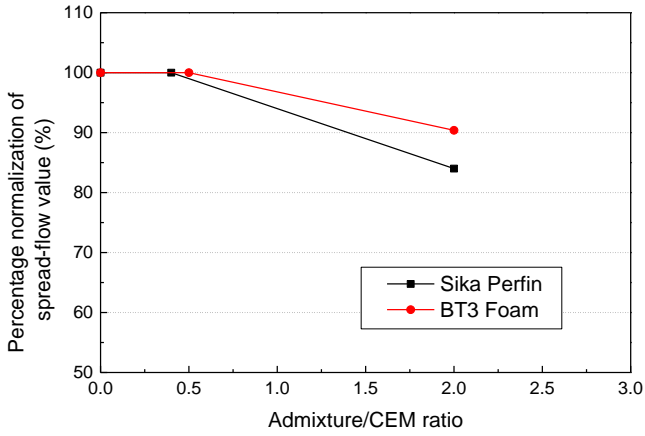
4.4.5.1 Preliminary experiments

In the beginning, preliminary experiments to investigate the influence of each admixture/cement ratio on the properties of UHPC were performed, as shown in Table 4.15. Detailed mix recipes and properties of these UHPC mixtures can be found in Table A.4 in the appendix. In the names of the UHPC mixtures, “750”, “860” and “720” are the cement contents, and “0.25” and “0.27” are the W/C ratios. Each UHPC mixture was mixed with a small Hobart mixer to test the spread-flow value, P_{fresh} and cast one $100 \times 100 \times 100 \text{mm}^3$ cube to test the compressive strength.

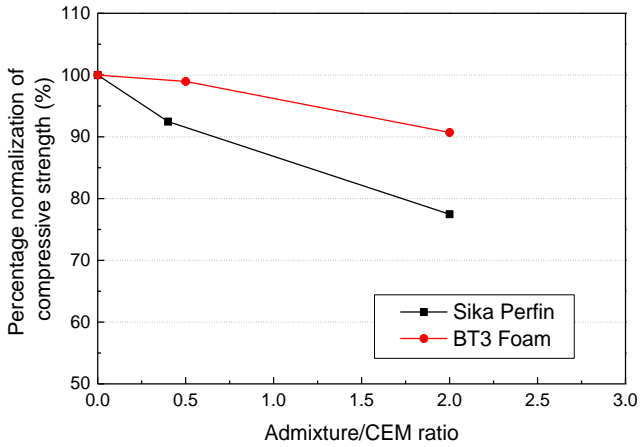
Table 4.15 UHPC groups tested in this section

Group	Name	Admixture	Admixture/cement ratio
4.4.5.1-1	750 0.27	Perfin	0%, 0.4%
4.4.5.1-2	860 0.25	Perfin	0%, 2%
4.4.5.1-3	720 0.25	Foam	0%, 0.5%, 2%

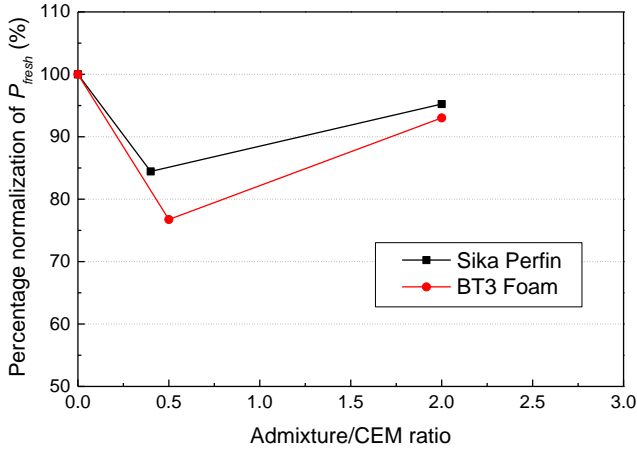
After percentage normalization from the UHPC mixtures without Perfin or Foam and statistical analysis, the measured flowability, compressive strength and P_{fresh} are shown in Figure 4.30. It can be found that when 2% of the admixture/cement mass ratio (Admixture/CEM ratio) for both Perfin and Foam is mixed in the concrete, the flowability of UHPC may decrease significantly, and the compressive strength may also undergo a remarkable reduction. P_{fresh} will reduce when 0.4~0.5% admixture/cement ratio is added. But when 2%, due to the decrease in flowability, P_{fresh} will increase again. These results are consistent with that reported by Yu R et al. [121]. Accordingly, it seems that an excessive amount of defoaming agent may not benefit to enhance the de-airing behaviours in UHPC, but reduce the strength.



(a) Flowability



(b) Compressive strength



(c) Measured P_{fresh}

Figure 4.30 Influence of Perfin/CEM ratio on the properties and P_{fresh} of UHPC

4.4.5.2 Further investigation

As shown in Table 4.16, in order to fully explore the actual impact, 2 groups of UHPC mixtures with the same raw materials and mix proportion were mixed with an Eirich mixer. The admixture/cement mass ratios (Admixture/CEM ratio) are 0%, 0.5%, 1%, 1.5%, and 2%, respectively. Detailed mix recipes and properties of these UHPC mixtures can be found in Table A.4 in the appendix. For the higher admixture/cement ratio, a slightly higher W/C ratio is considered (in the names of the UHPC mixtures as “0.25”, “0.255”, “0.26” and “0.264”) to keep the flowability and viscosity constant to study the influence of the defoaming agent on P_{fresh} . These 2 groups were mixed on different days and the cement could vary in quality, leading to different flowability and P_{fresh} of the concrete when without a defoaming agent.

Table 4.16 UHPC groups tested in this section

Group	Admixture	Admixture/cement ratio	Adjusted W/C ratio	Spread-flow (cm)	T_{200} (s)
Sika Perfin	Perfin	0%, 0.5%, 1%, 1.5%, 2%	0.25, 0.25, 0.255, 0.26, 0.264	28.5	12
BT3 Foam	Foam	0%, 0.5%, 1%, 1.5%, 2%	0.25, 0.25, 0.255, 0.26, 0.264	26	19

The measured compressive strength of the UHPC mixture is shown in Figure 4.31. It is interesting to find that the UHPC mixtures with more Sika Perfin will have quite lower compressive strengths, but the UHPC mixtures with more BT3 Foam seem to only have

slightly lower compressive strengths. It can therefore be deduced that the slight decrease in compressive strength for the UHPC with BT3 Foam may be due to the higher W/C ratio and the slight influence of this admixture, while the decrease in compressive strength for the UHPC with Sika Perfin may be due to the large effect of this admixture. This means that compared with BT3 Foam, Sika Perfin may have a large negative effect on the compressive strength of UHPC. Thus, the application of Sika Perfin must take this into account.

Figure 4.32 shows the results of measured P_{fresh} , examined P_{bubble} and calculated ($P_{fresh} - P_{bubble}$) value, it could be found that both Sika Perfin and BT3 Foam can decrease the P_{fresh} , but the ($P_{fresh} - P_{bubble}$) value seems not to change, Sika Perfin may have a slightly stronger effect than BT3 Foam. This means that the defoaming agent can influence the de-airing during mixing, but not the de-airing after mixing. The maximum amount of defoaming agent is preferably no more than 0.5% of the cement mass, because after 0.5%, more admixture/cement ratio will not have a big benefit on de-airing but a loss on hardening performance.

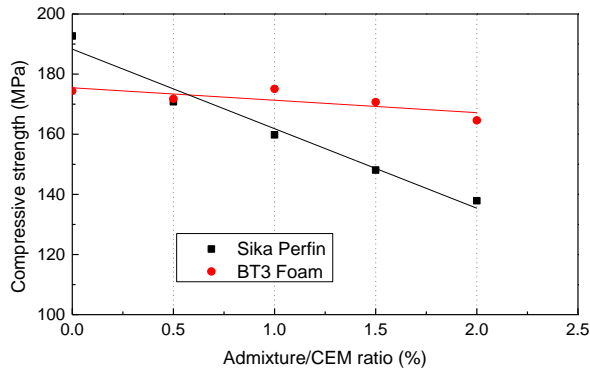
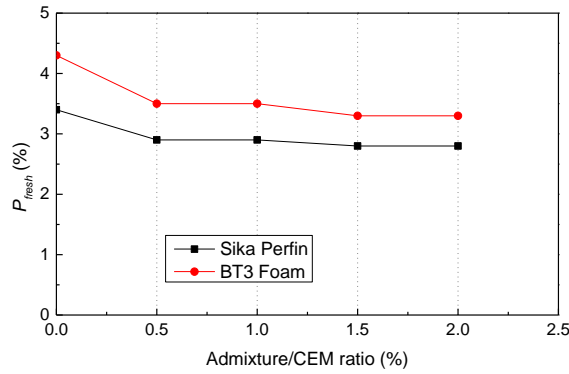
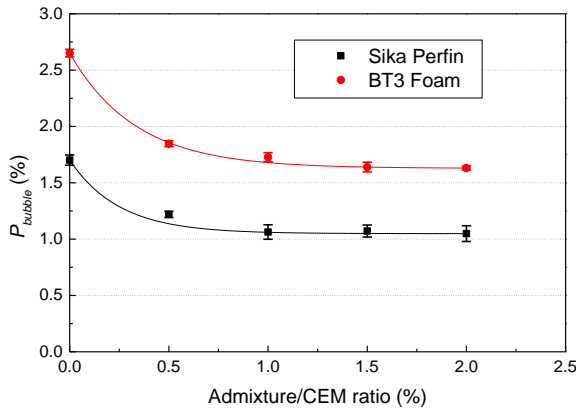


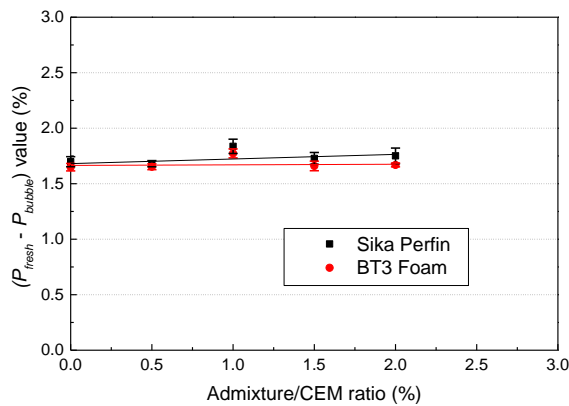
Figure 4.31 Influence of the Admixture/CEM ratios on the compressive strength of UHPC



(a) Measured P_{fresh}



(b) Examined P_{bubble}

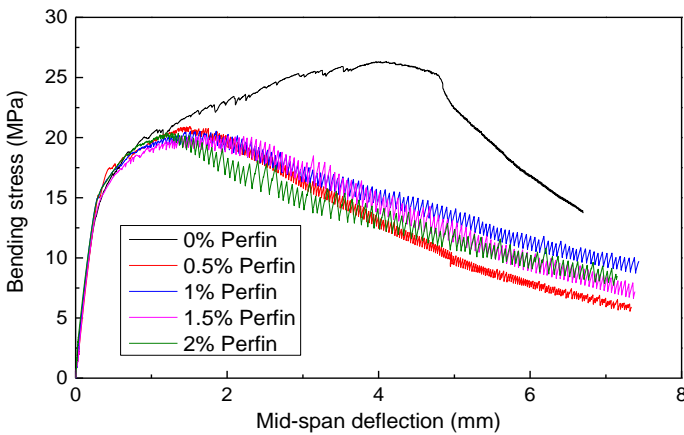


(c) Calculated $P_{fresh} - P_{bubble}$

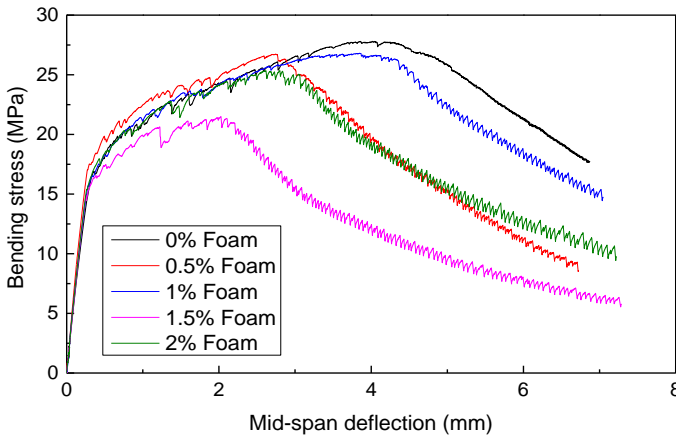
Figure 4.32 Influence of the Admixture/CEM ratios on the de-airing behaviours of UHPC

4.4.5.3 4-point bending test

Additionally, 4-point bending tests were also performed on the $50 \times 150 \times 550 \text{mm}^3$ beams for these two groups of UHPC mixtures according to ÖBV-Richtlinie “UHPC” [20]. The bending stress-mid-span deflection curves are shown in Figure 4.33. It can be found that the bending stress of UHPC beams containing Sika Perfin no longer rises soon after cracking; while the bending stress of UHPC beams containing BT3 Foam continues to rise after cracking, which is similar to the bending stress of normal fibre-reinforced UHPC. These results demonstrate that Sika Perfin might also decrease the bond strength between UHPC and StF.



(a) 4-point bending tests of UHPC mixtures with Perfin



(b) 4-point bending tests of UHPC mixtures with Foam

Figure 4.33 Influence of defoaming agents on the bending performance of UHPC

In summary, the added amount of the defoaming agent is better to not exceed 0.5% of the mass of cement. Since the superplasticiser used in this research is a product of the BT3 company, it is also possible that the incompatibility of Sika Perfin with the superplasticiser leads to a reduction in hardened properties. BT3 Foam, on the other hand, has better effects in comparison. Further research is still needed.

4.4.6 Release agent

The formwork release agent refers to a substance applied on the inner surfaces of formwork before casting, to prevent the formwork from sticking to the concrete surface after the hardening of the concrete. Otherwise, it will not be easy to remove the formwork, and the smoothness of the concrete surface may also be affected. Its main function is to form a film on the surface between formwork and concrete to isolate them.

Compared with traditional engine oil or waste engine oil, the formwork release agent has the advantages of easy releasing, no contamination to the concrete surface, no corrosion of the formwork, easy painting, and low price. However, not all types of release agents are suitable for formworks made of different materials. For formworks of different materials and concrete with different construction conditions and finishing requirements, a suitable release agent must be selected for a good effect.

In particular, in order to make the surface of concrete smoother, some high-efficiency release agents can not only play a separation role but also play a certain de-airing role, such as allowing air bubbles to rise along the formwork and then discharge. Therefore, it is of great significance to investigate whether the formwork release agent can also enhance the de-airing after mixing.

4.4.6.1 Test results in Section 4.4.2

As introduced in Section 4.4.2, 2 kinds of release agents for formwork (“MFRL 456” and “SPSP IQ P08”) were used for each column. The “MasterFinish RL 456” (MFRL 456) from the company “Master Builders Solutions GmbH” is a chemical-physical release agent made from process oils with anti-corrosion additives and dearomatized alkanes. It can keep the formwork clean, ensure easy demoulding and enable the production of clean, spotless, and void-free concrete surfaces. The “Trennmittel Separate Spezial IQ P08” (SPSP IQ P08) from the company “Baustofftechnik GmbH” is a water-immiscible release agent based on mineral oil for all common types of formworks. It can provide excellent corrosion protection for steel formworks, protect wood formworks from leaching and rot and also keep no discolouration

of the concrete surface. The technical specifications of these two release agents are seen in Table 4.17.

Table 4.17 Technical specifications of these 2 release agents

	Raw material base	State	Density (kg/l)
MFRL 456	process oil	fluid	0.79
SPSP IQ P08	mineral oil	fluid	0.86

For the tests in Section 4.4.2, when P_{fresh} was 2.5%, the influence of these 2 release agents on P_{bubble} for the three casting methods is shown in Figure 4.34 after percentage normalization from the results of UHPC mixtures with “MFRL 456”. Figure 4.35 also shows the appearance of the surface of the concrete samples under the casting method “GEN 70°” with the two release agents. It can be found that the release agent “MFRL 456” seems to be able to yield a smoother surface and lower P_{bubble} than “SPSP IQ P08”. This means that the rising speed of air bubbles on the surface of the concrete samples using the release agent “MFRL 456” significantly increases. However, whether this will accelerate the rising speed of air bubbles inside the concrete sample still needs further investigation.

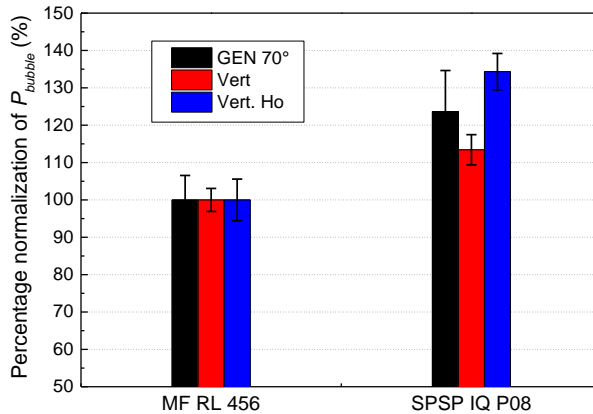
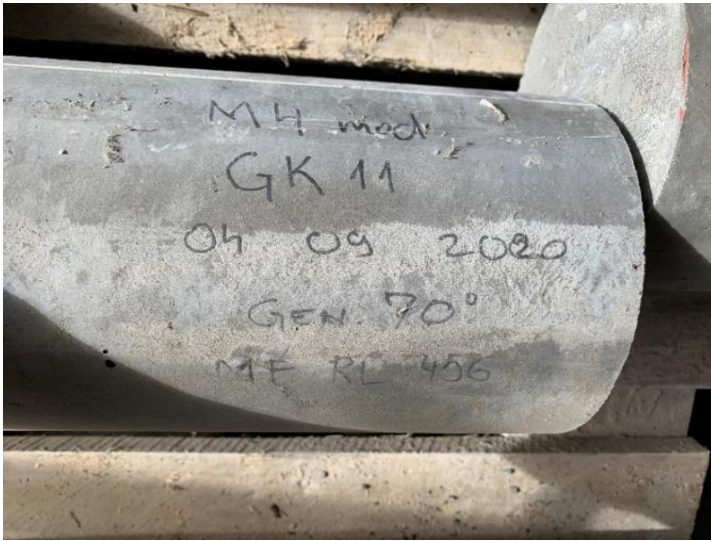


Figure 4.34 Influence of the 2 release agents on P_{bubble}



(a) UHPC with “MFRL 456” under “GEN 70°”



(b) UHPC with “SPSP IQ P08” under “GEN 70°”

Figure 4.35 Appearance of the surface of the UHPC samples with the two release agents.

4.4.6.2 Some existing research

There has been some existing research on the effect of different types of release agents on the air pores on the concrete surface. For example, Ichimiya K et al. [133] studied the influence of the wettability and angle of form on the characteristics of surface pores in self-

compacting concrete. They found that water-based formwork release agents might create fewer surface voids on the surface of concrete compared to oil-based agents. Besides, they also found that the surface air pore diameter seemed to have a relationship with the depth of the air pore from the surface. This indicates that the release agent may not influence the air pores in the concrete but only the air pores near the surface.

In addition, Savukaitis G et al. [134] also conducted research on the influence of new and used formwork coated with different release agents on the appearance of the formed concrete surface. They tested the surface of concretes with different release agents on the old and new formwork. As shown in Figure 4.36 (copyright permitted), it could be found that the concrete had a better surface with fewer air pores when “RA No.1” and “RA No.4” were used. This means that the water-based formwork release agent may probably have the best effect, followed by the mineral oil-based one, while the silicone oil-based and liquid wax-based release agents may not be able to efficiently decrease the air pores in the concrete.

Nonetheless, existing research has not shown the effect of formwork release agents on the internal de-airing of concrete after casting. It is also critical to reduce air pores inside the concrete as compared to reducing air pores on the surface of the concrete because the former directly affects the hardened properties of concrete. Therefore, whether the formwork release agent, which can reduce the air pores on the concrete surface, can also increase the de-airing after mixing to reduce the air pores inside the concrete or not, is also required to be investigated.

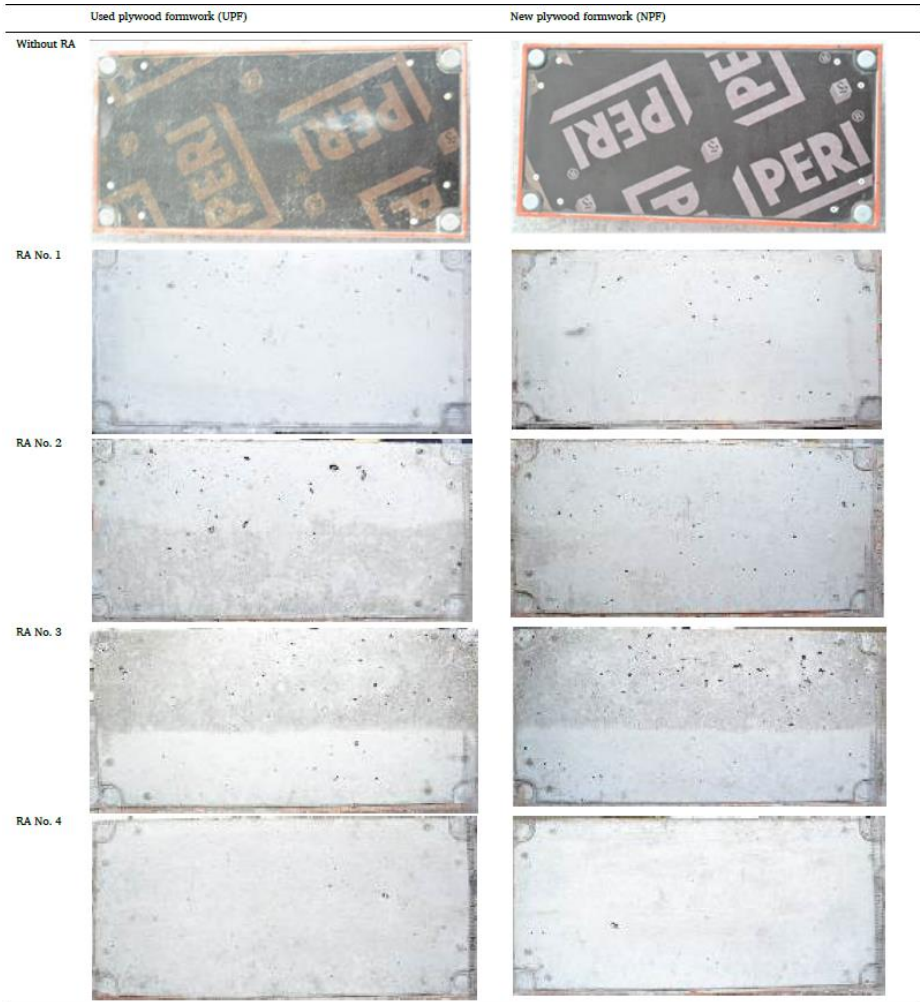


Figure 4.36 Appearance of plywood formworks and the formed concrete surface with different release agents (RA No.1: a solvent-free release agent based on water-soluble emulsion; RA No.2: a release agent based on liquid wax; RA No.3: a release agent based on silicon oil; RA No.4: a release agent based on mineral oil.) [134]

4.4.6.3 Investigation of the function of the formwork release agent

To further investigate the function of the formwork release agent, each UHPC mixture in Group 4.4.4.4-1 was also cast in four $\Phi 100 \times H 200 \text{ mm}^3$ cylinders with different release agents. After 2~3 days, the cylinders were observed on the surface first and then examined the air pores in three positions with the method introduced in Section 4.2.

A total of 4 kinds of formwork release agents were used for the cylinders for each UHPC mixture, which are the oil-based formwork release agent “Premadd Trennmittel Z-BC” (Z-BC), and the water-based formwork release agent “Premadd Trennmittel Z-SP” (Z-SP) from the company “BT3 Betontechnik”, the chemical-physical, low-odour fair-faced formwork release agent “MasterFinish RL 450” (MFRL 450) from the company “Master Builders Solutions GmbH”, and the ordinary cooking oil (Pflanzenöl) as a reference for comparison. The technical specifications of these 4 tested release agents are shown in Table 4.18.

Table 4.18 Technical specifications of these 4 tested release agents

	Raw material base	State	Density (kg/l)
Z-BC	solvent	fluid	1.02
Z-SP	oil	fluid	0.78
MFRL 450	Process oil	fluid	0.77
Pflanzenöl	oil	fluid	0.8

Figure 4.37, Figure 4.38 and Figure 4.39 show the appearances of the cylinder surface of the 3 UHPC mixtures with different formwork release agents, respectively. By visual observation alone, it can be roughly detected that the surfaces of UHPC cylinders with “Z-SP” and “MFRL 450” are significantly better than those with “Z-BC” and “Pflanzenöl” for all the 3 mixtures, indicating that water-based and mineral oil-based formwork release agents may benefit for decreasing the air bubbles on the surface of UHPC. This result is consistent with the existing research findings [133, 134].

Figure 4.40 shows the examined P_{bubble} of these 3 UHPC mixtures with 4 kinds of formwork release agents after percentage normalization from the mixture with release agent “Z-BC”. After calculation with the P_{fresh} in Table 4.11, the results of the $(P_{fresh} - P_{bubble})$ value can be shown in Figure 4.41. It is interesting that the cylinders with “Z-SP” and “Pflanzenöl” have relatively lower P_{bubble} and higher $(P_{fresh} - P_{bubble})$ values than those with “MF RL450” and “Z-BC”.

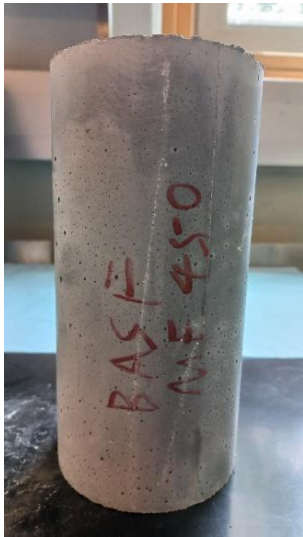
Combined with the results of surface observations, it can be assumed that “Z-SP” has the best effect on enhancing the de-airing near the surface of the concrete; “MF RL450” has a good effect on decreasing the air bubbles on the surface, but the influencing extent in the concrete may be very low; “Z-BC” has no effect on the air bubbles on the surface, thereby very high P_{bubble} ; “Pflanzenöl” is actually not a formwork release agent with no effect on the air bubbles on the surface, but its chemical composition (fatty acids, vitamin E, etc.) might interact with concrete to slightly affect de-airing behaviours.



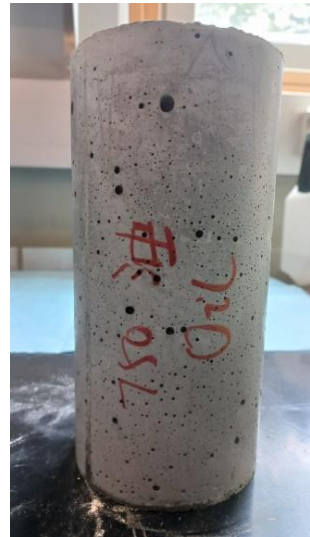
(a) Premadd Trennmittel Z-BC



(b) Premadd Trennmittel Z-SP



(c) MasterFinish RL 450

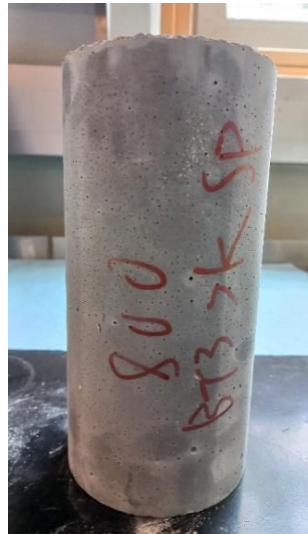


(d) Pflanzenöl

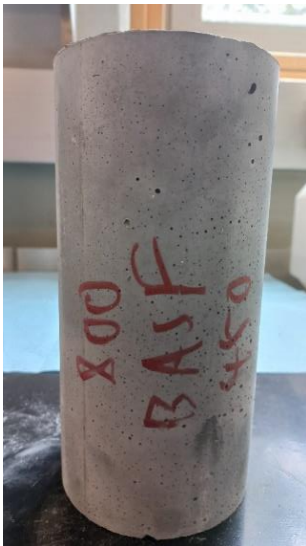
Figure 4.37 Appearances of UHPC cylinders using Recipe “750 0.25”



(a) Premadd Trennmittel Z-BC



(b) Premadd Trennmittel Z-SP



(c) MasterFinish RL 450



(d) Pflanzenöl

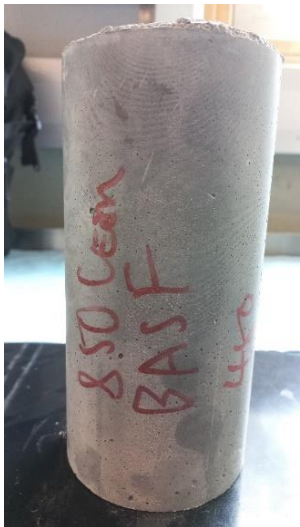
Figure 4.38 Appearances of UHPC cylinders using Recipe “800 0.25”



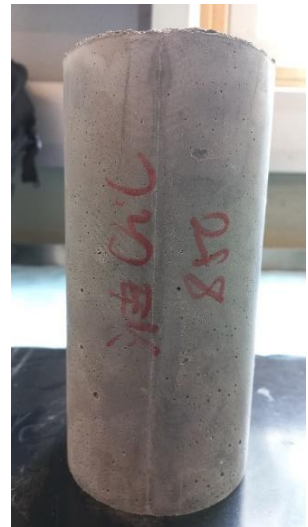
(a) Premadd Trennmittel Z-BC



(b) Premadd Trennmittel Z-SP



(c) MasterFinish RL 450



(d) Pflanzenöl

Figure 4.39 Appearances of UHPC cylinders using Recipe “850 0.25”

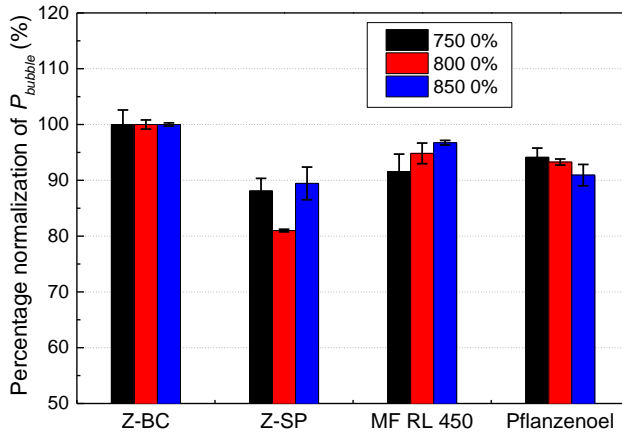


Figure 4.40 Examined P_{bubble} with 4 kinds of formwork release agents

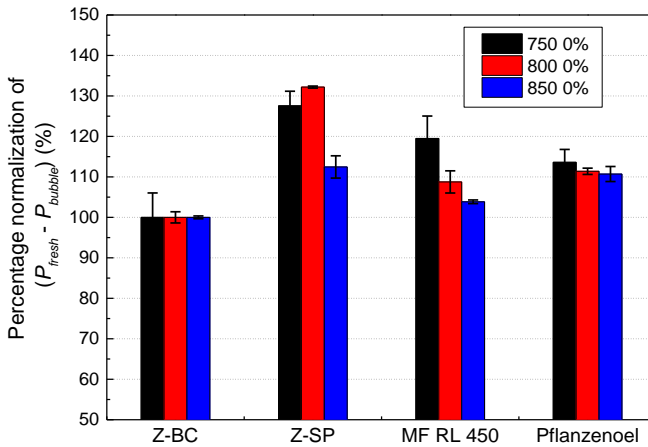


Figure 4.41 Calculated $(P_{fresh} - P_{bubble})$ value with 4 kinds of formwork release agents

Therefore, it can be deduced from these results that, some good release agents that work on decreasing the air pores on the surface of concrete may be beneficial for the reduction of air bubbles near the surface but seem to have little effect on internal air bubbles. However, in some practical engineering applications, this kind of formwork release agent can also be used according to the requirements.

4.5 Air bubbles formation and de-airing mechanisms

4.5.1 Distribution of air bubbles in UHPC columns

To analyse the air bubbles formation and de-airing mechanisms, it is necessary to investigate the distribution of air bubbles in vertical UHPC columns. Thus, in order to observe the air bubble distribution of UHPC mixtures containing different recipes, 5 batches of UHPC mixtures were mixed with an ELBA mixer, as shown in Table 4.19. Detailed mix recipes and properties of these UHPC mixtures can be found in Table A.5 in the appendix.

Table 4.19 Mix proportions of UHPC mixtures for columns

Group	UHPC mixture	Cement content (kg/m ³)	W/B ratio	SP/B ratio (%)	Spread-flow (cm)	P_{fresh} (%)
4.5.1-1	Column 1	720	0.241	4.46	25	4.2
	Column 2	860	0.212	3.13	25	4.2
	Column 3	720	0.232	3.13	25	4.2
	Column 4	860	0.232	2.68	31	3
	Column 5	720	0.241	3.13	25	4.2

Table 4.20 Casted samples to investigate the air bubble distribution

UHPC mixture	Specimen
Column 1	1 $\Phi 100 \times H200\text{mm}^3$ cylinder, 3 $100 \times 100 \times 100\text{mm}^3$ cubes, 1 $\Phi 110 \times H1000\text{mm}^3$ column
Column 2	1 $\Phi 100 \times H200\text{mm}^3$ cylinder, 3 $100 \times 100 \times 100\text{mm}^3$ cubes, 1 $\Phi 110 \times H1000\text{mm}^3$ column
Column 3	1 $\Phi 100 \times H200\text{mm}^3$ cylinder, 3 $100 \times 100 \times 100\text{mm}^3$ cubes, 1 $\Phi 110 \times H1000\text{mm}^3$ column
Column 4	1 $\Phi 100 \times H200\text{mm}^3$ cylinder, 3 $100 \times 100 \times 100\text{mm}^3$ cubes, 1 $\Phi 110 \times H1000\text{mm}^3$ column, 1 $\Phi 110 \times H500\text{mm}^3$ column
Column 5	1 $\Phi 100 \times H200\text{mm}^3$ cylinder, 3 $100 \times 100 \times 100\text{mm}^3$ cubes, 1 $\Phi 50 \times H1000\text{mm}^3$ column, 1 $\Phi 50 \times H2000\text{mm}^3$ column, 1 $\Phi 75 \times H1000\text{mm}^3$ column, 1 $\Phi 100 \times H1000\text{mm}^3$ column

As shown in Table 4.20, each UHPC mixture was cast into one $\Phi 100 \times H200\text{mm}^3$ cylinder and three $100 \times 100 \times 100\text{mm}^3$ cubes. Additionally, the UHPC mixtures “Column 1”, “Column 2” and “Column 3” were cast into one $\Phi 110 \times H1000\text{mm}^3$ column. The UHPC mixture “Column 4” was cast into one $\Phi 110 \times H500\text{mm}^3$ column and one $\Phi 110 \times H1000\text{mm}^3$ column. The UHPC mixture “Column 5” was cast into four columns with different diameters and lengths, which were $\Phi 50 \times H1000\text{mm}^3$, $\Phi 50 \times H2000\text{mm}^3$, $\Phi 75 \times H1000\text{mm}^3$, and $\Phi 100 \times H1000\text{mm}^3$. 7 days after casting, all the columns and cylinders were cut from different positions to check the air pores in the sections, as shown in Figure 4.42.

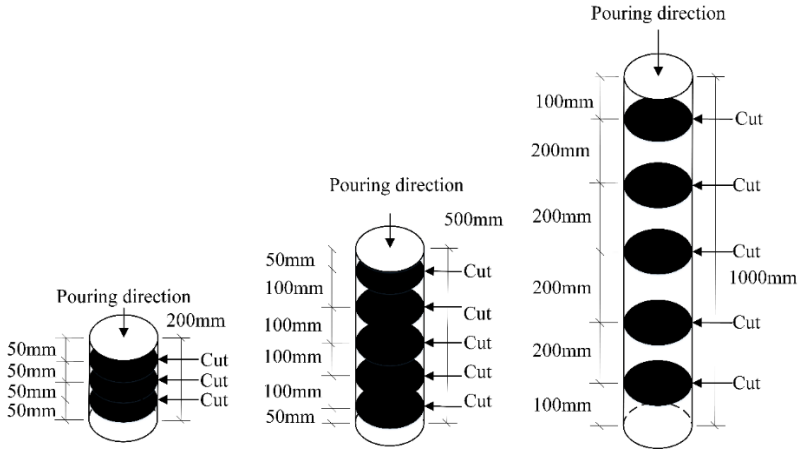


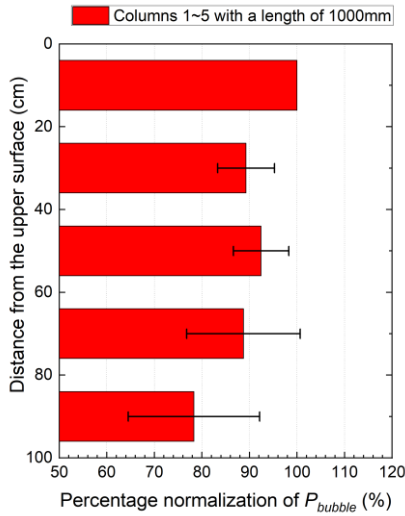
Figure 4.42 Schematic diagram of the cutting positions of the columns and cylinders

The air pores distribution along the longitudinal direction for Columns 1~5 with a length of 1000mm (7 columns) is shown in Figure 4.43(a) after percentage normalization from the topmost position (distance from the upper surface is 100mm) and statistical analysis. Figure 4.43(b) and (c) show the result of Column 4 with a length of 500mm and the result of Column 5 with a length of 1000mm. It can be found that except for Column 5 with a length of 2000mm, in almost all the other columns the lower sections (larger distances from the upper surface) would have a lower P_{bubble} , which is consistent with the findings of Li T et al. [123].

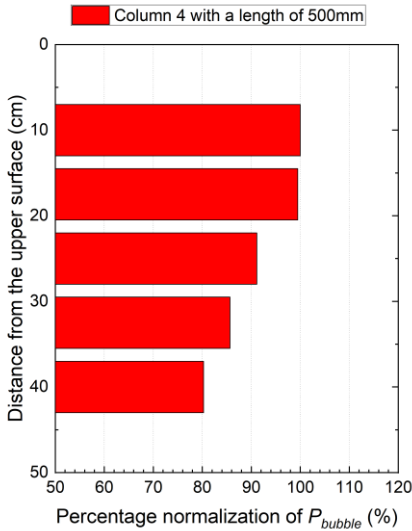
Due to the relatively uniform distribution of air bubbles in the fresh concrete and the same pouring process for these columns, it can be deduced that normally the de-airing behaviours after mixing in the fresh UHPC mixture might be uniform from bottom to top. However, for a slender column with a length of 2m and a diameter of 50mm, due to the effect of the formwork release agent (introduced in the last section), the air bubbles may have uneven de-airing behaviours and be stuck somewhere, leading to irregular results. In this case, the uneven application of the formwork release agent may also have an influence. What is the slenderness ratio of the column that can make the distribution of air bubbles more affected by the release agent still needs further investigation.

Figure 4.44 shows the air pores distribution along the longitudinal direction in the cylinders ($\Phi 100 \times H 200 \text{mm}^3$) for these 5 UHPC mixtures. It can be seen that for very short cylinders the distribution of the pores is more homogeneous, which is the reason that the cylinders cast in the previous sections didn't consider the effect of the distribution of the air pores along the longitudinal direction. This is due to the fact that for short cylinders when pouring concrete in the longitudinal direction, the concrete tends to flow more along the edges rather than

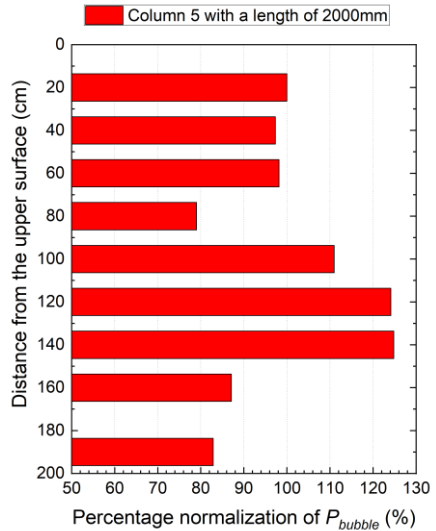
falling straight down. This triggers the covering of more air as shown in Figure 4.18, which increases the air pores in the lower part as well. These results provide a basis for analysing the air bubbles formation and de-airing mechanisms.



(a) Columns 1~5 with a length of 1000mm



(b) Column 4 with a length of 500mm



(c) Column 5 with a length of 2000mm

Figure 4.43 Air pores distribution along the longitudinal direction for the 9 columns

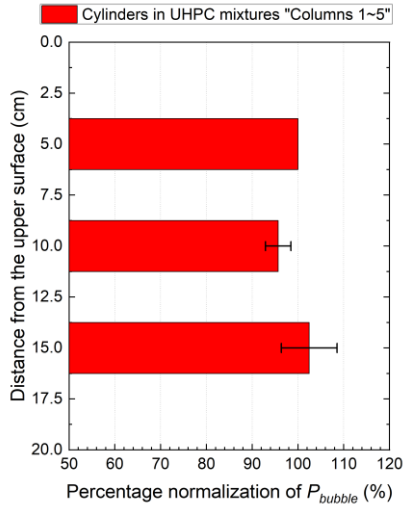


Figure 4.44 Air pores distribution along the longitudinal direction for the cylinders

4.5.2 Influences of the specimen sizes on the percentage of air pores

For the group “Column 5”, 3 columns with different diameters (50mm, 75mm and 100mm) were tested. When considering the influence of the diameter on P_{bubble} , the results can be shown in Figure 4.45 after percentage normalization from the column with a diameter of 100mm in each cutting section and statistical analysis. In the figure, the diameter is represented by the surface area, because the latter is more directly related to air bubbles on the cutting positions. It can be found that for each position, P_{bubble} seems not to be affected by the surface area. The percentage of air pores in the slender elements is still large, which also illustrates the significance of this research. Additionally, based on this result it can be concluded that the air bubbles barely move horizontally during the de-airing process after casting.

For investigating the influence of the length of the column on the de-airing behaviours in UHPC, owing to the results that the diameter may not have a large influence on P_{bubble} , the columns and cylinders of these 5 UHPC mixtures with a diameter of 100mm or 110mm and different lengths can be compared together. The results of the examined P_{bubble} in different positions are shown in Figure 4.46. It can be found that except for the slender column “Column 5 50mm”, the longer columns seem to have a slightly lower P_{bubble} than the shorter columns.

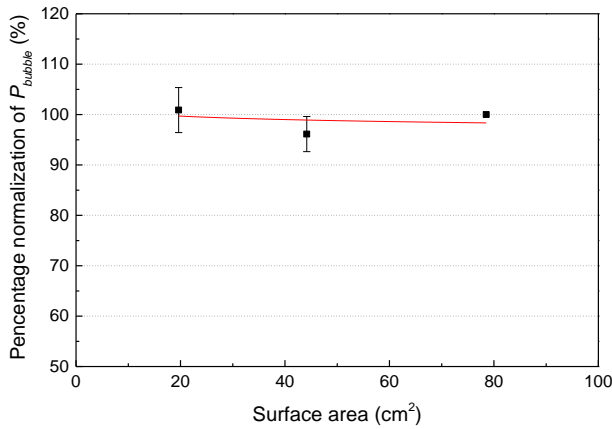


Figure 4.45 Influence of surface area on the de-airing behaviours in UHPC

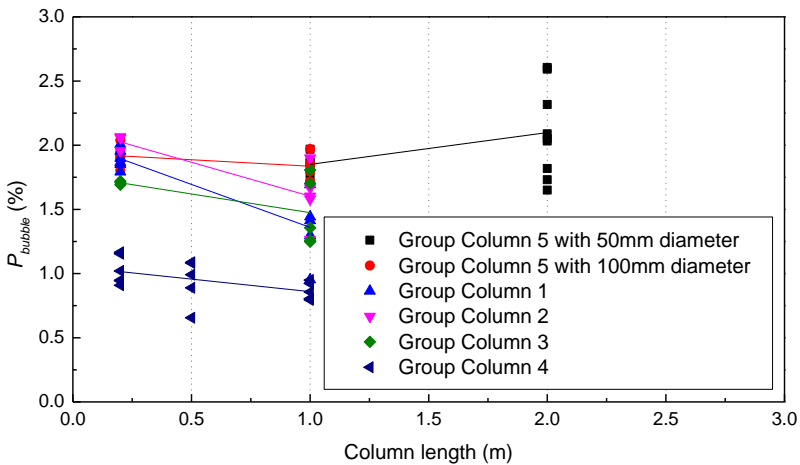


Figure 4.46 Influence of column length on the de-airing behaviours in UHPC

Since all the columns in this study produced similar results, it can be assumed that for short cylinders, the casting process is similar to the “Gen 70”, which may entrap more air as the concrete flows along the edge of the formwork to the bottom, which is also consistent with the results in Section 4.5.1. However, for long columns, the concrete falls more directly to the bottom, which may not only entrap less air but also reduce the amount of entrapped air due to the impact of old and new concrete. As a result, the length of the sample will certainly influence P_{bubble} . In this research, only the test results of UHPC mixtures with the same sample length can be compared.

4.5.3 Influences on the size of air bubbles

To investigate the formation and de-airing mechanisms of air bubbles, the influences of different factors on the size of air bubbles should also be considered, which is examined as the mean Feret diameters of air pores in different positions by the methods introduced in Section 4.2, where the maximum air pore diameter can be obtained for each UHPC mixture. As shown in Figure 4.9, there may be some very large air pores existing in the hardened concrete. Compared with small air pores, these large air pores may have a greater impact on structural performances. At the same time, how these big air pores are formed is an important issue that needs to be studied. Thus, compared with the average air pore diameter, the maximum air pore diameter can better reflect the results of large air pores. In this section, the influence of various factors on the maximum air pore diameter in the UHPC mixture is analysed based on the results in previous sections.

4.5.3.1 Influence of the flowability

According to the results in Section 4.4.3.1, the flowability of UHPC mainly affects the de-airing during mixing but not after mixing. Figure 4.47 shows the relationship between the measured spread-flow values and the percentage normalization of the maximum air pore diameter from the UHPC mixtures with a spread-flow value of 26cm for the 4 groups of UHPC mixtures tested in Section 4.4.3.1. It can be found that, although there is a certain amount of scattering, a higher flowability may be able to lead to a lower maximum air bubble size, indicating that big air bubbles may be generated during the mixing process.

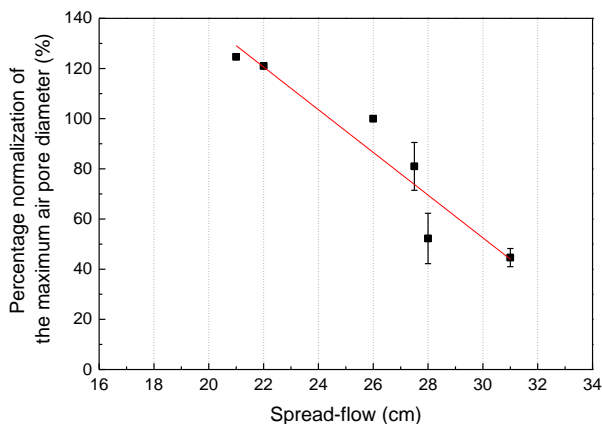


Figure 4.47 Relationship between the measured spread-flow values and the maximum air pore diameters

4.5.3.2 Influence of the viscosity

According to the results in Section 4.4.3.2, the viscosity of concrete mainly influences the de-airing process after mixing but not during mixing. Figure 4.48 shows the relationship between the measured T_{200} values and the percentage normalization of the maximum air pore diameter from the UHPC mixtures with a T_{200} value of 9s for the 3 groups of UHPC mixtures tested in Section 4.4.3.2. It can be found that a higher viscosity may not have an obvious influence on the maximum air bubble size, which means the de-airing process after mixing may have little effect on the air bubble size.

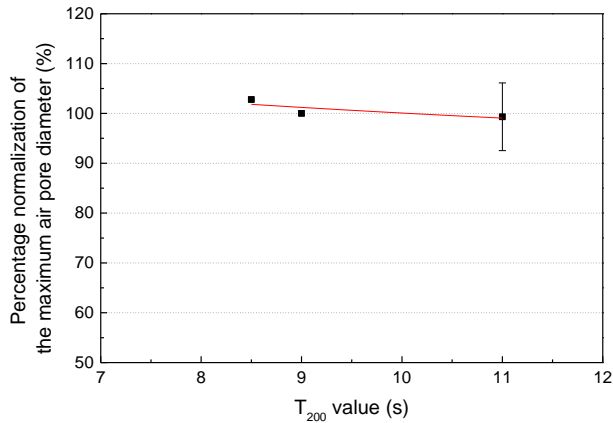


Figure 4.48 Relationship between the measured T_{200} values and the maximum air pore diameters

4.5.3.3 Changing of the consistency over time

According to the results in Section 2.3.3.2 and Section 4.4.4.3, the changing of the consistency of UHPC over time is affected by the SP/B ratio when the flowability is constant, which also affects P_{bubble} but doesn't influence the P_{fresh} , because there can be more time for the de-airing process after mixing. When only considering the SP/B ratio exceeding the critical value to make the flowability constant for the UHPC mixtures in Group 2.3.3-3 and Group 2.3.3-7, the relationship between the SP/B ratio and the percentage normalization of the maximum air pore diameter from the UHPC mixtures with an SP/B ratio of 2.23% for these 2 groups of UHPC mixtures can be seen in Figure 4.49. It can be found that the SP/B ratio as well as the changing of the consistency of UHPC over time may not have an obvious influence on the air bubble size. This also illustrates that the de-airing process after mixing may have little effect on the air bubble size.

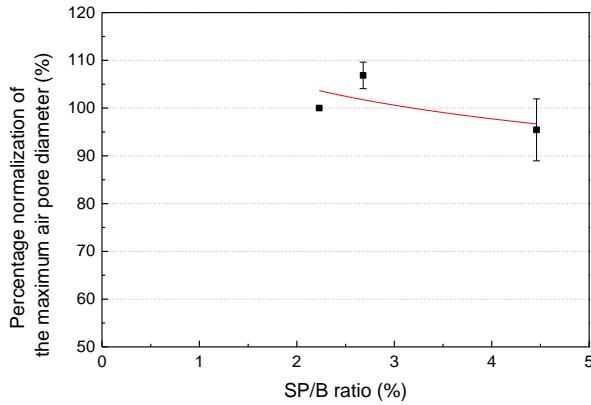


Figure 4.49 Relationship between the SP/B ratio and the maximum air pore diameter when the flowability is constant

4.5.3.4 Mixing time and casting time

According to the results in Section 4.4.1.1, longer mixing time may decrease the P_{fresh} and increase the flowability of the UHPC mixture. For the study in this section, in order to be able to determine the influencing factors of the air bubble size, different casting time was also considered in the tests in Section 4.4.1.1. For the two groups of 4 batches of UHPC mixtures (Group 4.4.1.1-1 and Group 4.4.1.1-2), each UHPC is cast into 2 $\Phi 100 \times H200\text{mm}^3$ cylinders at 2 different times, as shown in Table 4.21. One cylinder was cast just after mixing (casting time: 2min), and the other cylinder was cast after storing the concrete in an open bucket for 90min and 95min (casting time: 90min and 95min) when the air bubbles had largely escaped from the UHPC mixtures, as shown in Figure 4.50. Although the initial setting of UHPC mixtures might already start, the concretes were still soft enough for the casting of the cylinders. Consequently, the cylinders can be divided into 4 groups (Group 4.5.3.4-1~4.5.3.4-4) with different mixing times and casting times.

Table 4.21 UHPC mixtures in Groups 4.4.1.1-1 and 4.4.1.1-2

Mixing time group	Casting time group	UHPC mixture	Mixing time (min)	Casting time (min)
4.4.1.1-1	4.5.3.4-1	720 0.223 7min	7	2
		720 0.223 7min	7	90
	4.5.3.4-2	720 0.223 23min	23	2
		720 0.223 23min	23	90
4.4.1.1-2	4.5.3.4-3	750 0.223 8min	8	2
		750 0.223 8min	8	95
	4.5.3.4-4	750 0.223 22min	22	2
		750 0.223 22min	22	95



Figure 4.50 UHPC mixtures stored in the open buckets for 90min of the de-airing process

Figure 4.51 shows the influence of casting time on the P_{bubble} for the 4 groups of UHPC cylinders with different mixing times. It can be seen that a longer casting time can decrease the P_{bubble} due to the larger de-airing degree after mixing in the bucket than in the formwork. Figure 4.52 shows the relationship between the casting time and the maximum air pore diameters of these 4 groups of UHPC mixtures. At this time, a delayed casting time seems not to have a clear relationship with the maximum air bubble size.

Accordingly, Figure 4.53 shows the relationship between the mixing time and the maximum air pore diameters for Group 4.4.1.1-1 and Group 4.4.1.1-2. It can be found that a longer mixing time leads to a lower maximum air bubble size. Combining this result with the results in Section 4.4.1.1 and Section 4.5.3.1, it can be surmised that the maximum air bubble size is closely related to the de-airing during mixing, but not to the de-airing after mixing.

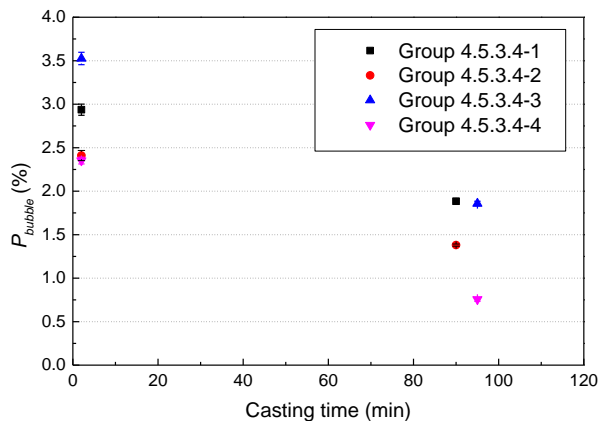


Figure 4.51 Influence of casting time on the de-airing behaviours in UHPC

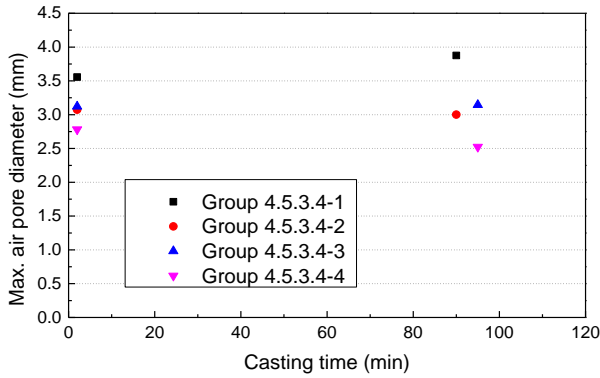


Figure 4.52 Relationship between casting time and maximum air pore diameter

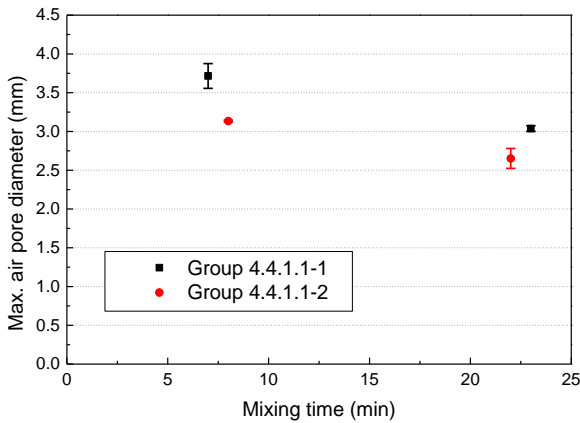


Figure 4.53 Relationship between mixing time and maximum air pore diameter

4.5.4 Air bubbles formation and de-airing mechanisms analysis

Based on the results in this chapter, the mixing parameters including mixing time, type of mixer and so on can influence P_{fresh} by affecting the de-airing during mixing; different casting methods may lead to different entrapped air during casting to influence P_{bubble} ; the flowability of concrete has a near liner influence on P_{fresh} by affecting the de-airing during mixing, the viscosity of concrete has a near liner influence on the $(P_{fresh} - P_{bubble})$ value by affecting the de-airing after mixing, but the temperature of concrete has no obvious effect; the coarse aggregates and steel fibres can influence P_{fresh} by affecting the de-airing during mixing; slower changing of consistency of UHPC over time can provide more time for the de-airing process after casting; some defoaming agent can also influence P_{fresh} by affecting the de-

airing during mixing; the formwork release agent mostly influences the air bubbles on the surface of the concrete but not that inside.

Therefore, the air bubbles formation and de-airing mechanisms can be assumed as follows: when the raw materials are added before mixing, part of the air may be covered between the materials, and soon after the mixing starts, the raw materials, water and superplasticizer will form a very thick mortar. Afterwards, due to UHPC's extremely impermeable, honey-like properties, the air is entrapped between the concrete and forms air bubbles.

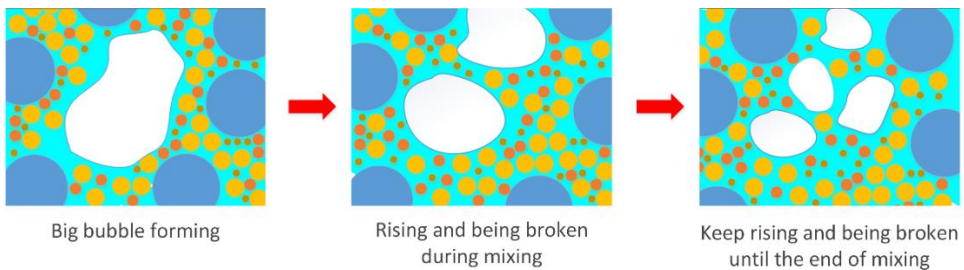


Figure 4.54 Schematic diagram of the formation, de-airing and breaking of large air bubbles during the mixing process

As shown in Figure 4.54, when the mixing process continues, these air bubbles will be broken up, reunited, and partly discharged during the mixing process. Then after mixing, the air bubbles start to rise and escape from the mixture due to their low density, but the rising process is almost in the vertical direction, as shown in Figure 4.55. When the UHPC being cast into the formwork, some of the new air is also entrapped in the concrete. Then in the formwork, the air bubbles continue to rise vertically until the concrete sets, and the air bubbles near the formwork may be accelerated due to the function of the release agent.

A comparison of the experimental findings with the proposed mechanisms are given as follows: firstly, casting with a hose from the bottom can minimize the entrapped air during casting, thereby reducing P_{bubble} ; secondly, an increase in mixing time, a large mixer, a good flowability of concrete, coarse particles present can all enhance the de-airing process during mixing, making more air bubbles be broken up and discharged; thirdly, the defoaming agent may also play a role in increasing the de-airing during the mixing process because of chemical effects; fourthly, low viscosity, long setting time can enhance the de-airing process after mixing; lastly, the air bubble size has more relationship with the de-airing during mixing, and after mixing during the vertical de-airing process in the formwork the air bubble size may not be influenced by the de-airing process. Therefore, in this research, the proposed formation and de-airing mechanisms of air bubbles agree with most of the test observations.

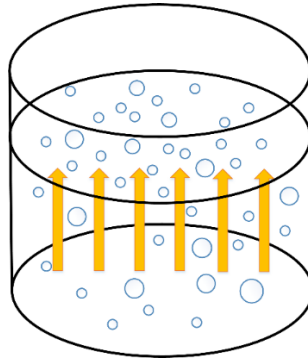


Figure 4.55 Schematic diagram of the movement process of air bubbles

4.6 3D X-ray irradiation to detect air pores distribution

To further verify the formation and de-airing mechanisms, the X-ray CT scanning of air pores in samples was also performed with the specific instrument. Afterwards, the 3D analysis software was used to more realistically present the distribution of air pores in UHPC. In this research, the UHPC mixture with the same recipe as “750 0.223” in Table 4.2 and Table A.4 in the appendix was mixed with an ELBA mixer to cast four big $\Phi 110 \times H1000 \text{mm}^3$ columns, four small $\Phi 100 \times H200 \text{mm}^3$ cylinders and four $100 \times 100 \times 100 \text{mm}^3$ cubes. The cast method is all poured directly from the top. The spread-flow was tested to be 25.5cm and the T_{200} was 17s. The maximum compressive strength of cubes was tested to be 173MPa.

Table 4.22 Tested samples with 3D X-ray

UHPC mixture	Elephant skin	Casting time (min)	P_{fresh} (%)	Specimen
IC_ES	With	2	5.2	1 $\Phi 110 \times H1000 \text{mm}^3$ column, 1 $\Phi 100 \times H200 \text{mm}^3$ cylinder
IC_noES	Without	2	5.2	1 $\Phi 110 \times H1000 \text{mm}^3$ column, 1 $\Phi 100 \times H200 \text{mm}^3$ cylinder
DC_ES	With	95	4.2	1 $\Phi 110 \times H1000 \text{mm}^3$ column, 1 $\Phi 100 \times H200 \text{mm}^3$ cylinder
DC_noES	Without	95	4.2	1 $\Phi 110 \times H1000 \text{mm}^3$ column, 1 $\Phi 100 \times H200 \text{mm}^3$ cylinder

As shown in Table 4.22, the specimens were divided into 4 groups of 1 column and 1 cylinder. 2 groups were cast just after mixing (casting waiting time: 2min), and 2 groups were

cast after storing the concrete in the ELBA mixer for 95min when the air bubbles were largely discharged. For each 2 groups, to investigate the influence of the “elephant skin” on the de-airing behaviours in UHPC, one group was sprayed with water on the surface and covered with a plastic membrane after casting, and the other group was directly exposed to the air to form the “elephant skin”. Thus, the 4 groups were named “IC_ES”, “IC_noES”, “DC_ES” and “DC_noES”, where “IC” and “DC” represented “immediately cast (2min)” and “delayed cast (95min)” and “ES” stood for the “elephant skin”, as shown in Figure 4.56.



Figure 4.56 4 groups of cylinders and columns in this research

As shown in Figure 4.57, the scanning machine is the “UniTOM XL” from the company “TESCAN GmbH”, which is a multi-resolution micro-CT optimized for high throughput, diverse sample types and flexibility for the research. Micro-CT provides direct 3D information on the porosity, mineral distribution and microstructure of geological samples with micrometre resolution. The TESCAN UniTOM XL micro-CT system enables μ CT images with the best possible resolution of approx. 4 μ m in 3D of almost any material. Sample size ranges from a few millimetres up to 1 m high and 600 mm in diameter with a maximum weight of 45 kg. Therefore, it is of great research value to use this instrument to scan air pores in concrete.



Figure 4.57 “UniTOM XL” from the company “TESCAN GmbH”

Figure 4.58 shows the samples in one group and the scanning position. Owing to the very dense microstructure of UHPC, its material requires higher irradiation intensity than general geological samples, which is also one of the biggest problems limited to scan quality.



(a) $\Phi 100 \times H 200 \text{mm}^3$ cylinder



(b) $\Phi 100 \times H 1000 \text{mm}^3$ column

Figure 4.58 Scanning of one group of cylinder and column

The results were analyzed in the software “Dragonfly” from the company “Object Research Systems (ORS) Inc.”. “Dragonfly” is the premier software platform for scientific image processing, which is powerful, flexible, and user-friendly. It is a professional supporting analysis software for the equipment “TESCAN UniTOM XL”. For comparison with the test

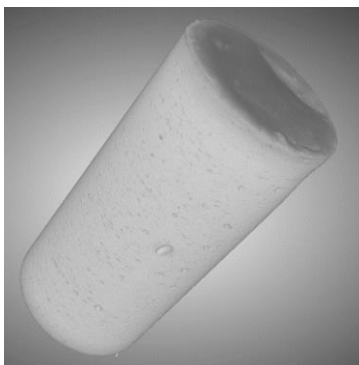
method of cutting cylinders in the previous sections, in this test, also air pores larger than 0.5mm were recognized.

4.6.1 Results of the short cylinders

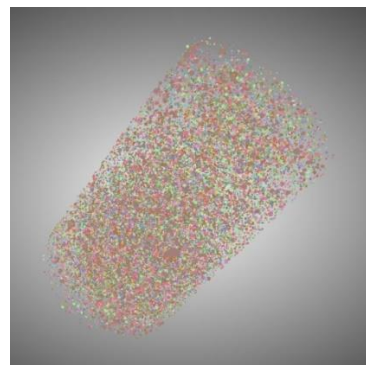
Figure 4.59 shows the 3D vision of the cylinder “IC_ES” and the recognized air pores in the “Dragonfly”. It can be clear to see the stereoscopic image of the air pore distribution in the cylinder.

Figure 4.60 and Figure 4.61 show the distribution of the air pores along the longitudinal direction of the cylinder “IC_ES” and “IC_noES”, respectively. Since the top of the cylinder was uneven and the bottom was in contact with the support, the air pore distribution near these two surfaces couldn’t be identified clearly, so the data near 0 and 200mm of distance from the upper surface couldn’t be obtained. But from the air pores distributions, it can be seen that for the immediately cast small cylinders, the lower part seems to have more pores than the upper part. This result seems to be unexpected, which is not consistent with the results in Section 4.5.1 and the findings of Li T et al. [123]. Besides, by comparison of these two cylinders, the “elephant skin” caused more air bubbles to accumulate under the top surface.

Figure 4.62 and Figure 4.63 show the distribution of the air pores along the longitudinal direction of the cylinder “DC_ES” and “DC_noES”, respectively. It can be found that in addition to more air pores accumulating under the top surface caused by the “elephant skin” in the cylinder “DC_ES”, for the delayed cast small cylinders it can also be seen that the lower part seems to have slightly more pores than the upper part.



(a) 3D image of the cylinder



(b) Identified air pores

Figure 4.59 3D analysis results of cylinder “IC_ES” by software “Dragonfly”

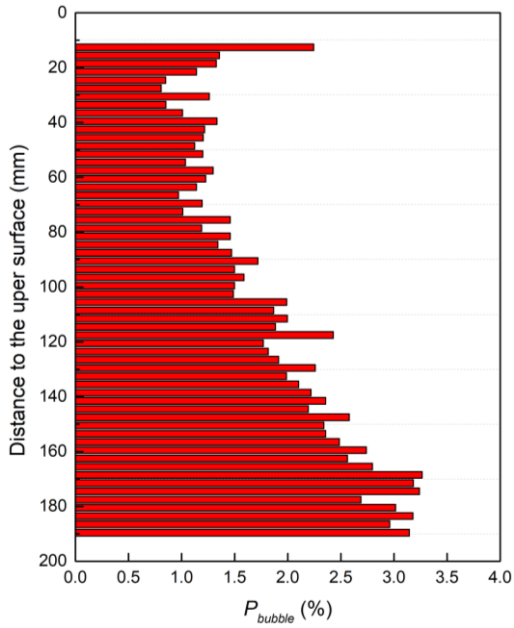


Figure 4.60 Distribution of the air pores along the longitudinal direction in the cylinder “IC_ES”

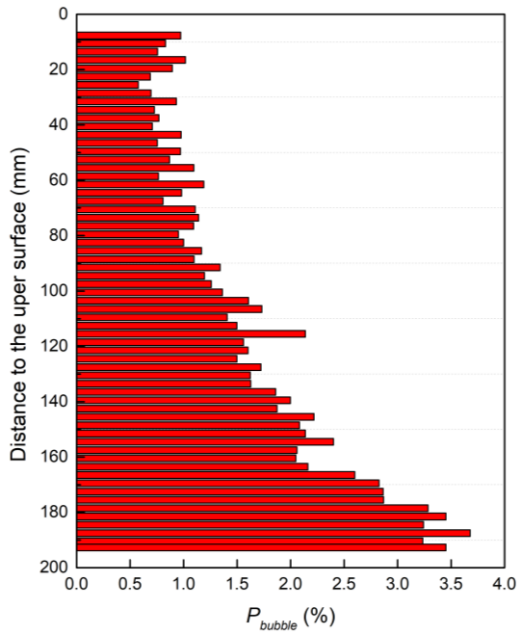


Figure 4.61 Distribution of the air pores along the longitudinal direction in the cylinder “IC_noES”

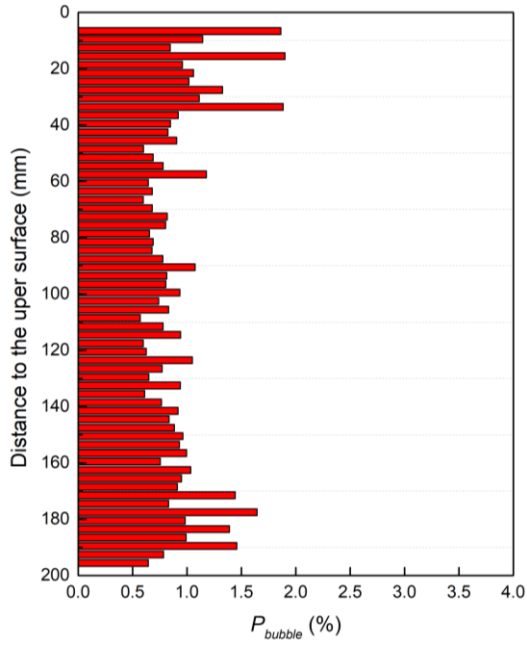


Figure 4.62 Distribution of the air pores along the longitudinal direction in the cylinder “DC_ES”

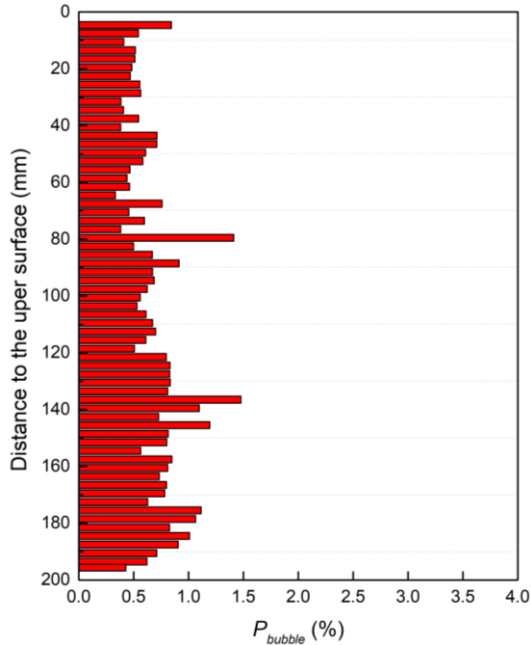


Figure 4.63 Distribution of the air pores along the longitudinal direction in the cylinder “DC_noES”

The reasons for these results can be analysed according to Figure 4.64. When comparing a scanned section of the upper half of the cylinder “DC_noES” with a scanned section of the lower half of the cylinder “DC_noES”, it can be found that the brightness of the upper half section is slightly higher than that of the lower half. This may be caused by the X-ray perspective problem of the scan. All the four cylinders show this phenomenon. And since the recognition software “Dragonfly” identifies the numbers and sizes of air pores mainly according to the lightness in the images, the air pores identified in the upper half are smaller than those in the lower half. Therefore, there are still some problems in using this method to study the distribution of air pores, and the detection accuracy of the instrument needs to be improved.

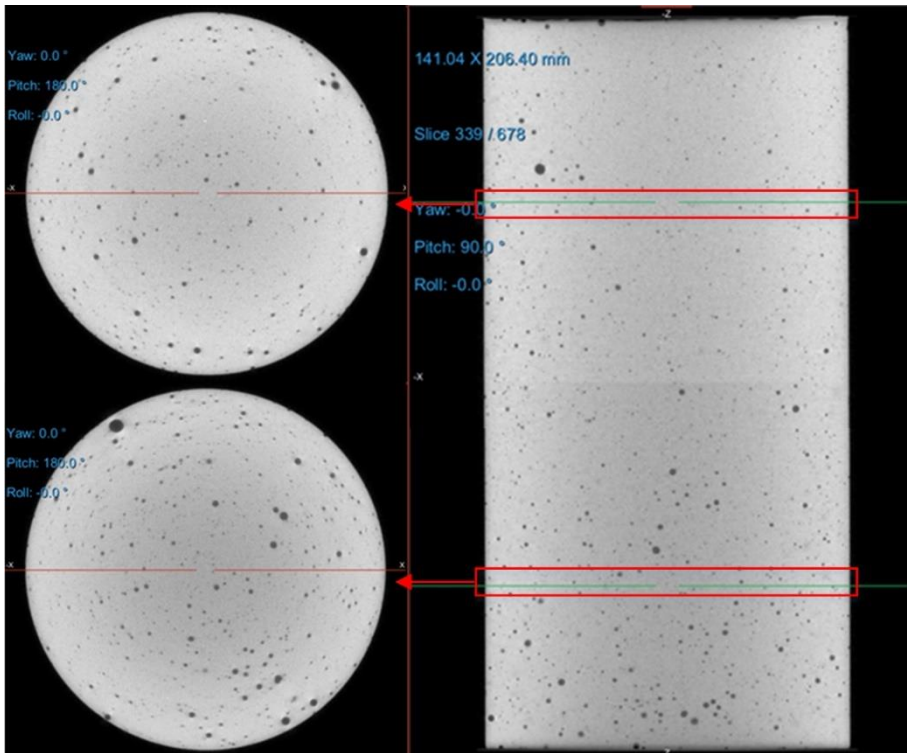


Figure 4.64 Scanned brightness of the upper part is slightly higher than that of the lower part in cylinder “IC_noES”

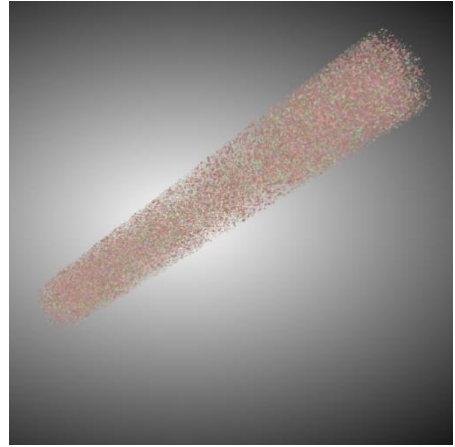
Nevertheless, when comparing the results for the immediately cast cylinders (“IC_ES” and “IC_noES”) and the delayed cast cylinders (“DC_ES” and “DC_noES”), the air pore content is significantly reduced in the delayed cast cylinders, which is consistent with the results in Section 4.5.3.4.

4.6.2 Results of the long columns

Figure 4.65 shows the 3D vision of the long column “IC_ES” and the recognized air pores in the “Dragonfly”. It can also be clear to see the stereoscopic image of the air pore distribution in the whole column.



(a) 3D image of the column



(b) recognized air bubbles

Figure 4.65 3D analysis of long column “IC_ES” by software “Dragonfly”

Figure 4.66 and Figure 4.67 show the distribution of the air pores along the longitudinal direction in the 4 columns, respectively. Since the top of the column was uneven and the bottom was in contact with the support, the air pore distribution near these two surfaces could also not be identified clearly, so the data near 0 and 1000mm of distance from the upper surface couldn't be obtained. But from the air pores distributions, at this time, the uneven light brightness (as shown in Figure 4.68, the middle section is lighter in the column “IC_noES”) leads to a more irregular distribution of air pores along the axial direction. Thus, when only comparing the results of the immediate cast columns and the delayed cast columns, it can be seen that the air pore content is also significantly reduced in the delayed cast columns. Besides, the “elephant skin” also causes more air bubbles to accumulate under the top surface.

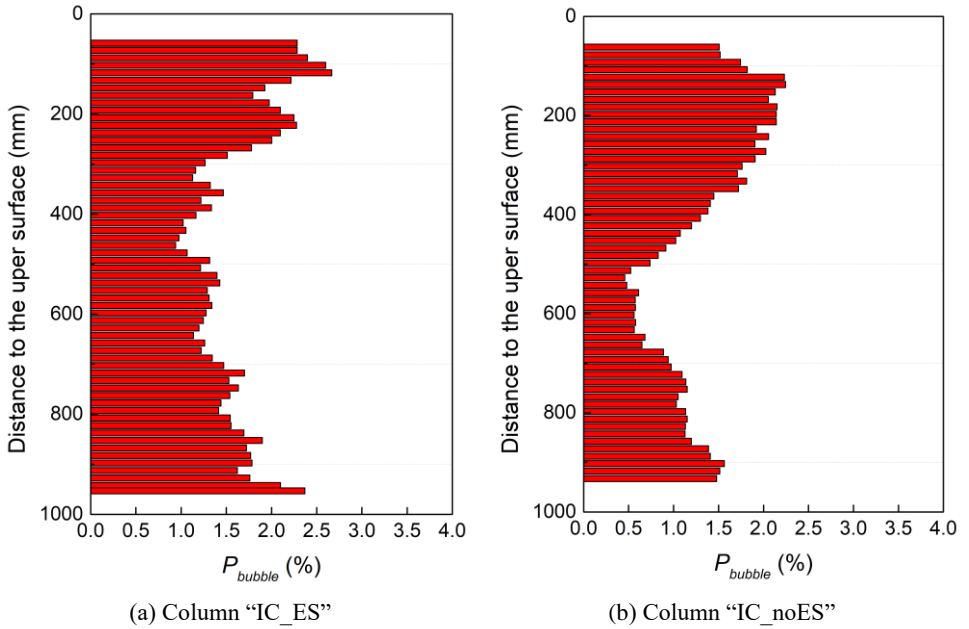


Figure 4.66 Distributions of air pores along the longitudinal direction in the immediate cast columns

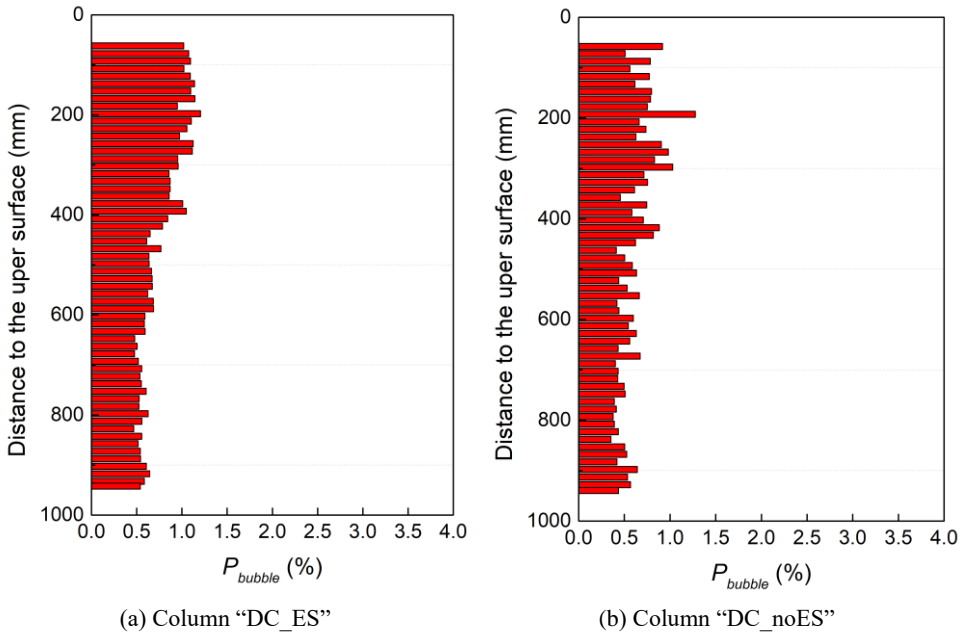


Figure 4.67 Distributions of air pores along the longitudinal direction in the delayed cast columns

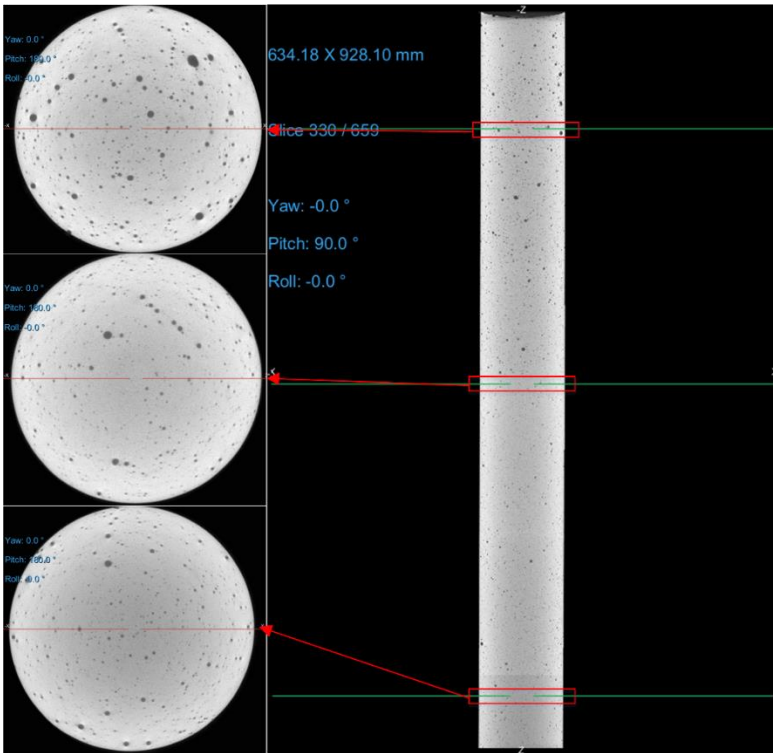


Figure 4.68 Scanned brightness of the middle part is slightly higher than those of the upper part and lower part in column “IC_noES”

Figure 4.69 shows the scanned and examined percentages of air pores in the whole sample of the cylinders and columns by the machine “UniTOM XL” and software “Dragonfly”. As mentioned above, the two ends of the samples couldn’t be recognized, and the maximum penetration of the instrument is still insufficient for scanning the highly dense material like UHPC, leading to the result of the percentage of air pores being generally smaller than that obtained in the previous sections by the test method of cutting cylinders. Thus, this is actually the percentage of scanned air pores but not true $P_{bubble-all}$, which is named $P_{bubble-scan}$. Nevertheless, when comparing these 4 groups, it can also be found that: firstly, the samples cast after waiting for a period of time (DC) have significantly smaller $P_{bubble-scan}$ than the samples without waiting (IC), which is consistent with the results in Section 4.5.3.4; secondly, the samples with the “elephant skin” have a slightly larger $P_{bubble-scan}$ than the samples without the “elephant skin”, indicating that the “elephant skin” may have an influence on the de-airing behaviours in UHPC, which needs further investigation; thirdly, the short cylinders seem to have larger $P_{bubble-scan}$ than the long columns, which is consistent with the findings in Section 4.5.2.

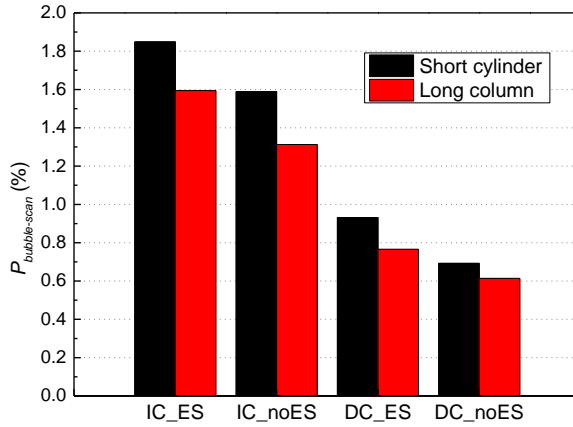


Figure 4.69 Scanned percentages of air pores in the whole sample of the cylinders and columns

In conclusion, 3D X-ray irradiation scanning is not accurate enough for the dense microstructure of UHPC, and there are still some problems in the results that cannot be quantitatively analysed but can only be qualitatively analysed. Considering that 3D X-ray irradiation can display the results more intuitively and stereoscopically if the penetration ability of the instrument can be improved in the future, the microstructure in the concrete can be more truly reflected.

4.7 Summary

This chapter mainly investigates the methods to enhance the de-airing behaviours in UHPC mixtures during and after mixing. By analysing the different factors that may affect the formation and de-airing of the air bubbles during and after mixing, the presumable formation and de-airing mechanisms of air bubbles in UHPC have been studied. In addition, several feasible methods to reduce the air pores in UHPC structures could be proposed. The main conclusions are drawn as follows:

- (1) In order to ensure that the air pores in hardened UHPC elements do not adversely affect mechanical properties and structural safety, and to provide sufficient surface quality and confidence from the people, the percentage of air pores in the element should be less than 1.7%. In order to meet this requirement, the air content in the fresh UHPC mixture is preferably less than 4% within the scope of this research;

- (2) A longer mixing time, a mixer with a larger capacity and a higher power can decrease the air content in the fresh UHPC mixture. The reference mix proportion used in this study (see Chapter 2) mixed with an Eirich mixer hardly fulfils the requirements in Conclusion (1) regarding the air content in fresh UHPC mixture. However, in large-scale applications, the mixers with larger capacities and higher powers can be used. And it is also possible to adjust the mix proportion based on the study in Chapter 2.
- (3) Partial adjustments from the reference mix proportion within the scope of this research can be based on the calculation of the air content of fresh UHPC mixtures and the percentage of air pores in hardened UHPC elements according to equations (4.19) and (4.20), thus fulfilling the requirements in conclusion (1).
- (4) A higher flowability can enhance the de-airing during mixing, a lower viscosity can enhance the de-airing after mixing. Both can benefit from fulfilling the requirements in conclusion (1). The influence of the flowability on the air content in the fresh UHPC mixture can be calculated according to equation (4.3).
- (5) Coarse aggregates, steel fibres and some defoaming agents can enhance the de-airing during mixing and thus reduce the air content of fresh UHPC mixtures. Formwork release agents can only enhance the de-airing after mixing near the concrete surface, which can help to improve the quality of the concrete surface.
- (6) Some casting methods like casting with a hose can decrease the entrapped air bubbles during casting to decrease the air pores in the elements;

In conclusion, based on the requirements of different large-scale engineering applications of UHPC, on the premise of maintaining performances, corresponding methods to enhance the de-airing behaviours in UHPC can decrease the air pores in the UHPC structures to increase reliability and confidence. However, further experimental and theoretical research work is still needed in the future.

5 Influence of the RCA on the workability of UHPC

5.1 Literature review

According to the research results in the previous chapters and the deduced formation mechanisms of the “elephant skin” and the air bubbles formation and de-airing mechanisms, when UHPC contains coarse aggregates or steel fibres and the flowability remains consistent, the large particle would make the internal moisture to take a long way round to rise, which enhances the growing of the “elephant skin” over time; at the same time, the de-airing during the mixing process can also be enhanced, resulting in reduced air content in fresh concrete. In order to further verify these mechanisms, so as to solve the workability issues for large-scale applications of UHPC, this chapter introduces a special coarse aggregate—recycled concrete aggregate (RCA) to study its influence on these workability issues.

Compared with conventional NAs, RCAs have higher water absorption and lower density. Compared with the basalts used in UHPC, the strength and sharpness of RCAs are also lower. At present, there have been many studies on the application of RCAs in concrete. It is generally known that the RCAs are high-value sorting recycled from construction and demolition waste (C&D W). In construction projects, whether it is new construction, renovation and repair, or demolition of buildings, many waste materials will be generated during the process, such as waste concrete, bricks, tiles, etc. The construction industry generates the highest amount of waste among all industries, which is about 2 billion tons of waste per year worldwide [135, 136]. In Flanders Belgium alone, the construction industry generates around 15 million tons of waste per year [137].

For the treatment of C&D W, there are several different ways [138]. Since the landfill of C&D W is forbidden in many European countries due to its harm, the method currently mostly used in Europe is recycling [139]. Among them, the low-value recycling method to recycle the C&D W is to directly use them as low-grade bricks, road cushions, etc. [140] This kind of utilization method is relatively simple, the utilization rate is insufficient, and the

utilization value is low. The best solution for C&D W treatment is high-value sorting recycling, which is to sort and recycle the C&D W and re-use them in application fields such as concrete, bricks, masonry blocks, etc. The utilization rate can reach 90% [141].

As shown in Figure 5.1, the production of most RCAs is composed of the following steps [142, 143]: first of all, the part of C&D W containing concrete is separated and crushed by a specific type of crusher. There are different crushers including jaw crushers, cone crushers, impact crushers, etc. Each crusher has its own advantages, disadvantages and scope of application. The concrete fragments are normally crushed several times to achieve thoroughness. Then, the impurities which are not desirable for the production of RCAs are removed from the debris, containing plastics, glass, metals, etc. Hereafter, the aggregates pass through different sieves and are sorted into fine and coarse fractions.



Figure 5.1 Production of RCAs in a recycling factory (<http://www.obbc.be/nl/installaties>)

Therefore, the reason for the high water absorption and low density of RCA compared with NA is mainly because its surface is covered with a layer of old mortar, as shown in Figure 5.2 [57] (copyright permitted). From a microstructural point of view, RCA consists of the original NA, attached old mortar, and the interfacial zone (ITZ) between them. When using RCAs to replace part of the NAs in new concrete, there can be four ITZs: the old ITZ between old NA and old mortar in RCA, the new ITZ-1 between new NA and new mortar, the new ITZ-2 between old NA in RCA and new mortar, and the new ITZ-3 between old mortar in RCA and new mortar. Due to ITZ being characterized by the high capillary pore size on

average, and oriented layers of coarse $\text{Ca}(\text{OH})_2$ crystals, it has been well-known as the primary weak link in concrete [144-146].

As a result, on the one hand, concrete containing RCAs (RAC) will have more ITZs compared to NAC, resulting in more pores; On the other hand, there can be relatively many pores in the old dry mortar contained in RCA, and the greater the amount of residual mortar, the greater the porosity of RCA. These lead to a decrease in the density and an increase in the water absorption of the aggregates.

According to the existing studies about the performances of RAC such as mechanical properties, fresh properties, freeze-thaw characteristics, carbonization characteristics, etc. [147-150], when RCAs are used to directly replace NAs in concrete, the fresh and hardened performances of RAC may generally be lower than that of NAC. Thus, in order to prevent the fresh performances of RAC from being greatly reduced, it is usually considered to add a certain amount of additional water to compensate for the high water absorption of the RCAs [151, 152]. The amount of compensation water is a very important issue in the study of the workability of RAC.

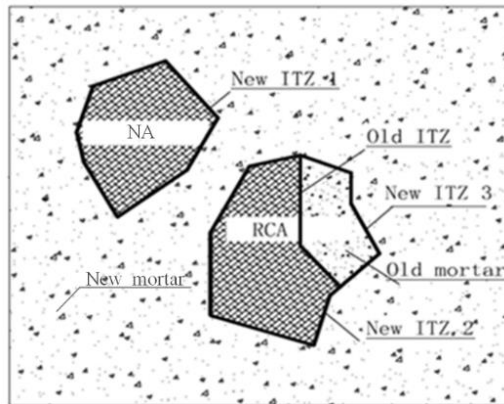


Figure 5.2 Schematic diagram of recycled aggregate surface wrapped with mortar [57]

In addition, as mentioned before, UHPC may have higher requirements on workability, and due to its very low water/cement ratio, the high water absorption and low density of RCAs may have large influences on the related workability issues of UHPC. Consequently, it is of great significance to investigate the influence of RCAs on the workability of UHPC to verify the proposed formation mechanisms of the “elephant skin” and the air bubbles formation and de-airing mechanisms in UHPC.

The results of this research can also be used to preliminarily develop the new UHPC material contained in RCAs. It is gradually possible to use RCAs to replace the coarse aggregates in UHPC [153]. However, there is still relatively little research in this area in the world. Since RCAs are weaker, their incorporation may result in a decrease in the compressive strength. Nevertheless, considering that UHPC has a very high amount of cementitious materials, UHPC containing RCAs can still have a high compressive strength even if the strength is reduced in comparison to UHPC with NAs. With the current increasing popularity of the use of UHPC in the world, considering the large number of C&D W in some countries such as Belgium, where there is a shortage of NAs, the use of RCAs in UHPC can also help to reduce the cost and contribute to sustainable development in the field of engineering materials. Therefore, the development of UHPC containing RCAs is also meaningful.

In this chapter, firstly the research on the influence of RCAs on the properties of normal strength RAC is analyzed through literature collection and experimental study; secondly, the influence of the replacement ratio of RCAs and the content of compensation water (percentage of the water absorbed by RCAs) on the fresh and hardened properties of UHPC are investigated; thirdly, the effect of RCAs on the formation of the “elephant skin” and the de-airing processes in UHPC are explored. Finally, the influence mechanisms of RCAs on the workability of UHPC is discussed.

5.2 Influence of RCA on the properties of normal strength concrete

Most research that has been done already on the use of recycled aggregate in concrete is focused on the hardened properties of concrete and the fresh concrete properties are often neglected. Besides, slump, air content, and hardening speed will also have a certain influence on the hardened properties of concrete.

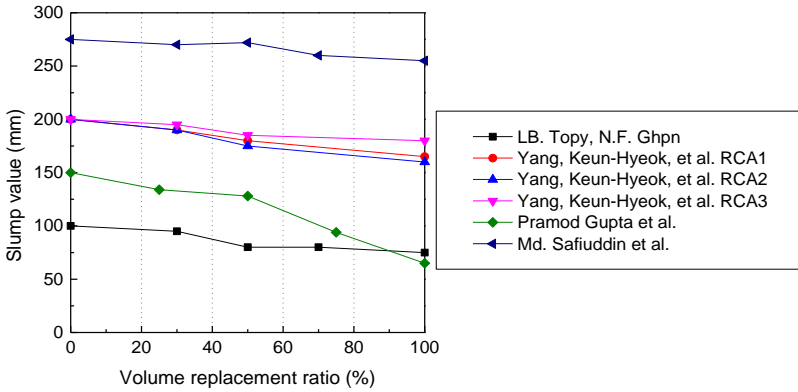
Thus, this research on the influence of RCA on the properties of normal strength RAC is divided into two parts: conventional vibrated concrete (CVC) and self-compacting concrete (SCC), in order to explore the effect of RCAs and compensation water and provide a basis for the investigation of UHPC with RCAs.

5.2.1 Results in literature

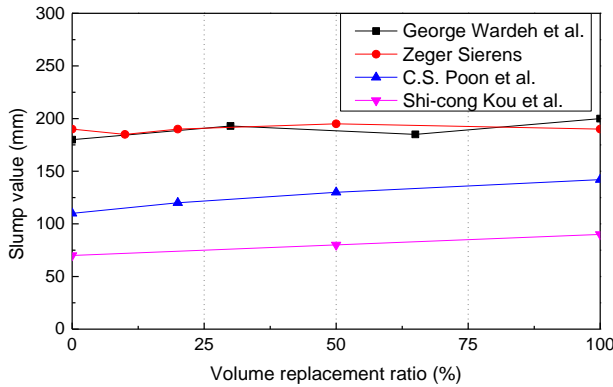
It is well known that for CVC the slump value is the most important property to determine the consistency of fresh concrete, which is measured according to EN 12350-2 [154]. For the SCC, the consistency is evaluated by the filling ability, which measures the ability of the concrete to flow under its own weight without any vibration being applied and fully fill the formwork [155]. The filling ability of SCC is an important property especially when it is used to fill up spaces. The tests that can be performed to assess the filling ability are the slump flow test and the V-funnel test. Through a slump flow test according to EN 12350-8 [156], the slump flow and T_{500} values can be obtained. And the V-funnel value can be measured according to EN 12350-9 [157].

In order to investigate the influence of RCAs and compensation water on the slump value of CVC and the slump flow value of SCC, this study first collected the results in literature based on a recent master thesis "The influencing factors on the workability of recycled aggregate concrete" [158] incorporated by the authors of this thesis.

The results of the influence of RCAs and the content of compensation water on the slump value of CVC are shown in Figure 5.3 [59, 159-165]. It can be clearly seen that when RCA is incorporated without compensation water, the slump value decreases with an increase in the RCA content. But when RCA is with 100% compensation water, the slump value would increase with an increase of RCA content. Figure 5.4 [59, 159-165] shows the results of the influence of RCAs and the content of compensation water on the compressive strength of CVC, it can also be seen that when RCA is without compensation water, the compressive strength decreases with an increase of RCA content. But when RCA is with 100% compensation water, with the increase of RCA content, although the compressive strength still decreases, the magnitude seems to have weakened. This result also illustrates the necessity of compensation water, which benefits both the fresh and hardening performance of the concrete.

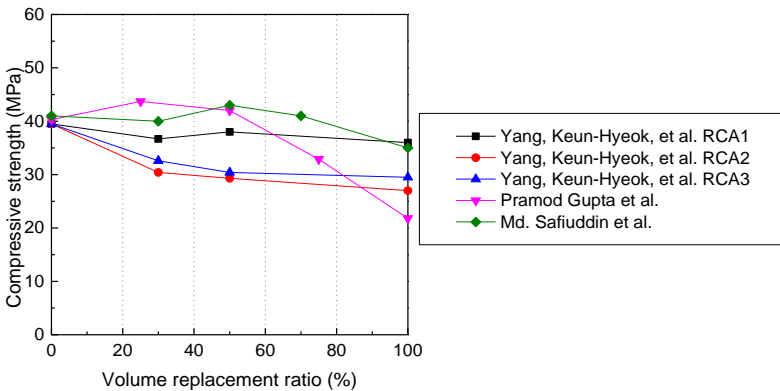


(a) With 0% compensation water

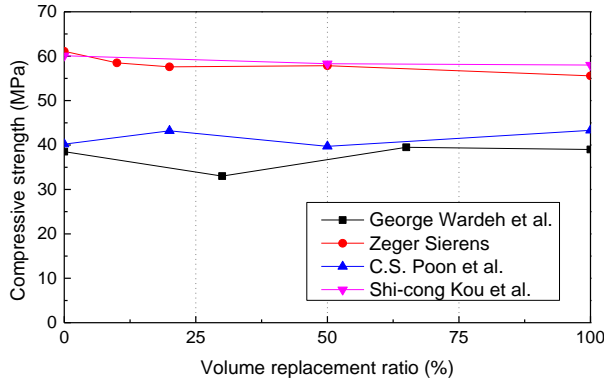


(b) With 100% compensation water

Figure 5.3 Influence of the volume replacement ratio of RCA and the content of compensation water on the slump value for CVC [59, 159-165]



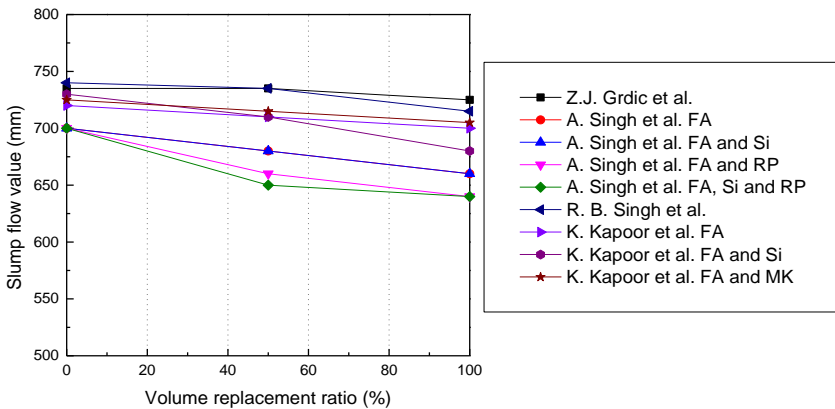
(a) With 0% compensation water



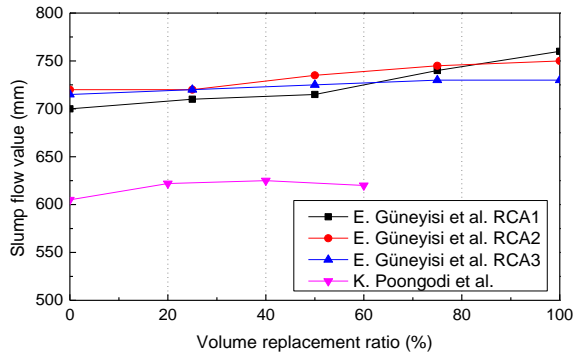
(b) With 100% compensation water

Figure 5.4 Influence of the volume replacement ratio of RCA and the content of compensation water on the compressive strength for CVC [59, 159-165]

The results of the influence of RCAs and the content of compensation water on the slump flow value of SCC are shown in Figure 5.5 [60, 166-170]. It can be found that similar to the results of CVC, when RCA is without compensation water, the slump flow value decreases with an increase in the RCA content. However, when RCA is with 100% compensation water, the slump flow value increases with the increase of the RCA content. Figure 5.6 [60, 166-170] shows the results of the influence of RCAs and the content of compensation water on the compressive strength of SCC. Due to the insufficient data for both slump flow value and compressive strength, the results in the figure cannot represent the laws, but it can be seen that the influence of the RCA content on the compressive strength of SCC is similar to that of CVC.

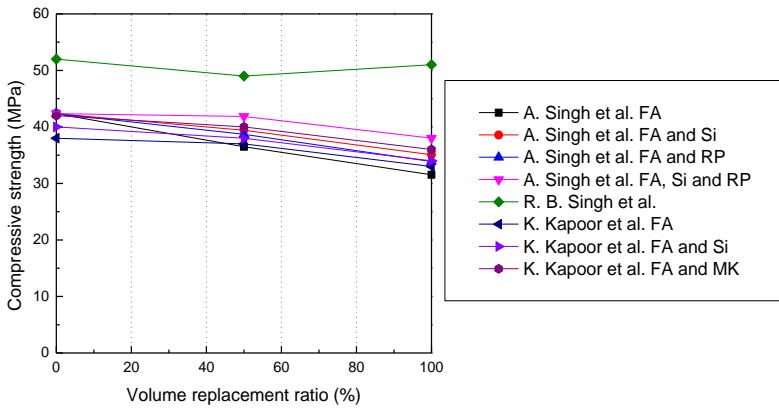


(a) With 0% compensation water

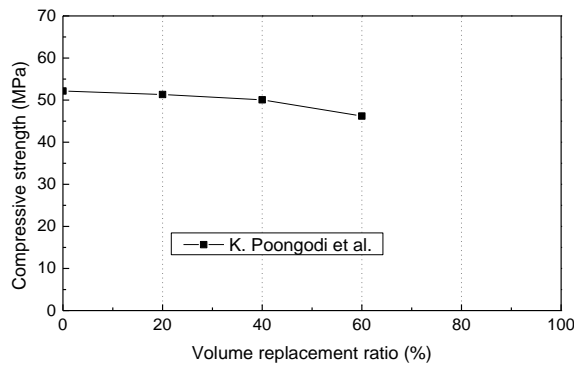


(b) With 100% compensation water

Figure 5.5 Influence of the volume replacement ratio of RCA and the content of compensation water on the flowability for SCC [60, 166-170]



(a) With 0% compensation water



(b) With 100% compensation water

Figure 5.6 Influence of the volume replacement ratio of RCA and the content of compensation water on the compressive strength for SCC [60, 166-170]

From the results in the literature, it can be analysed that when RCAs are used to replace part of NAs in concrete since RCAs have a higher water absorption rate than NAs, the free water in the concrete will be partially absorbed, and the slump flowabilities of both CVC and SCC will be reduced if no compensating water is added. At the same time, because RCAs have more pores, their strength is not as good as that of NAs, and when the consistency decreases, the porosity of concrete increases due to the lower particle packing density. Thus, even if the free water in the concrete is reduced, the compressive strength of concrete containing RCAs will still decrease. However, for SCC, because of its relatively low porosity itself, when RCAs have not so many pores, the compressive strength can also increase with the increase of the RCA content due to the decrease of free water in the concrete, which is the reason for the result of R.b. Singh et al. in Figure 5.6(a) [167].

When 100% compensation water is added, the free water absorbed by RCAs in concrete can be supplemented, and the slump flowabilities of both CVC and SCC don't decrease but increase. This is due to RCAs will not absorb free water with a 100% water absorption rate in concrete. Because the water absorption rate of RCAs is measured by the water absorption of 24h, while concrete usually reaches the final setting in 5-8h. However, in this case, the increased slump flow value depends on the pre-wetting and mixing procedure and on the time when the slump is measured, which is the reason for the scattering of the results. Besides, due to the decrease of porosity caused by the increase of consistency, for CVC, the decrease of concrete compressive strength with the increase of RCA content will be slowed down. But for SCC, due to its own low porosity, its compressive strength will continue to decrease with the increase of RCA content.

Accordingly, in order to ensure sufficient consistency of RAC and not to reduce the compressive strength due to excessive free water content, it is necessary to find an optimal compensation water content so that the slump fluidity of RAC is close to that of NAC. At this time, the compressive strength result may also be optimal.

5.2.2 Experimental research

To determine the optimal compensation water content, experiments to study the fresh and hardened properties of CVC contained RCAs were carried out. The RCA used in this research was from the company "Karl Schwarzl Betriebsgesellschaft m.b.H." in Austria. They are gravel aggregates for concrete recycled from the concrete regeneration tank in the mix station, which are crushed and collected from the hardened concrete recovered in the mix station with a fraction of 0-16mm. The parent concrete class ranges from C20/25-C70/85, as

shown in Figure 5.7. The RCA was washed and sieved into the size of 4-8mm. Figure 5.8 shows the particle size distributions of the RCA and NA with the same grade of 4-8mm, which have no large difference. The water absorption and the densities of the RCA were determined according to EN 1097-6 [171]. The measured average water absorption of the RCA was 3.7% and the apparent density was 2453kg/m^3 .



Figure 5.7 Photo of the used RCA

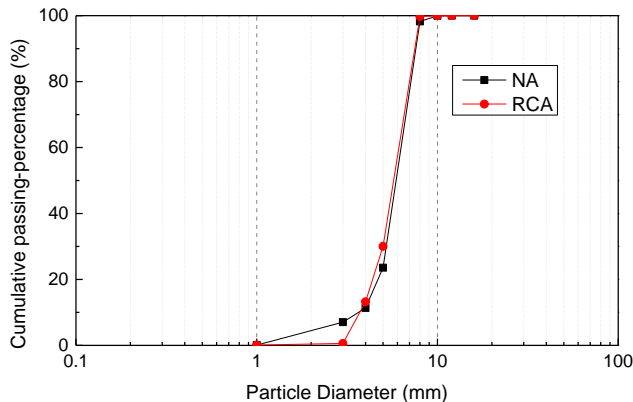


Figure 5.8 Particle size distribution of used NAs and RCAs in this section

3 batches of C50 concrete were mixed with an Eirich mixer, as shown in Table 5.1. Detailed mix recipes and properties of these NSCs can be found in Table A.6 in the appendix. The CEM C used for these NSCs is the “Alpen Zement CEM II/A-S 52.5N” from the company “W&P Zement GmbH”, which is a Portland slag cement for all common concrete applications. It is particularly suitable for ready-mixed concrete and concrete plants, as well as concreting work at low temperatures, especially when there are increased requirements for early strength. The technical parameters are shown in Table 5.2. A total of 3 kinds of NAs (Sand 0-4mm, Gravel 4-8mm, and Gravel 8-16mm) are from the company “Tieber GmbH”

in Austria. They are high-quality sand and gravel quarried from the mountains with very low water absorptions (<1%). The RCA replacement ratio was considered to be 0%, 50% and 100%.

Based on the results of the previous section and the results of the tests conducted by the colleagues of the institute, the optimum compensating water content should be around 80% of the water absorption of RCAs. In the master's study "The influencing factors on the workability of recycled aggregate concrete" [158], the effect of 0%, 78% and 100% compensating water on slump flow, air content and compressive strength of CVC as well as SCC was investigated. The results showed that the optimum compensating water content might vary slightly for different concretes, but was roughly in the range of 75% to 85%.

Consequently, in this research, the compensation water content was taken as 75% of the water absorption of RCAs, which are represented by "0/0", "50/75" and "100/75" in the name of the recipes in Table 5.1. For each batch of concrete, the consistency was tested and the mixture was then cast into two 150×150×150mm cubes to test the compressive strength after being cured in room-temperature water for 28 days.

Table 5.1 The CVCs tested for investigating the RCAs

Concrete	RCAs Replacement ratio	Compensation water content	Slump flow value (cm)	Average compressive strength (MPa)
CVC 0/0	0	0	48	53.2
CVC 50/75	50%	75%	47.5	50.3
CVC 100/75	100%	75%	47	48.1

Table 5.2 Technical parameters of the CEM C

2-day compressive strength	28-day compressive strength	Initial setting time	Fineness	Density
32 MPa	60 MPa	150 min	4300 cm ² /g	3.08 g/cm ³

In this research, the consistency of the concrete mixture was tested using a flow table after compacting 15 times according to EN 12350-5 [172], as shown in Figure 5.9 and Figure 5.10 [173]. Figure 5.11 shows the photos of the flow table tests of concrete mixtures. From the results of slump flow values and average compressive strengths in Table 5.1, it can be found that in these tests, the compensation water contents of 75% of the water absorption of RCAs is very close to the optimal value. The slump flow values of the tested concrete mixtures are

nearly the same and the compressive strength is also not reduced so much as the increase of the volume replacement ratio of the RCA.

Therefore, when an optimal compensation water content is added to the concrete, the compressive strength could be optimal, and the workability of the concrete would also be favourable. However, the optimal compensation water content for concrete with RCAs may depend on the type of concrete mixtures, properties of RCAs, and the amount of RCAs, which still require further research work.

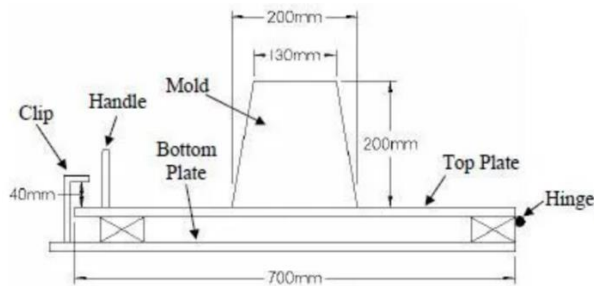


Figure 5.9 Flow table test apparatus [172]

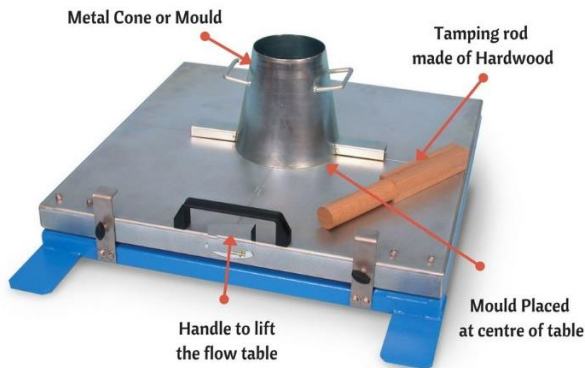


Figure 5.10 Photo of the flow table test apparatus [173]

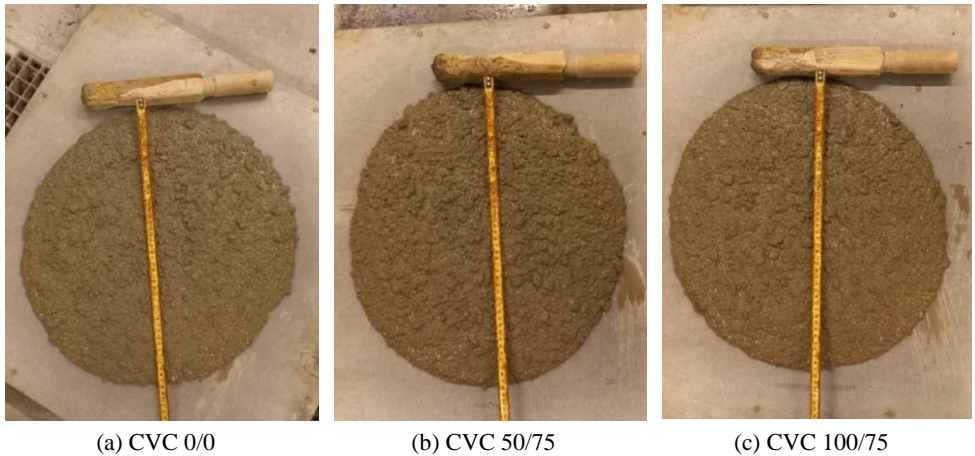


Figure 5.11 Photos of the flow table tests of concrete mixtures

5.3 Influence of RCA on the properties of UHPC

Based on the test results on the influence of RCA on the workability of normal-strength concrete, its influence on the workability of UHPC can be preliminarily explored. Considering that there is little research and the relevant literature is not sufficient, this section mainly investigates the fresh properties of UHPC with RCAs by means of experimental research and theoretical analysis.

The RCA from the company “Karl Schwarzl Betriebsgesellschaft m.b.H.” in Austria were used to replace the BA2 (introduced in Section 2.1.4) in UHPC. According to the fraction of BA2, the RCA with a size of 4-8mm was also used to replace the BA2. The particle size distribution of the BA and RCA is shown in Figure 5.12.

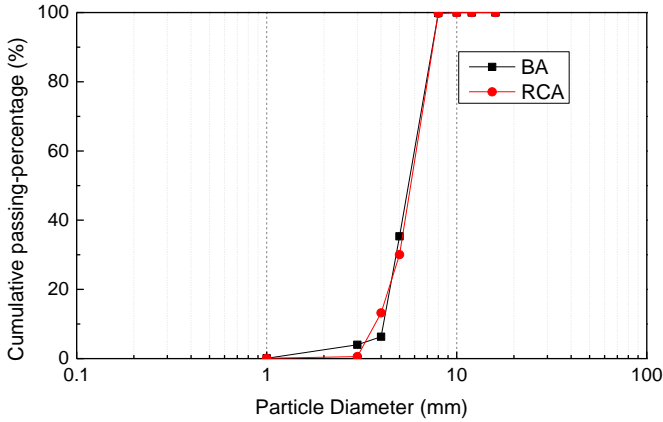


Figure 5.12 Particle size distribution of used BAs and RCAs in this section

5.3.1 Preliminary tests at the first stage

To investigate the influence of RCAs on the fresh properties of UHPC, preliminary laboratory tests were performed. The RCA volume replacement ratios of 0%, 50% and 100% are used to investigate the effect of RCA on the compressive strength of UHPC, air content and the “elephant skin”. According to the existing research and previous test results, in this research, compensation water should be correctly considered based on the water absorption of the RCA to achieve the same flowability. Thus, 2 groups of concrete are preliminarily tested in the first stage, in which one group is with StF1 and the other is without StF, as shown in Table 5.3. Detailed mix recipes and properties of these UHPC mixtures can be found in Table A.7 in the appendix.

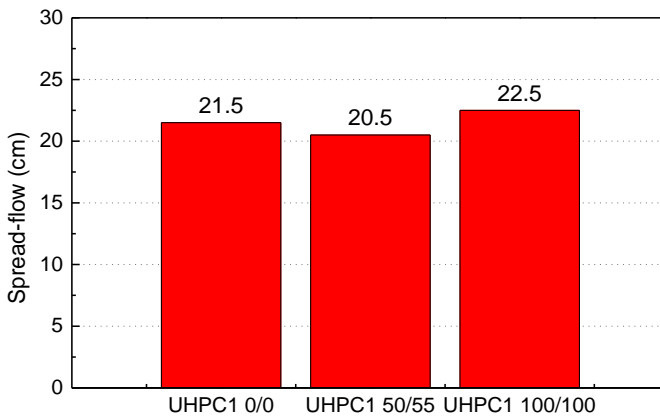
For initially determining the optimal compensation water content, the compensation water content for the RCA was adjusted according to the flowability of the UHPC mixtures, which is represented by “0/0”, “50/55”, “100/100”, “50/80” and “100/75” in the name of the UHPC mixtures, where “0”, “50” and “100” before the slash represent the RCA volume replacement ratio. Each concrete was mixed with a small Hobart mixer (Figure 2.4) to test the flowability, and air content (only for Group 2) and cast one $100 \times 100 \times 100 \text{ mm}^3$ cube to test the compressive strength after being cured in room temperature water for 28 days.

The results of the flowabilities of these 2 groups of UHPC mixtures are shown in Figure 5.13. Figure 5.14 shows the photos of the flowability test of UHPC mixtures. Similar to normal strength concrete, the content of compensation water has a great influence on the flowability

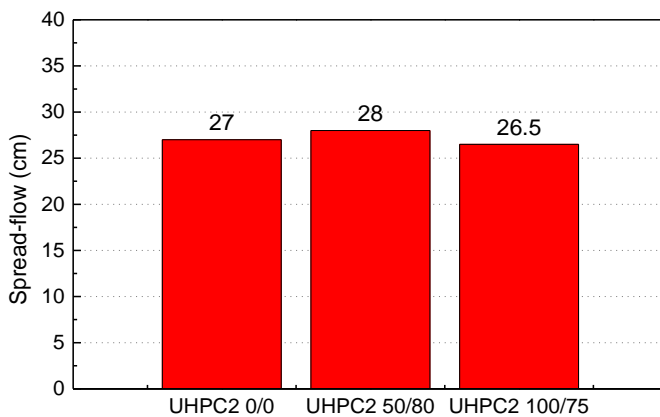
of the mixtures. In order to obtain a similar flowability to that of UHPC with natural BA, the optimal compensation water content should be between 75% and 80%.

Table 5.3 Tested UHPC mixtures with RCAs in preliminary tests

Group	UHPC mixture	RCA replacement ratio (%)	Compensation water content (%)
UHPC1 with StF1	UHPC1 0/0	0	0
	UHPC1 50/55	50	55
	UHPC1 100/100	100	100
UHPC2 without StF	UHPC2 0/0	0	0
	UHPC2 50/80	50	80
	UHPC2 100/75	100	75



(a) Group UHPC1 with StF1



(b) Group UHPC2 without StF

Figure 5.13 Flowability of 2 groups of UHPC mixtures

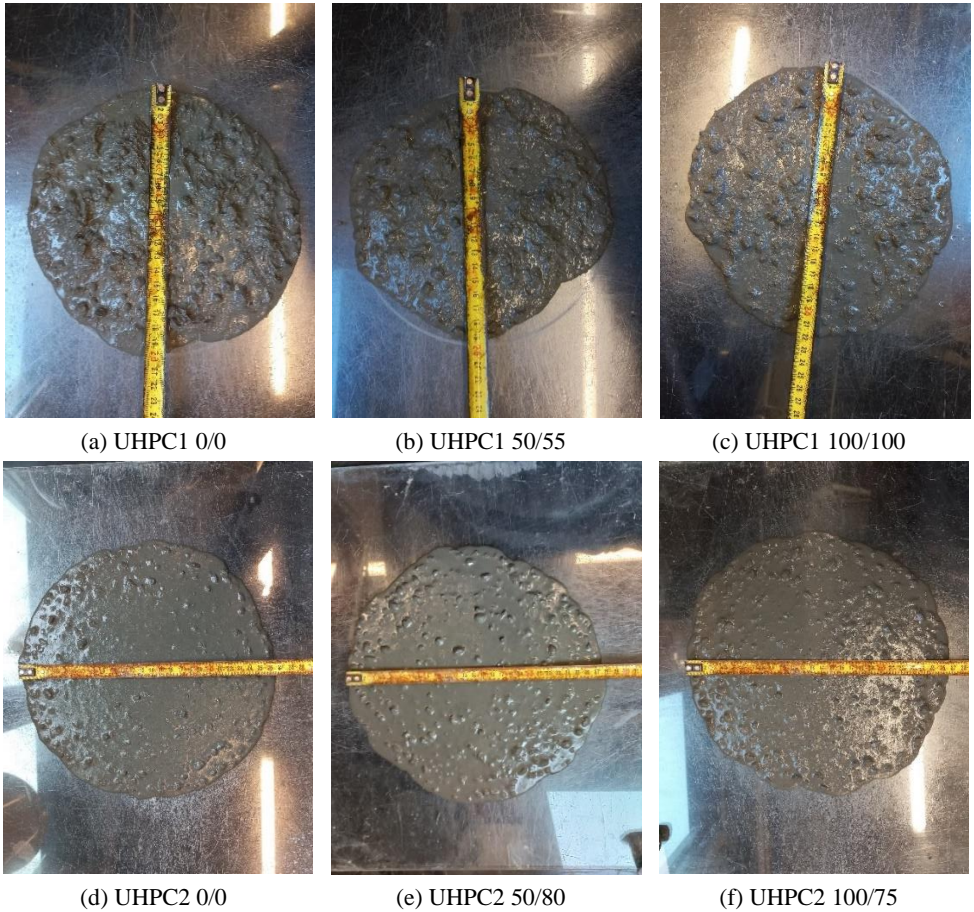
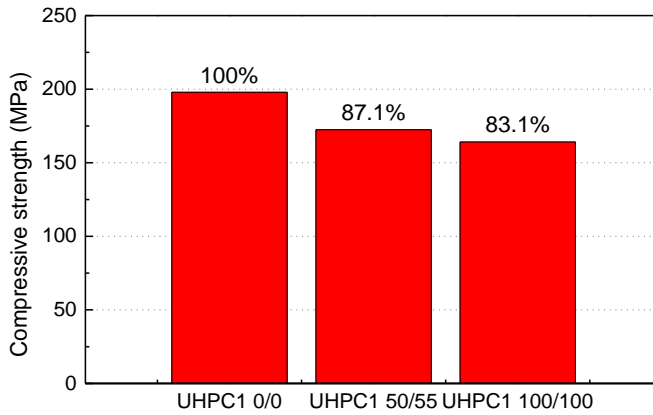


Figure 5.14 Photos of the flowability test of UHPC mixtures

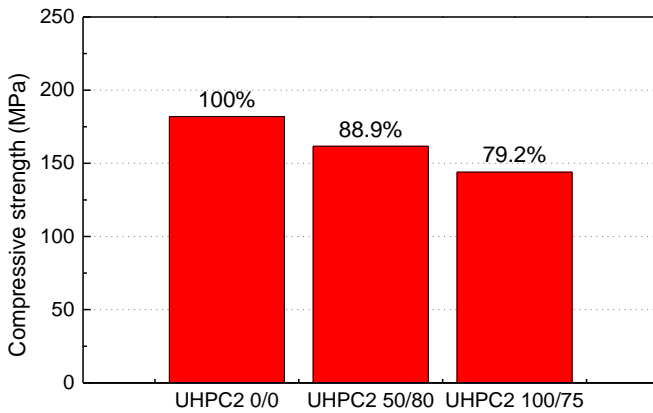
The results of the compressive strength of the 2 groups of UHPC mixtures are shown in Figure 5.15. It could be found that the compressive strength of UHPC with 50% RCA is about 10-13% lower than that without RCA, and the compressive strength of UHPC with 100% RCA is about 17-21% lower than that without RCA. Owing to the different content of the compensation water, the specific influence still requires further investigation.

Figure 5.16 shows the measured air contents of the fresh UHPC mixtures (P_{fresh}) in Group “UHPC2 without StF”. It should be noted that the flowability of the UHPC with a RCA replacement ratio of 50% in Group “UHPC2 without StF” is slightly higher than that of the reference UHPC without RCA due to excessive water compensation (Figure 5.13), leading to the air content also shown to be slightly lower, which is consistent with the findings in

Section 4.5.2. The influence of the RCA on P_{fresh} still needs to be further investigated for UHPC mixtures with the same flowability.

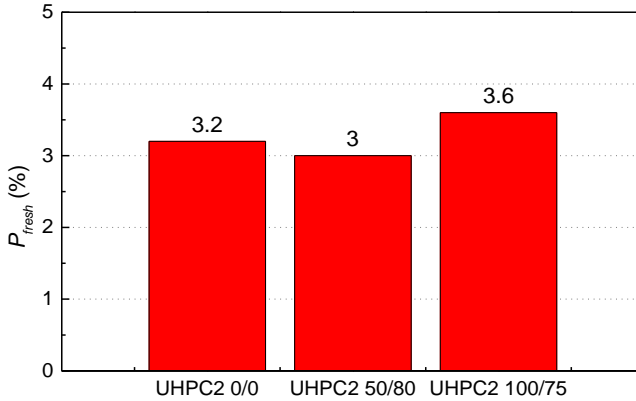


(a) Group UHPC1 with StF1



(b) Group UHPC2 without StF

Figure 5.15 Compressive strengths of these 2 groups of UHPC mixtures

Figure 5.16 P_{fresh} of the UHPC mixtures in Group “UHPC2 without StF”

5.3.2 Optimal compensation water content investigation

To further investigate the influence of RCA on the workability of UHPC, an optimal compensation water content value should be found to keep the flowability similar. According to the results in Section 5.3.1, the optimal compensation water content could be between 75-80%. Hence, 7 batches of UHPC mixtures were mixed with the small Hobart mixer, as shown in Table 5.4. Detailed mix recipes and properties of these UHPC mixtures can be found in Table A.7 in the appendix. The RCA volume replacement ratio was taken as 0%, 50% and 100%, and the compensation water contents of 0%, 100% and 78% of the water absorption of RCA were tested to investigate the influence of the compensation water content, which are represented by “0/0”, “50/0”, “50/78”, “50/100”, “100/0”, “100/78” and “100/100” in the names of UHPC mixtures in Table 5.4. For each batch of concrete, the flowability and air content were tested and one $100 \times 100 \times 100 \text{mm}^3$ cube was cast to test the compressive strength after being cured in room-temperature water for 28 days.

Table 5.4 Tested UHPC mixtures with RCAs and different compensation water content

UHPC mixture	RCA replacement ratio (%)	Compensation water content (%)
UHPC3 0/0	0	0
UHPC3 50/0	50	0
UHPC3 50/78	50	78
UHPC3 50/100	50	100
UHPC3 100/0	100	0
UHPC3 100/78	100	78
UHPC3 100/100	100	100

Figure 5.17 shows the results of the measured flowabilities of these UHPC mixtures. Figure 5.18 shows the photos of the flowability test of UHPC mixtures. It can be found that similar to normal strength concrete, when without compensation water, the flowability decreases with the increase of RCA replacement ratio, and when with 100% compensation water, the flowability increases. In this case, when with 78% compensation water, the flowability of the UHPC mixture barely changes as the RCA replacement ratio increases, indicating that 78% could be considered as the optimal compensation water content for the UHPC with RCAs.

Figure 5.19 shows the measured 28d compressive strength of the UHPC mixtures. It can be found that, regardless of whether compensation water is added, an increase in the RCA replacement ratio leads to a decrease in the compressive strength of concrete, which is due to the strength of RCAs (mainly gravel) being much lower than that of natural basalt aggregates. Besides, the compressive strength seems to drop a little more after the addition of compensation water, because the porosity of UHPC is already very low, the addition of compensation water may only increase the free water content at this time. Nevertheless, the difference is relatively slight, indicating that for UHPC, the addition of different contents of compensation water may have little effect on the compressive strength, but have a main impact on the workability.

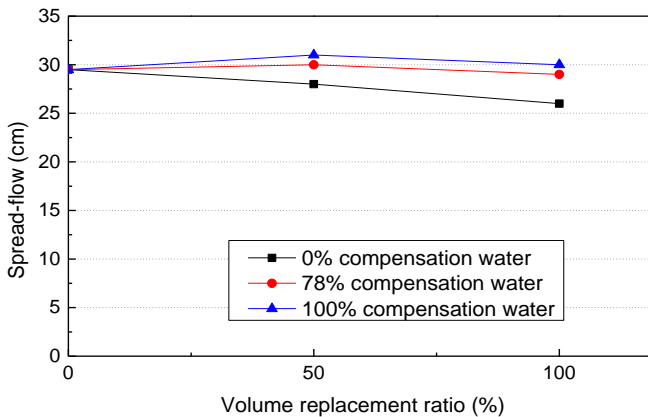


Figure 5.17 Measured flowabilities of UHPC mixtures



(a) UHPC3 0/0



(b) UHPC3 50/0



(c) UHPC3 50/78



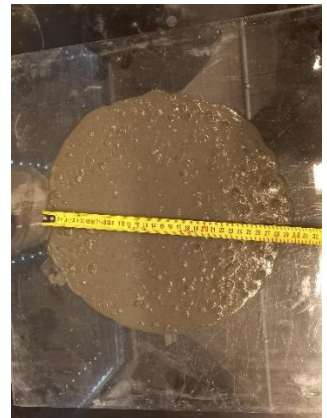
(d) UHPC3 50/100



(e) UHPC3 100/0



(f) UHPC3 100/78



(g) UHPC3 100/100

Figure 5.18 Photos of the flowability test of UHPC mixtures

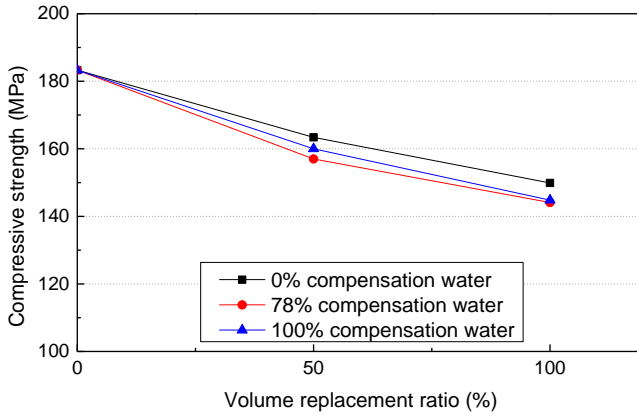


Figure 5.19 Measured 28d compressive strength of UHPC mixtures

Figure 5.20 shows the measured P_{fresh} . It can also be found that when there is no compensation water, P_{fresh} would increase significantly with the increase of the RCA replacement ratio; when the compensation water content is 100%, as the RCA replacement ratio increases, P_{fresh} would hardly increase due to the increase of flowability; when the compensation water is 78% and the flowabilities are almost the same, P_{fresh} still slightly increases with the increase of the RCA replacement ratio. This indicates that the use of RCA may increase the air content in fresh UHPC mixture.

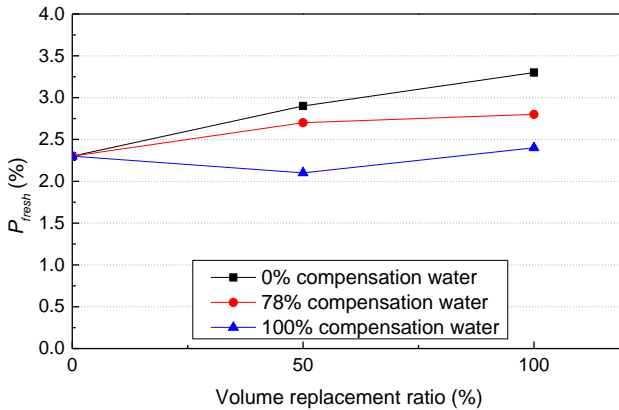


Figure 5.20 Measured P_{fresh} of the UHPC mixtures

5.3.3 Influence of RCA on the de-airing and the “elephant skin”

Assuming that 78% is the optimal compensation water content, which can keep the flowability almost unchanged, the influence of RCA on the de-airing and the “elephant skin” in UHPC is investigated. In the research of this section, 3 batches of UHPC mixtures were mixed with the Eirich mixer as shown in Table 5.5. Detailed mix recipes and properties of these UHPC mixtures can be found in Table A.7 in the appendix. The RCA replacement ratio was also varied as 0%, 50% and 100% and the compensation water content was 78%, which are represented by “0/0”, “50/78” and “100/78” in the names of the UHPC mixtures in Table 5.5. For each batch of UHPC, the flowability, viscosity and air content were tested, one $100 \times 250 \times 30 \text{mm}^3$ plate was cast to test the growing of the “elephant skin” over time, one $\Phi 100 \times H 200 \text{mm}^3$ cylinder was cast to test the air pores in the sections and three $100 \times 100 \times 100 \text{mm}^3$ cubes were cast to test the compressive strength after cured in room temperature water for 28 days.

Table 5.5 Tested UHPC mixtures with RCAs to investigate the workability issues

UHPC mixture	RCA replacement ratio (%)	Compensation water content (%)	Spread-flow (cm)	T_{200} (s)
UHPC4 0/0	0	0	29.5	7
UHPC4 50/78	50	78	29.5	7
UHPC4 100/78	100	78	29.5	7

Figure 5.21 shows the photos of the flowability test of UHPC mixtures. From the results of spread-flow values and T_{200} values in Table 5.5, the flowabilities and viscosities are nearly the same for the UHPC mixtures with the different replacement ratios of RCAs. Figure 5.22 shows the measured compressive strengths of UHPC mixtures. The decrease in the compressive strength of UHPC with RCAs is also consistent with the previous test results shown in Figure 5.15. The 28d compressive strength of UHPC containing 100% RCA can also reach a compressive strength higher than 140MPa.



(a) UHPC4 0/0 (b) UHPC4 50/78 (c) UHPC4 100/78

Figure 5.21 Photos of the flowability test of UHPC mixtures

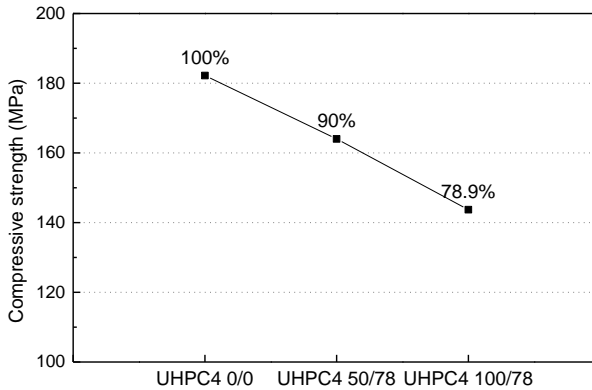
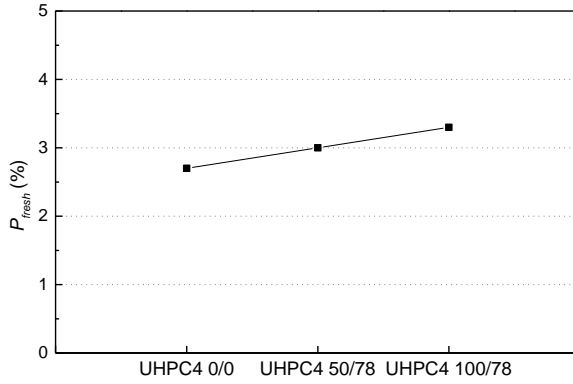
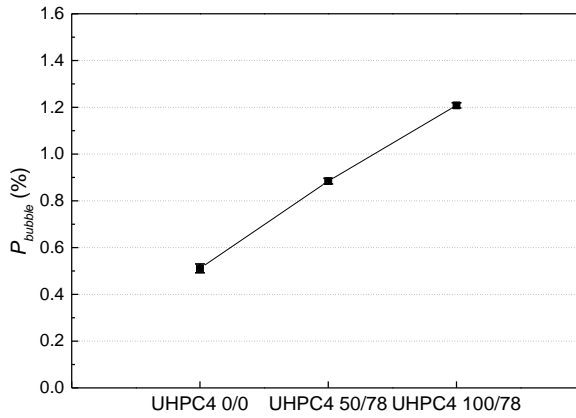


Figure 5.22 Measured compressive strengths of UHPC mixtures

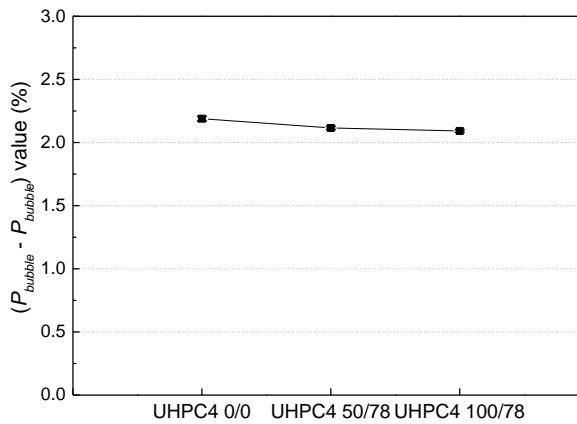
Figure 5.23 shows the measured and calculated P_{fresh} , P_{bubble} , $(P_{fresh} - P_{bubble})$ value and the maximum air bubble diameter of these 3 batches of UHPC mixtures. It can be found that the RCAs have a large influence on P_{fresh} , resulting in a change of P_{bubble} , while the $(P_{fresh} - P_{bubble})$ value is almost unchanged, indicating that the RCA would mainly impact the de-airing process during mixing, but not on the de-airing process after mixing. From the results of the maximum air bubble diameter, it can be found that the UHPC with RCAs would have larger maximum air bubble diameters than that without RCAs, which also proves the influence of RCA on the de-airing process during mixing according to the results in Section 4.5.3.



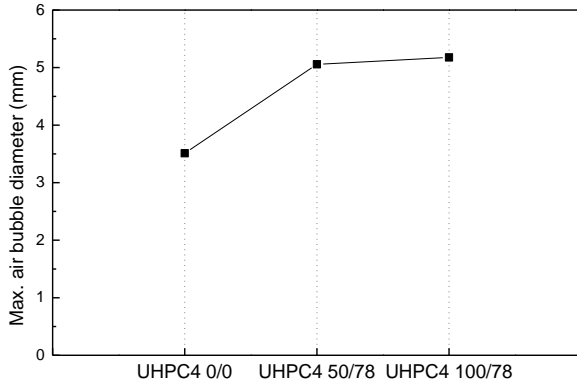
(a) Measured P_{fresh}



(b) Measured P_{bubble}



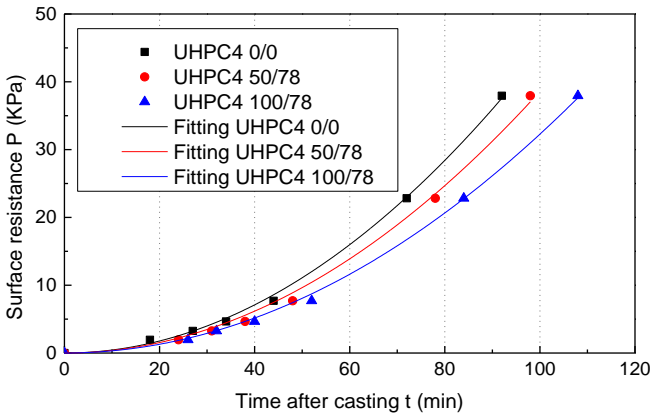
(c) Calculated $P_{fresh} - P_{bubble}$



(d) Measured maximum air bubble diameter

Figure 5.23 Influence of RCA on the de-airing behaviours in UHPC

Figure 5.24 shows the results of the growing of the “elephant skin” over time ($R^2=0.999$). It can be found that the use of RCA may decrease the growing of the “elephant skin” over time. This can be attributed to the fact that when more RCA is incorporated, and the compensation water content is 78%, although the flowability remains similar, the actual free water in the concrete increases because the rough surface of the RCA requires more free water to obtain flowability. More free water in the UHPC helps to supplement moisture that evaporates from the surface, slowing down the growing of the “elephant skin” over time. This further verifies the formation mechanisms of the “elephant skin”.



(a) Surface resistance-time curves

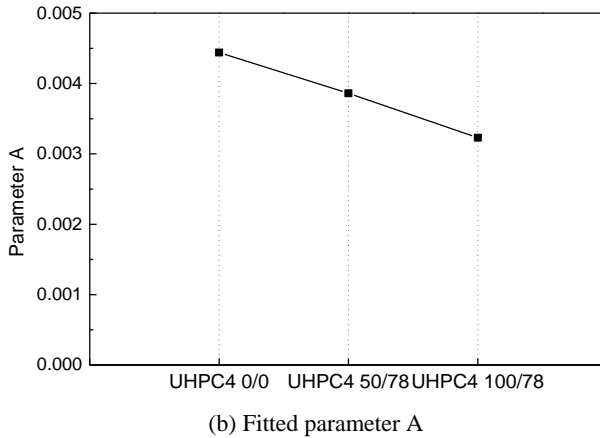


Figure 5.24 Influence of the RCAs on the growing of the “elephant skin” over time

5.4 Discussion of the influence mechanisms

As shown in Figure 5.2, the biggest difference between RCA and NA is that the surface of RCA is covered with an old mortar porous layer and there are more ITZs when RCA is used in the new concrete. These results in the high water absorption and low density of RCA in comparison to NA.

Therefore, regarding the effect of RCA and compensation water content on the consistency of concrete, when the concrete is mixed with RCA without adding compensating water, the free water in the concrete will be largely absorbed by RCA, resulting in a loss of consistency. But when the compensating water is added by 100% of the water absorption of RCA in the concrete, there will be an increase in flowability due to the inability of the RCA to absorb the free water by 100% of the water absorption before the final set of the concrete. This result is true for both NSC and UHPC.

Regarding the effect of RCA and compensation water content on the compressive strength of concrete, based on the results in collected literature and experiments, the reason can be assumed to be the following analysis:

For CVC, when no compensation water is added to the concrete, with the increase of the RCA content, since the compressive strength of RCA is lower than that of NA due to its own porosity, even if more free water is absorbed, the decrease in concrete consistency will also

increase the porosity, and the compressive strength of CVC will be reduced. But when 100% compensation water is added to the concrete, with the increase of the RCA content, although the compressive strength of RCA is lower than that of NA, and the free water in concrete increases, the increase of concrete consistency can reduce the porosity, causing the rate of decrease in compressive strength of CVC is slowed down.

For SCC, due to its high consistency, when no compensation water is added to the concrete, with the increase of the RCA content, more free water will be absorbed, and considering that the compressive strength of RCA is lower than that of NA, the compressive strength of SCC may increase or decrease. But when 100% compensation water is added to the concrete, with the increase of the RCA content, the free water in the concrete will also increase, leading to the compressive strength of SCC decreases.

For UHPC, since the compressive strength of RCA is much lower than that of basalt aggregate, the compressive strength of UHPC may decrease significantly with the increase of RCA content regardless of the addition of compensation water. And since UHPC has very low porosity, more compensation water only increases the free water content in concrete, thereby further reducing the compressive strength.

Consequently, in order to prevent segregation and the influence of excess free water on the hardening performance, the optimal compensation water content should be considered to make the flowability of the concrete containing RCA very close to that of the concrete without RCA. According to the test results, the value may be between 75% and 85% and vary for different concrete.

In addition, when the optimum compensating water content is added, more RCAs may decrease the de-airing during mixing in UHPC and decrease the growing of the “elephant skin” over time. This reason can be assumed to be as follows:

Although not measured in this study, based on the characteristics of the aggregate, the sharpness of RCA is lower than that of basalt, and the surface roughness of RCA is higher than that of basalt. Therefore, for the UHPC containing RCAs, the lower density and sharpness of RCA may cause a lack of intensity during the mixing process, leading to a larger P_{fresh} . At the same time, when the flowability is the same, owing to the rougher surface of RCA, there would be more free water in the UHPC containing RCAs, resulting in the decreased growing of the “elephant skin” over time.

Accordingly, the test results on UHPC with RCA further verified the proposed formation mechanisms of the “elephant skin” and the air bubbles formation and de-airing mechanisms.

5.5 Summary

Based on the research on the influence of RCA on the properties of NSC (CVC and SCC), this chapter investigates the influence of RCA on the workability of UHPC, and at the same time verifies the the proposed formation mechanisms of the “elephant skin” and the air bubbles formation and de-airing mechanisms. The main conclusions can be drawn as follows:

- (1) RAC would absorb free water in the concrete, making the concrete with RCA less consistent than that with NA. Adding optimal compensation water content according to the water absorption of RCA can maintain consistency and avoid detrimental effects of RCA on the hardened properties of concrete. The optimal compensation water content may be in the range of 75%~85% in the scope of this research, and may be different for the different concrete mixtures;
- (2) The compressive strength of RCA is lower than that of NA and much lower than that of basalt aggregate. So when RCA absorbs a certain amount of free water in the concrete, for NSC containing RCA, the compressive strength may increase or decrease; for UHPC containing RCA, the compressive strength usually decreases. The compressive strength of UHPC contains 100% RCAs may decrease by about 20%;
- (3) When an optimal compensation water content is added, for the UHPC with RCA, the de-airing process during mixing can be reduced, leading to higher air content in fresh concrete in comparison to the UHPC with basalt aggregate;
- (4) When an optimal compensation water content is added, for the UHPC with RCA, the internal moisture will rise more slowly due to the lower density and rougher surface of RCA, leading to a slower growing of the “elephant skin” over time in comparison to the UHPC with basalt aggregate.

In conclusion, as a special aggregate with high water absorption and low density, RCA has a certain degree of influence on the workability of UHPC, which needs further theoretical and experimental analysis in the future. However, RCA-containing UHPC mixtures with sufficient fresh and hardened properties can be preliminarily developed, which is also conducive to large-scale and sustainable engineering applications of UHPC.

6 Conclusions and recommendations

This doctoral dissertation mainly performs investigations on the workability issues that impede UHPC's large-scale applications. The extremely high performances of UHPC enable it to be applied more and more widely in various projects without increasing the cost. However, due to some workability issues, it is still difficult to realize large-scale applications. This thesis mainly investigates various factors affecting the workability issues of the “elephant skin” and de-airing in UHPC, hypothesizes and summarizes the impact mechanisms of each issue, and then puts forward relevant solutions in some aspects based on UHPC material and mix proportion. Through the analysis of each chapter, the following conclusions, significances and contents that need further research in the future can be drawn.

6.1 Main findings

According to the results in Chapter 2, based on the existing developed UHPC with the optimal raw materials and mix proportion and the requirements for the UHPC performances, the range of content of each UHPC component was determined in order to solve the workability issues. The influences of the content of each component on the flowability, viscosity, temperature of fresh UHPC and the compressive strength of hardened UHPC were investigated. The results of this chapter explain the raw materials and mix design of the UHPC mixtures in this research, and provide an important basis for the research in the following chapters.

According to the results in Chapter 3, a layer of the “elephant skin” will appear on the concrete surface as short as 3-5min after casting, which may affect the surface performance of the concrete, making the connection of multi-layer UHPC invalid, and hinder the air bubbles in the concrete from rising. By using the Vicat experimental method to investigate various influencing factors, it is found that the generation of the “elephant skin” is mainly because of the rather limited amount of free water in the UHPC mixture, the loss of water on the concrete surface is often significant. On the other hand, due to the high viscosity of UHPC, the rising rate of internal water in the mixture is generally very low, which is normally (much) lower than the evaporation rate of water on the concrete surface, resulting in the rapid

formation of a hard layer on the surface. Thus, if changing the external environment is possible, a decrease in the evaporation rate can help to decrease the growing of the “elephant skin” over time on the UHPC surface. Otherwise, from the perspective of the raw material and mix proportion of UHPC, increasing the paste content, water/binder ratio, or superplasticizer dosage within the range given in Chapter 2 may be helpful for decreasing the growing of the “elephant skin” over time. Besides, the UHPC without coarse aggregates and steel fibre may also be beneficial. These ways could contribute to providing sufficient time for watering the surface in large-scale applications, thereby completely avoiding the harm of the “elephant skin”.

According to the results in Chapter 4, due to UHPC’s ultra-high performance, it can be applied to very fine structures, while because of its dense microstructure, the de-airing behaviours in UHPC during and after mixing is very slow, causing many air bubbles entrapped in fresh UHPC mixture. Although UHPC has a large packing density, small capillary porosity, and high compressive strength and durability, the entrapped air bubbles (diameter > 0.5mm) will form big air pores in the hardened structure to cause safety hazards, which is not conducive to the large-scale application of UHPC. By analyzing the different factors that may affect the generation and de-airing behaviours of the air bubbles during and after mixing, it is found that the air bubbles are usually generated when the raw materials are added, some can escape during the mixing process, but some will remain in the concrete after mixing and rise vertically. After that, some new air may also be entrapped during casting, and in the end all the air bubbles will slowly rise vertically until the UHPC sets. In order to reduce the air pores in hardened concrete, it is necessary to enhance the de-airing behaviours of UHPC during and after mixing. Additionally, decreasing the air bubbles entrapped during casting can also help. Hence, the UHPC with constituents to achieve high flowability, with coarse aggregate or steel fibre, or with some kinds of defoaming agent, which would not strongly affect the hardening performance of concrete, can increase the de-airing behaviour during the mixing process. The UHPC with constituents to achieve low viscosity or longer setting time without strongly affecting the hardening performance of concrete can enhance the de-airing behaviour of UHPC after mixing. Some casting methods like casting with a hose can decrease the entrapped air bubbles during casting.

According to the results in Chapter 5, owing to the surface of recycled aggregate being covered with an old mortar layer and can form more interfacial zones when mixed in the new concrete, the density of recycled aggregate is lower and the water absorption of recycled aggregate is higher than the natural aggregate. Thus, the using of recycled aggregates to replace natural aggregates in concrete not only has a certain influence on the hardening

performance but also has a great influence on workability. Based on the research on the influence of recycled aggregates on normal-strength concrete, the influence of recycled aggregates on workability issues was investigated to verify the proposed mechanisms. It is found that recycled aggregates can absorb free water in the concrete, making the concrete with recycled aggregate less consistent than that with natural aggregate. Adding an optimal compensation water content can supplement a certain amount of free water to keep the consistency. Due to the low density, low sharpness, and rough surface of recycled aggregate, the de-airing process during mixing of UHPC with recycled aggregate can be slower, the amount of free water in UHPC with recycled aggregate should also be larger to keep sufficient flowability. These lead to higher air content in fresh UHPC and slower growing of the “elephant skin” over time, which further verified the formation mechanisms of the “elephant skin” and the air bubbles formation and de-airing mechanisms in UHPC. In addition, the compressive strength of UHPC containing 100% RCAs may decrease by only about 20%. Considering the shortage of natural aggregates and the excess of construction and demolition waste in some regions, the use of recycled aggregates in UHPC can be a significant cost reduction and sustainable development as UHPC becomes increasingly popular.

6.2 Valorisations

With the development of concrete technology, most research that has been done already on the production and implementation of concrete is focused on the hardened properties of concrete. Especially for UHPC, the research on the fresh properties is far from sufficient. Nevertheless, the fresh performance of concrete, especially the workability is also very important in industrial engineering, which directly affects the practical application of concrete. For example, the consistency of concrete directly affects how evenly the concrete can be distributed in the formwork after it has been cast. In some cast-in-place concrete projects with a slope, proper consistency is a necessary requirement for realizing the slope of the road surface. In addition, the workability of concrete could also have a certain influence on the hardening performance of concrete.

Now that UHPC technology is developing day by day, more and more UHPC materials can be applied in practical engineering due to their ultra-high performance. However, some properties of UHPC such as high viscosity, low water content, etc., which are different from normal strength concrete also hinder its large-scale application, which is one of the fundamental reasons why UHPC cannot be fully popularized in structural engineering.

This doctoral dissertation focuses on resolving some workability issues of UHPC such as the “elephant skin” and air bubbles. At the same time, it initially investigates the feasibility of using recycled aggregates in UHPC. Through the research conclusions of this thesis, in future UHPC applications, engineers can achieve larger-scale, more material-saving, and more sustainable production, which has greatly promoted the further popularization of UHPC. The future structural design tends to be safer, more durable, simpler and more environmentally friendly. Therefore, as a material with high development value, the use of UHPC has great significance in many aspects.

6.3 Future investigation

6.3.1 More types of raw material

Considering the raw materials for UHPC in the European market in recent years, especially in Austria, the types of raw materials used in this thesis have proven to be the most beneficial raw materials for UHPC performance as of 2019 (starting of this research). However, with the continuous development of material technology, some new high-performance raw materials may have been developed in the past five years, some of which can also achieve the ultra-high performance and good workability of UHPC. Consequently, the research on these different types of raw materials will be one of the key topics in future research, such as different kinds of cement, superplasticizer, silica fume, quartz powder and other reactive and inert powders etc.

6.3.2 More in-depth study of the “elephant skin”

This research mainly uses the experimental method to summarize the formation mechanisms of the “elephant skin” based on the hypothesis of the results. However, with the maturity of computer simulation calculation and instrument perspective scanning technology, more in-depth research on the “elephant skin” can be gradually carried out. For example, appropriate methods can be used to simulate and calculate the interaction between particles and moisture on the micro-scale of concrete to trigger the formation process of elephant skin; the development of the “elephant skin” can be scanned in real-time through X-ray CT technology, so as to explore the fundamental methods to prevent the formation of elephant skin. In the future, relevant research in this area can be carried out if conditions permit, which can investigate the actual process in a more scientific way with higher precision.

6.3.3 More in-depth study of air bubbles

Similar to the research on elephant skin, the investigation of air bubbles can also be calculated using the method of micro-scale finite element simulation, so as to compare with the experimental results. In addition, the X-ray CT scanning used to observe the actual air bubble distribution in concrete can make the results more accurate and intuitive. But the insufficient permeability of X-rays to UHPC irradiation is still a big problem, which needs to be improved urgently. To this end, more X-ray CT scans may be performed in the future, including test blocks of different sizes, concrete with coarse aggregate or steel fibres, etc. Moreover, the influence of the “elephant skin” on the distribution of air bubbles in concrete columns also needs to be further explored.

6.3.4 A detailed study on UHPC with recycled aggregate

In this research, the influence of recycled aggregates on the fresh and hardened properties of UHPC was preliminarily studied, and a recycled aggregate UHPC with a high strength was developed. Despite that, in order to make UHPC with recycled aggregates more popular and widely applied, relevant detailed investigation needs to be further completed, including the best concrete mix proportion, different types of recycled aggregates, other influencing factors on the workability of concrete, etc.

In addition, when the recycled aggregates can be recovered and processed from the waste UHPC, these recycled basalts may have much higher strength, which would also make the recycled aggregate UHPC have higher performance. At this time, the fresh properties as well as the mechanical properties such as elastic modulus, stress-strain curve, etc. are also worthy of research. This part can also be carried out by means of experimental analysis or theoretical simulation, which would have significant development and application value in the future.

Reference

- [1] R. AGUERO, C. KORZENOWSKI, J. AGUIRRE, A. CAMPOS FILHO, L. da SILVA FILHO, and C. MALLMANN, "Experimental study of concrete mixtures to produce UHPRC using sustainable brazilians materials Estudio experimental de mezclas de concreto para producir UHPRC usando materiales brasileños sustentables," 2019.
- [2] E. Fehling, M. Schmidt, J. Walraven, T. Leutbecher, and S. Fröhlich, "Ultra-high performance concrete: fundamental–design–example," *Wilhelm Ernst & Sohn, Verlag für Architektur und technische Wissenschaften GmbH & Co. KG, Rotherstraße*, vol. 21, p. 10245, 2014.
- [3] P. Richard and M. Cheyrezy, "Composition of reactive powder concretes," *Cement and concrete research*, vol. 25, no. 7, pp. 1501-1511, 1995.
- [4] H. H. Bach, "Densified Cement/Ultra-Fine Particle-Based materials," in *Second International Conference on Superplasticizers in Concrete, Ottawa Canada, 1981*, 1981.
- [5] P. Richard and M. H. Cheyrezy, "Reactive powder concretes with high ductility and 200-800 MPa compressive strength," *Special Publication*, vol. 144, pp. 507-518, 1994.
- [6] O. Abdulkareem, "Microstructure and Durability Properties of Environmentally Friendly Ultra-High Performance Concrete (UHPC)," Nantes, 2017.
- [7] V. Perry, "Case studies on innovative applications and challenges of introducing breakthrough technologies (UHPC) in the construction industry," *Ref*, vol. 10, pp. 33-41, 2015.
- [8] P.-C. Aïtcin, M. Lachemi, R. Adeline, and P. Richard, "The Sherbrooke reactive powder concrete footbridge," *Structural Engineering International*, vol. 8, no. 2, pp. 140-144, 1998.
- [9] P. C. Aïtcin and P. Richard, "The pedestrian/bikeway bridge of Sherbrooke," in *Proceedings 4th International Symposium on Utilization of High-Strength/High-Performance Concrete, Paris*, 1996, pp. 1399-1406.
- [10] B. Graybeal, "UHPC in the US Highway Infrastructure," *Designing and Building with UHPFRC*, pp. 221-234, 2011.
- [11] E. Fehling, K. Bunje, and M. Schmidt, "Gärtnerplatz–Bridge over River Fulda in Kassel: Multispan Hybrid UHPC-Steel Bridge," *Designing and Building with UHPFRC*, 2011.
- [12] M. Schmidt and D. Jerebic, "UHPC: basis for sustainable structures-the Gaertnerplatz bridge in Kassel," *Ultra High Performance Concrete (UHPC)*, vol. 2, pp. 05-07, 2008.

- [13] H. oved. "https://commons.wikimedia.org/wiki/File:Haneda_Airport_D_Runway.jpg." (accessed).
- [14] E. Fehling, M. Schmidt, and S. Stürwald, *Ultra High Performance Concrete:(UHPC); Proceedings of the Second International Symposium on Ultra High Performance Concrete, Kassel, Germany, March 05-07, 2008*. kassel university press GmbH, 2008.
- [15] N. M. Azmee and N. Shafiq, "Ultra-high performance concrete: From fundamental to applications," *Case Studies in Construction Materials*, vol. 9, p. e00197, 2018.
- [16] F. Toutlemonde, G. Génèreux, J. Resplendino, and M. Delort, "Product and design standards for UHPFRC in France," in *International Interactive Symposium on Ultra-High Performance Concrete*, 2016, vol. 1, no. 1: Iowa State University Digital Press.
- [17] N. Afnor, "P18–710," *Specific Rules for Ultra-High Performance Fiber-Reinforced Concrete (UHPFRC)*, 2016.
- [18] Y. Uchida, J. Niwa, Y. Tanaka, and M. Katagiri, "Outlines of ‘Recommendations for design and construction of ultra high strength fiber reinforced concrete structures’ by JSCE," in *Proc., Int. Workshop on High Performance Fiber Reinforced Cementitious Composites in Structural Applications*, 2005.
- [19] SIA, "Ultra-high performance fibre reinforced cement-based composites (UHPFRC): Materials design, and application," ed: EPFL-Swiss Federal Institute of Technology Lausanne, Switzerland, 2016.
- [20] B. Freytag, V. T. Nguyen, M. Huß, and M. Kleiser, "ÖBV-Richtlinie UHPC," in *Beton Graz'22: 5. Grazer Betonkolloquium 01./02. September 2022*: Verlag der Technischen Universität Graz, 2022, p. 123.
- [21] M. Di Prisco, G. Plizzari, and L. Vandewalle, "Fibre reinforced concrete: new design perspectives," *Materials and structures*, vol. 42, pp. 1261-1281, 2009.
- [22] E. Fehling, M. Schmidt, and T. Teichmann, "Dauerhaftigkeit und Berechnung Ultrahochfester Betone (UHPC), Forschungsbericht," 2005.
- [23] W. GmbH. "<https://www.wild.at/unternehmen/evolution/>." (accessed).
- [24] M. Reichel, L. Sparowitz, and B. Freytag, "Bridge WILD Volkermarkt-prestressed arched structure made of precast UHPC-segments. Part 1-Design and detailing," *BETON-UND STAHLBETONBAU*, vol. 106, no. 11, pp. 760-769, 2011.
- [25] M. Reichel, L. Sparowitz, and B. Freytag, "Bridge WILD Volkermarkt-prestressed arched structure made of precast UHPC-segments. Part 2-Erection, accompanying research, quality control," *Beton-Und Stahlbetonbau*, vol. 106, no. 12, pp. 827-835, 2011.
- [26] Denistriademerignac. "<https://pixabay.com/de/photos/mucem-marseille-museum-2041900/>." (accessed).
- [27] J. Resplendino and F. Toutlemonde, "The UHPFRC revolution in structural design and construction," in *RILEM-Fib-AFGC int. symposium on ultra-high performance fibre-reinforced concrete, UHPFRC*, 2013, pp. 791-804.
- [28] R. R. Architecte. "https://www.architectmagazine.com/project-gallery/jean-bouin-stadium_o." (accessed).

- [29] P. Mazzacane, R. Ricciotti, G. Lamoureux, and D. Corvez, "Roofing of the stade Jean Bouin in UHPFRC," in *Proceedings of International Symposium on Ultra-High Performance Fibre-Reinforced Concrete*, 2013, pp. 59-68.
- [30] Y. Tanaka, K. Maekawa, Y. Kameyama, A. Ohtake, H. Musha, and N. Watanabe, "The innovation and application of UHPFRC bridges in Japan," *Designing and Building with UHPFRC*, pp. 149-188, 2011.
- [31] T. Stengel and P. SCHIEBL, "Life cycle assessment of UHPC bridge constructions: Sherbrooke footbridge, Kassel Gärtnerplatz footbridge and Wapello road bridge," *Archit. Civ. Eng. Environ*, vol. 1, pp. 109-118, 2009.
- [32] K. H. Hoang, "A Systematic Mix Design Approach for Ultra High Performance Fibre Reinforced Concrete," Doctor, Graz University of Technology, Graz University of Technology, Austria, 2017.
- [33] O. Mishra and S. Singh, "An overview of microstructural and material properties of ultra-high-performance concrete," *Journal of Sustainable Cement-Based Materials*, vol. 8, no. 2, pp. 97-143, 2019.
- [34] K. Wille, A. E. Naaman, S. El-Tawil, and G. J. Parra-Montesinos, "Ultra-high performance concrete and fiber reinforced concrete: achieving strength and ductility without heat curing," *Materials and structures*, vol. 45, pp. 309-324, 2012.
- [35] A. Sajna, E. Denarié, and V. Bras, "Assessment of UHPFRC based bridge rehabilitation in Slovenia, two years after application," in *Proceedings of 3rd International Symposium on Ultra-High Performance Concrete*, 2012, vol. 1, no. CONF: Uni Kassel, pp. 1-8.
- [36] H. Uchikawa, S. Hanehara, and D. Sawaki, "The role of steric repulsive force in the dispersion of cement particles in fresh paste prepared with organic admixture," *Cement and concrete research*, vol. 27, no. 1, pp. 37-50, 1997.
- [37] C. Shi, Z. Wu, J. Xiao, D. Wang, Z. Huang, and Z. Fang, "A review on ultra high performance concrete: Part I. Raw materials and mixture design," *Construction and Building Materials*, vol. 101, pp. 741-751, 2015.
- [38] A. Arora *et al.*, "Microstructural packing-and rheology-based binder selection and characterization for Ultra-high Performance Concrete (UHPC)," *Cement and Concrete Research*, vol. 103, pp. 179-190, 2018.
- [39] A. Bentur, S.-i. Igarashi, and K. Kovler, "Prevention of autogenous shrinkage in high-strength concrete by internal curing using wet lightweight aggregates," *Cement and concrete research*, vol. 31, no. 11, pp. 1587-1591, 2001.
- [40] A. Wetzel, C. Glotzbach, K. Maryamh, and B. Middendorf, "Microstructural investigations on the skinning of ultra-high performance concrete," *Cement and Concrete Composites*, vol. 57, pp. 27-33, 2015.
- [41] M. Olipitz, "A universal UHPC shell element for consideration of future building with precast elements," in *20th Congress of IABSE 2019: The Evolving Metropolis New York 2019*, 2019, pp. 2271-2280.
- [42] O. Budd, S. Pottle, and M. Stacy, "UHPC in the UK," in *International Interactive Symposium on Ultra-High Performance Concrete*, 2019, vol. 2, no. 1: Iowa State University Digital Press.
- [43] J. Binard, "UHPC: A game-changing material for PCI bridge producers," *PCI Journal*, 2017.

- [44] Y. Chen, F. Matalkah, W. Rankothge, A. Balachandra, and P. Soroushian, "Improvement of the surface quality and aesthetics of ultra-high-performance concrete," *Proceedings of the Institution of Civil Engineers-Construction Materials*, vol. 172, no. 5, pp. 246-255, 2019.
- [45] K. A. Riding, C. C. Ferraro, H. Hamilton, M. S. Voss, and R. Alrashidi, "Requirements for Use of Field-Cast, Proprietary Ultra-High-Performance Concrete in Florida Structural Applications," Florida. Department of Transportation, 2019.
- [46] J. C. Scheydt, G. Herold, and H. S. Müller, "Ultrahochfester Beton," in *Symposium Baustoffe und Bauwerkserhaltung in Karlsruhe*, 2006, vol. 3, pp. 33-44.
- [47] J. von Werder, P. Fontana, J. Hoppe, S. Bilgin, and B. Meng, "Composite Facade Elements with Self-Cleaning Surface made of Ultra-High-Performance Concrete (UHPC)," in *Current Topics and Trends on Durability of Building Materials and Components-Proceedings of the XV edition of the International Conference on Durability of Building Materials and Components (DBMC 2020)*, 2020: International Center for Numerical Methods in Engineering (CIMNE), pp. 1289-1297.
- [48] Ç. Yalçınkaya, "A preliminary study on the development of the normal concrete-UHPC composite beam via wet casting," *J. Struct. Eng.*, vol. 4, no. 1, pp. 046-056, 2021.
- [49] F. Mendonca, M. A. El-Khier, G. Morcoux, and J. Hu, "Feasibility Study of Development of Ultra-High Performance Concrete (UHPC) for Highway Bridge Applications in Nebraska," University of Nebraska--Lincoln, 2020.
- [50] C. G. Alexander Wetzel, Benjamin Scheffler, "Mikrostrukturelle Untersuchungen zu Entstehungsmechanismen von Elefantenhaut auf UHPC," 53. *Forschungskolloquium am 9. und 10. Oktober*, vol. 53, pp. 125-133, 2012.
- [51] H. Huang, X. Gao, and A. Zhang, "Numerical simulation and visualization of motion and orientation of steel fibers in UHPC under controlling flow condition," *Construction and Building Materials*, vol. 199, pp. 624-636, 2019.
- [52] L. Xu, Q. Lu, Y. Chi, Y. Yang, M. Yu, and Y. Yan, "Axial compressive performance of UHPC filled steel tube stub columns containing steel-polypropylene hybrid fiber," *Construction and Building Materials*, vol. 204, pp. 754-767, 2019.
- [53] M. M. Norhasri, M. Hamidah, A. M. Fadzil, and O. Megawati, "Inclusion of nano metakaolin as additive in ultra high performance concrete (UHPC)," *Construction and Building Materials*, vol. 127, pp. 167-175, 2016.
- [54] J. Dils, V. Boel, and G. De Schutter, "Influence of cement type and mixing pressure on air content, rheology and mechanical properties of UHPC," *Construction and Building Materials*, vol. 41, pp. 455-463, 2013.
- [55] R. Kumar and B. Bhattacharjee, "Porosity, pore size distribution and in situ strength of concrete," *Cement and concrete research*, vol. 33, no. 1, pp. 155-164, 2003.
- [56] P. E. Claude Goguen, LEED AP. (2022, August 8) How Pores in Concrete Influence Durability. *Precast Magazines*.
- [57] J. Xiao, *Recycled Aggregate Concrete Structures*. Springer, 2017.

- [58] N. Hamiruddin, R. A. Razak, K. Muhamad, M. M. Zahid, and C. C. A. Aziz, "The Effect of Different Sand Gradation with Ultra High Performance Concrete (UHPC)," *Solid State Phenomena*, vol. 280, pp. 476-480, 2018.
- [59] C. S. Poon, Z. Shui, L. Lam, H. Fok, and S. Kou, "Influence of moisture states of natural and recycled aggregates on the slump and compressive strength of concrete," *Cement and concrete research*, vol. 34, no. 1, pp. 31-36, 2004.
- [60] Z. J. Grdic, G. A. Toplicic-Curcic, I. M. Despotovic, and N. S. Ristic, "Properties of self-compacting concrete prepared with coarse recycled concrete aggregate," *Construction and Building Materials*, vol. 24, no. 7, pp. 1129-1133, 2010.
- [61] D. G. I. f. Standardization, "DIN EN 196-1: Methods of Testing Cement–Part 1: Determination of Strength," ed: Beuth Verlag Berlin, Germany, 2016.
- [62] S. Abbas, W. Abbass, M. L. Nehdi, A. Ahmed, and M. Yousaf, "Investigation of alkali-silica reactivity in sustainable ultrahigh performance concrete," *Sustainability*, vol. 13, no. 10, p. 5680, 2021.
- [63] N. Ö. EN, "197-1: 2011 10 15: Zement–Teil 1: Zusammensetzung, Anforderungen und Konformitätskriterien von Normalzement," *Wien: Austrian Standards Institute*, 2011.
- [64] S. Mindess, J. F. Young, and D. Darwin, "Mineral admixtures and blended cements," *Chapter*, vol. 5, pp. 93-114, 2003.
- [65] P. K. Mehta and P. J. Monteiro, *Concrete: microstructure, properties, and materials*. McGraw-Hill Education, 2014.
- [66] V. G. Papadakis, "Effect of fly ash on Portland cement systems: Part I. Low-calcium fly ash," *Cement and concrete research*, vol. 29, no. 11, pp. 1727-1736, 1999.
- [67] V. G. Papadakis, "Experimental investigation and theoretical modeling of silica fume activity in concrete," *Cement and Concrete Research*, vol. 29, no. 1, pp. 79-86, 1999.
- [68] V. G. Papadakis, "Effect of fly ash on Portland cement systems: Part II. High-calcium fly ash," *Cement and Concrete Research*, vol. 30, no. 10, pp. 1647-1654, 2000.
- [69] S. Fennis, "Design of ecological concrete by particle packing optimization," 2011.
- [70] E. ÖNORM, "13263-1: 2009-06–Silikastaub für Beton–Teil 1: Definitionen, Anforderungen und Konformitätskriterien," 2009.
- [71] P. Schießl *et al.*, "Effect of Superplasticizers and Silica Fume on Mixing and Workability of UHPC," in *The 3rd International fib Congress incorporating the PCI Annual Convention and Bridge Conference.*, 2010.
- [72] E. Sakai, K. Yamada, and A. Ohta, "Molecular structure and dispersion-adsorption mechanisms of comb-type superplasticizers used in Japan," *Journal of advanced concrete technology*, vol. 1, no. 1, pp. 16-25, 2003.
- [73] Y. Fang *et al.*, "Study on Dispersion, Adsorption, and Hydration Effects of Polycarboxylate Superplasticizers with Different Side Chain Structures in Reference Cement and Belite Cement," *Materials*, vol. 16, no. 11, p. 4168, 2023.
- [74] X. Liu *et al.*, "Synthesis, characterization and performance of a polycarboxylate superplasticizer with amide structure," *Colloids and Surfaces A: Physicochemical and Engineering Aspects*, vol. 448, pp. 119-129, 2014.

- [75] L. Lei, T. Hirata, and J. Plank, "40 years of PCE superplasticizers-History, current state-of-the-art and an outlook," *Cement and Concrete Research*, vol. 157, p. 106826, 2022.
- [76] S. Chen *et al.*, "Dispersion, fluidity retention and retardation effect of polyacrylate-based ether superplasticizer nanomicelles in Portland cement," *Construction and Building Materials*, vol. 290, p. 123149, 2021.
- [77] J. Plank, C. Schroefl, M. Gruber, M. Lesti, and R. Sieber, "Effectiveness of polycarboxylate superplasticizers in ultra-high strength concrete: the importance of PCE compatibility with silica fume," *Journal of Advanced Concrete Technology*, vol. 7, no. 1, pp. 5-12, 2009.
- [78] R. J. Flatt and Y. F. Houst, "A simplified view on chemical effects perturbing the action of superplasticizers," *Cement and concrete research*, vol. 31, no. 8, pp. 1169-1176, 2001.
- [79] N. V. Tue, J. Ma, and M. Orgass, "Influence of addition method of superplasticizer on the properties of fresh UHPC," in *Proceedings of the 2nd International Symposium on Ultra-High Performance Concrete, Kassel, Germany, 2008*, pp. 93-100.
- [80] EN-934-1, "Admixtures for Concrete, Mortar and Grout. Common Requirements," ed: Comité Européen de Normalisation (CEN) Brussels, Belgium, 2008.
- [81] E. DIN, "934-2: 2009+ A1: 2012," *Admixtures for Concrete, Mortar and Grout. Part, vol. 2.*
- [82] B. ÖNORM, "4710-1: 2018 01 01: Beton–Festlegung, Eigenschaften, Herstellung, Verwendung und Konformität–Teil 1: Regeln zur Umsetzung der ÖNORMEN EN 206 für Normal-und Schwerbeton," ed: Vienna: Austrian Standards, 2018.
- [83] D. D. I. f. Normung, *DIN 1045-2: Plain, Reinforced and Prestressed Concrete Structures. Part 2: Concrete, Specification, Performance, Production and Conformity. Application Rule for DIN EN 206-1.* DIN, 2008.
- [84] D. -, "Concrete, reinforced and prestressed concrete structures–Part 2: Concrete–Specifications, properties, production and conformity–Application rules for DIN EN 206-1," ed: Beuth Verlag Berlin, Germany, 2008.
- [85] B. EN, "1097-2, 2010, "Tests for mechanical and physical properties of aggregates: methods for the determination of resistance to fragmentation."," *British Standards Institution*, 2010.
- [86] R. Park, "Ductility evaluation from laboratory and analytical testing," in *Proceedings of the 9th world conference on earthquake engineering*, 1988, vol. 8: Tokyo-Kyoto Japan, pp. 605-616.
- [87] M. Shafieifar, M. Farzad, and A. Azizinamini, "Experimental and numerical study on mechanical properties of Ultra High Performance Concrete (UHPC)," *Construction and Building Materials*, vol. 156, pp. 402-411, 2017.
- [88] E. DIN, "14889-1: 2006-11–Fasern für Beton–Teil 1: Stahlfasern-Begriffe," *Festlegungen und Konformität*, pp. 14889-1.
- [89] C. Wen, P. Zhang, J. Wang, and S. Hu, "Influence of fibers on the mechanical properties and durability of ultra-high-performance concrete: A review," *Journal of Building Engineering*, vol. 52, p. 104370, 2022.
- [90] H. Kim, P. Hadl, and V. T. Nguyen, "A New mix design method for UHPC based on stepwise optimization of particle packing density," in *International Interactive*

- Symposium on Ultra-High Performance Concrete*, 2016, vol. 1, no. 1: Iowa State University Digital Press.
- [91] H. Okamura and M. Ouchi, "Self-compacting concrete," *Journal of advanced concrete technology*, vol. 1, no. 1, pp. 5-15, 2003.
- [92] A. ASTM, "C1064-86-standard test method for temperature of freshly mixed portland cement concrete," *Annual book of ASTM standards*, vol. 4, 1986.
- [93] Y. Kusumawardaningsih, E. Fehling, and M. Ismail, "UHPC compressive strength test specimens: Cylinder or cube?," *Procedia Engineering*, vol. 125, pp. 1076-1080, 2015.
- [94] E. DIN, "12390-3: 2019-10," *Testing hardened concrete—Part*, vol. 3, pp. 12390-3, 2019.
- [95] H. H. Kim, M. Huß, G. Vojvodic, and V. T. Nguyen, "Optimization of Coarse Aggregate UHPC Composition for UHPC-Filled Steel Tubes/Hollow Precast Concrete Columns," in *Ultra-High Performance Concrete and High Performance Construction Materials: Proceedings of HiPerMat 2020: Schriftenreihe Baustoffe und Massivbau*: Kassel University Press, 2020, pp. 5-6.
- [96] J. Oppeneder, L. Sparowitz, B. Freytag, P. Hadl, and V. T. Nguyen, "MATERIAL DEVELOPMENT FOR THE QUICKWAY SYSTEM," in *Central European Congress on Concrete Engineering*, 2017.
- [97] M. Mayer, M. Huß, H. H. Kim, and N. V. Tue, "Übergangskonstruktionen aus UHPFRC für den Integralbrückenbau," *Beton-und Stahlbetonbau*, vol. 117, no. 2, pp. 78-89, 2022.
- [98] B. Sagmeister, M. Reichel, M. Huß, and M. Mayer, "UHFB-Overlay auf Fuß-und Radwegbrücke Karl-Heine-Bogen in Leipzig," *Beton-und Stahlbetonbau*, 2023.
- [99] Y. He, X. Zhang, S. Liu, R. Hooton, T. Ji, and Y. Kong, "Impacts of sulphates on rheological property and hydration performance of cement paste in the function of polycarboxylate superplasticizer," *Construction and Building Materials*, vol. 256, p. 119428, 2020.
- [100] A. Wetzel and C. Glotzbach, "Microstructural characterisation of elephant skin on ultra-high performance concrete," *14th Euroseminar on Microscopy Applied to Building Materials*, 2013.
- [101] *ASTM C403, Test Method for Time of Setting of Concrete Mixtures by Penetration Resistance*, Vol. 04.02, W. C. ASTM International, PA., Annual Book of ASTM Standards, 2008.
- [102] Ç. Yalçınkaya and O. Çopuroğlu, "Elephant skin formation on UHPC surface: Effects of climatic condition and blast furnace slag content," *Construction and Building Materials*, vol. 268, p. 121126, 2021.
- [103] Ç. Yalçınkaya and H. Yazıcı, "Effects of ambient temperature and relative humidity on early-age shrinkage of UHPC with high-volume mineral admixtures," *Construction and Building Materials*, vol. 144, pp. 252-259, 2017.
- [104] M. Küchler, *Verbundmittel für Hybridkonstruktionen mit Ultrahochleistungsbeton*. BoD—Books on Demand, 2009.
- [105] E. DIN, "196-3: 2009-02: Methods of testing cement—Determination of setting times and soundness," ed: Beuth Publishers, Berlin.

- [106] B. A. Graybeal, "Material property characterization of ultra-high performance concrete," United States. Federal Highway Administration. Office of Infrastructure ..., 2006.
- [107] M. Bajaber and I. Hakeem, "UHPC evolution, development, and utilization in construction: A review," *Journal of Materials Research and Technology*, vol. 10, pp. 1058-1074, 2021.
- [108] C.-W. Chung, M. Mroczek, I.-Y. Park, and L. J. Struble, "On the evaluation of setting time of cement paste based on ASTM C403 penetration resistance test," *Journal of Testing and Evaluation*, vol. 38, no. 5, pp. 527-533, 2010.
- [109] R. Faserbeton, "Österreichische Bautechnik Vereinigung (ÖVB)," ed: Wien, 2008.
- [110] B. En, "196-1, Methods of testing cement," *Determination of strength, Br. Stand. Inst.*, vol. 25, 2005.
- [111] I. Standard, "Plain and reinforced concrete-code of practice," *New Delhi: Bureau of Indian Standards*, 2000.
- [112] P. J. Uno, "Plastic shrinkage cracking and evaporation formulas," *ACI Materials Journal*, vol. 95, pp. 365-375, 1998.
- [113] H. weather Concreting, "ACI 305R," *American Concrete Institute, Farmington Hills, MI*.
- [114] P. E. Baldwin and A. D. Maynard, "A survey of wind speeds in indoor workplaces," *The Annals of occupational hygiene*, vol. 42, no. 5, pp. 303-313, 1998.
- [115] X. Xu and Z. Hou, "Experimental study on one-way BFRP bar-reinforced UHPC slabs under concentrated load," *Materials*, vol. 13, no. 14, p. 3077, 2020.
- [116] A. Valikhani, A. Jaberi Jahromi, I. M. Mantawy, and A. Azizinamini, "Numerical modelling of concrete-to-UHPC bond strength," *Materials*, vol. 13, no. 6, p. 1379, 2020.
- [117] J. Cui, Z. He, and X. Cai, "Mechanical properties and key intrinsic factors of sprayed ultra-high performance concrete (SUHPC) with alkali-free accelerator," *Construction and Building Materials*, vol. 349, p. 128788, 2022.
- [118] S. Wang *et al.*, "Effect of steel fiber distribution on the mechanical properties of UHPC caused by vehicle-bridge coupling vibration," *Composites Part B: Engineering*, vol. 245, p. 110201, 2022.
- [119] I. Schachinger, J. Schubert, and O. Mazanec, "Effect of mixing and placement methods on fresh and hardened ultra high performance concrete (UHPC)," in *International Symposium on Ultra High Performance Concrete*, 2004, pp. 575-586.
- [120] H. Huang, X. Gao, and D. Jia, "Effects of rheological performance, antifoaming admixture, and mixing procedure on air bubbles and strength of UHPC," *Journal of Materials in Civil Engineering*, vol. 31, no. 4, p. 04019016, 2019.
- [121] R. Yu *et al.*, "Uncovering the approach to develop ultra-high performance concrete (UHPC) with dense meso-structure based on rheological point of view: Experiments and modeling," *Construction and Building Materials*, vol. 271, p. 121500, 2021.
- [122] R. Wang, X. Gao, J. Zhang, and G. Han, "Spatial distribution of steel fibers and air bubbles in UHPC cylinder determined by X-ray CT method," *Construction and Building Materials*, vol. 160, pp. 39-47, 2018.

- [123] T. Li *et al.*, "The mechanism of anticorrosion performance and mechanical property differences between seawater sea-sand and freshwater river-sand ultra-high-performance polymer cement mortar (UHPC)," *Polymers*, vol. 14, no. 15, p. 3105, 2022.
- [124] K. Shi, H. Deng, J. Hu, J. Zhou, X. Cai, and Z. Liu, "Effects of Steel Slag Powder Content and Curing Condition on the Performance of Alkali-Activated Materials Based UHPC Matrix," *Materials*, vol. 16, no. 10, p. 3875, 2023.
- [125] H. Huang, X. Gao, H. Wang, and H. Ye, "Influence of rice husk ash on strength and permeability of ultra-high performance concrete," *Construction and Building Materials*, vol. 149, pp. 621-628, 2017.
- [126] E. 12350-7:, "Testing fresh concrete. Air content. Pressure methods," *European standards*, 2009.
- [127] G. Heinzele and B. Freytag, "Zerstörungsfreie Qualitätskontrolle-WILD-Brücke," 2009.
- [128] H. G. Merkus, *Particle size measurements: fundamentals, practice, quality*. Springer Science & Business Media, 2009.
- [129] E. DIN, "12390-13: 2021-09; Testing Hardened Concrete—Part 13: Determination of Secant Modulus of Elasticity in Compression," *Deutsches Institut für Normung: Berlin, Germany*, 2021.
- [130] A. C. I. Committee, "347.3R-13: Guide to Formed Concrete Surfaces," *Technical Documents*, 1/1/2014.
- [131] M. Pauser, "UHPC-Anwendung in der Praxis," ed: Forschungsbericht. FFG Projektnummer FO999887033, 2022.
- [132] B. EN, "934-2, Admixtures for concrete, mortar and grout-Part 2: Concrete admixtures-Definitions, requirements, conformity, marking and labelling," *British Standards Institution*, 2009.
- [133] K. ICHIMIYA, T. IDEMITSU, and T. YAMASAKI, "INFLUENCE OF THE WETTABILITY AND ANGLE OF FORM ON THE CHARACTERISTICS OF SURFACE VOIDS IN SELF-COMPACTING CONCRETE," *Doboku Gakkai Ronbunshu*, vol. 2002, no. 704, pp. 143-150, 2002.
- [134] G. Savukaitis, M. Daukšys, S. Juočiūnas, A. Grinys, and D. Kriptavičius, "The influence of new and used formwork coated with different release agents on the appearance of the formed concrete surface," *Journal of Building Engineering*, vol. 42, p. 102807, 2021.
- [135] A. A. Gulghane and P. Khandve, "Management for construction materials and control of construction waste in construction industry: a review," *International Journal of Engineering Research and Applications*, vol. 5, no. 4, pp. 59-64, 2015.
- [136] S. Nagapan, I. A. Rahman, A. Asmi, A. H. Memon, and I. Latif, "Issues on construction waste: The need for sustainable waste management," in *2012 IEEE colloquium on Humanities, Science and Engineering (CHUSER)*, 2012: IEEE, pp. 325-330.
- [137] S. Delvoie, L. Courard, J. Hubert, Z. Zhao, and F. Michel, "Construction and Demolition Wastes: specific conditions for recycling in North West Europe," *Cement, Wapno, Beton*, vol. 1, 2020.
- [138] K. Kabirifar, M. Mojtahedi, C. Wang, and V. W. Tam, "Construction and demolition waste management contributing factors coupled with reduce, reuse, and

- recycle strategies for effective waste management: A review," *Journal of Cleaner Production*, vol. 263, p. 121265, 2020.
- [139] S. Ulubeyli, A. Kazaz, and V. Arslan, "Construction and demolition waste recycling plants revisited: management issues," *Procedia Engineering*, vol. 172, pp. 1190-1197, 2017.
- [140] A. Di Maria, J. Eyckmans, and K. Van Acker, "Use of LCA and LCC to help decision-making between downcycling versus recycling of construction and demolition waste," in *Advances in Construction and Demolition Waste Recycling*: Elsevier, 2020, pp. 537-558.
- [141] M. J. Whittaker *et al.*, "Novel construction and demolition waste (CDW) treatment and uses to maximize reuse and recycling," *Advances in Building Energy Research*, vol. 15, no. 2, pp. 253-269, 2021.
- [142] J. Xiao, J. Li, and Y. Lan, "Research on recycled aggregate concrete—A review," *Concrete*, 2003.
- [143] S. Desai, "Sustainable development and recycling of concrete aggregate," in *Sustainable Construction: Use of Recycled Concrete Aggregate: Proceedings of the International Symposium organised by the Concrete Technology Unit, University of Dundee and held at the Department of Trade and Industry Conference Centre, London, UK on 11–12 November 1998*, 1998: Thomas Telford Publishing, pp. 381-388.
- [144] G. Prokopski and J. Halbiniak, "Interfacial transition zone in cementitious materials," *Cement and Concrete Research*, vol. 30, no. 4, pp. 579-583, 2000.
- [145] A. Elsharief, M. D. Cohen, and J. Olek, "Influence of aggregate size, water cement ratio and age on the microstructure of the interfacial transition zone," *Cement and concrete research*, vol. 33, no. 11, pp. 1837-1849, 2003.
- [146] H. Zhang, T. Ji, and H. Liu, "Performance evolution of the interfacial transition zone (ITZ) in recycled aggregate concrete under external sulfate attacks and dry-wet cycling," *Construction and Building Materials*, vol. 229, p. 116938, 2019.
- [147] F. Yang *et al.*, "A new stress-strain model for concrete containing recycled concrete aggregates subjected to uniaxial compression," in *Brittle Matrix Composites 12-Proceedings of the 12th International Symposium on Brittle Matrix Composites*, 2019: Institute of Fundamental Technological Research (IFTR) of the Polish Academy ...
- [148] E. Serreyn, "A review on the frost resistance of recycled aggregate concrete."
- [149] X. Zeng, "Progress in the research of carbonation resistance of RAC," *Construction and Building Materials*, vol. 230, p. 116976, 2020.
- [150] J. Xiao, J. Li, and C. Zhang, "Mechanical properties of recycled aggregate concrete under uniaxial loading," *Cement and concrete research*, vol. 35, no. 6, pp. 1187-1194, 2005.
- [151] H. Zhang, X. Xu, W. Liu, B. Zhao, and Q. Wang, "Influence of the moisture states of aggregate recycled from waste concrete on the performance of the prepared recycled aggregate concrete (RAC)—A review," *Construction and Building Materials*, vol. 326, p. 126891, 2022.
- [152] Z. Sierens and J. Li, "Mechanical properties of concrete with recycled aggregate at early ages," *Aci Special Publications*, pp. 39.1-39.10, 2018.

- [153] Z. Sierens, M. Joseph, B. Vandevyvere, and J. Li, "High quality recycled concrete aggregates in UHPC-A preliminary study," *Progress of Recycling in the Built Environment*, pp. 1-8, 2018.
- [154] E. DIN, "12350-2. 2009," *Testing fresh concrete—Part*, vol. 2, pp. 12350-2.
- [155] H. Rasekh, A. Joshaghani, S. Jahandari, F. Aslani, and M. Ghodrat, "Rheology and workability of SCC," in *Self-compacting concrete: materials, properties and applications*: Elsevier, 2020, pp. 31-63.
- [156] E. DIN, "12350-8: 2010-12. Testing Fresh Concrete—Part 8: Self-Compacting Concrete—Slump-Flow Test, German version EN 12350-8: 2010," *German Institute for Standardisation (Deutsches Institut für Normung), Beuth Verlag GmbH: Berlin, Germany*, 2010.
- [157] E. 12350-9, "Testing Fresh Concrete-Part 9: Self-Compacting Concrete—V-Funnel Test," ed, 2009.
- [158] T. MONKERHEY and S. THERY, "The influencing factors on the workability of recycled aggregate concrete."
- [159] N. F. Günçan, "Using waste concrete as aggregate," *Cement and concrete research*, vol. 25, no. 7, pp. 1385-1390, 1995.
- [160] K.-H. Yang, H.-S. Chung, and A. F. Ashour, "Influence of Type and Replacement Level of Recycled Aggregates on Concrete Properties," 2008.
- [161] P. K. Gupta, Z. A. Khaudhair, and A. K. Ahuja, "A new method for proportioning recycled concrete," *Structural concrete*, vol. 17, no. 4, pp. 677-687, 2016.
- [162] U. J. Alengaram, A. Salam, M. Z. Jumaat, F. F. Jaafar, and H. B. Saad, "Properties of high-workability concrete with recycled concrete aggregate," *Materials Research*, vol. 14, pp. 248-255, 2011.
- [163] G. Wardeh, E. Ghorbel, and H. Gomart, "Mix design and properties of recycled aggregate concretes: applicability of Eurocode 2," *International Journal of Concrete Structures and Materials*, vol. 9, pp. 1-20, 2015.
- [164] Z. Sierens, "The use of high-quality recycled concrete aggregates in precast non-prestressed and prestressed concrete," 2021.
- [165] S.-c. Kou, C.-s. Poon, and F. Agrela, "Comparisons of natural and recycled aggregate concretes prepared with the addition of different mineral admixtures," *Cement and Concrete Composites*, vol. 33, no. 8, pp. 788-795, 2011.
- [166] A. Singh, S. Arora, V. Sharma, and B. Bhardwaj, "Workability retention and strength development of self-compacting recycled aggregate concrete using ultrafine recycled powders and silica fume," *Journal of Hazardous, Toxic, and Radioactive Waste*, vol. 23, no. 4, p. 04019016, 2019.
- [167] R. B. Singh and B. Singh, "Rheological behaviour of different grades of self-compacting concrete containing recycled aggregates," *Construction and Building Materials*, vol. 161, pp. 354-364, 2018.
- [168] K. Kapoor, S. Singh, and B. Singh, "Durability of self-compacting concrete made with Recycled Concrete Aggregates and mineral admixtures," *Construction and Building Materials*, vol. 128, pp. 67-76, 2016.
- [169] E. Güneysi, M. Gesoglu, Z. Algin, and H. Yazıcı, "Rheological and fresh properties of self-compacting concretes containing coarse and fine recycled concrete aggregates," *Construction and Building Materials*, vol. 113, pp. 622-630, 2016.

- [170] K. Poongodi, P. Murthi, P. Awoyera, R. Gobinath, O. Olalusi, and OB, "Durability Properties of Self-compacting concrete made with recycled aggregate for pavement application," *Silicon*, doi.org/10.1007/s12633-020-00635-7, 2020.
- [171] E. -6, "Tests for mechanical and physical properties of aggregates—Part 6: Determination of particle density and water absorption," *European Committee for Standardization: Brussels, Belgium*, 2013.
- [172] D. E. 12350–5, "Testing fresh concrete—Part 5: Flow table test; German version EN 12350–5: 2009," ed: Deutshes Institut für Normung Berlin, 2009.
- [173] Krishna. "Flow table test of concrete to test workability of concrete <https://civilread.com/flow-table-test-concrete/>." <https://civilread.com/flow-table-test-concrete/>. (accessed.

Appendix: Detailed UHPC recipes and properties

Table A.1: Detailed mix recipe and properties of each UHPC mixture in Chapter 2

	720 12% 30% (0.223)	720 18% 30% (0.212)	720 12% 40% (0.223)	720 18% 40% (0.212)	860 12% 30%	860 18% 30%	860 12% 40%	860 18% 40%
CEM A (kg/m ³)	720	720	720	720	860	860	860	860
Si (kg/m ³)	86.4	129.6	86.4	129.6	103.2	154.8	103.2	154.8
QP (kg/m ³)	216	216	288	288	258	258	344	344
WA (kg/m ³)	164.9	164.9	164.9	164.9	196.9	196.9	196.9	196.9
SP (kg/m ³)	21.6	21.6	21.6	21.6	25.8	25.8	25.8	25.8
QS1 (kg/m ³)	236.6	226.2	222.1	211.7	181.6	169.2	164.3	151.8
QS2 (kg/m ³)	946.4	904.7	888.3	846.7	726.4	676.7	657.1	607.4
Water-to-cement (W/C) ratio	0.25	0.25	0.25	0.25	0.25	0.25	0.25	0.25
Water-to-binder (W/B) ratio	0.223	0.212	0.223	0.212	0.223	0.212	0.223	0.212
Si/C ratio	12%	18%	12%	18%	12%	18%	12%	18%
QP/C ratio	30%	30%	40%	40%	30%	30%	40%	40%
SP/C ratio	3%	3%	3%	3%	3%	3%	3%	3%
QS1/(QS1+QS2)	20V%	20V%	20V%	20V%	20V%	20V%	20V%	20V%
QS2/(QS1+QS2)	80V%	80V%	80V%	80V%	80V%	80V%	80V%	80V%
Spread-flow (cm)	29.5	26	28.5	26.5	27.1	24.1	27	24
Temperature in fresh mix (°C)	29.3	27.5	29.9	28.5	4.3	5	4.35	5.05
Compressive strength (MPa)	208.3 184.8	191.8 198.1	204 205	193.7 183.4	175.2 169.2	172 168.7	170.1 169.2	170.9 165.9
	720 12% 30% 0241	720 18% 30% 0.225	720 12% 40% 0.228	720 18% 40% 0.225	620 CEM A 0% 0.223	620 CEM A 0% 0.25	860 CEM A 0% 0.205	860 CEM A 0% 0.223
CEM A (kg/m ³)	720	720	720	720	620	620	860	860
Si (kg/m ³)	86.4	129.6	86.4	129.6	74.4	74.4	103.2	103.2
QP (kg/m ³)	216	216	288	288	186	186	258	258
WA (kg/m ³)	179.3	175.7	168.5	175.7	142	163.7	179.7	196.9
SP (kg/m ³)	21.6	21.6	21.6	21.6	18.6	18.6	25.8	25.8
QS1 (kg/m ³)	229	220.5	220.2	206	275.9	264.4	190.7	181.6
QS2 (kg/m ³)	915.8	881.8	880.7	823.8	1103.5	1057.5	762.9	726.4
StF1 (kg/m ³)	0	0	0	0	0	0	0	0
Water-to-cement (W/C) ratio	0.27	0.264	0.255	0.264	0.25	0.285	0.23	0.25
Water-to-binder (W/B) ratio	0.241	0.223	0.228	0.223	0.223	0.25	0.205	0.223

Si/C ratio	12%	18%	12%	18%	12%	12%	12%	12%
QP/C ratio	30%	30%	40%	40%	30%	30%	30%	30%
SP/C ratio	3%	3%	3%	3%	3%	3%	3%	3%
QS1/(QS1+QS2)	20V%	20V%	20V%	20V%	20V%	20V%	20V%	20V%
QS2/(QS1+QS2)	80V%	80V%	80V%	80V%	80V%	80V%	80V%	80V%
StF volume content	-	-	-	-	-	-	-	-
Spread-flow (cm)	32.5	29.5	30	30	22	29.5	29.5	34
Temperature in fresh mix (°C)	27	27.1	29.2	27.8	31.2	27.3	29.6	28.1
Compressive strength (MPa)	195.7	198.1	203	183.4	186.4	196.3	211.1	210.2
	176.7	194.3	201.5	188.3	181.3	208.9	184.6	204.7
					161.8	191.5	195.9	197.8

	720	720	720	720	720	720	720	720
	CEM	CEM	CEM	CEM	0.223	0.223	0.223	0.241
	A 2%	A 2%	B 2%	B 2%	2.05	2.68	4.46	1.52
	0.223	0.25	0.223	0.232				
CEM A (kg/m ³)	720	720	-	-	-	-	-	720
CEM B (kg/m ³)	-	-	720	720	720	720	720	-
Si (kg/m ³)	86.4	86.4	86.4	86.4	86.4	86.4	86.4	86.4
QP (kg/m ³)	216	216	216	216	216	216	216	216
WA (kg/m ³)	164.9	190.1	164.9	172.1	168.4	164.9	154.8	185.8
SP (kg/m ³)	21.6	21.6	21.6	21.6	16.6	21.6	36	12.2
QS1 (kg/m ³)	226	212.6	226	222.2	237.2	236.6	234.8	230.1
QS2 (kg/m ³)	904	850.5	904	888.7	948.9	946.4	939.2	920.5
StF1 (kg/m ³)	157	157	157	157	0	0	0	0
Water-to-cement (W/C) ratio	0.25	0.285	0.25	0.26	0.25	0.25	0.25	0.27
Water-to-binder (W/B) ratio	0.223	0.25	0.223	0.232	0.223	0.223	0.223	0.241
Si/C ratio	12%	12%	12%	12%	12%	12%	12%	12%
QP/C ratio	30%	30%	30%	30%	30%	30%	30%	30%
SP/C ratio	3%	3%	3%	3%	2.3%	3%	5%	1.7%
QS1/(QS1+QS2)	20V%	20V%	20V%	20V%	20V%	20V%	20V%	20V%
QS2/(QS1+QS2)	80V%	80V%	80V%	80V%	80V%	80V%	80V%	80V%
StF volume content	2%	2%	2%	2%	-	-	-	-
Spread-flow (cm)	22	27.5	26	27.5	29.5	29.5	29.5	24.5
Temperature in fresh mix (°C)	31.4	26	29.8	26.1	29	29.3	29.1	27.5
Compressive strength (MPa)	171.6	167.4	170.6	169.8	207.1	208.3	205.2	175.9
	174.4	166.2	168.3	166	200.8	199.9	198.2	155.7
					206.4	194.8	190.5	159.3
					194.7	200.4	183.5	

	720	720	720	720	720	720	720	750
	0.241	0.241	0.25	0.25	0.25	0.25	0.25	0.223
	1.65	2.68	2%	2%	2%	2%	2%	2.68
			1.52	1.79	2.23	2.68	4.46	
CEM A (kg/m ³)	720	720	720	720	720	720	720	750
Si (kg/m ³)	86.4	86.4	86.4	86.4	86.4	86.4	86.4	90
QP (kg/m ³)	216	216	216	216	216	216	216	225
WA (kg/m ³)	185.1	179.3	196.6	195.1	192.6	190.1	180	171.8
SP (kg/m ³)	13.3	21.6	12.2	14.4	18	21.6	36	22.5
QS1 (kg/m ³)	230	229	213.8	213.5	213.1	212.6	210.8	224.8

QS2 (kg/m ³)	920	915.8	855.2	854.1	852.3	850.5	843.4	899.2
StF1 (kg/m ³)	-	-	157	157	157	157	157	-
Water-to-cement (W/C) ratio	0.27	0.27	0.285	0.285	0.285	0.285	0.285	0.25
Water-to-binder (W/B) ratio	0.241	0.241	0.25	0.25	0.25	0.25	0.25	0.223
Si/C ratio	12%	12%	12%	12%	12%	12%	12%	12%
QP/C ratio	30%	30%	30%	30%	30%	30%	30%	30%
SP/C ratio	1.85%	3%	1.7%	2%	2.5%	3%	5%	3%
QS1/(QS1+QS2)	20V%	20V%	20V%	20V%	20V%	20V%	20V%	20V%
QS2/(QS1+QS2)	80V%	80V%	80V%	80V%	80V%	80V%	80V%	80V%
StF volume content	-	-	2%	2%	2%	2%	2%	-
Spread-flow (cm)	29.5	32.5	21	26	28	28	28	27
Temperature in fresh mix (°C)	28.1	27	26.1	26.4	25.2	25.1	26	-
Air content in fresh mix (%)	-	-	5	4.2	3.7	3.7	3.7	-
Compressive strength (MPa)	192.4	195.7	158.8	168.8	174.4	173.3	162.5	183.8
	175.4	176.7	158.0	168.4	174.2	168.8	160.2	184
	163.6	165.6						

	750	750	750	860	860	860	860	860
	0.223	0.241	0.241	0.223	0.223	0.223	0.223	0.223
	4.46	2.68	4.46	1.52	1.61	2.68	2%	2%
							2.23	2.68
CEM A (kg/m ³)	750	750	750	860	860	860	860	860
Si (kg/m ³)	90	90	90	103.2	103.2	103.2	103.2	103.2
QP (kg/m ³)	225	225	225	258	258	258	258	258
WA (kg/m ³)	161.3	186.8	176.3	204.8	204.2	196.9	200	196.9
SP (kg/m ³)	37.5	22.5	37.5	14.6	15.5	25.8	21.5	25.8
QS1 (kg/m ³)	222.9	216.9	215	183	182.9	181.6	171.5	171
QS2 (kg/m ³)	891.8	867.4	860	732	731.5	726.4	686.1	684
StF1 (kg/m ³)	-	-	-	-	-	-	157	157
Water-to-cement (W/C) ratio	0.25	0.27	0.27	0.25	0.25	0.25	0.25	0.25
Water-to-binder (W/B) ratio	0.223	0.241	0.241	0.223	0.223	0.223	0.223	0.223
Si/C ratio	12%	12%	12%	12%	12%	12%	12%	12%
QP/C ratio	30%	30%	30%	30%	30%	30%	30%	30%
SP/C ratio	5%	3%	5%	1.7%	1.8%	3%	2.5%	3%
QS1/(QS1+QS2)	20V%	20V%	20V%	20V%	20V%	20V%	20V%	20V%
QS2/(QS1+QS2)	80V%	80V%	80V%	80V%	80V%	80V%	80V%	80V%
StF volume content	-	-	-	-	-	-	2%	2%
Spread-flow (cm)	27	25.5	25.5	25.5	29.5	34.0	27.5	27.5
Temperature in fresh mix (°C)	-	-	-	29.1	29.2	29.6	27.6	28.1
Compressive strength (MPa)	186.9	180.9	176.1	193.9	194.5	194.6	180	185.5
	183.8	174.5	176.8	184.2	187.8	190.7	184	175.2
	860	0.223	0.223	0.223	0.223	0.223		
	0.223	2.68	2.68	2.68	2.68	2.68		

	2%	0%	0%	0%	2%	2%
	4.46	479.5	553.6	657.4	553.6	657.4
CEM A (kg/m ³)	860	620	720	860	720	860
Si (kg/m ³)	103.2	74.4	86.4	103.2	86.4	103.2
QP (kg/m ³)	258	186	216	258	216	258
WA (kg/m ³)	184.9	142	164.9	196.9	164.9	196.9
SP (kg/m ³)	43	18.6	21.6	25.8	21.6	25.8
QS1 (kg/m ³)	168.9	275.9	236.6	181.6	226	171
QS2 (kg/m ³)	675.5	1103.5	946.4	726.4	904	684
StF1 (kg/m ³)	157	-	0	-	157	157
Water-to-cement (W/C) ratio	0.25	0.25	0.25	0.25	0.25	0.25
Water-to-binder (W/B) ratio	0.223	0.223	0.223	0.223	0.223	0.223
Si/C ratio	12%	12%	12%	12%	12%	12%
QP/C ratio	30%	30%	30%	30%	30%	30%
SP/C ratio	5%	3%	3%	3%	3%	3%
QS1/(QS1+QS2)	20V%	20V%	20V%	20V%	20V%	20V%
QS2/(QS1+QS2)	80V%	80V%	80V%	80V%	80V%	80V%
StF volume content	2%	-	-	-	2%	2%
Spread-flow (cm)	27.5	19	29.5	34	22	27.5
Temperature in fresh mix (°C)	28	31.2	29.3	28.1	31.4	27.8
Compressive strength (MPa)	186.1	186.4	208.3	210.2	186.7	168.8
	173.2	181.3	184.8	204.7	181.8	165.6
		161.8	179	197.8		

	(1)	(1)	(1)	(2)	(2)	(3)	(3)	(3)
	0.25	0.25	0.25	0.25	0.25	0.27	0.27	0.27
	0% BA	30%	30%	0% BA	30%	0% BA	30%	30%
		BA1	BA2		BA1		BA1	BA2
CEM A (kg/m ³)	720	660	630	720	660	720	660	630
Si (kg/m ³)	86.4	79.2	75.6	86.4	79.2	86.4	79.2	75.6
QP (kg/m ³)	216	198	189	216	198	216	198	189
WA (kg/m ³)	164.9	151.1	144.3	164.9	151.1	179.3	164.3	156.9
SP (kg/m ³)	21.6	19.8	18.9	21.6	19.8	21.6	19.8	18.9
QS1 (kg/m ³)	236.6	260.2	271.9	236.6	260.2	229	253.2	265.3
QS2 (kg/m ³)	946.4	650.4	679.9	946.4	650.4	915.8	632.9	663.2
BA1 (kg/m ³)	-	449.1	-	-	449.1	0	437.1	0
BA2 (kg/m ³)	-	-	458.4	-	0	0	0	458
Water-to-cement (W/C) ratio	0.25	0.25	0.25	0.25	-	-	-	-
Water-to-binder (W/B) ratio	0.223	0.223	0.223	0.223	0.25	0.27	0.27	0.27
Si/C ratio	12%	12%	12%	12%	0.223	0.241	0.241	0.241
QP/C ratio	30%	30%	30%	30%	12%	12%	12%	12%
SP/C ratio	3%	3%	3%	3%	30%	30%	30%	30%
QS1/(QS1+QS2+BA1+BA2)	20V%	20V%	20V%	20V%	3%	3%	3%	3%
QS2/(QS1+QS2+BA1+BA2)	80V%	50V%	50V%	80V%	20V%	20V%	20V%	20V%
BA1/(QS1+QS2+BA1+BA2)	-	30V%	-	-	50V%	80V%	50V%	50V%

BA2/(QS1+QS2+BA1+BA2)	-	-	30V%	-	30V%	-	30V%	-
StF volume content	-	-	-	-	-	-	-	30V%
Spread-flow (cm)	24.5	24.5	24.5	25	25	24	24	24
Temperature in fresh mix (°C)	29.4	29.4	29.2	27.4	26.4	27.1	26.8	27.4
Compressive strength (MPa)	196.9	199	193.6	171.8	174	186.9	180.9	184.3
	190.4	193.3	192.9	161.1	165.3	167.6	176.8	184.1
	188.1	187.3	193.8					

	(1)	(1)	(2)	(2)	0.27	0.27	0.27
	0.25	0.25	0.25	0.25	0% StF	2%	2%
	0% StF	2% StF1	0% StF	2% StF1		StF1	StF2
CEM A (kg/m ³)	720	750	720	750	720	790	780
Si (kg/m ³)	86.4	90	86.4	90	86.4	94.8	93.6
QP (kg/m ³)	216	225	216	225	216	237	234
WA (kg/m ³)	164.9	171.8	164.9	171.8	179.3	196.7	194.2
SP (kg/m ³)	21.6	22.5	21.6	22.5	21.6	23.7	23.4
QS1 (kg/m ³)	236.6	214.2	236.6	214.2	229	190.1	194.2
QS2 (kg/m ³)	946.4	856.8	946.4	856.8	915.8	760.5	776.6
StF1 (kg/m ³)	0	157	0	157	0	157	0
StF2 (kg/m ³)	0	0	0	0	0	-	157
Water-to-cement (W/C) ratio	0.25	0.25	0.25	0.25	0.27	0.27	0.27
Water-to-binder (W/B) ratio	0.223	0.223	0.223	0.223	0.241	0.241	0.241
Si/C ratio	12%	12%	12%	12%	12%	12%	12%
QP/C ratio	30%	30%	30%	30%	30%	30%	30%
SP/C ratio	3%	3%	3%	3%	3%	3%	3%
QS1/(QS1+QS2)	20V%	20V%	20V%	20V%	20V%	20V%	20V%
QS2/(QS1+QS2)	80V%	80V%	80V%	80V%	80V%	80V%	80V%
StF volume content	0%	2%	0%	2%	0%	2%	2%
Spread-flow (cm)	24.5	24.5	25	25	26	26	26
Temperature in fresh mix (°C)	29.4	29.2	27.4	27.8	27.3	26	27
Compressive strength (MPa)	196.9	197.9	171.8	178.6	180.8	173.9	176.6
	190.4	197.1	161.1	173.8	164.6	169.8	171
	188.1	195					

	720	720	750	750
	0.25	0.25	0.27	0.27
	CEM A	CEM B	CEM A	CEM B
CEM A (kg/m ³)	720	-	750	-
CEM B (kg/m ³)	-	720	-	750
Si (kg/m ³)	86.4	86.4	90	90
QP (kg/m ³)	216	216	225	225
WA (kg/m ³)	164.9	164.9	186.8	186.8
SP (kg/m ³)	21.6	21.6	22.5	22.5
QS1 (kg/m ³)	226	226	206.3	206.3
QS2 (kg/m ³)	904	904	825	825
StF1 (kg/m ³)	157	157	157	157

Water-to-cement (W/C) ratio	0.25	0.25	0.25	0.25
Water-to-binder (W/B) ratio	0.223	0.223	0.223	0.223
Si/C ratio	12%	12%	12%	12%
QP/C ratio	30%	30%	30%	30%
SP/C ratio	3%	3%	3%	3%
QS1/(QS1+QS2)	20V%	20V%	20V%	20V%
QS2/(QS1+QS2)	80V%	80V%	80V%	80V%
StF volume content	2%	2%	2%	2%
Spread-flow (cm)	22	26	26	31
Temperature in fresh mix (°C)	31.4	29.8	26.8	25.8
Compressive strength (MPa)	186.7 181.8	170.6 168.3	169 165.2	167.4 157.2

Table A.2: Detailed mix recipe of each UHPC mixture in Sections 3.2 and 3.3

	720 CEM B		720 CEM A		620 30% BA2		620 30% BA2 1% StF	
CEM A (kg/m ³)	-		720		620		620	
CEM B (kg/m ³)	720		-		-		-	
Si (kg/m ³)	86.4		86.4		74.4		74.4	
QP (kg/m ³)	216		216		248		248	
WA (kg/m ³)	164.9		164.9		142		142	
SP (kg/m ³)	21.6		21.6		18.6		18.6	
QS1 (kg/m ³)	236.6		236.6		263.4		258.1	
QS2 (kg/m ³)	946.4		946.4		658.4		645.2	
QS3 (kg/m ³)	0		0		0		0	
BA2 (kg/m ³)	0		0		454.7		445.5	
StF1 (kg/m ³)	0		0		0		78.5	
Water-to-cement (W/C) ratio	0.25		0.25		0.25		0.25	
Water-to-binder (W/B) ratio	0.223		0.223		0.223		0.22	
Si/C ratio	12%		12%		12%		12%	
QP/C ratio	30%		30%		40%		40%	
SP/C ratio	3%		3%		3%		3%	
QS1/(QS1+QS2+QS3+BA2)	20V%		20V%		20V%		20V%	
QS2/(QS1+QS2+QS3+BA2)	80V%		80V%		50V%		50V%	
QS3/(QS1+QS2+QS3+BA2)	-		-		-		-	
BA2/(QS1+QS2+QS3+BA2)	-		-		30V%		30V%	
StF volume content	-		-		-		1%	
Parameter A	RH 40%	0.01803	RH 46%	0.00415	RH 70%	0.00531	RH 68%	0.01078
	RH 76%	0.00296	RH 60%	0.00215	RH 85%	0.00058	RH 85%	0.00135
	RH 100%	0.00073	RH 76%	0.00039	RH 100%	0.00025	RH 100%	0.00044

			RH 80%	0.00015				
			RH 100%	0.00010				
	860 QS3 3% StF1		720 CEM A (3-point bending beams)		720 CEM A (3- point bending prisms)		750 1%	860 2%
CEM A (kg/m ³)	860		720		720		750	860
CEM B (kg/m ³)	-		-		-		-	-
Si (kg/m ³)	154.8		86.4		86.4		90	103.2
QP (kg/m ³)	344		216		216		225	258
WA (kg/m ³)	196.9		164.9		164.9		171.8	196.9
SP (kg/m ³)	25.8		21.6		21.6		22.5	25.8
QS1 (kg/m ³)	0		236.6		236.6		219.5	171
QS2 (kg/m ³)	0		946.4		946.4		878	684
QS3 (kg/m ³)	679.7		0		0		0	0
StF1 (kg/m ³)	235.5		0		0		78.5	157
Water-to-cement (W/C) ratio	0.25		0.25		0.25		0.25	0.25
Water-to-binder (W/B) ratio	0.21		0.223		0.223		0.223	0.223
Si/C ratio	18%		12%		12%		12%	12%
QP/C ratio	40%		30%		30%		30%	30%
SP/C ratio	3%		3%		3%		3%	3%
QS1/(QS1+QS2+QS3)	-		20V%		20V%		20V%	20V%
QS2/(QS1+QS2+QS3)	-		80V%		80V%		80V%	80V%
QS3/(QS1+QS2+QS3)	100V%		-		-		-	-
StF volume content	3%		-		-		1%	2%
Parameter A	RH 64%	0.00489	Un-spray water	0.01129	0.0113		0.0061	0.0019
	RH 87%	0.00080						
	RH 100%	0.00015	Spray water	0.00052				

Table A.3: Detailed mix recipe and properties of each UHPC mixture in Section 3.4

	720 0.223 2.23	720 0.223 2.68	720 0.223 4.46	860 0.223 (high) 1.96	860 0.223 (high) 2.68	860 0.223 (high) 4.46
CEM A (kg/m ³)	720	720	720	860	860	860
Si (kg/m ³)	86.4	86.4	86.4	103.2	103.2	103.2
QP (kg/m ³)	216	216	216	258	258	258
WA (kg/m ³)	167.4	164.9	154.8	201.8	196.9	184.9
SP (kg/m ³)	18	21.6	36	18.9	25.8	43
QS1 (kg/m ³)	237	236.6	234.8	182.5	181.6	179.5
QS2 (kg/m ³)	948.2	946.4	939.2	729.8	726.4	717.9
Water-to-cement (W/C) ratio	0.25	0.25	0.25	0.25	0.25	0.25

Water-to-binder (W/B) ratio	0.223	0.223	0.223	0.223	0.223	0.223
Si/C ratio	12%	12%	12%	12%	12%	12%
QP/C ratio	30%	30%	30%	30%	30%	30%
SP/C ratio	2.5%	3%	5%	2.2%	3%	5%
QS1/(QS1+QS2)	20V%	20V%	20V%	20V%	20V%	20V%
QS2/(QS1+QS2)	80V%	80V%	80V%	80V%	80V%	80V%
Spread-flow (cm)	29.5	29.5	29.5	34.0	34.0	34.0
Temperature in fresh mix (°C)	29	29.3	29.1	25.5	25.1	24.9
Compressive strength (MPa)	201.7	208.3	198.2	197.2	194.6	196.6
	201.5	184.8	190.5	188.5	190.7	192.8
	191.6	179	183.5	187.9	193.5	191.2
Parameter A	0.00423	0.00275	0.00165	0.00309	0.00215	0.00121

Table A.4: Detailed mix recipe and properties of each UHPC mixture in Sections 4.3 and 4.4

	860	860	860	860	720	720	750	750
	0.25	0.25	0.25	0.25	0.241	0.241	0.223	0.223
	ELBA	ELBA	ELBA	ELBA	7min	23min	8min	22min
	1.15	1.51	2.68	4.46				
CEM A (kg/m ³)	860	860	860	860	720	720	750	750
Si (kg/m ³)	103.2	103.2	103.2	103.2	86.4	86.4	90	90
QP (kg/m ³)	258	258	258	258	216	216	225	225
WA (kg/m ³)	205.7	204.8	196.9	184.9	179.3	179.3	171.8	171.8
SP (kg/m ³)	13.3	14.6	25.8	43	21.6	21.6	22.5	22.5
QS1 (kg/m ³)	183.2	183	181.6	179.5	229	229	224.8	224.8
QS2 (kg/m ³)	732.6	732	726.4	717.9	915.8	915.8	899.2	899.2
Water-to-cement (W/C) ratio	0.25	0.25	0.25	0.25	0.27	0.27	0.25	0.25
Water-to-binder (W/B) ratio	0.22	0.22	0.22	0.22	0.241	0.241	0.22	0.22
Si/C ratio	12%	12%	12%	12%	12%	12%	12%	12%
QP/C ratio	30%	30%	30%	30%	30%	30%	30%	30%
SP/C ratio	1.55%	1.7%	3%	5%	3%	3%	3%	3%
QS1/(QS1+QS2)	20V%	20V%	20V%	20V%	20V%	20V%	20V%	20V%
QS2/(QS1+QS2)	80V%	80V%	80V%	80V%	80V%	80V%	80V%	80V%
Spread-flow (cm)	21	27	32	32	20.5	24	23	27
Temperature in fresh mix (°C)	-	-	-	-	24.7	30.7	26.8	29
Air content in fresh mix (%)	4.8	4	3.6	3.6	4.6	4.4	5.4	4.6
Compressive strength (MPa)	179.7	188.9	194.8	185.4	171.9	173	164.2	165.7
	179.3	186.8	190.1	182.9	163.8	173.6	161.9	167.3
	175.5	173	193.2	176.7				
	170.3	185.3	194.8	178				
	151.5		186.3					
P_{bubble} in all sections (%)	2.9776	1.6924	1.1606	0.7328	2.8581	2.4386	3.5587	2.3209
	3.4308	1.6416	1.0744	0.5764	2.9368	2.4634	3.4269	2.3283
	3.3956	1.7611	1.0861	0.6078	3.0159	2.3287	3.5914	2.4076
	2.9173	1.7487	1.119	0.8446				
	3.085	1.7704	1.1288	0.6935				
	3.083	1.7496	1.0904	0.7284				

	720 0.223 6min	720 0.223 10min	720 0.223 15min	720 0.223 20min	750 0.223 Temp1	750 0.223 Temp2	750 0.223 Temp3
CEM A (kg/m ³)	720	720	720	720	750	750	750
Si (kg/m ³)	86.4	86.4	86.4	86.4	90	90	90
QP (kg/m ³)	216	216	216	216	225	225	225
WA (kg/m ³)	164.9	164.9	164.9	164.9	171.8	171.8	171.8
SP (kg/m ³)	21.6	21.6	21.6	21.6	22.5	22.5	22.5
QS1 (kg/m ³)	236.6	236.6	236.6	236.6	224.8	224.8	224.8
QS2 (kg/m ³)	946.4	946.4	946.4	946.4	899.2	899.2	899.2
Water-to-cement (W/C) ratio	0.25	0.25	0.25	0.25	0.25	0.25	0.25
Water-to-binder (W/B) ratio	0.223	0.223	0.223	0.223	0.22	0.22	0.22
Si/C ratio	12%	12%	12%	12%	12%	12%	12%
QP/C ratio	30%	30%	30%	30%	30%	30%	30%
SP/C ratio	3%	3%	3%	3%	3%	3%	3%
QS1/(QS1+QS2)	20V%	20V%	20V%	20V%	20V%	20V%	20V%
QS2/(QS1+QS2)	80V%	80V%	80V%	80V%	80V%	80V%	80V%
Spread-flow (cm)	25	28.5	29.5	30	24	24	24
Temperature in fresh mix (°C)	24.6	27.4	28.5	28.6	30.2	33.2	37.1
Air content in fresh mix (%)	5.6	5.2	4.8	4.6	5.7	5.7	5.7
Compressive strength (MPa)	168.9 177.2	172.7 188.6	180.8 192.3	186.6 189	178.1 162.6	178 164.3	178.3 171.9
P_{bubble} in all sections (%)	-	-	-	-	3.6395 3.6088 3.6602	3.5404 3.5151 3.6776	3.6068 3.6369 3.5885

	720 CEM B Hobart	720 CEM B Eirich	720 CEM B ELBA	750 1% StF1 Eirich	750 1% StF1 TU Graz	750 2% StF1 Hobart	750 2% StF1 Eirich	750 2% StF1 TU Graz
CEM A (kg/m ³)	-	-	-	750	750	750	750	750
CEM B (kg/m ³)	720	720	720	-	-	-	-	-
Si (kg/m ³)	86.4	86.4	86.4	90	90	90	90	90
QP (kg/m ³)	216	216	216	300	300	300	300	300
WA (kg/m ³)	169.6	169.6	169.6	186.8	186.8	186.8	186.8	186.8
SP (kg/m ³)	25.2	25.2	25.2	22.5	22.5	22.5	22.5	22.5
QS1 (kg/m ³)	232.3	232.3	232.3	196.4	196.4	191.1	191.1	191.1
QS2 (kg/m ³)	929.3	929.3	929.3	785.8	785.8	764.6	764.6	764.6
StF1 (kg/m ³)	-	-	-	78.5	78.5	157	157	157
Water-to-cement (W/C) ratio	0.26	0.26	0.26	0.27	0.27	0.27	0.27	0.27
Water-to-binder (W/B) ratio	0.23	0.23	0.23	0.24	0.24	0.24	0.24	0.24
Si/C ratio	12%	12%	12%	12%	12%	12%	12%	12%
QP/C ratio	30%	30%	30%	40%	40%	40%	40%	40%
SP/C ratio	3.5%	3.5%	3.5%	3%	3%	3%	3%	3%
QS1/(QS1+QS2)	20V%	20V%	20V%	20V%	20V%	20V%	20V%	20V%
QS2/(QS1+QS2)	80V%	80V%	80V%	80V%	80V%	80V%	80V%	80V%
StF volume content	-	-	-	1%	1%	2%	2%	2%
Spread-flow (cm)	27.5	27.5	25	29	26	24	29	29

Air content in fresh mix (%)	3.6	2.9	3.2	3.6	3.6	3.4	4.2	2.4
Compressive strength (MPa)	186.8	188.1 184.9	183.8 189.9	190.6	153 144 142.2 142.5 144.5 142.6	184.6	179.4 179.9 178.4	-
P_{bubble} in all sections (%)	-	1.56 1.7552 1.7948	1.6923 1.7102 1.72	1.3093 1.3207 1.2693	0.9915 1.0133 1.0453	-	2.2623 2.1344 2.2192	-

	750 2% StF1 Schwarzl	750 2% StF1 Habau	750 2% StF1 Oberndorfer	750 2.5% StF1 Eirich	750 2.5% StF1 TU Graz			
CEM A (kg/m ³)	750	750	750	750	750			
Si (kg/m ³)	90	90	90	90	90			
QP (kg/m ³)	300	300	300	300	300			
WA (kg/m ³)	186.8	186.8	186.8	186.8	186.8			
SP (kg/m ³)	22.5	22.5	22.5	22.5	22.5			
QS1 (kg/m ³)	191.1	191.1	191.1	188.5	188.5			
QS2 (kg/m ³)	764.6	764.6	764.6	754	754			
StF1 (kg/m ³)	157	157	157	196.3	196.3			
Water-to-cement (W/C) ratio	0.27	0.27	0.27	0.27	0.27			
Water-to-binder (W/B) ratio	0.24	0.24	0.24	0.24	0.24			
Si/C ratio	12%	12%	12%	12%	12%			
QP/C ratio	40%	40%	40%	40%	40%			
SP/C ratio	3%	3%	3%	3%	3%			
QS1/(QS1+QS2)	20V%	20V%	20V%	20V%	20V%			
QS2/(QS1+QS2)	80V%	80V%	80V%	80V%	80V%			
StF volume content	2%	2%	2%	2.5%	2.5%			
Spread-flow (cm)	30	28	30	24.5	25			
Air content in fresh mix (%)	2.3	2.5	2.1	3.6	1.8			
Compressive strength (MPa)	152.1 151.4 150.0 149 148.0 142.9	154.9 153.4 146.8 149.8 147.3 144	159.3 156.4 156.7 157.9 156 158.3	178.4 179.9	168.9 166.1 162 161.7 161.1 168.2			
P_{bubble} in all sections (%)	0.3265 0.442	1.0115 1.1832	-	2.3080 2.2221 2.2793	0.3631 0.2764 0.3612			

	720 0.223 StF	720 0.25 StF	860 0.223 StF	750 0.241 StF	720 CEM B 0.223	720 CEM B 0.232	750 CEM B 0.241	860 0.223 1.51%
CEM A (kg/m ³)	720	720	860	750	-	-	-	860
CEM B (kg/m ³)	-	-	-	-	720	720	750	-
Si (kg/m ³)	86.4	86.4	103.2	90	86.4	86.4	90	103.2

QP (kg/m ³)	216	216	258	225	216	216	225	258
WA (kg/m ³)	164.9	190.1	196.9	186.8	164.9	172.1	186.8	204.8
SP (kg/m ³)	21.6	21.6	25.8	22.5	21.6	21.6	22.5	14.6
QS1 (kg/m ³)	226	212.6	171	206.3	226	222.2	206.3	177.7
QS2 (kg/m ³)	904	850.5	684	825	904	888.7	825	710.8
StF1 (kg/m ³)	157	157	157	157	157	157	157	78.5
Water-to-cement (W/C) ratio	0.25	0.285	0.25	0.27	0.25	0.26	0.27	0.25
Water-to-binder (W/B) ratio	0.223	0.25	0.223	0.241	0.223	0.232	0.241	0.223
Si/C ratio	12%	12%	12%	12%	12%	12%	12%	12%
QP/C ratio	30%	30%	30%	30%	30%	30%	30%	30%
SP/C ratio	3%	3%	3%	3%	3%	3%	3%	1.7%
QS1/(QS1+QS2)	20V%	20V%	20V%	20V%	20V%	20V%	20V%	20V%
QS2/(QS1+QS2)	80V%	80V%	80V%	80V%	80V%	80V%	80V%	80V%
StF volume content	2%	2%	2%	2%	2%	2%	2%	1%
Spread-flow (cm)	22	27.5	27.5	26	26	27.5	31	26
Air content in fresh mix (%)	4.3	3.5	3.5	3.8	3.6	3.2	2.6	4.5
Compressive strength (MPa)	171.6	167.4	168.8	169	170.6	169.8	167.4	188.9
	174.4	166.2	165.6	165.2	168.3	166	157.2	186.8
								173
								185.3
P_{bubble} in all sections (%)	2.6426	1.9094	1.9118	2.2706	2.4913	1.56	0.5064	1.9038
	3.3498	1.7302	1.8683	2.1121	2.9249	1.7552	0.6238	2.1313
	2.7082	1.8613	1.6089	2.2578	2.5008	1.7948	0.5649	2.0112
								1.8666
								1.9290
								1.9052

	860	750	750	750	800	850	0%	750	750
	0.223	0.241	0.223	0%	0%	0%	0%	0.27	0.27
	4.46%	1% StF	0% StF					0%	0.4%
CEM A (kg/m ³)	860	750	750	750	800	850	750	750	
Si (kg/m ³)	103.2	90	90	90	96	102	90	90	
QP (kg/m ³)	258	225	225	225	240	255	225	225	
WA (kg/m ³)	184.9	186.8	171.8	171.8	183.2	194.7	186.8	184.7	
SP (kg/m ³)	43	22.5	22.5	22.5	24	25.5	22.5	22.5	
Perfin (kg/m ³)	-	-	-	-	-	-	0	3	
Foam (kg/m ³)	-	-	-	-	-	-	0	0	
QS1 (kg/m ³)	174.2	211.6	224.8	224.8	205.2	185.5	216.9	216.5	
QS2 (kg/m ³)	696.7	846.2	899.2	899.2	820.7	742.1	867.4	865.9	
StF1 (kg/m ³)	78.5	78.5	0	0	0	0	0	0	
Water-to-cement (W/C) ratio	0.25	0.27	0.25	0.25	0.25	0.25	0.27	0.27	
Water-to-binder (W/B) ratio	0.223	0.241	0.223	0.223	0.223	0.223	0.241	0.241	
Si/C ratio	12%	12%	12%	12%	12%	12%	12%	12%	
QP/C ratio	30%	30%	30%	30%	30%	30%	30%	30%	
SP/C ratio	5%	3%	3%	3%	3%	3%	3%	3%	
Perfin/CEM ratio	-	-	-	-	-	-	0%	0.4%	
Foam/CEM ratio	-	-	-	-	-	-	0%	0%	
QS1/(QS1+QS2)	20V%	20V%	20V%	20V%	20V%	20V%	20V%	20V%	
QS2/(QS1+QS2)	80V%	80V%	80V%	80V%	80V%	80V%	80V%	80V%	

StF volume content	1%	1%	0%	0%	0%	0%	0%	0%
Spread-flow (cm)	31	29	29	22	25.5	29	27	27
Air content in fresh mix (%)	3.7	3.6	3.6	5.2	4.9	4.6	4.5	3.8
Compressive strength (MPa)	182.9 176.7 178 185.4	178.4 179.9	192.9 185.6	178.8 176.4 164.8	174.1 172.2	176.5 166.8	188.5	174.3
P_{bubble} in all sections (%)	0.8913 0.9144	2.2706 2.1121	1.8454 1.7503	3.6317 3.7469	3.0495 3.0828	2.4821 2.5001	-	-
(Release agent Z-BC)	1.0442 0.8661 0.9394 0.8577	2.2578	1.8079	3.5154	3.111	2.4899		

	860 0.25 0%	860 0.25 2%	720 0.25 0%	720 0.25 0.5%	720 0.25 2%	0% 0.25 Perfin	0.5% 0.25 Perfin	1% 0.255 Perfin
CEM A (kg/m ³)	860	860	720	720	720	750	750	750
Si (kg/m ³)	103.2	103.2	86.4	86.4	86.4	90	90	90
QP (kg/m ³)	258	258	216	216	216	225	225	225
WA (kg/m ³)	196.9	184.9	164.9	162.4	154.8	171.8	169.1	170.3
SP (kg/m ³)	25.8	25.8	21.6	21.6	21.6	22.5	22.5	22.5
Perfin (kg/m ³)	0	17.2	0	0	0	0	3.75	7.5
Foam (kg/m ³)	0	0	0	3.6	14.4	0	0	0
QS1 (kg/m ³)	181.6	179.5	236.6	236.1	234.8	214.2	213.7	211.3
QS2 (kg/m ³)	726.4	717.9	946.4	944.6	939.2	856.8	855	845.2
StF1 (kg/m ³)	-	-	-	-	-	157	157	157
Water-to-cement (W/C) ratio	0.25	0.25	0.25	0.25	0.25	0.25	0.25	0.255
Water-to-binder (W/B) ratio	0.223	0.223	0.223	0.223	0.223	0.223	0.223	0.228
Si/C ratio	12%	12%	12%	12%	12%	12%	12%	12%
QP/C ratio	30%	30%	30%	30%	30%	30%	30%	30%
SP/C ratio	3%	3%	3%	3%	3%	3%	3%	3%
Perfin/CEM ratio	0%	2%	0%	0%	0%	0%	0.5%	1%
Foam/CEM ratio	0%	0%	0%	0.5%	2%	0%	0%	0%
QS1/(QS1+QS2)	20V%	20V%	20V%	20V%	20V%	20V%	20V%	20V%
QS2/(QS1+QS2)	80V%	80V%	80V%	80V%	80V%	80V%	80V%	80V%
StF volume content	-	-	-	-	-	2%	2%	2%
Spread-flow (cm)	25	21	26	26	23.5	28.5	28.5	28.5
Air content in fresh mix (%)	4.2	4	4.3	3.3	4	3.4	2.9	2.9
Compressive strength (MPa)	186.4	144.4	174.4	172.6	158.2	192.7	170.8	159.8
P_{bubble} in all sections (%)	-	-	-	-	-	1.6508 1.6938 1.7605	1.1996 1.2589 1.2003	1.005 1.153 1.0315

	1.5% 0.26 Perfin	2% 0.264 Perfin	0% 0.25 Foam	0.5% 0.25 Foam	1% 0.255 Perfin	1.5% 0.26 Perfin	2% 0.264 Perfin
CEM A (kg/m ³)	750	750	750	750	750	750	750

Si (kg/m ³)	90	90	90	90	90	90	90
QP (kg/m ³)	225	225	225	225	225	225	225
WA (kg/m ³)	171.4	171.8	171.8	169.1	170.3	171.4	171.8
SP (kg/m ³)	22.5	22.5	22.5	22.5	22.5	22.5	22.5
Perfin (kg/m ³)	11.25	15	0	0	0	0	0
Foam (kg/m ³)	0	0	0	3.75	7.5	11.25	15
QS1 (kg/m ³)	208.8	206.8	214.2	213.7	211.3	208.8	206.8
QS2 (kg/m ³)	835.3	827.1	856.8	855	845.2	835.3	827.1
StF1 (kg/m ³)	157	157	157	157	157	157	157
Water-to-cement (W/C) ratio	0.26	0.264	0.25	0.25	0.255	0.26	0.264
Water-to-binder (W/B) ratio	0.232	0.236	0.223	0.223	0.228	0.232	0.236
Si/C ratio	12%	12%	12%	12%	12%	12%	12%
QP/C ratio	30%	30%	30%	30%	30%	30%	30%
SP/C ratio	3%	3%	3%	3%	3%	3%	3%
Perfin/CEM ratio	1.5%	2%	0%	0%	0%	0%	0%
Foam/CEM ratio	0%	0%	0%	0.5%	1%	1.5%	2%
QS1/(QS1+QS2)	20V%	20V%	20V%	20V%	20V%	20V%	20V%
QS2/(QS1+QS2)	80V%	80V%	80V%	80V%	80V%	80V%	80V%
StF volume content	2%	2%	2%	2%	2%	2%	2%
Spread-flow (cm)	28.5	28.5	26	26	26	26	26
Air content in fresh mix (%)	2.8	2.8	4.3	3.5	3.5	3.3	3.3
Compressive strength (MPa)	148.1	137.9	174.4	171.8	175.1	170.7	164.6
P_{bubble} in all sections (%)	1.1327 1.0803 1.0028	1.1285 0.9581 1.0602	2.6173 2.6971 2.639	1.8706 1.8604 1.8103	1.6779 1.7769 1.7261	1.5999 1.62 1.6996	1.6392 1.6071 1.6464

Table A.5: Detailed mix recipe and properties of each UHPC mixture in Section 4.5

	Column 1	Column 2	Column 3	Column 4	Column 5
CEM A (kg/m ³)	720	860	0	860	720
CEM B (kg/m ³)	0	0	720	0	0
Si (kg/m ³)	86.4	103.2	86.4	103.2	86.4
QP (kg/m ³)	216	258	216	258	216
WA (kg/m ³)	169.2	185.3	169.6	205.5	176.8
SP (kg/m ³)	36	30.1	25.2	25.8	25.2
QS1 (kg/m ³)	227.2	185.6	232.3	177	228.5
QS2 (kg/m ³)	908.7	742.5	929.3	708.2	914.1
Water-to-cement (W/C) ratio	0.27	0.24	0.26	0.26	0.27
Water-to-binder (W/B) ratio	0.24	0.21	0.23	0.23	0.24
Si/C ratio	12%	12%	12%	12%	12%
QP/C ratio	30%	30%	30%	30%	30%
SP/C ratio	5%	3.5%	3.5%	3%	3.5%
QS1/(QS1+QS2)	20V%	20V%	20V%	20V%	20V%
QS2/(QS1+QS2)	80V%	80V%	80V%	80V%	80V%
Spread-flow (cm)	25	25	25	31	25
Air content in fresh mix (%)	4.2	4.2	4.2	3	4.2

Compressive strength (MPa)		181.3	189.8	183.8	192.3	194.9		
		180.4	183.8	177.4	191.3	182.1		
		178.6	186.6	180.9	186.4	191		
	Distance from the upper surface (cm)					Diameter 50mm	Diameter 75mm	Diameter 100mm
P_{bubble} (%)	10	1.69331	1.89989	1.85673	0.94888	1.86336	1.85744	1.96924
	30	1.29797	1.6666	1.80683	0.85658	1.74352	1.64005	1.79527
	50	1.44234	1.58052	1.70172	0.92251	1.87202	1.77656	1.84573
	70	1.41281	1.60333	1.25952	0.79462	1.96873	1.89193	1.85502
	90	0.95287	1.26448	1.24766	0.80474	1.80566	1.66073	1.71666
	10				1.08776			
	17.5				1.08201			
	25				0.99125			
	32.5				0.88826			
	40				0.65531			
	20					2.08821		
	40					2.03209		
	60					2.04981		
	80					1.65012		
	100					2.31709		
	120					2.59221		
	140					2.60596		
	160					1.8188		
	190					1.73059		
	5	1.95432	2.05671	1.69233	1.02016			1.90829
	10	1.85176	1.9559	1.71023	0.9487			1.80361
	15	1.89902	2.06466	1.71998	1.16527			1.88644

Table A.6: Detailed mix recipe and properties of each UHPC mixture in Section 5.2.2

	CVC 0/0	CVC 50/75	CVC 100/75
CEM C (kg/m ³)	350	350	350
Water (kg/m ³)	209	209	209
SP (kg/m ³)	1.9	1.9	1.9
Sand 0-4mm (kg/m ³)	906	906	906
Gravel 4-8mm (kg/m ³)	543	272	0
Gravel 8-16mm (kg/m ³)	362	362	362
RCA 4-8mm (kg/m ³)	0	247	494
Compensation water (kg/m ³)	0	7	13
Water-to-cement (W/C) ratio	0.6	0.6	0.6
SP/C ratio	0.55%	0.55%	0.55%
V(Sand 0-4mm)/V(Ag)	50%	50%	50%
V(Gravel 4-8mm)/V(Ag)	30%	15%	0%
V(Gravel 8-16mm)/V(Ag)	20%	20%	20%
V(RCA 4-8mm)/V(Ag)	0%	15%	30%
Compensation water content (%)	75%	75%	75%
Slump flow value (cm)	48	47.5	47
Compressive strength (MPa)	52.8	52.7	48.2

53.6

47.9

48

Table A.7: Detailed mix recipe and properties of each UHPC mixture in Section 5.3

	UHPC1 0/0	UHPC1 50/55	UHPC1 100/100	UHPC2 0/0	UHPC2 50/80	UHPC2 100/75
CEM A (kg/m ³)	670	670	670	680	680	680
Si (kg/m ³)	80.4	80.4	80.4	81.6	81.6	81.6
QP (kg/m ³)	201	201	201	204	204	204
WA (kg/m ³)	166.8	166.8	166.8	169.3	169.3	169.3
SP (kg/m ³)	20.1	20.1	20.1	20.4	20.4	20.4
QS1 (kg/m ³)	238.5	238.5	238.5	245.1	245.1	245.1
QS2 (kg/m ³)	596.3	596.3	596.3	612.7	612.7	612.7
BA2 (kg/m ³)	402.1	201	0	413.2	206.6	0
RCA 4-8mm (kg/m ³)	0	167.1	334.2	0	170.2	340.3
StF1 (kg/m ³)	157	157	157	-	-	-
Compensation water (kg/m ³)	0	3.4	12.4	0	5.1	9.5
Water-to-cement (W/C) ratio	0.27	0.27	0.27	0.27	0.27	0.27
Water-to-binder (W/B) ratio	0.24	0.24	0.24	0.24	0.24	0.24
Si/C ratio	12%	12%	12%	12%	12%	12%
QP/C ratio	30%	30%	30%	30%	30%	30%
SP/C ratio	3%	3%	3%	3%	3%	3%
QS1/(QS1+QS2+ BA2+RCA)	20V%	20V%	20V%	20V%	20V%	20V%
QS2/(QS1+QS2+ BA2+RCA)	50V%	50V%	50V%	50V%	50V%	50V%
BA2/(QS1+QS2+ BA2+RCA)	30V%	15V%	-	30V%	15V%	-
RCA/(QS1+QS2+ BA2+RCA)	-	15V%	30V%	-	15V%	30V%
StF volume content	2%	2%	2%	-	-	-
Compensation water content	-	55%	100%	-	80%	75%
Spread-flow (cm)	21.5	20.5	22.5	27	28	26.5
Air content in fresh mix (%)	-	-	-	3.2	3	3.6
Compressive strength (MPa)	197.9	172.4	164.1	181.9	161.7	144

	UHPC3 0/0	UHPC3 50/0	UHPC3 50/78	UHPC3 50/100	UHPC3 100/0	UHPC3 100/78	UHPC3 100/100
CEM A (kg/m ³)	680	680	680	680	680	680	680
Si (kg/m ³)	81.6	81.6	81.6	81.6	81.6	81.6	81.6
QP (kg/m ³)	204	204	204	204	204	204	204
WA (kg/m ³)	169.3	169.3	169.3	169.3	169.3	169.3	169.3
SP (kg/m ³)	20.4	20.4	20.4	20.4	20.4	20.4	20.4
QS1 (kg/m ³)	245.1	245.1	245.1	245.1	245.1	245.1	245.1
QS2 (kg/m ³)	612.7	612.7	612.7	612.7	612.7	612.7	612.7
BA2 (kg/m ³)	413.2	206.6	206.6	206.6	0	0	0
RCA 4-8mm (kg/m ³)	0	170.2	170.2	170.2	340.3	340.3	340.3

StF1 (kg/m ³)	-	-	-	-	-	-	-
Compensation water (kg/m ³)	0	0	4.9	6.3	0	9.8	12.6
Water-to-cement (W/C) ratio	0.27	0.27	0.27	0.27	0.27	0.27	0.27
Water-to-binder (W/B) ratio	0.24	0.24	0.24	0.24	0.24	0.24	0.24
Si/C ratio	12%	12%	12%	12%	12%	12%	12%
QP/C ratio	30%	30%	30%	30%	30%	30%	30%
SP/C ratio	3%	3%	3%	3%	3%	3%	3%
QS1/(QS1+QS2+BA2+RCA)	20V%	20V%	20V%	20V%	20V%	20V%	20V%
QS2/(QS1+QS2+BA2+RCA)	50V%	50V%	50V%	50V%	50V%	50V%	50V%
BA2/(QS1+QS2+BA2+RCA)	30V%	15V%	15V%	15V%	-	-	-
RCA/(QS1+QS2+BA2+RCA)	-	15V%	15V%	15V%	30V%	30V%	30V%
StF volume content	-	-	-	-	-	-	-
Compensation water content	-	0%	78%	100%	0%	78%	100%
Spread-flow (cm)	29.5	28	30	31	26	29	30
Air content in fresh mix (%)	2.3	2.9	2.7	2.1	3.3	2.8	2.4
Compressive strength (MPa)	183.3	163.4	157	160	149.9	144.1	144.8

	UHPC4 0/0	UHPC4 50/78	UHPC4 100/78
CEM A (kg/m ³)	680	680	680
Si (kg/m ³)	81.6	81.6	81.6
QP (kg/m ³)	204	204	204
WA (kg/m ³)	169.3	169.3	169.3
SP (kg/m ³)	20.4	20.4	20.4
QS1 (kg/m ³)	245.1	245.1	245.1
QS2 (kg/m ³)	612.7	612.7	612.7
BA2 (kg/m ³)	413.2	206.6	0
RCA 4-8mm (kg/m ³)	0	170.2	340.3
StF1 (kg/m ³)	-	-	-
Compensation water (kg/m ³)	0	4.9	9.8
Water-to-cement (W/C) ratio	0.27	0.27	0.27
Water-to-binder (W/B) ratio	0.24	0.24	0.24
Si/C ratio	12%	12%	12%
QP/C ratio	30%	30%	30%
SP/C ratio	3%	3%	3%
QS1/(QS1+QS2+BA2+RCA)	20V%	20V%	20V%
QS2/(QS1+QS2+BA2+RCA)	50V%	50V%	50V%
BA2/(QS1+QS2+BA2+RCA)	30V%	15V%	-

RCA/(QS1+QS2+ BA2+RCA)	-	15V%	30V%
StF volume content	-	-	-
Compensation water content	-	78%	78%
Spread-flow (cm)	29.5	29.5	29.5
Air content in fresh mix (%)	2.7	3	3.3
Compressive strength (MPa)	182.2 181.3	164 149.9	143.7 135.5
Parameter A	0.00444	0.00386	0.00323
P_{bubble} in all sections (%)	0.48466 0.5272	0.87916 0.87281	1.20032 1.20036
	0.52171	0.90116	1.22391

Monographic Series TU Graz

Schriftenreihe des Instituts Betonbau

Series Editor:

Univ.-Prof. Dipl.-Wirtsch.-Ing. Dr.techn. Dirk Schlicke

- Volume 1 Reichel, Michael Maria
Dünnwandige Segmentfertigteilm Bauweisen im Brückenbau aus gefasertem Ultrahochleistungsbeton (UHFB)
2011; ISBN 978-3-85125-168-5
- Volume 2 Li, Jiabin
Development and Validation of a new Material Model for Concrete on the Basis of Microplane Theory
2011; ISBN 978-3-85125-184-5
- Volume 3 Schwarz, Sören
Einfluss der Bewehrungsführung im Lasteinleitungsbereich von Flachdecken auf die Tragfähigkeit von Randstützen-Decken-Knoten
2012; ISBN 978-3-85125-205-7
- Volume 4 Schlicke, Dirk
Mindestbewehrung für zwangbeanspruchten Beton
2014 | 2. überarbeitete Auflage 2016
DOI 10.3217/978-3-85125-473-0
ISBN print 978-3-85125-363-4
ISBN e-book 978-3-85125-473-0
- Volume 5 Illich, Günther Werner
Ein Beitrag zur allgemeinen Beschreibung des Tragverhaltens von schlanken Betondruckgliedern
2015; DOI 10.3217/978-3-85125-405-1
ISBN print 978-3-85125-405-1
ISBN e-book 978-3-85125-410-5

- Volume 6 Pilch, Erwin
Integrale Brücken
2016; DOI 10.3217/978-3-85125-443-3
ISBN print 978-3-85125-443-3
ISBN e-book 978-3-85125-444-0
- Volume 7 Hadl, Philipp
Streuung im Zugtragverhalten von Stahlfaserbeton
2017; DOI 10.3217/978-3-85125-539-3
ISBN print 978-3-85125-539-3
ISBN e-book 978-3-85125-540-9
- Volume 8 della Pietra, Regina
Integralisierung von Bestandsbrücken
2018; DOI 10.3217/978-3-85125-587-4
ISBN print 978-3-85125-587-4
ISBN e-book 978-3-85125-588-1
- Volume 9 Laggner, Thomas Markus
Ganzheitliche 3D-Gebäudemodelle in der statischen Tragwerksanalyse
2022; DOI 10.3217/978-3-85125-904-9
ISBN print 978-3-85125-904-9
ISBN e-book 978-3-85125-905-6
- Volume 10 Mayer, Michael
Verhalten integraler Stahlbetonbrücken unter allgemeiner Beanspruchung
2022; DOI 10.3217/978-3-85125-928-5
ISBN print 978-3-85125-928-5
ISBN e-book 978-3-85125-929-2
- Volume 11 Yuan, Shuai
Investigation of some Workability Issues Impeding the Large-scale Application of UHPC
2024; DOI 10.3217/978-3-99161-026-7
ISBN print 978-3-99161-026-7
ISBN e-book 978-3-99161-027-4